



National Library
of Canada

Bibliothèque nationale
du Canada

Canadian Theses Service

Service des thèses canadiennes

Ottawa, Canada
K1A 0N4

NOTICE

The quality of this microform is heavily dependent upon the quality of the original thesis submitted for microfilming. Every effort has been made to ensure the highest quality of reproduction possible.

If pages are missing, contact the university which granted the degree.

Some pages may have indistinct print especially if the original pages were typed with a poor typewriter ribbon or if the university sent us an inferior photocopy.

Previously copyrighted materials (journal articles; published tests, etc.) are not filmed.

Reproduction in full or in part of this microform is governed by the Canadian Copyright Act, R.S.C. 1970, c. C-30.

AVIS

La qualité de cette microforme dépend grandement de la qualité de la thèse soumise au microfilmage. Nous avons tout fait pour assurer une qualité supérieure de reproduction.

S'il manque des pages, veuillez communiquer avec l'université qui a conféré le grade.

La qualité d'impression de certaines pages peut laisser à désirer, surtout si les pages originales ont été dactylographiées à l'aide d'un ruban usé ou si l'université nous a fait parvenir une photocopie de qualité inférieure.

Les documents qui font déjà l'objet d'un droit d'auteur (articles de revue, tests publiés, etc.) ne sont pas microfilmés.

La reproduction, même partielle, de cette microforme est soumise à la Loi canadienne sur le droit d'auteur, SRC 1970, c. C-30.

THE UNIVERSITY OF ALBERTA

STUDY OF THE ORIGIN OF EXCESSIVE BANDBROADENING ON
PRP-1

by

TERRY ANN DUBETZ

A THESIS

SUBMITTED TO THE FACULTY OF GRADUATE STUDIES AND RESEARCH
IN PARTIAL FULFILMENT OF THE REQUIREMENTS FOR THE DEGREE
DOCTOR OF PHILOSOPHY

DEPARTMENT OF CHEMISTRY

EDMONTON, ALBERTA

FALL 1988

Permission has been granted to the National Library of Canada to microfilm this thesis and to lend or sell copies of the film.

The author (copyright owner) has reserved other publication rights, and neither the thesis nor extensive extracts from it may be printed or otherwise reproduced without his/her written permission.

L'autorisation a été accordée à la Bibliothèque nationale du Canada de microfilmer cette thèse et de prêter ou de vendre des exemplaires du film.

L'auteur (titulaire du droit d'auteur) se réserve les autres droits de publication; ni la thèse ni de longs extraits de celle-ci ne doivent être imprimés ou autrement reproduits sans son autorisation écrite.

ISBN 0-315-45740-6

THE UNIVERSITY OF ALBERTA

RELEASE FORM

NAME OF AUTHOR TERRY ANN DUBETZ
TITLE OF THESIS STUDY OF THE ORIGIN OF EXCESSIVE
BANDBROADENING ON PRP-1
DEGREE FOR WHICH THESIS WAS PRESENTED Ph.D.
YEAR THIS DEGREE WAS GRANTED 1988

Permission is hereby granted to the UNIVERSITY OF ALBERTA
LIBRARY to reproduce single copies of this thesis and to lend or sell such
copies for private, scholarly or scientific research purposes only.

The author reserves other publication rights, and neither the thesis nor
extensive extracts from it may be printed or otherwise without the author's
written permission.

(Signed) *Terry Ann Dubetz*

PERMANENT ADDRESS:

2268 Norton

Rochester Hills, Michigan

U.S.A. 48063

DATED September 15 1988

THE UNIVERSITY OF ALBERTA
FACULTY OF GRADUATE STUDIES AND RESEARCH

The undersigned certify that they have read, and recommend to the Faculty of
Graduate Studies and Research, for acceptance, a thesis entitled STUDY OF THE
ORIGIN OF EXCESSIVE BANDBROADENING ON PRP-1
submitted by TERRY A. DUBETZ
in partial fulfilment of the requirements for the degree of DOCTOR OF PHILOSOPHY

F. F. Cantwell

F.F. Cantwell, Supervisor

B. Kratochvil

B. Kratochvil

James A. Plambeck

J.A. Plambeck

L. Hepler

L. Hepler

A. E. Mather

A.E. Mather


D. B. Marshall

D.B. Marshall, External Examiner

DATE

ABSTRACT

A polystyrene-divinylbenzene stationary phase (PRP-1) used for reversed-phase liquid chromatography (RPLC) is characterized to determine the origin of excessive bandbroadening.

Compared to other stationary phases used in RPLC, such as bonded phases, PRP-1 produces broad, asymmetrical peaks. This decreases the efficiency of PRP-1 for separations and limits its utility as a stationary phase. PRP-1 is chemically more stable than bonded phases, so it does have potential usefulness in RPLC. Therefore, it is of interest to determine the source of the bandbroadening on PRP-1 in order to minimize it. 

Chromatograms were run on both PRP-1 and a bonded phase in order to determine the relative magnitude of the bandbroadening on PRP-1 and to find relations between plate height and sample capacity factor, mobile phase linear velocity and type of sample. All samples chromatographed on PRP-1 produced bandbroadening 3x to 25x greater than the bonded phase. The bandbroadening on PRP-1 was not dependent on capacity factor but was much larger for more highly conjugated aromatics. The bandbroadening decreased with decreasing mobile phase linear velocity but was still large at low linear velocities.

Adsorption isotherms, adsorption-desorption kinetics and sample velocity profiles were measured on PRP-1 in order to estimate their contributions to bandbroadening.

The adsorption isotherm of a sample which produced large plate heights was measured and found to be only slightly curved, indicating isotherm non-linearity is not the cause of the bandbroadening. A program was written to predict the peak shape resulting from both a non-linear isotherm and column non-ideality.

Equipment was developed to measure adsorption-desorption kinetics; the kinetic process was found not to contribute significantly to the bandbroadening.

Velocity profiles on a packed bed of PRP-1 were determined by injecting a dye onto a short column of PRP-1, extruding the bed after partial migration of the dye and observing the dye profile. The profiles were non-uniform and changed shape with the manner in which mobile phase entered and left the column. It was concluded that the packing structure of PRP-1 is not stable or uniform and produces a non-uniform velocity profile which contributes significantly to bandbroadening.

ACKNOWLEDGEMENTS

The author is sincerely grateful to Dr. Frederick F. Cantwell for his guidance throughout the course of this work. Thanks are also extended to D.P. Lee of Hamilton Company for the donation of PRP-1 stationary phase which was used in this thesis.

TABLE OF CONTENTS

CHAPTER	PAGE
1. INTRODUCTION	1
2. EXPERIMENTAL	
2.1 Characterization of Bandbroadening by Chromatography	
2.1.1 Procedure	5
2.1.2 Apparatus	5
2.1.3 Chemicals	8
2.1.4 Solvents and Mobile Phases	8
2.2 Naphthalene Adsorption Isotherm	
2.2.1 Procedure	9
2.2.2 Apparatus	11
2.2.3 Chemicals	12
2.2.4 Solvents and Mobile Phases	12
2.2.5 Sample Solutions	12
2.2.6 Procedure for the Measurement of the Precolumn Hold-up Volume	13
2.3 Naphthalene Adsorption-Desorption Kinetics on PRP-1	
2.3.1 Apparatus and Procedure	13
2.3.2 Shallow Bed Cartridge Design	16
2.3.3 Chemicals	17
2.3.4 Solvents and Mobile Phases	17
2.3.5 Columns	19
2.3.6 Injection Loop Calibration	19

CHAPTER	PAGE
2.3.7 Measurement of Quantity of Naphthalene Adsorbed at Equilibrium	20
2.3.8 Hold-up Volume Measurements	20
2.4 Velocity Profile Studies	
2.4.1 Bed Extrusion Procedure	21
2.4.2 Apparatus, Column Packing and Chromatographic Characterization Procedures	22
2.4.3 Chemicals	25
2.4.4 Solvents and Mobile Phases	27
2.4.5 Stationary Phases	27
3. CHARACTERIZATION OF BANDBROADENING BY CHROMATOGRAPHY	
3.1 Theory	
3.1.1 Equilibrium Aspects of Chromatography	29
3.1.2 Bandbroadening	33
3.1.3 Longitudinal Diffusion	35
3.1.4 Adsorption-Desorption Kinetics	37
3.1.5 Mass Transfer Through the Stagnant Mobile Phase	39
3.1.6 Mass Transfer Through the Mobile Phase	40
3.1.7 Eddy Diffusion and the Coupled Plate Height Term	42
3.1.8 Summary of Column Bandbroadening	43
3.1.9 Extracolumn Bandbroadening	44
3.1.10 Total Plate Height	45
3.1.11 Measurement of Chromatographic Parameters	45
3.2 Results and Discussion	
3.2.1 Plate Height vs Stationary Phase	48
3.2.2 Plate Height vs Capacity Factor	50

CHAPTER	PAGE
3.2.3 Plate Height vs Mobile Phase Linear Velocity	55
3.3 Conclusions	63
4. NAPHTHALENE ADSORPTION ISOTHERM	
4.1 Theory	
4.1.1 Sorption Isotherms	65
4.1.2 Measuring Sorption Isotherms	69
4.1.3 Relation of Chromatographic Peak Shape and Isotherm Curvature	74
4.2 Results and Discussion	
4.2.1 Precolumn Hold-up Volume Determination	83
4.2.2 Naphthalene Adsorption Isotherm	86
4.2.3 Comparison of Results from Elution Chromatograms to Results Predicted from the Adsorption Isotherm	92
4.2.4 Simulation of Peak Shape Due to Isotherm Curvature	100
4.3 Conclusions	109
5. NAPHTHALENE ADSORPTION-DESORPTION KINETICS	
5.1 Theory	
5.1.1 Kinetic Processes in Chromatography	111
5.1.2 Methods Used to Measure the Rates of Adsorption and Desorption	115
5.1.3 Shallow Bed Procedure	117
5.2 Results and Discussion	
5.2.1 Measurement of Flow Profile	121
5.2.2 Injection Loop Volumes	122
5.2.3 Measurement of Quantity of Naphthalene Adsorbed at Equilibrium	124

CHAPTER	PAGE
5.2.4 Hold-up Volume Measurements	126
5.2.5 Measurement of the Naphthalene Desorption Rate	190
5.2.6 Effect of Fast Flow Rates on Particle Outer Film Diffusion	130
5.3 Relation of Adsorption-Desorption Rate Curves to Plate Height	
5.3.1 Calculation of the Adsorption-Desorption Plate Height	135
5.3.2 Infinite Solution Volume Assumption	140
5.4 Conclusions	146
6. VELOCITY PROFILE STUDIES	
6.1 Introduction	149
6.1.1 Packing Structure Heterogeneity and a Non-uniform Velocity Profile Due to Varying Permeability	149
6.1.2 Packing Structure Heterogeneity and Non-uniform Phase Ratio	152
6.1.3 Calculation of Plate Height Based on Varying Permeability and Non-uniform Phase Ratio Across the Column	154
6.2 Results and Discussion	
6.2.1 Packing Structure Non-uniformity Caused by Bed Compression or Expansion	160
6.2.2 Short Column Characterizations by Chromatography	166
6.2.3 Velocity Profile Results Using the Constricted Flow Configuration	171
6.2.4 Velocity Profile Results Using the Uniform Flow Configuration	176
6.2.5 Velocity Profiles Obtained on C18 Columns	184

CHAPTER	PAGE
6.2.6 Conclusions from the Velocity Profile Experiments	188
6.2.7 Plate Height Calculation Based on Velocity Profile	188
6.3 Conclusions	195
7. CONCLUSIONS AND FUTURE WORK	198

BIBLIOGRAPHY	201
APPENDIX I: Peak Simulation Program	210
APPENDIX II: Tables of parameters used in the peak simulation program	249
APPENDIX III: The Possibility of a Second Slower Reaction	253
APPENDIX IV: Program H(WS) used to calculate the effect on plate height due to a non-uniform packing density across the column	260

LIST OF TABLES

TABLE	PAGE
2.1 Characteristics of PRP-1	28
3.1 Plate heights and asymmetry factors for naphthalene on PRP-1 and C18	49
3.2 Plate height vs capacity factor on PRP-1	52
3.3 Naphthalene and methyl paraben plate heights vs mobile phase linear velocity on PRP-1	57
3.4 Calculated values of H_{ij} for naphthalene and methyl paraben at various mobile phase linear velocities	59
3.5 Extracolumn variance and total peak variance vs u_0 for naphthalene	61
3.6 Extracolumn variance and total peak variance vs u_0 for methyl paraben	62
4.1 Chromatographic parameters measured from the simulated peak and theoretical values for linear, non-ideal chromatography	82
4.2 Volume of calcium nitrate solution pumped through the PRP-1 precolumn vs V_m'	84
4.3 V_m' vs percent methanol in the mobile phase	85
4.4 V_m' vs calcium nitrate concentration	87
4.5 Naphthalene peak area vs equilibration time on PRP-1 precolumn	89
4.6 Naphthalene - 90% methanol(aq) adsorption isotherm on PRP-1	90
4.7 Naphthalene injected solution concentrations and the corresponding mobile phase equilibrium concentrations	95
4.8 Comparison of chromatographic parameters measured from simulated naphthalene peaks and experimental values from elution chromatograms	102

TABLE	PAGE
4.9 Chromatographic parameters measured from simulated naphthalene peaks using various injection profiles and isotherm shapes	106
5.1 Calibration of injection loops used in shallow bed method	125
5.2 V_m results for desorption rate experiment	128
5.3 Moles of naphthalene still adsorbed vs contact time of mobile phase for the desorption rate experiment	131
5.4 Plate heights calculated from desorption results	139
5.5 Error resulting from the departure from the ISV assumption in the desorption rate experiment	147
6.1 Values of permeability coefficient at various mobile phase linear velocities and column pressures	163
6.2 Permeability coefficients obtained for various columns and mobile phases	165
6.3 Plate heights for methyl paraben and 4-phenylazo-1-naphthylamine on PRP-1 short columns used in the velocity profile experiments	167
6.4 Plate heights for C18 columns used in the velocity profile experiments	170
6.5 Solvent volume passed through the columns prior to extrusion using constricted flow conditions	173
6.6 Sample velocities at the column wall and center using constricted flow conditions	175
6.7 Solvent volume passed through the columns prior to extrusion using uniform flow conditions	177
6.8 Sample velocities at the column wall and center using uniform flow conditions	179

TABLE	PAGE
6.9 Solvent volume passed through the columns prior to extrusion using constricted flow initially and then switching to uniform flow	181
6.10 Sample velocities at the column wall and center using constricted flow initially and then switching to uniform flow	183
6.11 Solvent volume passed through the C18 columns	185
6.12 Sample velocities at the column wall and center for the C18 columns	187
6.13 Variables used for the program H(WS) to predict the effect of an uneven packing density on plate height	190
6.14 Comparison of simulated values from the H(WS) program and experimental values measured from elution chromatograms on PRP-1	194
A2.1 Parameters used in the peak simulation program for a linear isotherm and a non-linear, convex isotherm	250
A2.2 Parameters used in the peak simulation program based on the experimental naphthalene adsorption isotherm	251
A2.3 Parameters used in the peak simulation program based on the experimental naphthalene adsorption isotherm and asymmetric injection profiles	257
A3.1 Calculated H at various u_0 for reactions 1 and 2	258

LIST OF FIGURES

FIGURE	PAGE
2.1 Schematic diagram of apparatus used for chromatography	6
2.2 Schematic diagram of the equipment used to measure the adsorption isotherm by the column equilibration method	10
2.3 Schematic diagram of the equipment used in the adsorption-desorption rate measurements by the shallow bed method	14
2.4 Shallow bed cartridge used to contain PRP-1 for the adsorption - desorption rate experiments	18
2.5 Schematic diagram of the equipment used to pack short columns for velocity profile experiments	23
2.6 Column outlet endfittings used in velocity profile studies	26
3.1 Measurement of peak width to calculate resolution	32
3.2 An ideal and a real chromatogram	34
3.3 Bandbroadening due to inability to achieve equilibrium between phases in chromatography	38
3.4 Measurement of variables used to calculate peak center of gravity and variance by moments analysis and the asymmetry factor	47
3.5 Chromatograms of naphthalene obtained on PRP-1 and a C18 column	51
3.6 Plate height vs capacity factor on PRP-1	54
3.7 Plate height vs mobile phase linear velocity on PRP-1 and C18	58
4.1 A sorption isotherm and calculation of the distribution coefficient using the sorption isotherm	66
4.2 Shapes of common sorption isotherms and the corresponding elution peak profile	67

FIGURE	PAGE
4.3 Breakthrough curve	71
4.4 Diagram of the initial portion of the "column" used in the peak simulation	77
4.5 Non-linear adsorption isotherm used to simulate a peak	79
4.6 Simulated elution peaks assuming a linear and a non-linear isotherm	81
4.7 Naphthalene - 90% methanol(aq) adsorption isotherm on PRP-1	91
4.8 Retention volume vs naphthalene concentration	97
4.9 Asymmetry factor vs naphthalene concentration	98
4.10 Plate height vs naphthalene concentration	99
4.11 Simulated elution peaks for two naphthalene concentrations	101
4.12 Injection profiles used with the peak simulation program	105
4.13 Simulated peaks using an increasing ramp injection profile	107
4.14 Simulated peaks using a decreasing ramp injection profile	108
5.1 Diagram of a sample molecule undergoing steps in the adsorption - desorption process on a porous particle of stationary phase	112
5.2 Simulated desorption rate curve which would be obtained using the shallow bed technique	119
5.3 Dye patterns observed on the inlet end during the flow profile study of the shallow bed cartridge	123
5.4 V_m vs contact time for the desorption rate experiment	129
5.5 Moles still adsorbed vs contact time for the desorption rate experiment	132
5.6 First order plots of the naphthalene desorption rate data	137
5.7 Effect on shape of the desorption rate curve due to not meeting the ISV condition	141

FIGURE	PAGE
5.8 Diagram of the steps in the program used to calculate the error caused by not meeting the ISV condition	143
6.1 Measurement of Δd_{front} and Δd_{back} from a sample zone profile	159
6.2 Pressure vs average mobile phase linear velocity for a PRP-1 column	162
6.3 Sample profiles for a column with a uniform velocity profile assuming (a) non-linear convex isotherm and (b) linear isotherm	169
6.4 Sample profiles obtained on PRP-1 when columns were packed, conditioned and characterized using constricted flow conditions	174
6.5 Sample profiles obtained on PRP-1 when columns were packed, conditioned and characterized using uniform flow conditions	178
6.6 Sample profiles obtained on PRP-1 when columns were packed under constricted flow conditions and switched to uniform flow prior to injection of the dye	182
6.7 Sample profiles obtained on C18 columns under (a) constricted flow conditions and (b) uniform flow conditions during packing, conditioning and characterization	186
6.8 Simulated elution peaks using H(WS) for (a) methyl paraben $K_i = 1$ and (b) 4-phenylazo-1-naphthylamine $K_i = 45$	191
6.9 Diagrams of the model sample zone used in the H(WS) program and a real sample zone	192
A1.1 Diagram of steps which occur in the peak simulation program	212
A3.1 Plot of $\ln f(n'_{\text{ads}})$ vs t for reactions 1 and 2	257

CHAPTER 1

Introduction

Liquid chromatography is a technique commonly used to separate mixtures into their individual components. The separation process occurs as the sample components distribute themselves between the two phases present in a liquid chromatographic system. The two phases are a liquid mobile phase which flows over a bed of stationary phase particles. The stationary phase is tightly packed inside a column. The stationary phase may be a liquid coated onto solid "inert" support particles, substituent groups chemically bonded onto the solid support or a solid material. Probably the most widely used type of liquid chromatography is reversed-phase chromatography, where the mobile phase is a polar solvent mixture and the stationary phase is non-polar [1.1-1.2]. The liquid-coated types of stationary phases were found to be useful for separating mixtures of organic compounds but unfortunately, they were not always stable because of dissolution of the liquid coating into the mobile phase [1.3].

The next logical improvement was to chemically bond the nonpolar "liquid" molecule to the "inert" support to increase the stability. Presently, these are the most commonly used stationary phases in reversed-phase liquid chromatography. Most consist of alkyl chains which are eight or eighteen carbons long, bonded to a silica gel matrix. These type of stationary phases are known as reversed-phase "bonded phases". They have been used in many applications such as the analysis of oligopeptides [1.4], purification of recombinant proteins [1.5], determination of antibiotics [1.6] and others [1.7 - 1.12]. Bonded phases are very efficient at separating mixtures as they usually produce a narrow, Gaussian-shaped peak for each component in the mixture. When peaks are narrow and symmetrical, overlap between adjacent peaks is minimized and a greater number of components can be resolved.

Bonded phases do have some problems associated with them. First of all, the silica gel support matrix is not actually inert. Even with the layer of alkyl groups bonded to the silica surface there are acidic silanol groups which are accessible to the sample and the mobile phase. These silanol groups can react with basic samples and when they do, broad asymmetrical peaks are often produced [1.13]. This type of peak shape decreases the separating efficiency of the column. Also, the siloxane (Si-O-Si) groups are hydrolyzed by high pH (≥ 8) mobile phases, resulting in loss of the bound molecule or even dissolution of the stationary phase particles [1.14, 1.15]. Some researchers have found impurity peaks due to hydrolysis products from the bonded alkyl groups [1.16].

In order to circumvent these problems, the use of organic polymeric stationary phases has been increasing [1.17, 1.18]. These are highly cross-linked, rigid copolymer particles. They consist of many microspheres joined together in a cluster, forming a larger "macroporous" particle which has a large surface area [1.19, 1.20]. The microspheres, ideally, are non-porous and therefore not involved in the chromatographic separation process [1.17]. The macropores are due to the spaces between aggregates of microspheres and it is this porous surface upon which sample retention occurs [1.21]. These polymeric adsorbents have been used for several types of applications [1.22-1.24]. Researchers have separated mixtures of drugs [1.18, 1.25 - 1.27], thiamine derivatives [1.28], wine acids [1.29], nucleosides [1.30] and other samples [1.31 - 1.36] using polymers as a reversed-phase adsorbent.

Of particular interest in reversed-phase chromatography are polymers made of polystyrene-divinylbenzene. The adsorption of both ionic and neutral organic compounds has been studied by several researchers [1.21, 1.37-1.46]. Adsorption on these resins is the mechanism of retention for neutral organic compounds from mixtures of water and organic solvents [1.17, 1.37]. The amount of adsorption increases with surface area of the polymer, with the size and number of non-polar substituents on the sample and with increasing percent water in the mobile phase [1.21-1.24].

In contrast to silica-based bonded phases these polymers are chemically very stable [1.18, 1.30] and can be used over a pH range of 1 to 13. They do not dissolve in the organic mobile phases which are commonly used in reversed-phase liquid chromatography. Because of the high degree of cross-linking, they are mechanically stable and can be used at high pressures [1.17]. However, they do exhibit a problem which limits their utility. Polymeric adsorbents produce broad, asymmetrical peaks for most samples compared with the peak shapes obtained with silica-based bonded phases. As stated previously, this type of peak shape decreases the separating efficiency of a column. This problem is much worse for some non-polar aromatic samples [1.18, 1.47 - 1.49].

The purpose of the research described in this thesis is to discover the origin of this anomalously low column efficiency observed on the polymeric adsorbents. In this work Hamilton PRP-1, one of the most popular macroporous polystyrene-divinylbenzene stationary phases, was chosen for study. Naphthalene and 90% methanol(aq) were chosen as the model sample and mobile phase for this study, as this system produced poorly shaped peaks on PRP-1.

PRP-1 is available commercially as spherical 5 and 10 micrometer particles. The average pore diameter of the PRP-1 used in this thesis was 75 angstroms, although particles with larger pore diameters can be obtained. The polymer has a large surface area of 415 m² per gram. Pressures up to 4000 psig can be used with negligible compression of the particles. There is little swelling or shrinking of PRP-1 in typical reversed-phase mobile phases [1.30].

Chapter 2 gives experimental details, such as procedures and equipment, for all experiments done. Chapter 3 discusses the chromatographic experiments done to characterize the problem on PRP-1. Effects of flow rate, capacity factor and type of sample were studied in order to determine their relation to peak shape. This also helped determine which steps in the chromatographic process could be responsible for the problem and therefore, it directed the course of successive experiments.

In order to determine the cause of the broad, asymmetrical sample peaks observed on PRP-1, the chromatographic process was systematically studied. Each step in the separation process was evaluated for its effect on peak shape. Chapter 4 gives results for the measurement of the adsorption isotherm of naphthalene on PRP-1. Details are given for a program which was developed to predict a chromatographic peak shape based on isotherm curvature and other peak broadening phenomena. Chapter 5 presents the results of a kinetic experiment in which the naphthalene adsorption-desorption rate was measured. It also describes equipment which was especially developed for this experiment and which can be used to measure fast sorption rates on other particulate solids. Chapter 6 gives the results of sample velocity profile studies on the packed bed of PRP-1. A technique was developed for this experiment also. It was used to study a bonded phase adsorbent as well as PRP-1, in order to compare the two types of stationary phase materials. Finally, conclusions from all of these experiments are summarized in Chapter 7.

CHAPTER 2

Experimental

This chapter includes experimental details for all of the thesis work. The studies done on PRP-1 include chromatographic characterization of the packing material and measurements of adsorption isotherms, adsorption-desorption kinetics and velocity profile on the packed bed of resin.

2.1 Characterization of Bandbroadening by Chromatography

2.1.1 Procedure

A schematic diagram of the chromatographic system is shown in Figure 2.1. Mobile phase is delivered by pump P to column C and detector via injection valve V. Initially the injection valve is in the "LOAD" position (indicated by the solid lines in Figure 2.1) and loop L is filled with sample solution. To inject sample onto the column, V is switched to the "INJECT" position (dashed lines in Figure 2.1) which changes the path of mobile phase so it flushes out the loop. The sample peak is directly monitored as it elutes from the column into the detector.

The experiments which measured extracolumn bandbroadening were done using the same equipment except that the column was removed from the system.

2.1.2 Apparatus

Three different types of pumps were used depending upon the mobile phase flow rate desired. A Chromatronix model CMP-2VK (Laboratory Data Control, Riviera Beach, FL) was used for flow rates of 0.5 mL per minute or less. The high pressure pump from a

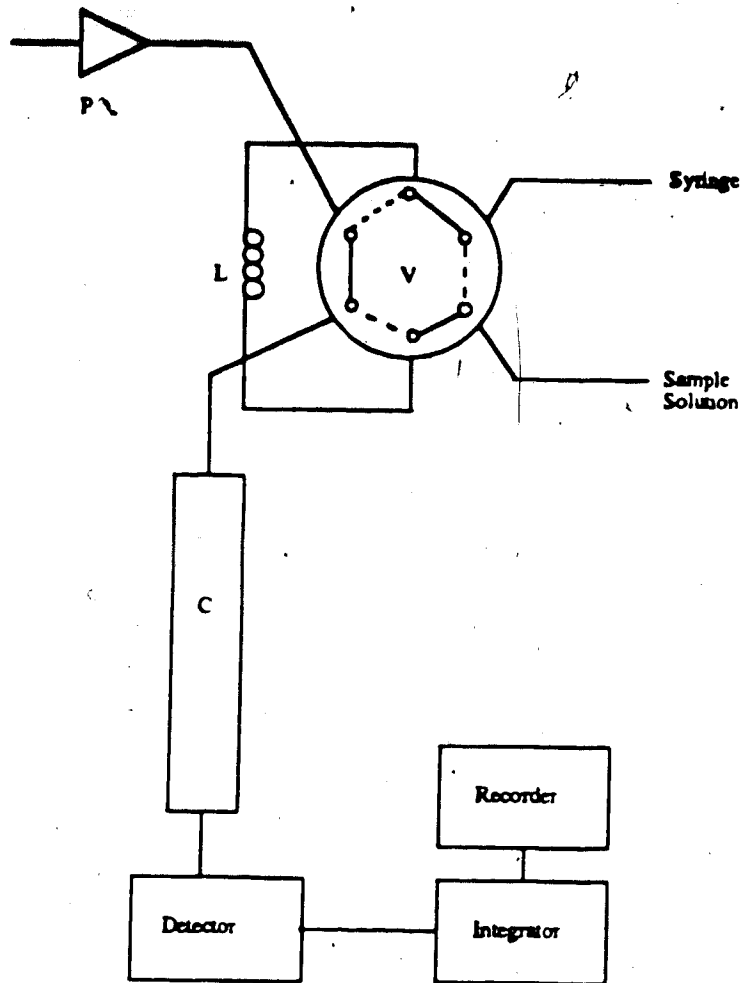


Figure 2.1 Schematic diagram of the apparatus used for elution chromatography. P = high pressure pump, V = injection valve, L = sample loop and C = analytical column.

Spectra Physics SP8000 liquid chromatograph (Spectra Physics, Santa Clara, CA) or a Waters M6000 pump (Waters Associates, Milford, MA) were used for higher flow rates.

A stainless steel injection valve (part no. 7010, Rheodyne Inc., Cotati, CA) was used to inject sample solution onto the chromatographic column from a 20 microliter loop (part no. 7022, Rheodyne Inc., Cotati, CA).

Several types of reversed-phase columns were used. The polystyrene-divinylbenzene copolymer column was PRP-1 (part no. SK 1120, Hamilton Co., Reno, NV). This column was 150 mm long with an id of 4.1 mm. The spherical macroporous copolymer beads had an average diameter of 10 micrometers and an average pore diameter of 75 angstroms. The column endfittings were a CPI compression type (Parker Hannifin). Two types of bonded phase columns were used, C8 and C18, and these consisted of an alkyl chain (eight carbons and eighteen carbons respectively) chemically bonded to a silica matrix. The C8 columns were supplied by two manufacturers. One was a LiChrosorb column (Spectra Physics, Santa Clara, CA) with 10 micrometer irregular-shaped particles having a column length of 250 mm and an internal diameter of 4.6 mm. The endfittings were a compression type. The other C8 column was a Partisil-10 C8 column (part no. 4229-001, Whatman Chemical Separations Inc., Clifton, NJ). This stationary phase consisted of irregular-shaped 10 micrometer particles. The column dimensions were 250 mm x 4.6 mm and the endfittings were Whatman compression screw endfittings.

The final column used was a Waters Novapak C18 (part no. 086344, Waters Associates, Milford, MA). The column was 150 mm x 3.9 mm with Waters compression type endfittings. The spherical C18 particles had an average diameter of 4 micrometers.

The detector used was a Spectroflow 757 UV-visible detector (Kratos Analytical Instruments, Ramsey, NJ). The chromatographic peak areas were measured using either a Hewlett-Packard Model 3390A (Hewlett-Packard, Avondale, PA) or a Vista 401 (Varian

Instruments, Palo Alto, CA) digital integrator. Eluted peaks were recorded using a Series 5000 Recordall (Fisher Scientific Co.) potentiometric chart recorder.

2.1.3 Chemicals

Naphthalene was supplied by Matheson, Coleman and Bell (Norwood, OH) and was recrystallized from methanol.

Methyl-p-hydroxybenzoate (methyl paraben) was used as received from Matheson, Coleman and Bell (Norwood, OH).

Phloroglucinol (1,3,5-trihydroxybenzene) was obtained from Fisher Scientific Co. (Fairlawn, NJ) and was recrystallized from water.

Calcium nitrate was supplied by Anachemia Ltd. (reagent grade, Montreal, Quebec) and was used as received.

All other chemicals were reagent grade and were used without further purification.

2.1.4 Solvents and Mobile Phases

Double distilled water was used to make all aqueous solutions. It was prepared by distilling the laboratory distilled water from alkaline permanganate in an all-glass still. The first 20% of this distillate was discarded and the middle portion was collected.

Methanol was obtained from two suppliers (Terochem Laboratories Ltd. and Anachemia Ltd.) and was distilled before use.

Acetonitrile was supplied by Caledon Laboratories Ltd. (Georgetown, Ontario) and was distilled before use.

Tetrahydrofuran with stabilizer was laboratory grade and was used as received from Caledon Laboratories Ltd. (Georgetown, Ontario).

Mobile phase concentrations are given as volume % organic solvent per volume of final solution. They were made by adding a known volume of organic solvent and diluting to the desired final volume with water. For example, 90% methanol(aq) was prepared by measuring 900 mL of methanol into a volumetric flask and then diluting to 1000 mL with water.

All solvents and mobile phases were filtered through a 0.45 micrometer porosity Nylon 66 membrane before use.

2.2 Naphthalene Adsorption Isotherm

2.2.1 Procedure

The procedure used to measure the adsorption isotherm of naphthalene from 90% methanol(aq) onto PRP-1 was the precolumn equilibration technique developed by May, Hux and Cantwell [2.1]. A schematic diagram of the equipment is shown in Figure 2.2. While injection valve V1 is in the "LOAD" position (solid lines in Figure 2.2) sample solution is pumped through precolumn C1 by pump P1 and out to waste until the adsorbent is equilibrated with the sample solution. Simultaneously, P2 is delivering a strong eluent through V1, V2 and the analytical column C2 and out to the detector. V2 is always in the "LOAD" position during the isotherm measurement.

After C1 is equilibrated V1 is switched to "INJECT" (dashed lines in Figure 2.2) so the strong eluent from P2 backflushes the precolumn, eluting adsorbed sample from C1. The sample continues through V1 and V2 onto column C2, where it is separated from interfering peaks before it reaches the detector.

The quantity of sample eluted from C1 is determined by comparison of the peak area with a calibration curve of peak area vs moles of sample. This quantity includes not only adsorbed sample but naphthalene present in tubing, valve V1 and the column void spaces of C1. The amount of naphthalene present in this hold-up volume is subtracted to

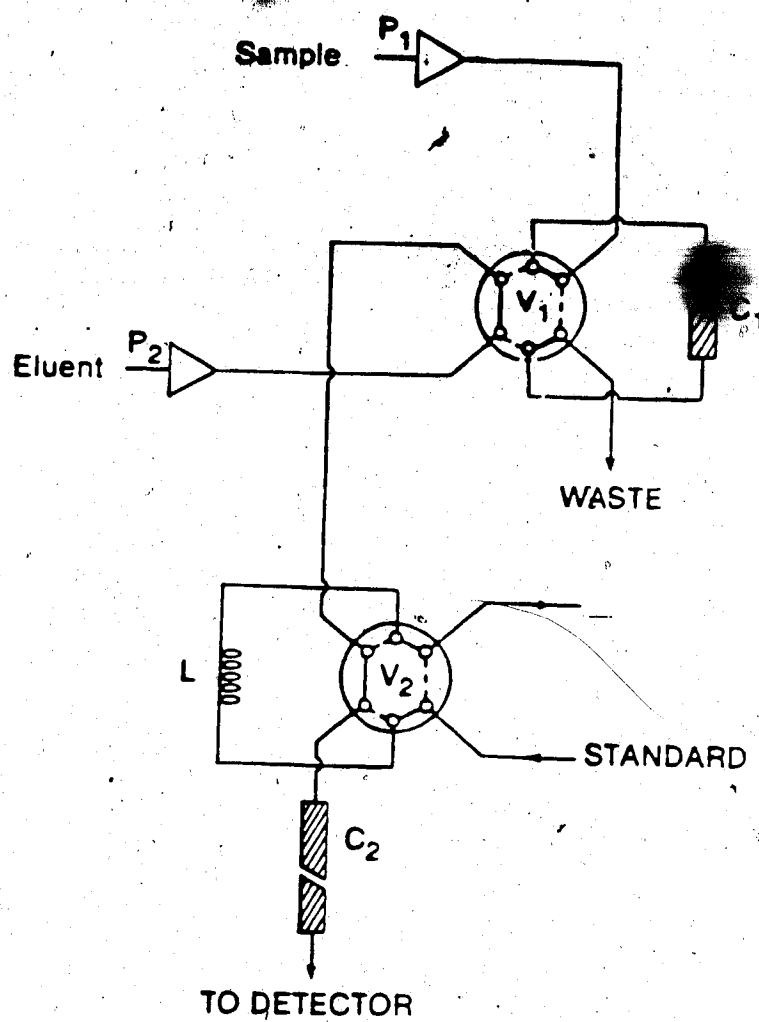


Figure 2.2 Schematic diagram of the equipment used for the adsorption isotherm experiment. P₁ and P₂ = pumps, C₁ = PRP-1 precolumn, C₂ = analytical column, V₁ and V₂ = injection valves and L = loop for standard solutions.

obtain the moles of sample adsorbed on the PRP-1. Section 2.2.6 gives details of the measurement of this hold-up volume. The calibration curve is determined in a separate experiment by injecting standard solutions from loop L with V2 onto the analytical column.

The distribution coefficient can be calculated using equations 4.6 and 4.7 described in Section 4.1.2. This procedure is repeated for several naphthalene solution concentrations to determine the adsorption isotherm.

2.2.2 Apparatus

Precolumn C1, which contained the PRP-1 adsorbent, was made from a piece of stainless steel tubing which was 4.2 mm long and had a 2 mm i.d. The adsorbent was held in place by a two micrometer pore diameter frit at each end and compression type endfittings. It was dry-packed with 6.25×10^{-5} kg of PRP-1.

The purpose of the analytical column, C2, was to separate the sample peak from any interfering peaks. A LiChrosorb C8 column (Spectra Physics, Santa Clara, CA) was used.

Pump P1 was a Milton Roy minipump Model 2396 (Laboratory Data Control, Riviera Beach, FL) while P2 was the pump from a Spectra Physics SP8000 chromatograph (Spectra Physics, Santa Clara, CA).

The injection valve and sample loop were described in Section 2.1.2. The exact volume of the sample loop, which had to be known for the calibration curve measurement, was previously measured by R.Hux [2.1] to have a volume of 23.88 ± 0.02 microliters.

Sample peaks were detected with a Kratos Spectroflow 757 UV-visible detector set at 254 nm. The eluted peaks were recorded using a Fisher Recordall chart recorder and were integrated with an HP Model 3390A integrator. All of these instruments were described in Section 2.1.2. Columns C1, C2 and valves V1, V2 were thermostated at $25.0 \pm 0.5^\circ \text{C}$ for all measurements using a forced air oven with copper cooling coils.

2.2.3 Chemicals

Naphthalene and calcium nitrate have been previously described in Section 2.1.3.

2.2.4 Solvents and Mobile Phases

The preparation of double distilled water, methanol and 90% methanol(aq) has been described in Section 2.1.4.

Acetonitrile was BDH Omnisolve (BDH Chemicals) suitable for spectrophotometry, chromatography and residue analysis. It was used without further purification.

15% acetonitrile in methanol was made by measuring 150 mL of acetonitrile into a volumetric flask and diluting to 1000 mL with methanol.

2.2.5 Sample solutions

The concentration range of naphthalene solutions used in the adsorption isotherm measurements was from 5×10^{-7} M to 1×10^{-4} M. They were prepared by serial dilution of a 9.87×10^{-4} M stock solution. The naphthalene standards used for the calibration curve were prepared by dilution of either the stock solution described above or a 9.85×10^{-3} M stock solution, and ranged from 2.57×10^{-5} M to 6.21×10^{-3} M.

Solutions of calcium nitrate ranging in concentration from 7.06×10^{-4} M to 1.008×10^{-2} M were used to measure the system void volume. The standard concentrations varied from 4.84×10^{-6} M to 1.61×10^{-4} M and were prepared by diluting a 5.00×10^{-4} M stock solution.

2.2.6 Procedure for the Measurement of the Precolumn Hold-up Volume

Calcium nitrate dissolved in 90% methanol_(aq) was used to measure the hold-up volume, V_m' , of the PRP-1 precolumn system. The same chromatographic system used for the adsorption isotherm (Figure 2.2) was used except the tubing which connected valve V1 to V2 was disconnected from V2. A volumetric flask was put here to collect the precolumn effluent upon elution of the calcium nitrate. In the loading step approximately 15 mL of a solution of 2.14×10^{-3} M calcium nitrate was pumped through the precolumn system to waste using pump P1 while V1 is in the "LOAD" position.

Next, V1 was switched from "LOAD" to "INJECT" so that approximately 25 mL of 90% methanol_(aq) from P2 was pumped through C1, the connecting tubing and the valve and collected in the volumetric flask. Any calcium nitrate present in the precolumn system was flushed into the volumetric flask during this step. This experiment was repeated two more times.

The nitrate absorbances of all three replicate solutions were read on a Cary 118 UV-visible spectrophotometer at a wavelength of 220 nm. The absorbances of these solutions were compared with a calibration curve made from standard solutions of calcium nitrate in order to determine the moles of calcium nitrate present in the hold-up volume.

2.3 Naphthalene Adsorption-Desorption Kinetics on PRP-1

2.3.1 Apparatus and Procedure

The purpose of this experiment is to measure the rate of naphthalene desorption from PRP-1 into 90% methanol_(aq). A schematic diagram of the equipment is shown in Figure 2.3. Helium is used to propel solutions through the tubing and the bed of PRP-1. Component C contains the PRP-1 adsorbent and will be referred to as the "shallow bed cartridge" or "s.b. cartridge". It is attached to an injection valve V (part no. 7010,

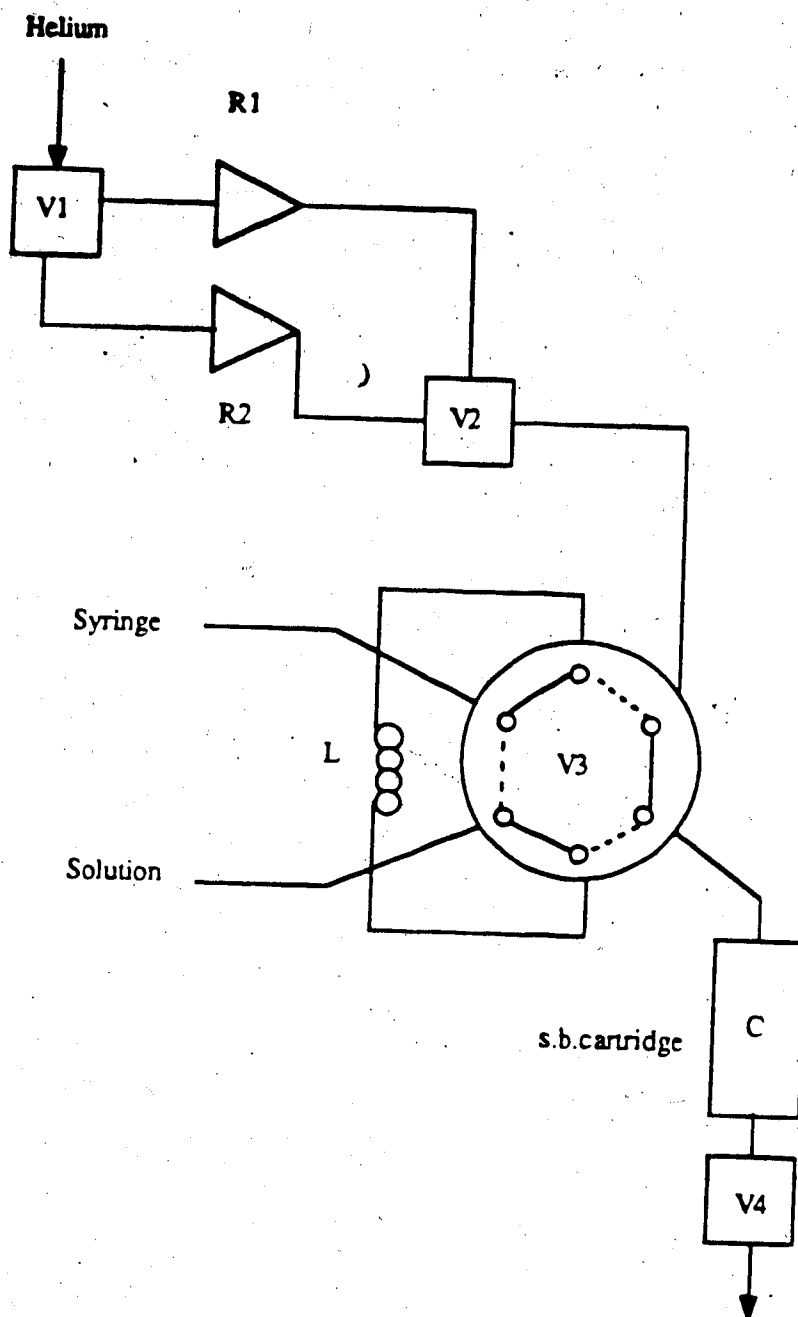


Figure 2.3 Schematic diagram of the equipment used in the adsorption-desorption rate measurements. V1, V2 and V4 = 2-way valves, V3 = injection valve, R1 and R2 = solution reservoirs, L = solution loop and C = shallow bed cartridge.

Rheodyne Inc., Cotati, CA). Two stainless steel cylinders R1 and R2 are pressurized with helium and act as reservoirs to hold solutions. Reservoir R2 contains glass wool and a small volume of 90% methanol(aq). The purpose of R2 is to saturate the helium with solvent before the helium passes through the s.b. cartridge in order to prevent drying of the PRP-1 by the gas. Valves V1 and V2 are teflon 3-way valves (part no. CAV3031, Laboratory Data Control, Riviera Beach, FL). These valves determine which reservoir the helium will flow through. Valve V4 is the same type of valve but is operating in a 2-way mode. Several pieces of stainless steel tubing of various volumes were used as loop L. The tubing dimensions are listed in Table 5.1.

The conditions and procedure for the desorption rate experiment is as follows. Reservoir R1 contains naphthalene dissolved in 90% methanol(aq) and injection valve V3 is in the "LOAD" position (solid lines in Figure 2.3). Valves V1 and V2 are switched so that the naphthalene solution is flushing the shallow bed cartridge, C, which contains the PRP-1. This is to ensure the PRP-1 adsorbent is thoroughly equilibrated by the sample. Valve V4 is open so the effluent from C flows to waste. V1 and V2 are then switched so that C is purged with solvent saturated helium. This step is intended to remove excess sample solution from the tubing, the frits and the interparticle spaces of C. After purging, V4 is closed so the pressure along the length of C is equalized. Loop L is filled with 90% methanol(aq) mobile phase solution and then V3 is switched to the "INJECT" position (dashed lines in Figure 2.3). V4 is opened and helium sweeps through L, propelling the slug of mobile phase solution through the bed of PRP-1 and then purging the excess liquid from the hold-up volume. The time in which the slug of mobile phase solution is in contact with the adsorbent is determined by the helium pressure and the volume of solution in L. The moles of naphthalene still adsorbed on the PRP-1 will be quantified but there is some naphthalene in the hold-up volume, V_m' . This quantity must be measured and subtracted from the total to give moles of sample actually adsorbed on the resin. The helium

purge minimizes the amount present in V_m' , but it does not remove it all. Details of the hold-up volume determination are given in Section 2.3.8.

After the slug of mobile phase solution has passed through the adsorbent, C is disconnected from V3 and V4. It is attached to an HPLC pump (Model M6000, Waters Associates, Milford, MA), which delivers a strong eluent (methanol) to elute all the naphthalene from C in a small volume. The eluted sample is collected in a 10 mL volumetric flask and diluted to volume with methanol. Reversed-phase liquid chromatography was chosen to quantify the naphthalene in this solution. Details of the chromatographic procedure and equipment were given in Sections 2.1.1 and 2.1.2. The pump used for the chromatography was from the Spectra Physics chromatograph and the integrator used was the VISTA 401.

The above procedure gives only one data point on a plot of moles of sample still adsorbed vs time and several more points must be measured to determine the desorption rate. To obtain these, the time was varied by keeping the flow rate constant and varying the volume of solution injected.

2.3.2 Shallow Bed Cartridge Design

In order to measure the amount of sample desorbed from the PRP-1 for fast contact times and under irreversible, first order conditions, it was necessary to have a very thin bed of the adsorbent material. The slug of mobile phase solution was pushed through this bed at fast flow rates which required moderately high pressures. Therefore, a suitable column for the PRP-1 had to be designed to meet these conditions and also, it was desirable to keep the hold-up volume minimized. A stainless steel in-line filter (part no. 7302, Rheodyne Inc., Cotati, CA) was modified for this purpose. This component is identified as "C" in Figure 2.3 and will be referred to as the "shallow bed cartridge" or "s.b.cartridge" for the remainder of the thesis. The shallow bed cartridge design is shown schematically in Figure

2.4. A thin bed of PRP-1 (approximately 0.5 mm high) was dry-packed in a teflon tube between two stainless steel frits. The weight of the resin used was 2.4×10^{-6} kg and the bed diameter was 3 mm. The frit at the s.b.cartridge inlet had a diameter of 0.125 inches and was 0.063 inches thick (part no. H2731, The Anspec Co. Inc., Ann Arbor, MI). The inlet frit pore diameter was 20 micrometers, while the frit at the s.b.cartridge outlet had a smaller pore diameter of 2 micrometers in order to retain the 10 micrometer PRP-1 particles. The larger pore diameter frit was used at the inlet in order to decrease the resistance to flow and decrease the pressure required. The outlet frit had a diameter of 0.125 inches and a thickness of 0.031 inches (part no. 4334-220, Whatman Chemical Separations Inc., Clifton, NJ). The frits were pressed partially closed in the center to help displace flow laterally. Also, at the s.b.cartridge inlet, two pieces of large mesh stainless steel screen were placed to help disperse the flow evenly across the bed of packing material. The teflon tube holding the packing and frits is placed inside the two filter end pieces and this entire assembly is put inside the Rheodyne filter cartridge cap and body.

2.3.3 Chemicals

Naphthalene and phloroglucinol were the two compounds used in this experiment and they were described previously in Section 2.1.3.

2.3.4 Solvents and Mobile Phases

Methanol, water and 90% methanol(aq) were described in Section 2.1.4. 65% methanol(aq) was the mobile phase used in the liquid chromatographic quantification of adsorbed naphthalene and was prepared by diluting 650 mL of methanol to 1000 mL with water.

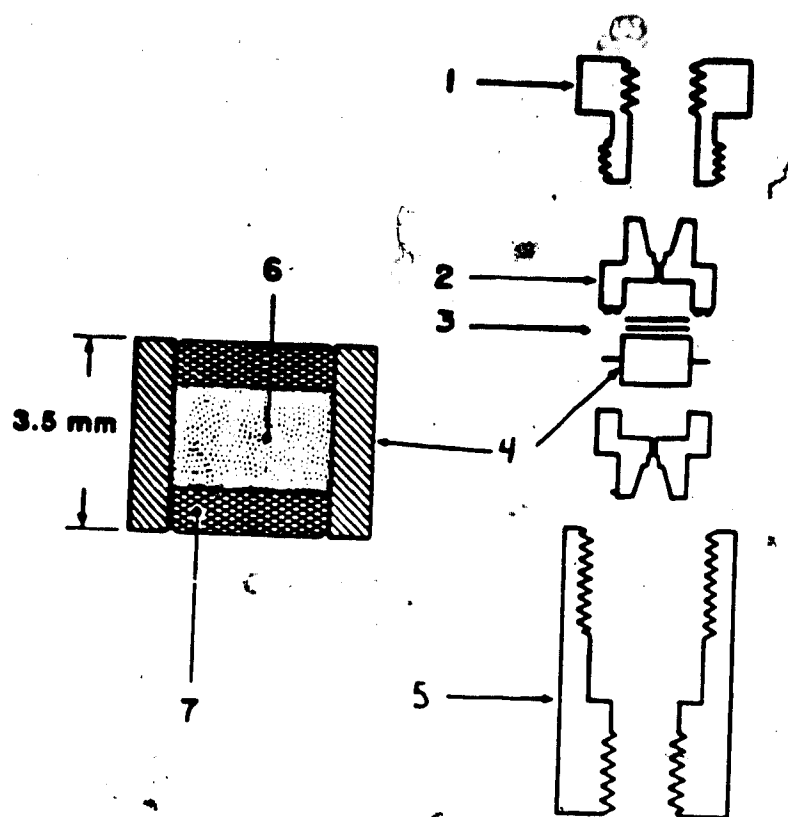


Figure 2.4 Shallow bed cartridge used to contain the PRP-1 stationary phase in the adsorption-desorption rate experiments.

1. Cap of in-line filter assembly (inlet)
2. Filter end piece
3. s.s. screens
4. Teflon tubing which contains the PRP-1
5. Body of the in-line filter assembly (outlet)
6. PRP-1 stationary phase
7. Frit (inlet frit = $20\ \mu\text{m}$ outlet frit = $2\ \mu\text{m}$)

2.3.5 Columns

Liquid chromatography was used to measure the amount of naphthalene adsorbed on the PRP-1 resin. The two bonded phase columns which were used were a LiChrosorb RP-8 and a Partisil-10 C8 column, both of which have been described in Section 2.1.2.

2.3.6 Injection Loop Calibration

The solution contact time (during which time sample was desorbed from the PRP-1) was varied by changing the volume of mobile phase solution injected through the shallow bed. Larger volumes gave longer contact times (see equation 5.3). The solution volumes were injected from calibrated pieces of stainless steel tubing (loop L in Figure 2.3). Stainless steel was found to work better than teflon tubing because the helium did not sweep solution from teflon very efficiently.

The volumes of the loops were measured in the following manner. The s.b. cartridge and valve V4 were removed from the shallow bed kinetic apparatus. The remaining kinetic apparatus was pressurized so helium from R1 could flow through the system. Next, V2 was closed to stop the flow of helium through the Rheodyne injection valve, V3. A volumetric flask was placed under the tubing which normally connected the s.b. cartridge to V3. Valve V3 was in the "LOAD" position and loop L was filled with a sample solution of known concentration. V3 was next switched to "INJECT" and V2 opened so the helium flow was sent to V3, through loop L and out to the volumetric flask. After 45 seconds V2 was shut and the flask removed. The contents of the flask were diluted to volume with methanol and the entire procedure repeated two more times.

The absorbances of all the solutions collected were read on a UV-visible spectrophotometer. Two types of spectrophotometers were used, a Cary 118 and a

Hewlett Packard 8451A diode array. The moles of sample in each flask were determined by comparing the absorbance of the unknown solution with that of a standard.

7 This procedure was also performed using methanol instead of helium to expel the sample from L. This was done in order to see how effective the helium was at displacing the solution from the loop.

2.3.7 Measurement of Quantity of Naphthalene Adsorbed at Equilibrium

The experimental procedure was performed as follows. A solution of naphthalene in 90% methanol(aq) was pumped through the s.b. cartridge of PRP-1. The solution concentration was 9.7×10^{-5} M. This solution concentration is past the linear region of the isotherm but this was necessary in order to have a sufficient amount of naphthalene to be accurately detected. Linearity was not a requirement for this experiment anyway, as long as the distribution coefficient for this concentration was known.

After 50 mL of naphthalene solution had flowed through the PRP-1, the s.b. cartridge was purged with helium for 45 seconds to remove most of the unadsorbed sample from the void volume. The remaining sample in the bed (adsorbed and a small amount in V_m') was eluted into a 10 mL volumetric flask using methanol. The contents of the flask were diluted to volume and the absorbance of this solution was read at 222 nm using a Cary 118 UV-visible spectrophotometer. The total moles of naphthalene eluted were calculated by comparing the absorbance of the unknown solution with a calibration curve made of standards.

2.3.8 Hold-up Volume Measurements

The procedure for measuring the hold-up volume, V_m' , will be described here. The shallow bed of PRP-1 was equilibrated with 20 mL of a solution of an unretained

sample compound. The unretained sample used was phloroglucinol dissolved in 90% methanol(aq). Valves V1 and V2 were in positions open to reservoir R2 (Figure 2.3) which contained the sample solution. Reservoir R1 contained a small amount of 90% methanol(aq) to saturate the helium with mobile phase before the gas encountered the PRP-1. Valve V4 was open.

V1 and V2 were now switched so that the PRP-1 was purged with helium for 45 seconds to remove excess phloroglucinol solution present in V_m . With V3 in the "LOAD" position, injection loop L was filled with a mobile phase solution of 90% methanol(aq). V4 was closed after filling L.

V3 was switched to "INJECT" and valve V4 re-opened so the mobile phase solution in L was propelled through the PRP-1 and out to waste and the system was then purged with helium. The contact time of the mobile phase solution was calculated using equation 5.3. After 45 seconds V4 was shut, V1 and V2 were switched so that neither helium nor sample solution from R2 and R1 would flow through the PRP-1, and the s.b.cartridge was removed from the kinetic apparatus. Any phloroglucinol remaining in the s.b.cartridge was eluted from into a 2 mL volumetric flask with methanol and the number of moles was measured. This procedure was repeated for all the injection loops in order to obtain a plot of hold-up volume versus contact time.

2.4 Velocity Profile Studies

2.4.1 Bed Extrusion Procedure

The purpose of the velocity profile experiment was to observe the radial distribution of sample axial velocities across the packed bed of stationary phase in a short chromatographic column. A dye was injected onto the column and allowed to elute approximately 3 / 4 down the column. At this point, the flow of 90% methanol(aq) mobile phase was stopped and replaced with 10% glycerin(aq). About 5 mL of glycerin solution

was delivered through the column to help the particles adhere. The column was removed from the chromatographic system and the inlet endfitting removed. The first 2 mm of packing were carefully scraped out and a teflon plug was inserted. The column was then placed in a Dewar flask filled with dry ice pellets for 15 minutes for additional cohesiveness of the stationary phase. After this, the outlet frit and endfitting were removed and the bed of packing material was extruded from the column tubing by pushing on the teflon plug with an aluminum rod. After extrusion, the packed bed was sliced longitudinally with a razor blade so that the pattern of the dye across the bed could be observed. This pattern corresponded with the sample velocity profile across the column.

This was repeated using different types of outlet endfittings. The various fittings were used both during the column packing step and during the chromatographic characterization of the columns. The procedures for packing and characterizing the columns are described below in Section 2.4.2. The endfittings provided either constricted or uniform outlet flow. These experiments were done on both PRP-1 and C18 stationary phases.

2.4.2 Apparatus, Column Packing and Chromatographic Characterization Procedures

The equipment used to pack the columns is shown in Figure 2.5. A Waters M6000 pump (Waters Associates, Milford, MA) was used to deliver slurry solvent into a stainless steel stirred slurry packing chamber. The cylinder holds about 150 mL of solution. A short (5 cm long) piece of s.s.tubing is attached to the top of the packing cylinder and the column to be packed is attached to the tubing with a connecting union. The piece of tubing and the column have the same i.d. (4.1 mm). Both the tubing and the column were made of 0.25 inch o.d. precision bore stainless steel tubing (part no. A-3014, Mandel Scientific Co. Ltd., Rockwood, Ontario). Columns varied in length from 4.5 cm to 5 cm. Stainless steel frits of 2 micrometer pore diameter and 0.25 inch diameter (part no. A-716525 ,

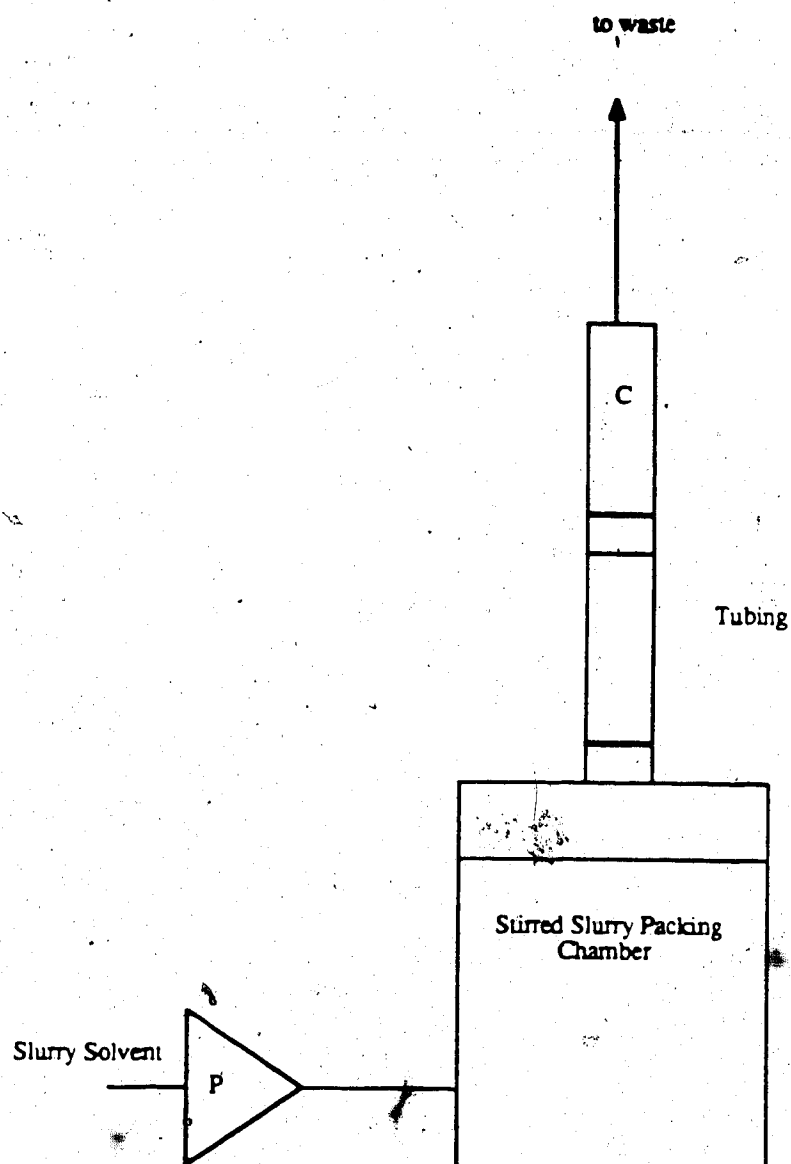


Figure 2.5 Schematic diagram of the apparatus used to pack the short columns (C) used in the velocity profile experiments. P = pump used for the slurry solvent.

Mandel Scientific Co. Ltd., Rockwood, Ontario) were placed at the ends of the column after packing. The column was sealed using compression type endfittings (part no. 400611, Mandel Scientific Co. Ltd., Rockwood, Ontario). During the packing of the column, the packing slurry was constantly agitated using a magnetic stirring bar in order to keep the stationary phase particles suspended.

When packing a column the stirred slurry packing chamber was connected at its base to a pump. A slurry of stationary phase and solvent was deaerated by bubbling with helium and then was poured into the chamber. The methods of Linder and Keller [2.3, 2.4] were used to pack all columns and a modification of the slurry solvent suggested by Lee [2.2] was used for the PRP-1 columns. After the stationary phase slurry was added, the chamber was sealed and the column and the short piece of s.s. tubing were attached. A frit and an endfitting were put on the column outlet and then the slurry solvent was delivered by the pump at a flow rate of 6 mL per minute which required a maximum pressure of 4500 psig. To ensure that both the tubing and column were filled, 70 mL of slurry solvent was used. After packing was completed, the pump was shut off and the system was allowed to depressurize for 15 minutes. The s.s. tubing (with the column still attached to it) was removed from the cylinder. The tubing was disconnected from the column and a frit and endfitting were placed at the open end of the column. Before the column was used it was flushed with 20 mL of water followed by 60 mL of methanol to remove any slurry solvent.

After packing, the plate height and void volume of each column was measured using the chromatographic system shown in Figure 2.1. A pump from a Spectra Physics SP8000 chromatograph was used to deliver mobile phase and peaks were integrated using a VISTA 401 integrator. These two pieces of equipment and the other instruments in the system have been described in Section 2.1.2.

After these column parameters were measured a dye was injected so the flow profile could be observed after extrusion of the bed of stationary phase from the column. The

packing material was extruded from the tubing using a teflon plug (4.1 mm diameter, 3 mm length) and an aluminum rod (3 mm diameter, 5 cm length), both of which were made by the chemistry department machine shop.

Two other types of outlet endfittings were used on the columns in addition to the standard compression fitting. All of these endfittings are shown in Figure 2.6. One of these used the commercial endfitting described above, but a thin stainless steel washer was placed between the frit and the endfitting. The washer dimensions were 0.25 inch o.d., 4.1 mm i.d. and a thickness of 0.5 mm. The third type of endfitting was a modification of the compression fitting. The 0.0625 inch end of the fitting was drilled out to a diameter of 4.1 mm and then a perforated plate was silver soldered across the opening. The perforated plate had nineteen 0.5 mm diameter holes evenly distributed across a 4.1 mm diameter, which aligned with the drilled-out hole. The purpose of both the washer and the perforated plate endfittings was to provide a uniformly distributed outlet flow from the column.

2.4.3 Chemicals

Methyl p-hydroxybenzoate and calcium nitrate were used to characterize the home-packed columns. Details on these compounds were given in Section 2.1.3.

The dyes 4-phenylazo-1-naphthylamine, 1-aminoanthraquinone and 4-phenylazoaniline were supplied by Eastman Organic Chemicals (Rochester, NY). The 1-aminoanthraquinone was practical grade. Amaranth (FDC Red #2) was supplied by Endo Laboratories (Garden City, N.Y.). All four dyes were used without further purification.

Sodium chloride was reagent grade from A & C American Chemicals (Ville St. Laurent, Quebec) and was used as received.

Glycerin (glycerol) was analytical reagent grade from BDH Chemicals and was used as received.

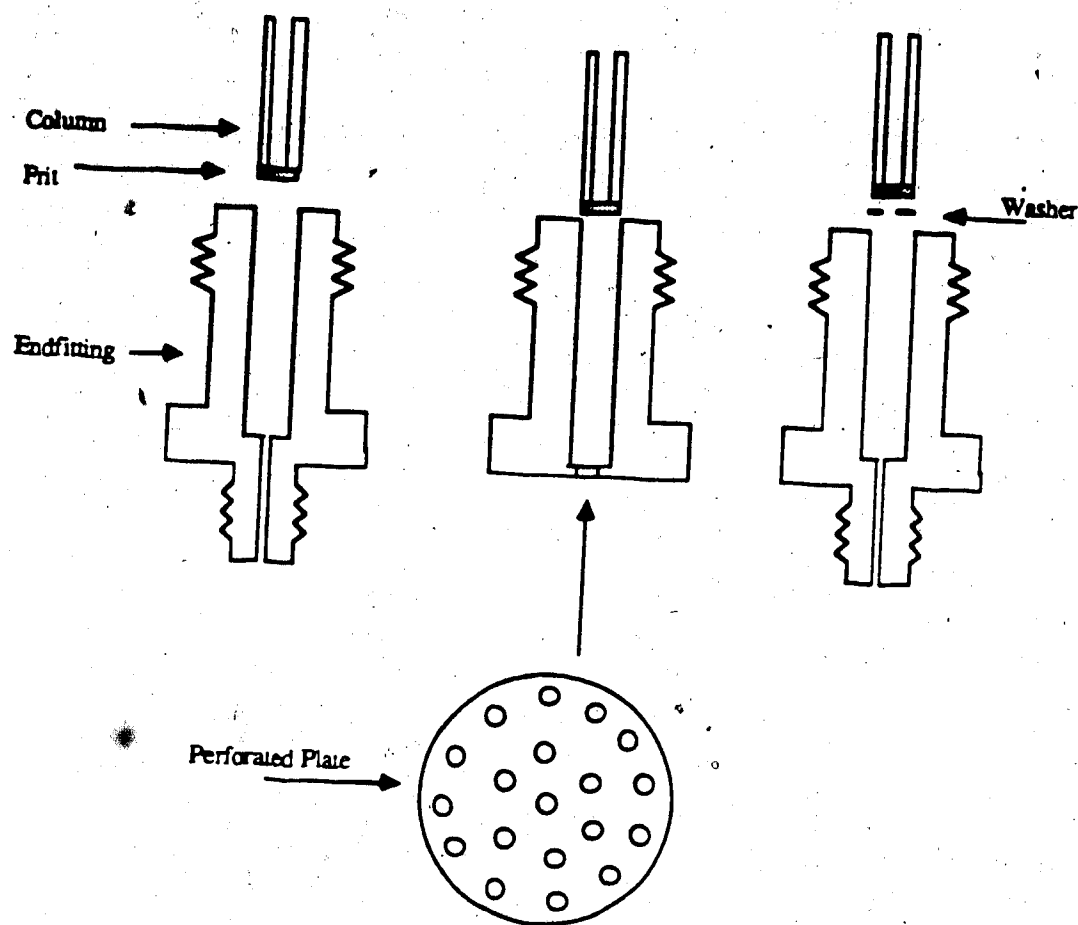


Figure 2.6 Column outlet endfittings used in the velocity profile experiments.
 (A) conventional Swagelok compression endfitting for constricted flow.
 (B) Perforated plate endfitting for uniform flow. The face of the plate is shown below. (C) Washer endfitting for uniform flow.

2.4.4 Solvents and Mobile Phases

The preparation of double distilled water, methanol and 90% methanol(aq) has been described in Section 2.1.4.

Two types of slurry solvents were used to pack the columns. A solution of 2.5% sodium chloride in 10% (v/v) glycerin(aq) was used for the PRP-1 columns. To prepare the slurry solvent, 12.5 grams of sodium chloride were dissolved in 50 mL of glycerin and diluted to 500 mL with water. The slurry solvent for C18 columns was a 1:1:1 mixture of ethanol, n-propanol and toluene. To prepare this, 170 mL of each solvent was used.

A 10% glycerin(aq) solution was made by diluting 50 mL of glycerin to 500 mL with water.

Toluene was reagent grade and was used without further purification. It was obtained from Aldrich Chemical Co. Inc. (Milwaukee, WI). 1-Propanol (certified, Fisher Scientific Co., Fairlawn, NJ) was used as received. The 98% ethanol contained 2% benzene.

2.4.5 Stationary Phases

Short columns were home-packed using two types of bulk stationary phase. PRP-1 was donated by Hamilton Co. (Reno, NV). The characteristics of this polystyrene-divinylbenzene copolymer are given in Table 2.1. The second packing material was Partisil-10 ODS-3- (part no. 4128-010, Whatman Inc., Clifton, NJ) which consisted of 10 micrometer diameter, irregular-shaped particles. An eighteen carbon chain is chemically bonded to a silica matrix (10% carbon loading) and is endcapped to provide 95% coverage of the surface silanol groups [2.5].

Table 2.1 Characteristics of PRP-1 2.2

Column bed density	0.42 g per cm ³
packing material	polystyrene-divinylbenzene
particle size	95 % within the range 8 - 12 μ m
particle shape	spherical
specific surface area	415 m ² per g
pore volume of packing	0.79 cm ³ per g
ave. pore diameter	75 angstroms
solvent restrictions	pH 1 - 13 , 0.5 N salt

CHAPTER 3

Characterization of Bandbroadening by Chromatography

3.1 Theory

3.1.1 Equilibrium Aspects of Chromatography

Chromatography is a technique used to separate mixtures so that the individual components in the mixture can be identified and quantified. The basic concepts of chromatography have been discussed by many authors [3.1-3.5]. In high performance liquid chromatography (HPLC) there are two phases, a solid matrix referred to as the stationary phase and a moving liquid called the mobile phase. The stationary phase is tightly packed into a column and the mobile phase flows continuously through the stationary phase. A sample mixture is applied to the top of the column and the components separate into bands based on differing interactions with both phases. Consider one compound in the sample mixture. The sample component (i) distributes itself between the mobile phase (m) and the stationary phase (s).



Several terms which are commonly used in chromatography will be defined and explained. The distribution coefficient is the concentration ratio of sample in the stationary phase to sample in the mobile phase and any units can be used for the concentration terms.

$$K_i = \frac{C_s}{C_m}$$

3.1

A unitless parameter which is related to K_i is the capacity factor k'_i . This is the ratio of moles of sample in the stationary phase (n_s) to moles in the mobile phase (n_m).

$$k'_i = \frac{n_s}{n_m}$$

3.2

In this thesis C_s is expressed in moles per kg of stationary phase while C_m is given in moles per liter of mobile phase. The capacity factor is related to the distribution coefficient by the phase ratio (ϕ) which is :

$$k_i' = K_i \phi \quad 3.3$$

where :

$$\phi = \frac{W_s}{V_m} \quad 3.4$$

W_s is the weight of stationary phase in the bed. V_m is the volume of mobile phase contained between the stationary phase particles and within the particle pores and is referred to as the void volume. This is the volume of mobile phase required to elute a sample which is not sorbed on the stationary phase (an unretained sample) but which enters the inter- and intraparticle spaces.

At the column outlet the separated sample compounds elute as peaks. Normally, the peaks are Gaussian shaped with each peak eluting at a characteristic time, the retention time (t_r). The time at which an unretained sample elutes (t_m) can be used to calculate the average linear velocity of the mobile phase (u_o).

$$u_o = \frac{L}{t_m} \quad 3.5$$

L is the length of the column. The average velocity at which a sample moves (u_i) is calculated using equation 3.6.

$$u_i = \frac{L}{t_r} \quad 3.6$$

The sample velocity is related to the capacity factor because the sample is moving only when it is in the mobile phase. Therefore, the sample velocity is dependent on the fraction of sample in the mobile phase ($f_{i,m}$).

$$f_{i,m} = \frac{n_m}{n_m + n_s} \quad 3.7$$

Since k_i' is equal to n_s divided by n_m the sample fraction in the mobile phase is also represented by equation 3.8.

$$f_{i,m} = \frac{1}{1 + k_i} \quad 3.8$$

The sample velocity is equal to the fraction of sample in the mobile phase multiplied by the mobile phase linear velocity.

$$u_i = f_{i,m} u_o = \frac{1}{1 + k_i} u_o \quad 3.9$$

Retention can also be expressed in volume units (V_R , the retention volume) which is related to t_r by the mobile phase flow rate, F .

$$V_R = t_r F \quad 3.10$$

The retention volume can be related to the capacity factor by equation 3.11.

$$k_i = \frac{V_R - V_m}{V_m} \quad 3.11$$

The resolution, R_s , between adjacent peaks is a measure of the ability of the chromatographic process to separate mixtures. The resolution is defined as the distance between the peak centers divided by the average peak width [3.6].

$$R_s = \frac{t_{r,2} - t_{r,1}}{0.5(w_1 + w_2)} \quad 3.12$$

R_s is unitless so the peak widths are measured in the same time units as the retention times. Figure 3.1 shows how the widths are measured on two peaks. The separation between the peaks increases as R_s increases. If the difference between the peak centers is increased, the separation between the two peaks will increase but it is not desirable to have retention times longer than necessary. From equation 3.12 it can be seen that the resolution can also be increased by decreasing the peak width. A smaller peak width also results in an increase in

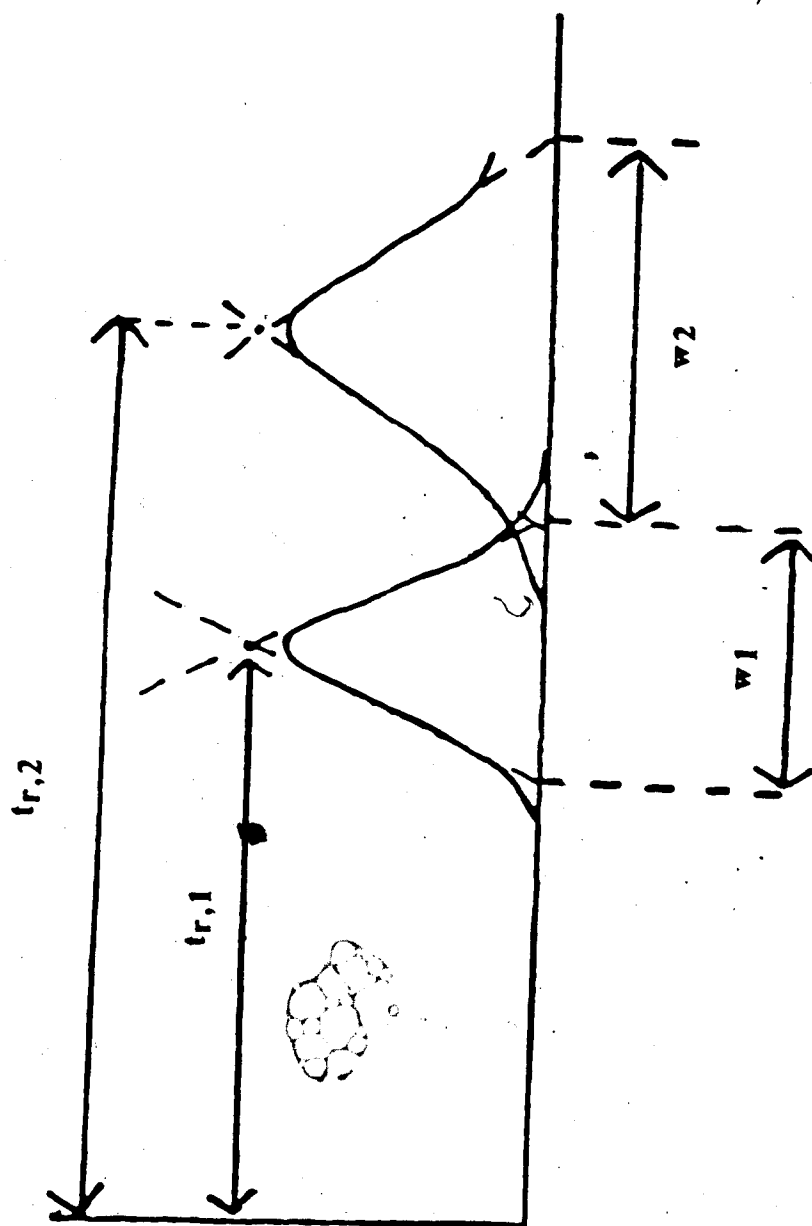


Figure 3.1 Measurement of peak width to calculate the resolution (R_s) between two adjacent peaks. To measure the peak width at the baseline, lines are drawn tangent to the sides of the peaks. The distance between the points at which the tangents cross the baseline is the peak width (w). This figure was taken from Figure 2.9 in reference 3.3.

the peak height which means peaks of lower concentrations can be detected. Therefore, it is of interest to know what processes contribute to peak broadening (bandbroadening) and how these processes can be minimized to decrease the peak width.



3.1.2 Bandbroadening

Ideally, if a multi-component sample were loaded onto the top of a chromatography column as an infinitely narrow band, the sample components having different values of k_i' would separate into infinitely thin bands on the column and elute as spikes. However, because several stochastic processes occur which broaden the band, Gaussian-shaped peaks result if the sample bands travel for a sufficiently long time. An ideal and a real chromatogram are shown in Figure 3.2. This bandbroadening or band dispersion degrades the separating ability of the column and therefore it is desirable to minimize this effect. The amount of band dispersion which occurs is described by the column plate height (H) which is related to the width of a sample peak and is defined in Equation 3.13.

$$H = \frac{\sigma_x^2}{X} \quad 3.13$$

σ_x^2 is the variance in distance units and is larger for wider peaks. X is the distance the sample has traveled down the column. For a peak which has eluted from the column X is equal to the column length L .

$$H = \frac{\sigma_x^2}{L} \quad 3.14$$

The plate height can be calculated in terms of V_r and t_r also :

$$H = \frac{\sigma_v^2}{V_r} * L \quad 3.15$$

$$H = \frac{\sigma_t^2}{t_r} * L \quad 3.16$$

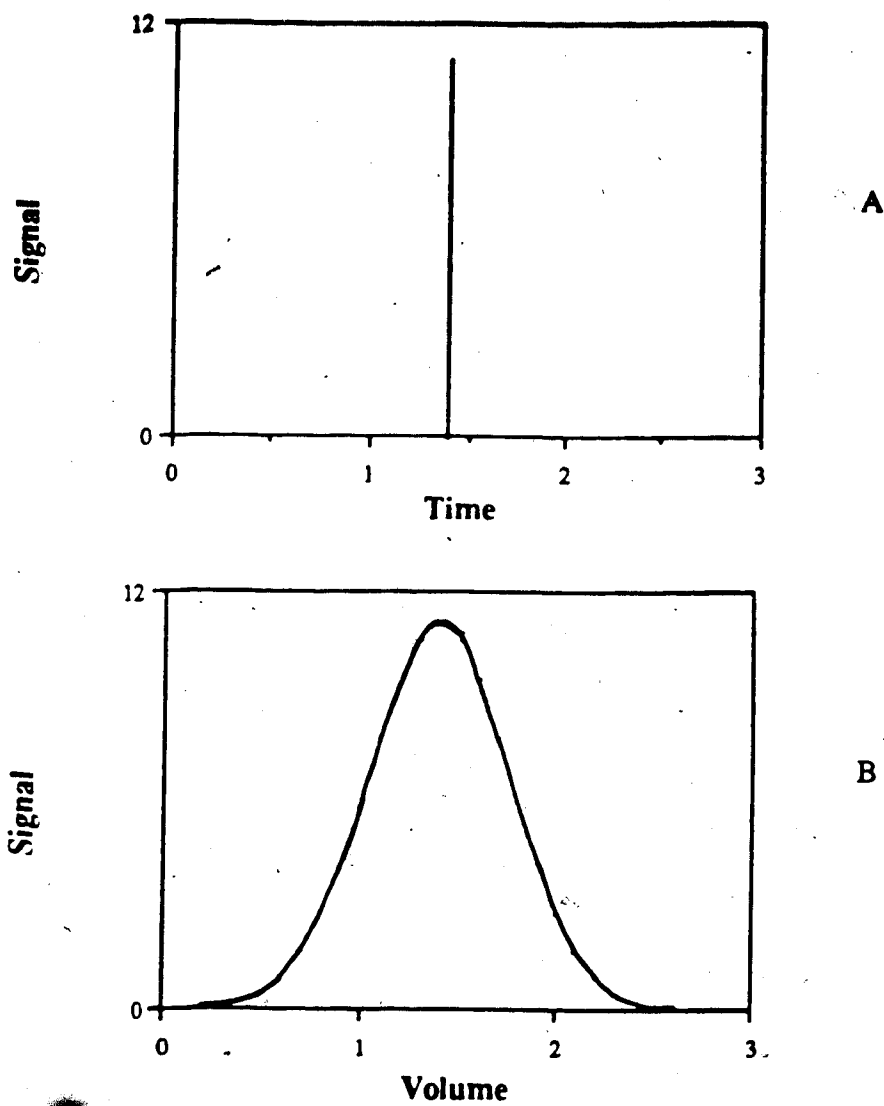


Figure 3.2 (A) An ideal chromatogram with no bandbroadening and (B) a real chromatogram (non-ideal) with a Gaussian shape due to bandbroadening processes.

In equations 3.15 and 3.16 the units for the variance are either volume squared or time squared, respectively. V_T and t_T are the peak center of gravity (in volume or time units).

The center of gravity and variance can be found by using a digital treatment of the data (this method will be discussed later in Section 3.1.11). Equations 3.14 through 3.16 are true for any peak shape.

There are several processes in the column which cause bandbroadening. These are axial diffusion, slow mass transfer within and between different phases and structural inhomogeneities in the packed bed of stationary phase which cause a non-uniform velocity profile. The mass transfer contribution includes the rate of adsorption-desorption onto the stationary phase, diffusion through the intraparticle pores and mass transfer through the mobile phase. The bandbroadening due to each of these phenomena can be described by individual plate height equations. Because plate height is directly proportional to the variance and the variances of independent processes are additive, plate heights are also additive. The plate height from each process can be measured or calculated and compared with the total observed column plate height to determine the significance of each. Bandbroadening processes have been discussed in detail by several authors [3.5, 3.7 - 3.13].

3.1.3 Longitudinal Diffusion

Longitudinal (or axial) diffusion is caused by the random movement of molecules from a high concentration region to areas of lower concentration. Solute will diffuse both forward and backward from the center of the band. This phenomena has been well characterized and can be described by a modified version of Einstein's diffusion equation [3.14].

$$\sigma_x^2 = 2 \gamma D_m t_d$$

γ is an obstruction factor which is less than 1 and is added to Einstein's original equation because the diffusion pathways are shorter in a packed bed since the particles obstruct the molecules. D_m is the solute diffusion coefficient in the mobile phase solvent and has units of cm^2 per second. The t_d in equation 3.17 is the time which the sample has available to diffuse. For axial diffusion in the mobile phase the time in which diffusion occurs is equal to the time spent in the mobile phase (t_m). This is equal to the distance traveled (the length of the column) divided by the speed (the average linear velocity of the mobile phase).

$$t_d = t_m = \frac{L}{u_o}$$

3.18

Substituting equation 3.18 into 3.17 gives :

$$\sigma_x^2 = \frac{2 \gamma D_m L}{u_o}$$

3.19

D_m is approximately 10^{-5} cm^2 per second for many organic compounds [3.15] and γ is about 0.5 to 0.7 for a uniformly packed bed [3.14,3.15,3.16]. Since plate height is proportional to variance equation 3.14 can be expressed in terms of H_{ld} :

$$H_{ld} = \frac{\sigma_x^2}{L}$$

$$H_{ld} = \frac{2 \gamma D_m}{u_o}$$

3.20

It can be seen that this term is inversely proportional to mobile phase velocity (or flow rate) and is more important at low linear velocities. For the flow rates commonly used in liquid chromatography H_{ld} is negligible.

Longitudinal diffusion can also occur in the stationary phase. However, because the diffusional pathways are generally more obstructed than those of the mobile phase, the contribution to bandbroadening is usually insignificant [3.17].

3.1.4 Adsorption - Desorption Kinetics

When a molecule is adsorbed onto the stationary phase it is temporarily immobilized. Meanwhile, the molecules which are still in the mobile phase will continue to move down the column, causing the sample zone to spread. The amount that the zone spreads or broadens is proportional to the time the molecule spends on the stationary phase before desorption occurs.

Another way to think of this phenomenon is to realize that equilibrium is not achieved between the stationary and mobile phases because of the finite time required for adsorption (and desorption) as the sample zone continuously moves down the column. The solute band is distributed in a Gaussian manner in the mobile phase. As the leading edge of the band encounters fresh stationary phase, it will start adsorbing, trying to reach equilibrium. However, this requires a certain amount of time and during this time the sample band has moved farther down the column. A higher concentration region of the zone is now contacting this region of stationary phase and more sample must adsorb to reach equilibrium. This process continues until the concentration maximum of the band passes, at which point the process reverses with sample desorbing into the mobile phase. Therefore, compared to the concentration required to be at equilibrium as specified by K_1 , there is a concentration deficiency in the stationary phase for the leading half of the sample zone and a concentration excess for the last half, while the opposite is true for the mobile phase. The effect that this process has on peak shape [3.7] is shown in Figure 2.3. The faster the rates of adsorption and desorption are, the smaller this effect is and less bandbroadening occurs. The amount of zone dispersion also depends on how fast the

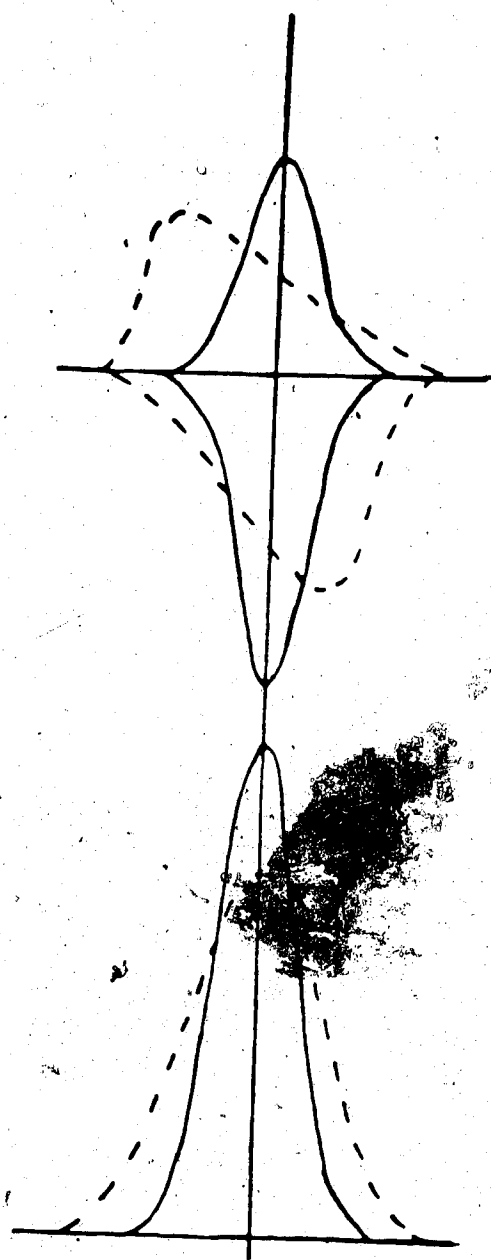


Figure 3.3 (A) Sample zone broadening resulting from non-equilibrium between the mobile and stationary phases. The solid line gives the zone profile if equilibrium is achieved and the dashed line is the profile due to non-equilibrium. (B) Elution peak profiles corresponding to attainment of equilibrium (—) and non-equilibrium (---). This figure is taken from reference 3.7.

sample is moving down the column (u_o) and the amount of sample in both phases (k_i').

The plate height contribution from the rate of adsorption-desorption [3.18] is given in equation 3.21.

$$H_s = 2 \left(\frac{k_i'}{1 + k_i'} \right) \frac{u_o}{k_d} \quad 3.21$$

The term k_d is the apparent 1st order desorption rate constant.

3.1.5 Mass Transfer through the Stagnant Mobile Phase

The mobile phase velocity within the pores of the stationary phase is assumed to be zero because of the large resistance to flow in the narrow, tortuous channels. Sample components can move through the pores only by diffusion and the rate of diffusion is dependent on the diffusion coefficient of the component in the mobile phase and on the geometry of the intraparticle channels. Tortuous, winding channels shorten the mean free path length of the molecule (the distance it can diffuse before encountering an obstruction such as a wall), while lengthening the overall distance the molecule must diffuse through the particle. Constricted channels decrease the area available for diffusion and will slow the rate of transport. The bandbroadening due to the finite rate of mass transfer through the pores is due to non-equilibrium between the moving and stagnant mobile phase and has the same effect on peak shape as the non-equilibrium described in Section 3.1.4.

Bandbroadening in the porous stagnant mobile phase is dependent on the rate of diffusion within the pores and the average mobile phase linear velocity. The slower the velocity of the mobile phase, the more time a molecule has to diffuse through the pores without the band center moving an appreciable distance down the column. The equation for this plate contribution was derived by Hawkes [3.19] and is given below.

$$H_{sm} = \frac{fct(f, k_i') d_p^2 u_o}{\gamma' D_m} \quad 3.22$$

$$fct(f, k_i') = \frac{(1 - f + k_i')^2}{[30(1 - f)(1 + k_i')^2]} \quad 3.23$$

$$f = \frac{\epsilon_{intra}}{\epsilon_t} \quad 3.24$$

γ' is another obstruction factor which accounts for the constricted, winding channels inside the particles and has a value less than 1. The particle diameter (d_p) appears because it is related to the distance the sample must diffuse through the pores. D_m , u_o and k_i' have all previously been defined. The capacity factor is important because much of the surface area of the adsorbent is within the pores, so solutes with larger k_i' values spend more time inside the particles. The parameter f is the ratio of intraparticle porosity (ϵ_{intra} , the pore volume divided by the total column geometric volume) to total porosity (ϵ_t , intra- and interparticle volume divided by the total column geometric volume). The amount of sample within the stagnant mobile phase will be dependent on the ratio of pore volume to total volume of mobile phase.

3.1.6 Mass Transfer through the Mobile Phase

In the packed bed of a column there are regions of different mobile phase velocities. Solute molecules which are in a faster velocity region move ahead of molecules in slower regions and this process disperses the sample band. These differing velocities occur because particles do not pack in a symmetrical manner but tend to group together, leaving small channels within the groups and larger channels between individual groups. This

leads to slower velocities in the narrow channels and faster velocities in the wider ones. There are also velocity inequalities across a single channel and across the entire column which produce bandbroadening. However, molecules do not stay in one path for the length of the column but exchange between faster and slower regions which narrows the range of average velocities experienced by different molecules in their passage along the column. This limits the extent of bandbroadening by "relaxing" the non-uniformities of the sample molecule velocities at different points in the column. The two exchange processes that relax the non-uniform velocity profile are lateral convection and lateral diffusion. Diffusion will be discussed in this section and convection will be discussed in Section 3(1.7).

If the relaxation process occurred infinitely fast, then all molecules would experience identical average velocities when in the mobile phase and there would be no bandbroadening from this phenomenon. However, relaxation occurs at a finite rate and the mobile phase plate height term is due to the finite rate of lateral diffusion. Because diffusion does not occur instantaneously, sample molecules will travel a distance down the column before they can diffuse into a neighboring stream.

The distances across which a molecule must diffuse to reach various velocity regions has been classified into the following five categories by Giddings [3.20]. The short range interchannel effect involves velocity variations in channels separated by a few particles while the long range interchannel effect involves velocity variations across a greater number of particles. On a grand scale these kinds of packing non-uniformities create a transcolumn effect. One special transcolumn effect, the wall effect is associated with the fact that the particles at the column tubing walls pack differently than do the particles in the center of the column. Usually, the packing is looser at the walls leading to faster velocities in this region. The difference between the mobile phase velocity in channels on opposite sides of a particle is the transparticle contribution. In channels between individual stationary phase particles, flow is laminar with the velocity slowest at

the particle surfaces and fastest in the center of the channel. This difference is the transchannel effect. The mobile phase plate height contribution from these phenomena is given in equation 3.25.

$$H_m = \frac{\omega d_p^2 u_o}{D_m} \quad 3.25$$

ω is a packing factor which takes into account the long and short range non-uniform velocity effects. ω is small for uniformly packed beds and it usually has a value of about 5. It increases for irregularly shaped particles and decreasing particle size, both of which lead to less uniform packing.

There is another contribution to bandbroadening from the mobile phase but it is negligible compared to the velocity inequality effect. This is associated with the inability to attain equilibrium with the stationary phase, which is a non-equilibrium effect analogous to the effects described in Sections 3.1.4 and 3.1.5.

3.1.7 Eddy Diffusion and the Coupled Plate Height Term

The second method of relaxing the nonuniform velocity profile is lateral convection. The lateral flow of mobile phase as it moves around particles and clusters of particles physically sweeps sample into the different channels. This method is generally more efficient than diffusion, except at low flow rates. Since eddy diffusion results from the packing geometry only, it is independent of mobile phase velocity. The contribution to plate height is caused by the finite time to transfer between channels [3.21] and is given in equation 3.26.

$$H_e = 2 \lambda d_p \quad 3.26$$

λ is a packing factor with typical values of less than 10. It decreases for particles with larger diameters because they are easier to pack uniformly and for columns with smaller radii because there is a smaller radial distance across which exchange must occur. In Section 3.1.2 it was said that plate heights of different processes were additive. However, the bandbroadening in the eddy diffusion and mobile phase terms have the same origin (a non-uniform velocity profile) and so the two processes are not independent and the plate heights cannot be simply added. Giddings [3.22] has combined the H_m and H_e contributions as shown in equation 3.27 and refers to this as the coupled plate height term.

$$H_{\text{couple}} = \left[\frac{1}{H_e} + \frac{1}{H_m} \right]^{-1} \quad 3.27$$

This simple equation gives results which correlate fairly well with experimental data but it is not a rigorous solution accounting for the interaction between the two processes. Of course, if one term, H_e or H_m , in the coupled equation is large compared to the other, the value of H_{couple} will approach the value predicted by the individual plate height equation of the smaller term.

3.1.8 Summary of Column Bandbroadening

The overall bandbroadening term is the sum of the plate height contributions of the processes which were just described and it is given in equation 3.28.

$$H_{\text{column}} = H_{ld} + H_s + H_{sm} + H_{\text{couple}} \quad 3.28$$

Since each term is dependent on parameters such as k' and u_0 in a different manner, the major contributor to bandbroadening in PRP-1 can be determined by varying one of the parameters and measuring the plate height. This was the approach taken to study

bandbroadening on PRP-1 using chromatographic characterization. Chromatograms were run in which the capacity factor and mobile phase linear velocity were varied and the effect on plate height was measured.

In addition to sample dispersion in the column, there are also bandbroadening effects from the extracolumn components such as the connecting tubing, the injector or the detector. This extracolumn contribution to plate height must be measured and subtracted from the overall plate height if one wishes to characterize only column bandbroadening effects.

3.1.9 Extracolumn Bandbroadening

Each component of the chromatographic system is responsible for additional spreading of the sample peak. This includes the injection valve, tubing, tubing connections, the detector flow cell and the finite electronic response times of the detector and recorder. These plate height contributions have been reviewed by Sternberg [3.23].

Ideally, sample would be injected onto the column as a spike or an impulse of zero width. Of course, this is impossible so the goal is to inject the sample solution as a very narrow square wave. With some injectors solute is flushed out of the injection valve exponentially, with the volume of sample solution within the injector decreasing rapidly at first and then more gradually. This not only broadens the injected zone of sample but gives it an asymmetric tailing profile. Sudden increases in tubing diameter can also exponentially distort the peak while straight lengths of tube disperse the zone because of the parabolic flow profile that occurs in the tube. Any dead spaces or voids in the chromatographic system can cause an exponential distortion of the signal.

Generally, it is desirable to keep extracolumn bandbroadening minimized (less than 10% of the total plate height). In this thesis the extracolumn plate height was measured

and subtracted from the total, to ensure extracolumn dispersion was not contributing significantly to the broad, distorted peaks eluted from PRP-1.

3.1.10 Total Plate Height

The overall plate heights experimentally measured on various columns represented a combination of column and extracolumn bandbroadening effects.

$$H_{\text{total}} = H_{\text{column}} + H_{\text{extracolumn}} \quad 3.29$$

$$H_{\text{total}} = H_{\text{ld}} + H_{\text{s}} + H_{\text{sm}} + H_{\text{couple}} + H_{\text{extracolumn}} \quad 3.30$$

The plate height from longitudinal diffusion was calculated and subtracted from the total as was the extracolumn contribution. H_{ld} was insignificant except at the lowest flow rates used. After subtracting these two terms the dispersion contributions responsible for bandbroadening on PRP-1 are given in equation 3.31.

$$H = H_{\text{s}} + H_{\text{sm}} + H_{\text{couple}} \quad 3.31$$

3.1.11 Measurement of Chromatographic Parameters

Various parameters can be obtained from chromatographic peaks which are related to the efficiency of the column. The most important is plate height which has been defined in Section 3.1.10 and is calculated by measuring the peak center of gravity and variance and substituting these values into equation 3.15. Both the center of gravity (which is the retention volume or retention time) and the variance were obtained by measuring the zeroeth, first and second statistical moments of the sample peak [3.24 - 3.27] using equations 3.32 through 3.34. The peak area (A) is the zeroeth moment, the retention volume (V_{r}) is the first moment and the variance (σ_{v}^2) is the second moment.

$$A = \sum (C_i \Delta V) \quad 3.32$$

$$V_r = \frac{1}{A} \left[\sum (V_i C_i \Delta V) \right] \quad 3.33$$

$$\sigma_v^2 = \left\{ \frac{1}{A} \left[\sum (V_i^2 C_i \Delta V) \right] \right\} - V_r^2 \quad 3.34$$

A typical peak is shown in Figure 3.4a with each of the variables indicated. The peak is divided into equal increments of ΔV . The term V_i is a volume on the x axis while C_i is the concentration which corresponds to V_i .

Another parameter used to describe peak shape is the asymmetry factor, A_s , [3.28] which indicates whether a peak is symmetrical, tailing or fronting. To obtain this parameter, a vertical line is drawn from the peak maximum to the baseline as shown in Figure 3.4b. A horizontal line is then drawn at 0.10 the height of the vertical line. The lengths of the two horizontal segments, a and b, are measured and substituted into equation 3.35.

$$A_s = \frac{b}{a} \quad 3.35$$

Here, b corresponds to the back portion of the peak and a to the front. If A_s is greater than 1 the back portion of the peak is longer and the peak is said to be tailing. If A_s is less than 1 the front portion is longer and the peak is fronting. An A_s equal to 1 indicates a symmetrical peak. Asymmetrical peaks can have several causes [3.29,3.30]. Some phenomena which produce tailing peaks are listed below.

- 1) slow adsorption - desorption kinetics
- 2) excessive extracolumn bandbroadening
- 3) a column with an insufficient plate number (less than 50) so that the stochastic processes have not yet operated sufficiently often to generate a symmetrical Gaussian shape

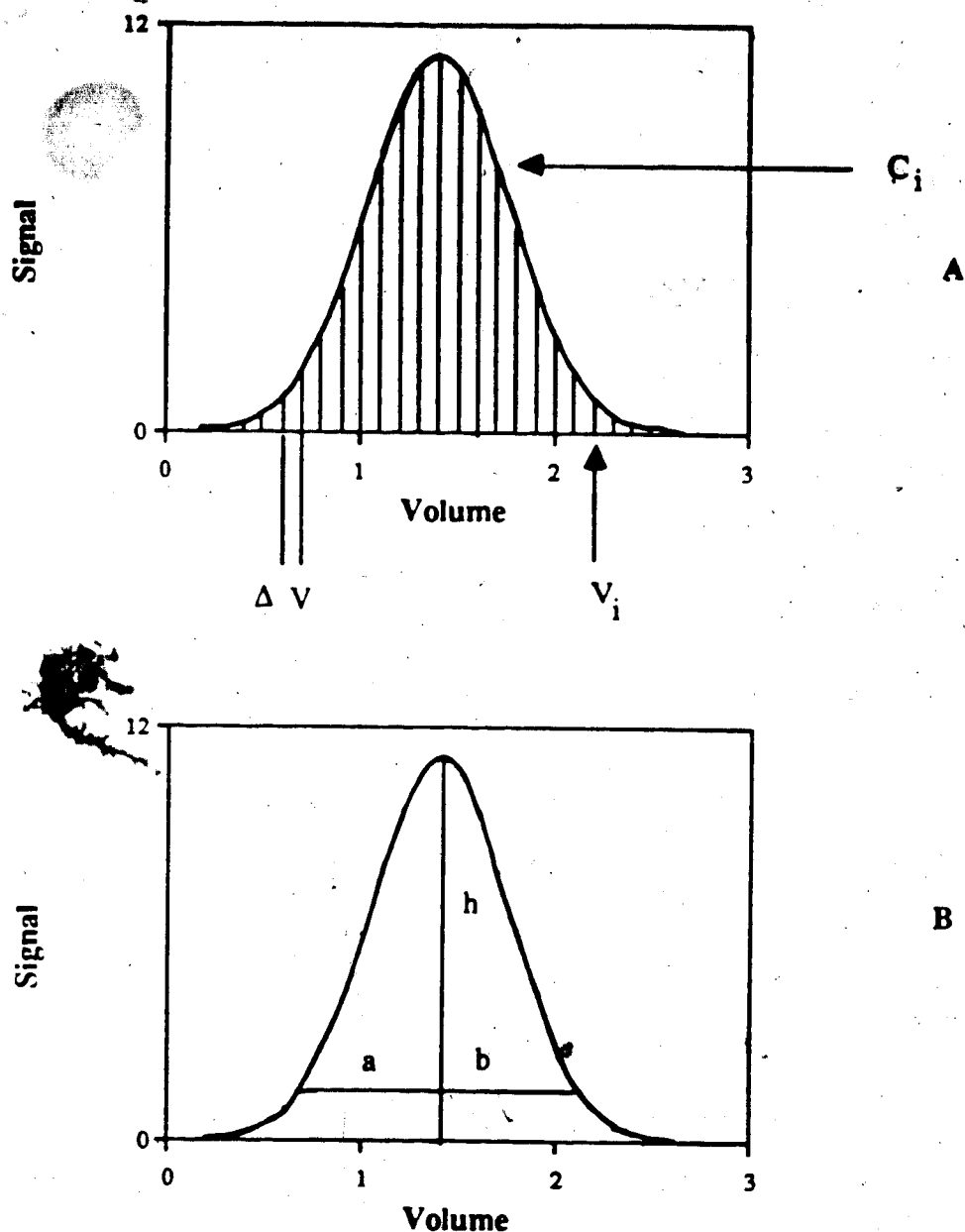


Figure 3.4 Measurement of variables on an elution peak for (A) calculation of statistical moments using equations 3.32 through 3.34. The increments along the x (volume) axis are ΔV and each point on this axis corresponds to a point V_i . C_i is the concentration from the y axis which corresponds to V_i . (B) Variables on an elution peak for the calculation of asymmetry factor (A_S). The variables a and b are measured by drawing a line (h) from the peak maximum to the baseline. At $0.1 h$, a horizontal line is drawn. The variable a is the initial portion of the horizontal line and b is the final portion.

- 4) an adsorption isotherm which is curved convex with respect to the y axis, for which K_i decreases with increasing solution concentration
- 5) non-uniform packing of the stationary phase
- 6) secondary chemical equilibria or reactions of the sample

Fronting peaks are less common in liquid chromatography but can be caused by a concave adsorption isotherm (where K_i increases with increasing solution concentration), secondary chemical reactions or packing non-uniformities.

3.2 Results and Discussion

3.2.1 Plate Height vs Stationary Phase

It has been observed that many compounds give broad asymmetrical peaks when chromatographed on PRP-1 [3.31,3.32]. Naphthalene was known to exhibit this behavior so it was chosen as the test compound as it was readily obtained and easily detected. The mobile phase was chosen to be 96% methanol(aq) because it gave a moderately large k_i' for naphthalene, which made certain aspects of measuring the adsorption isotherm and kinetics easier. Chromatograms of naphthalene were run on PRP-1 and on Waters Novapak C18 columns in order to compare the peak shapes between the two types of stationary phase. A C18 column was chosen because such columns are commonly used in chromatography and generally give narrow symmetrical peaks. Similar mobile phase velocities and k_i' values were used on each column, since plate height is dependent on both of these. Because C18 does not retain samples as strongly as PRP-1, a weaker mobile phase of 56% methanol(aq) had to be used with the C18 column so that naphthalene had the same k_i' on both columns. Results of this experiment are shown in Table 3.1. From these results, it can be seen that the PRP-1 plate height is approximately 20x larger than the C18 plate height and the PRP-1 peak is very tailed. The C18 naphthalene peak is also asymmetrical but it is fronting rather than tailing.

Table 3.1 Naphthalene plate height and asymmetry factor on PRP-1 and C18. The naphthalene concentration was 1×10^{-4} M.

Stationary Phase	Mobile Phase	Linear Velocity (cm / sec)	Capacity Factor	Plate Height (mm)	Asymmetry Factor
PRP-1	90% methanol(aq)	0.27	17.5	3.0	3.0
C18	56% methanol(aq)	0.24	16	0.13	0.4

The peak asymmetry on C18 was noticed for naphthalene in mobile phases which were 50% to 60% methanol(aq). When the mobile phase was 90% methanol(aq) the C18 naphthalene peak was no longer fronting. These peaks had an average asymmetry factor of 1.3, indicating the peak was slightly tailed in this mobile phase. The capacity factor for naphthalene on C18 in 90% methanol(aq) was 0.8. The origin of the peak fronting on C18 is unknown. The important point is that the C18 naphthalene plate height is significantly smaller than that on PRP-1. The naphthalene chromatograms on PRP-1 and the C18 column are shown in Figure 3.5 for a visual comparison of peak shapes on the polymer resin and a bonded phase column.

3.2.2 Plate Height vs Capacity Factor

Two terms in the column plate height equation are related to capacity factor. The stationary phase plate height (H_s) has a maximum value at k'_i equal to 1 and the stagnant mobile phase term (H_{sm}) increases with increasing k'_i . If either of these trends were observed on PRP-1, it could indicate that one of these processes is causing the bandbroadening.

Chromatograms of several sample compounds of varying k'_i using a 90% methanol(aq) mobile phase were run on PRP-1 to determine if the bandbroadening was dependent on capacity factor. Four of the samples were alkyl parabens. If there was a plate height dependence on capacity factor, then it should be apparent for related samples of increasing k'_i . All sample concentrations were 10^{-4} M and the mobile phase linear velocities are given in Table 3.2. The paraben compounds used were methyl paraben ($k'_i = 0.9$), n-hexyl paraben ($k'_i = 4.2$), n-heptyl paraben ($k'_i = 10.2$) and octyl paraben ($k'_i = 13.3$).

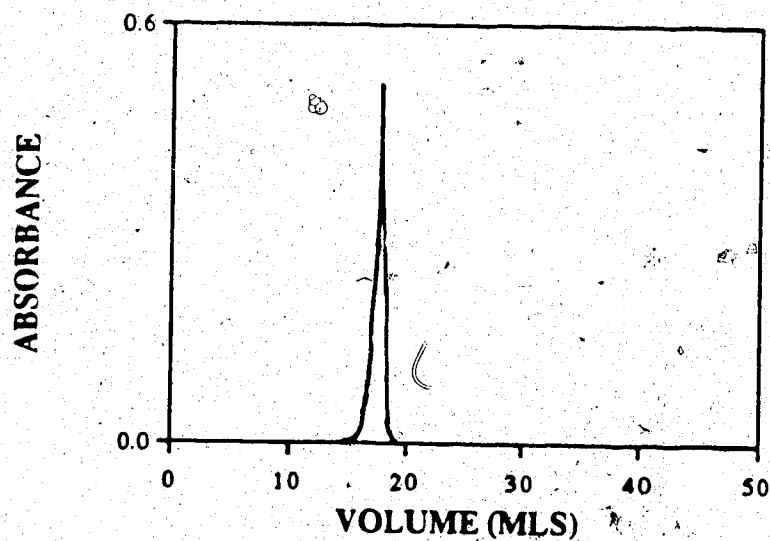
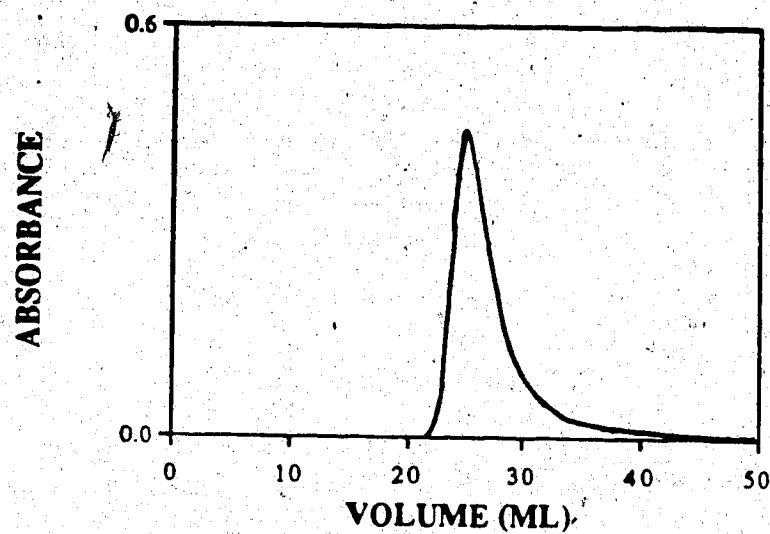


Figure 3.5 Chromatograms of 10^{-4} M naphthalene on (A) PRP-1 and (B) C18. The mobile phases and other chromatographic parameters are listed in Table 3.1.

Table 3.2 Plate height vs capacity factor on PRP-1. Two sets of samples were used, alkyl parabens and more highly conjugated aromatics. Sample concentrations were 10^{-4} M and the mobile phase was 90% methanol(aq).

Sample	Mobile Phase Linear Velocity (cm/sec)	Capacity Factor	Plate Height (mm)	Standard Deviation of Plate Height
Methyl Paraben	0.22	0.8	0.28	0.04
n-Hexyl Paraben	0.21	4.2	0.66	0.11
n-Heptyl Paraben	0.21	10.0	0.49	0.04
n-Octyl Paraben	0.30	13.3	0.75	0.13
4-Phenylazo - aniline	0.21	9.7	1.50	0.05
Naphthalene	0.22	17.5	2.42	0.13

The results of this experiment are shown in Figure 3.6 and are listed in Table 3.2. The paraben plate height is not dependent on capacity factor within one standard deviation of the measured H values.

Aromatic samples which contained more conjugation than the parabens were also tested. Chromatograms were run for 10^{-4} M solutions of naphthalene ($k'_1 = 17.5$) and p-phenylazoaniline ($k'_1 = 9.8$) using 90% methanol(aq) for the mobile phase and the linear velocities are listed in Table 3.2. The plate heights for these two samples were approximately 3x to 5x larger than the paraben plate heights as shown in Figure 3.6. Although the plate height appears to increase with increasing k'_1 for these two samples, the amount of bandbroadening is obviously dependent on the type of sample compound, rather than the capacity factor.

This sample dependence could be due to slow mass transfer or sorption processes which are specific to more highly conjugated aromatics. For example, if there were adsorption sites on the PRP-1 stationary phase which adsorbed these aromatics strongly, desorption could be slow. This would produce a large plate height due to k_d being small in the H_s term.

This experiment also indicates that the plate height is fairly large even for the parabens. This can be seen by comparing the paraben plate heights (average $H = 0.54$ mm) with the plate heights obtained for similar samples on C18. Values from the literature were taken for three samples on C18 [3.33]. The mobile phase is 1:1 (v/v) methanol : water and the mobile phase linear velocity was 0.28 cm per second. The C18 particles had an average diameter of 10 micrometers. The average C18 plate height was 0.08 mm, which is 7x smaller than the values obtained on PRP-1 at the same linear velocity.

Two conclusions can be drawn from these results. First, there is a process which produces a relatively large plate height (as compared to C18) for the parabens and which is independent of capacity factor. This indicates that the coupled plate height term could be

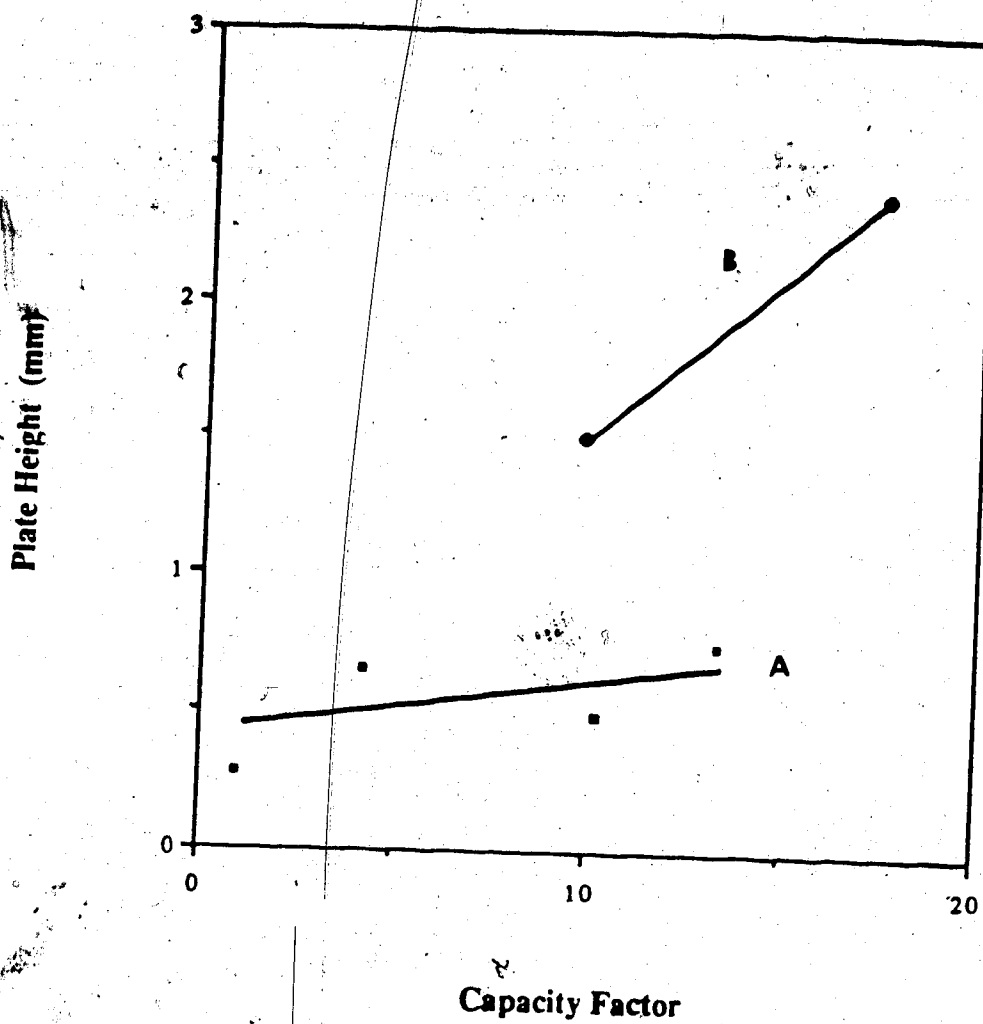


Figure 3.6 Plate height vs capacity factor on PRP-1 for (A) alkyl parabens and (B) 4-phénylazo-1-naphthylamine and naphthalene. Chromatographic conditions are listed in the text.

responsible for this plate height contribution, as this term is not dependent on capacity factor. The longitudinal diffusion term is also independent of k'_i but H_{ld} can be shown to be quite small by calculating it. Using a value of 0.6 for γ , 10^{-5} cm² per second for D_m and 0.27 cm per second for u_0 , H_{ld} is calculated to be 1.3×10^{-3} mm. The experimental values of H on PRP-1 are much larger than this, so H_{ld} is not the problem. Also, H_{ld} should increase with decreasing u_0 and the opposite trend is observed.

Second, the plate heights for more conjugated aromatics are much larger than plate heights of paraben samples. This contribution to plate height could be from a completely different process, such as slow adsorption-desorption kinetics. For this reason the adsorption-desorption kinetics of naphthalene in 90% methanol(aq) on PRP-1 were measured and are discussed in Chapter 5. Another possibility considered in this thesis was that the naphthalene and the 4-phenylazoaniline concentrations were in a non-linear region of their sorption isotherms. Isotherms and their effect on peak shape are discussed in Chapter 4. The sorption isotherm of naphthalene in 90% methanol(aq) on PRP-1 was measured to test this possibility.

3.2.3 Plate Height vs Mobile Phase Linear Velocity

It was stated previously that several of the terms in the plate height equation have a dependence on mobile phase velocity (u_0). The longitudinal diffusion term is inversely proportional and the stationary phase and stagnant mobile phase mass transfer terms are directly proportional. The coupled plate height term increases with increasing u_0 at low values of u_0 and then it reaches a plateau where it is independent of u_0 . The initial increasing portion of the curve occurs when the mobile phase linear velocity is low enough that lateral diffusion can contribute significantly to relaxing the non-uniform velocity profile. The plateau region occurs when u_0 is sufficiently high that there is not enough time for lateral diffusion to transport sample to different radial regions and therefore lateral

convection is the dominant process which relaxes the non-uniform velocity profile.

Chromatograms were run at several linear velocities and the plate heights were measured. Once the dependence of H on u_0 was known, some of the individual plate height terms could be specified as potential causes of the bandbroadening.

An H vs u_0 profile was run on PRP-1 using two samples, 1.03×10^{-4} M naphthalene ($k'_i = 17.5$) and 1.14×10^{-4} M methyl paraben ($k'_i = 0.88$). The mobile phase used was 90% methanol(aq). The range of mobile phase linear velocities used was 9.6×10^{-3} cm per second to 0.36 cm per second. These values correspond to flow rates of 0.055 mL per minute to 2.1 mL per minute on the PRP-1 column. Flow rate is related to mobile phase linear velocity by the column length (L) and void volume (V_m).

$$u_0 = \frac{L}{\left(\frac{V_m}{F}\right) 60}$$

3.36

The results for both samples are given in Table 3.3 and are plotted in Figure 3.7. The plate heights listed have the longitudinal diffusion term (H_{ld}) and the extracolumn contribution already subtracted. It was thought that at some of the lowest flow rates used the H_{ld} term may have been a significant fraction of the measured plate height. H_{ld} was calculated for each linear velocity using a D_m of 2×10^{-5} cm² per sec for naphthalene in methanol [3.34] and 1.0×10^{-5} cm² per sec for methyl paraben. γ was assumed to be 0.6 for both samples. The calculated values for H_{ld} for various mobile phase linear velocities are given in Table 3.4.

The extracolumn contribution was measured by removing the column from the chromatographic system and injecting 20 microliters of 1.1×10^{-5} M naphthalene into the system at each mobile phase linear velocity. The variance of each peak was calculated using moments analysis and was subtracted from the variance of the sample peaks eluted from the PRP-1 column at the corresponding linear velocity. The resulting difference between the two gave the variance due to column bandbroadening and this value

Table 3.3 Naphthalene and methyl paraben plate heights (H) vs mobile phase linear velocity (u_0) on PRP-1. Sample concentrations were 10^{-4} M and the mobile phase was 90% methanol(aq). Particle diameter was 10 micrometers. The plate heights listed in this table have had the extracolumn and longitudinal diffusion contributions subtracted. The error is listed as one standard deviation (s.d.) and the results are the average of duplicate chromatograms.

u_0 (cm / sec)	Naphthalene H (mm)	Overall s.d. for Naphthalene H	Methyl Paraben H (mm)	Overall s.d. for Methyl Paraben H
0.36	2.5	0.25	0.38	0.07
0.27	2.7	0.65	0.33	0.14
0.17	2.1	0.28	0.27	0.02
0.090	1.6	0.14	0.21	0.02
0.075	1.5	0.32	0.18	0.02
9.6×10^{-3}	0.72	0.19	0.10	0.05

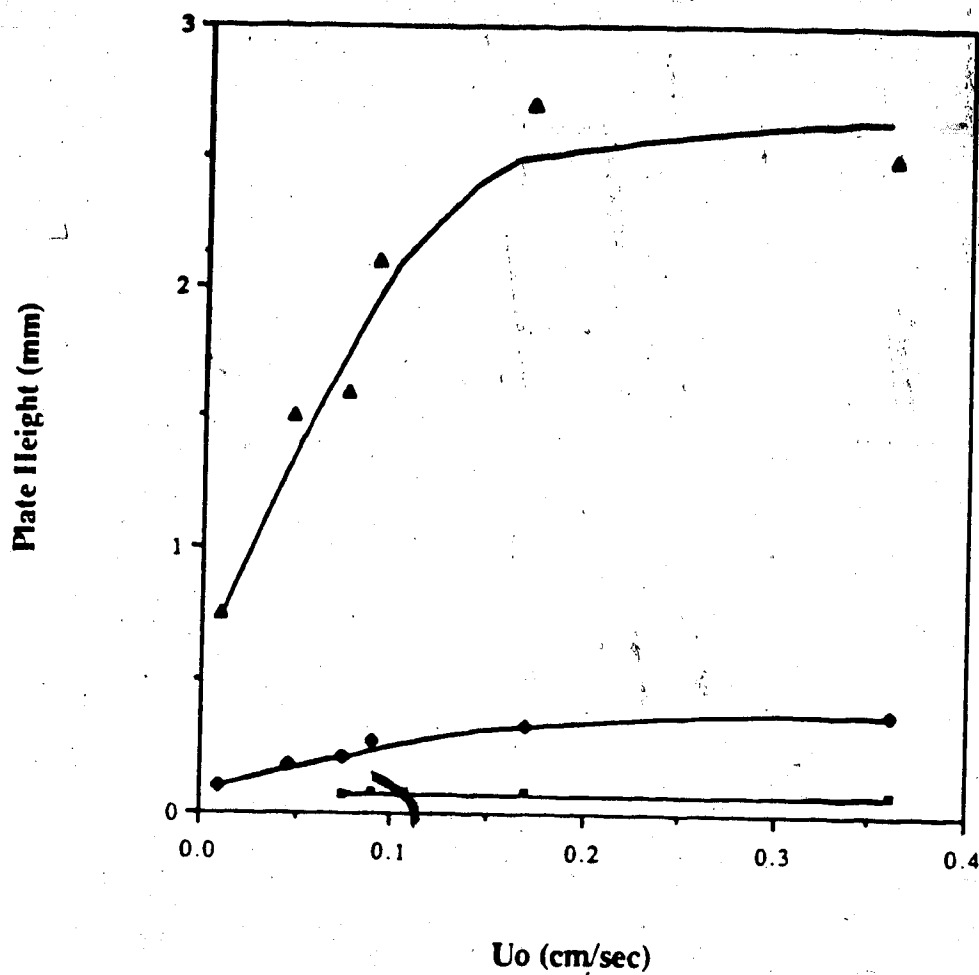


Figure 3.7 Plate height vs mobile phase linear velocity (u_o) on PRP-1 and C18. Conditions are : (▲) 10^{-4} M naphthalene on PRP-1 (◆) 10^{-4} M methyl paraben on PRP-1 and (■) average plate height on C18. The C18 values were calculated using Figure 6 in reference 3.33.

Table 3.4 Calculated values for naphthalene and methyl paraben H_{ld} vs mobile phase linear velocity (u_0) on PRP-1. The values used for D_m and γ are listed in the text. The standard deviation (s.d) for H_{ld} was calculated assuming 10% error in D_m and that γ had a range of 0.5 to 0.7.

u_0 (cm / sec)	Naphthalene H_{ld} (mm)	s.d for Naphthalene H_{ld}	Methyl Paraben H_{ld} ○ (mm)	s.d. for Methyl Paraben H_{ld}
0.36	6.7×10^{-4}	1.8×10^{-4}	3.8×10^{-4}	1.0×10^{-4}
0.27	8.9×10^{-4}	2.4×10^{-4}	5.2×10^{-4}	1.4×10^{-4}
0.17	1.4×10^{-3}	0.4×10^{-3}	8.1×10^{-4}	2.2×10^{-4}
0.090	2.7×10^{-3}	0.7×10^{-3}	1.6×10^{-3}	0.4×10^{-3}
0.075	3.2×10^{-3}	0.9×10^{-3}	1.9×10^{-3}	0.5×10^{-3}
9.6×10^{-3}	2.5×10^{-2}	0.7×10^{-2}	1.5×10^{-2}	0.4×10^{-2}

was used in equation 3.15 to calculate H_{column} . Tables 3.5 and 3.6 list the total sample peak variance for naphthalene and methyl paraben and the extracolumn variance measured for each mobile phase linear velocity.

As a comparison; the results for a C18 column are shown also [3.33]. The mobile phase for the C18 column was 1:1 (v/v) methanol:water. The C18 plate heights in Figure 3.7 are the average values of plate heights measured for three samples and were calculated using values from Figure 6 in reference 3.34. The samples were n-pentanol ($k_i' = 1.8$), phenol ($k_i' = 1.3$), and ethanol ($k_i' = 0.15$) but the concentrations were not given in the reference. The C18 particles had an average diameter of 10 micrometers. The extracolumn and H_{LD} contributions have not been subtracted for the C18 results. However at these linear velocities, H_{LD} is negligible.

First, comparing the results of methyl paraben on PRP-1 with the C18 results, one can see that the methyl paraben plate height is 3x to 4x larger on PRP-1 in the u_0 range which was studied on both C18 and PRP-1. Also, the plate heights obtained on PRP-1 are relatively large even at low flow rates. This can be seen clearly for naphthalene where H is 0.75 mm at a mobile phase linear velocity of 9.6×10^{-3} cm per second (flow rate = 0.055 mL per minute). The coupled plate height term could be causing the bandbroadening at low mobile phase linear velocities if velocity non-uniformities are occurring on a large enough scale that neither lateral diffusion nor lateral convection can relax the profile, even at low u_0 .

Although the PRP-1 plate heights are large at all values of u_0 , H does decrease with decreasing mobile phase velocity, especially for naphthalene. This dependence of plate height on mobile phase linear velocity indicates a mass transfer process is contributing to the large plate height values.

Both this experiment and the H vs k_i' experiment indicate that possibly there are two processes contributing to the excessive bandbroadening on PRP-1.

Table 3.5 Extracolumn σ_v^2 and total sample peak σ_v^2 vs mobile phase linear velocity (u_0) for naphthalene . The naphthalene concentration was 10^{-4} M for the total peak σ_v^2 . A solution of 10^{-4} M naphthalene was used for the extracolumn σ_v^2 measurements. The mobile phase was 90% methanol(aq) for all experiments. All results are the average of duplicate chromatograms. The error is listed as one standard deviation (s.d.).

u_0 (cm / sec)	Naphthalene σ_v^2 (mL^2)	s.d. for Naphthalene σ_v^2	Extracolumn σ_v^2 (mL^2)	s.d. for extracolumn σ_v^2
0.36	13.0	0.007	1.05×10^{-3}	0.10×10^{-3}
0.27	14.0	1.8	1.09×10^{-3}	0.10×10^{-3}
0.17	10.2	1.2	0.98×10^{-3}	0.10×10^{-3}
0.090	8.0	0.4	0.93×10^{-3}	0.03×10^{-3}
0.075	7.2	1.3	0.88×10^{-3}	0.03×10^{-3}
9.6×10^{-3}	3.6	0.2	0.38×10^{-3}	0.07×10^{-3}

Table 3.6 Extracolumn σ_v^2 and total sample peak σ_v^2 vs mobile phase linear velocity (u_0) for methyl paraben. The methyl paraben concentrations were 10^{-4} M for the total peak σ_v^2 . A solution of 10^{-4} M naphthalene was used for the extracolumn σ_v^2 measurements. The mobile phase was 90% methanol(aq) for all experiments. All results are the average of duplicate chromatograms. The error is listed as one standard deviation (s.d.).

u_0 (cm/sec)	Methyl Paraben σ_v^2 (mL ²)	s.d. for Methyl Paraben σ_v^2	Extracolumn σ_v^2 (mL ²)	s.d. for extracolumn σ_v^2
0.36	19.8×10^{-3}	1.8×10^{-3}	1.05×10^{-3}	0.10×10^{-3}
0.27	16.4×10^{-3}	5.5×10^{-3}	1.09×10^{-3}	0.10×10^{-3}
0.17	12.6×10^{-3}	0.8×10^{-3}	0.98×10^{-3}	0.10×10^{-3}
0.090	10.2×10^{-3}	0.8×10^{-3}	0.93×10^{-3}	0.03×10^{-3}
0.075	8.7×10^{-3}	0.8×10^{-3}	0.88×10^{-3}	0.03×10^{-3}
9.6×10^{-3}	5.6×10^{-3}	1.2×10^{-3}	0.38×10^{-3}	0.07×10^{-3}

3.3 Conclusions

The purpose of these experiments was first, to verify, as claimed in the literature, that elution peaks obtained with PRP-1 were broad and asymmetrical compared to those obtained on bonded phase columns and second, to determine the dependence of the PRP-1 plate height on capacity factor and mobile phase linear velocity. Since each term in the overall plate height equation is related to these parameters differently, it was thought the results of these experiments could help determine the process responsible for the excessive bandbroadening on PRP-1.

Chromatograms of naphthalene at a constant concentration, k_i' and u_0 were run on both PRP-1 and C18 using aqueous-methanol mobile phases. The plate height measured on PRP-1 was 20x larger than that measured for C18, indicating PRP-1 is much less efficient than C18.

The plate heights for samples of varying k_i' were measured and in general, plate height was independent of capacity factor. Two trends were noticed. First of all, the plate heights were much larger for more highly conjugated aromatics than for alkyl paraben compounds. This indicated the large plate height results from some chromatographic process specific to the more highly conjugated aromatic samples. This could be either a slow step in a mass transfer or kinetic process, or due to non-linearity of the sorption isotherms or another process which occurs only for the highly conjugated aromatic samples. Secondly, the PRP-1 plate heights were large even for the parabens compared to plate heights obtained on C18. The origin of this bandbroadening could be completely different than the process which broadens the more highly conjugated aromatic sample bands.

Results of the plate height vs mobile phase linear velocity study also indicate there are at least two processes contributing to bandbroadening on PRP-1. Two samples were used in this experiment, a more conjugated aromatic (naphthalene) and a paraben

(methyl paraben). Again, two trends were observed in plate heights for both samples were relatively large at low u_0 as compared to the plate heights measured on a C18 column. This means there is a velocity independent process contributing to the bandbroadening. This contribution most likely results from the coupled plate height term as was explained in Section 3.2.3. Therefore, a non-uniform velocity profile is probably causing some of the bandbroadening.

The second trend observed was that although the naphthalene plate height was always large, it did decrease with decreasing u_0 . This points to a mass transfer, kinetic or some other sample-specific process which is causing the bandbroadening observed for highly conjugated aromatic compounds.

Based on these results, it was decided that the sorption isotherm and adsorption-desorption kinetics of naphthalene should be measured to evaluate the contribution to bandbroadening from each of these. Also, in order to estimate the magnitude of the non-uniform velocity profile it was decided to measure sample profiles of dyes on packed beds of PRP[®]1.

CHAPTER 4

Naphthalene Adsorption Isotherm

4.1 Theory

4.1.1 Sorption Isotherms

As was mentioned in Chapter 3 a possible source of peak asymmetry is a non-linear adsorption isotherm. Adsorption isotherms and their relation to chromatography have been the subject of several discussions [4.1 - 4.3].

An isotherm is a plot of concentration of sample sorbed on the stationary phase (C_s) vs concentration in the mobile phase (C_m) at a constant temperature. The distribution coefficient, K_i , for a solute at any concentration is the slope of the line between the point corresponding to that concentration and the origin [4.4], as shown in Figure 4.1. Therefore, the isotherm gives the dependence of K_i upon concentration.

The shape of the isotherm depends upon the sorption mechanism [4.1]. Three common types of isotherms are shown in Figure 4.2 and the chromatographic peak shape which would be expected from each isotherm is drawn below it [4.4]. The first isotherm (Figure 4.2a) is linear. A linear isotherm occurs when the amount of sorbed sample is directly proportional to concentration in the mobile phase and therefore, K_i is a constant. For linearity to occur sample molecules must not interact with one another in either phase. Most isotherms approach linearity at sufficiently low sample concentrations. Generally, in order to be operating in the linear region the amount of sample adsorbed must be much less than the number of adsorption sites and the concentration of sample in the mobile phase must be much less than the concentrations of any other mobile phase species with which it interacts. The chromatographic peak shape which results from a linear isotherm is Gaussian, as shown in Figure 4.2a, assuming

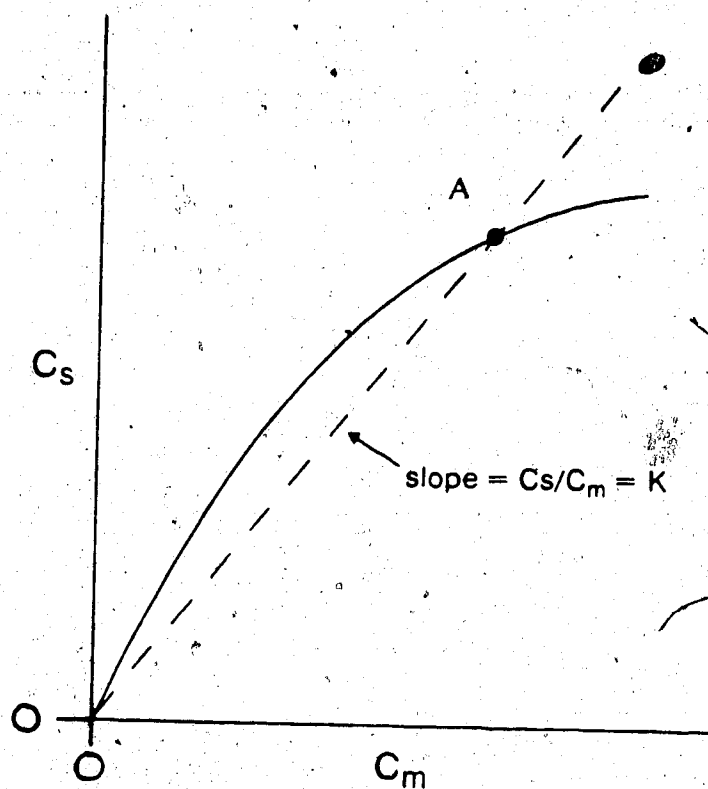


Figure 4.1 Sorption isotherm. The slope of the dashed line between the origin and point A is equal to the distribution coefficient, K_i , for solute i at concentration C_m .

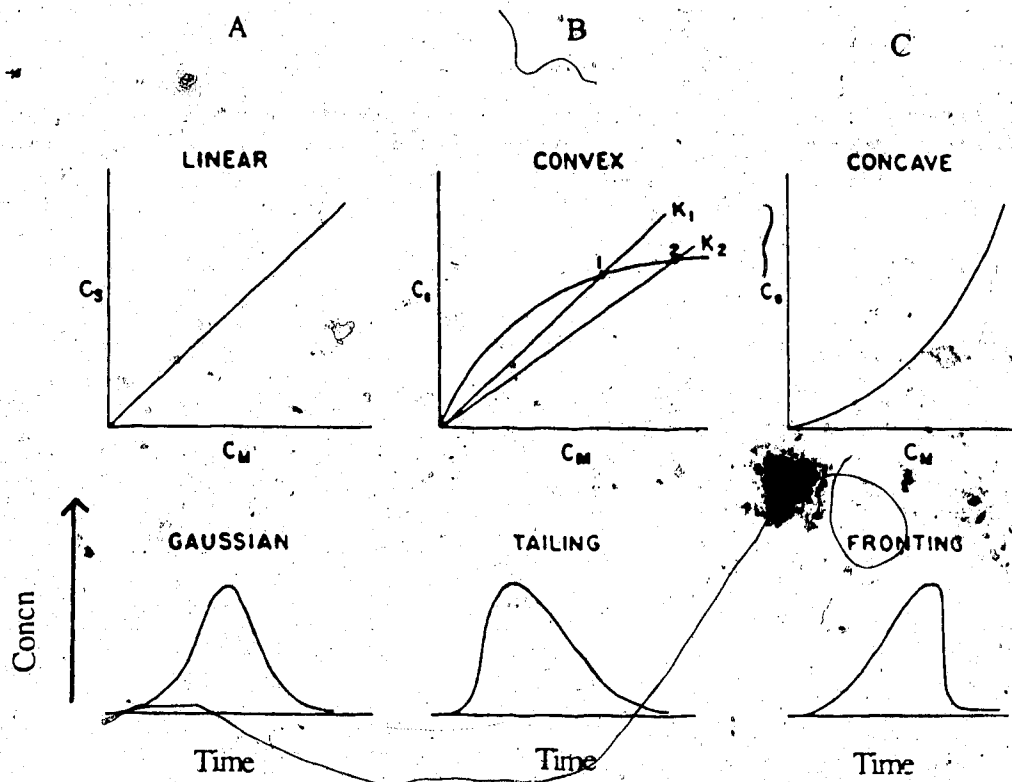


Figure 4.2 Shapes of common sorption isotherms and the corresponding elution peak profile. (a) Linear isotherm and Gaussian peak (b) Convex isotherm and tailed peak (c) Concave isotherm and fronting peak. (see reference 4.6).

there is some bandbroadening due to random, non-ideal chromatographic processes, such as diffusion.

The second isotherm (Figure 4.2b) is convex and here, K_i decreases with increasing sample concentration. This type of isotherm is common in liquid chromatography and gives rise to tailing peaks, as shown in Figure 4.2b. This peak shape can be understood if the distribution coefficients at two different concentrations (points 1 and 2) are considered. First, recall that the distribution coefficient and the capacity factor (k_i') are directly proportional to one another.

$$k_i' = K_i \phi$$

4.1

The phase ratio (ϕ) is equal to the weight of stationary phase (W_s) divided by the void volume (V_m). The void volume is defined here as the sum of the interparticle and intraparticle volume. The sample velocity is inversely proportional to ($1 + k_i'$) so the sample velocity decreases as k_i' (or K_i) increases:

$$u_i = u_o \frac{1}{1 + k_i'}$$

4.2

where u_i is the average sample velocity and u_o is the average linear mobile phase velocity. For sufficiently long columns, the sample distribution tends to acquire a Gaussian shape due to non-ideal bandbroadening processes which were described in Chapter 3. If the isotherm were linear, K_i and u_i would be constant for all concentrations along the sample zone and the sample would elute as a Gaussian peak. However, if u_i is dependent on concentration because of a changing distribution coefficient, the high concentration regions of the zone will move at a faster velocity than the low concentration regions. This causes the center of the band to catch up with the leading edge while the low concentration trailing edge moves more slowly and elutes as a

tail. Point 1 on the convex isotherm has a larger K_1 than point 2. Therefore, the portions of the zone with concentrations corresponding to point 1 will move more slowly and elute at a later time than those corresponding to point 2. Using analogous reasoning it can be seen that a concave isotherm, as shown in Figure 4.2c, will cause a fronting peak.

Since the retention volume (V_R) is proportional to $(1 + k_1')$ as shown in equation 4.3, V_R also will change with sample concentration in a non-linear region.

$$V_R = V_m (1 + k_1') \quad 4.3$$

V_m is the interparticle volume and pore volume of the bed of stationary phase and is determined by measuring the volume at which an unretained sample elutes. The unretained sample is a compound which is not adsorbed on the PRP-1 but enters the pore liquid. In the linear region V_R is a constant for a particular sample for a specific mobile and stationary phase.

4.1.2 Measuring Sorption Isotherms

Methods used to measure sorption isotherms in gas chromatography have been summarized by Huber and Gerritse [4.5] and by Conder and Young [4.6]. The same techniques applied to the determination of adsorption isotherms in liquid chromatography have been reviewed by Dondi et al [4.7], De Jong et al [4.8] and Jacobson et al [4.9]. These can be divided into two groups: equilibrium and non-equilibrium methods.

Two commonly used non-equilibrium methods are the breakthrough curve method and the elution chromatography method. The elution chromatography method [4.10] is an elution technique in which a narrow band of sample is injected at the column inlet. The sample band moves down the column at a velocity which is dependent on the

sample distribution coefficient and the mobile phase velocity. For a linear isotherm the volume at which the sample elutes is related to K_i , as given in equation 4.4.

$$K_i = \frac{V_r - V_m}{W_s}$$

4.4

V_r is the retention volume and W_s is the weight of stationary phase in the column.

One disadvantage to this method is that samples with large distribution coefficients will have long retention times, which is inconvenient. Also, since peaks become broader and shorter with increasing retention volumes, they may be very difficult to detect.

In the breakthrough method sample solution of a known concentration flows through a bed of adsorbent until the concentration of the effluent solution is equal to the concentration of the influent. At this point the adsorbent is at equilibrium with the sample solution. The signal expected from this experiment is called a breakthrough curve. A typical one is shown in Figure 4.3. The shape of a breakthrough curve can be explained as follows. Initially, as the sample solution encounters the stationary phase all the sample is adsorbed onto the stationary phase and none is detected in the column effluent. As the adsorbent begins to reach equilibrium with the solution, increasing concentrations of sample are detected until finally a plateau is reached. At the plateau the effluent concentration is equal to the influent concentration of the solution and the adsorbent is at equilibrium with the sample solution. If the adsorption isotherm is linear the eluent volume corresponding to the midpoint of the breakthrough curve is equal to the chromatographic retention volume. For an isotherm of any shape, the derivative of the breakthrough curve is the elution peak. The moles adsorbed at equilibrium is given by the hatched area between the breakthrough profile and V_m and the dashed line at C_m as shown in Figure 4.3 [4.11]. However, determining experimentally when the plateau on

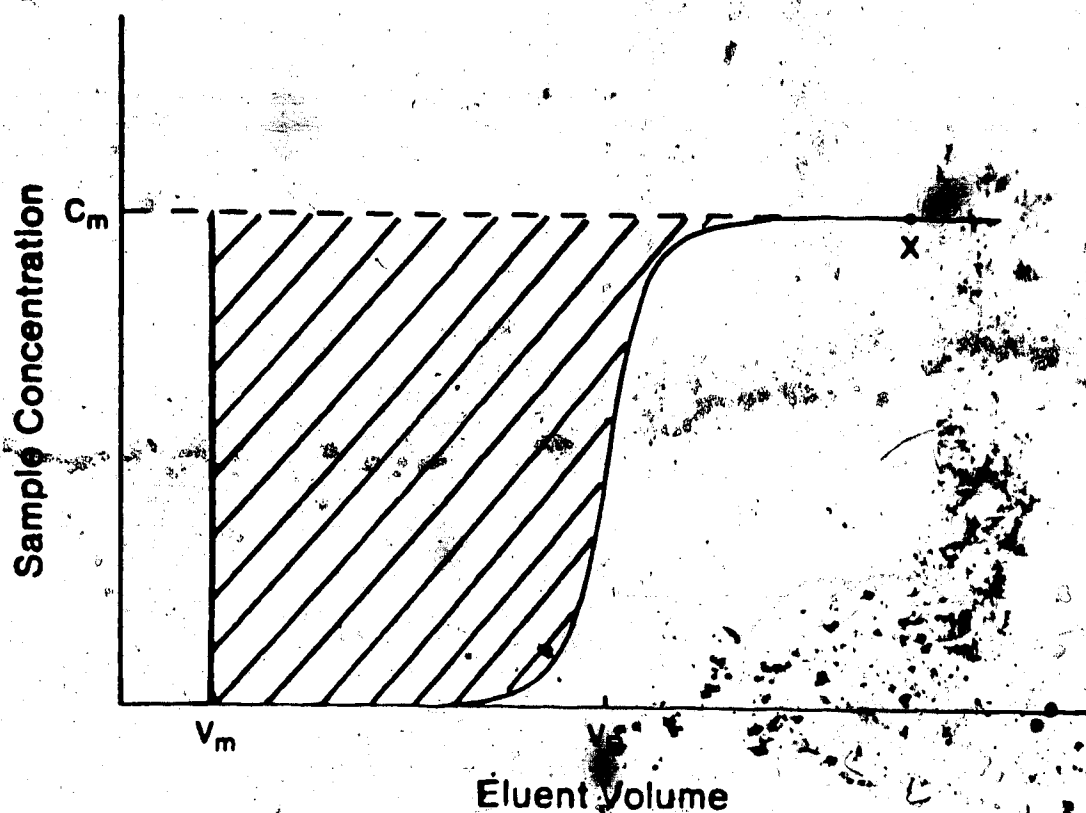


Figure 4.3 Breakthrough curve. Equilibrium between the two phases occurs at the plateau of the breakthrough curve. The effluent concentration at the plateau is equal to the influent solution concentration. For a linear isotherm, the midpoint of the rising portion of the breakthrough curve is equal to the retention volume, V_R .

the breakthrough curve has been reached becomes impossible when C_m is so small that the entire breakthrough curve is buried in baseline noise.

There are two commonly used equilibrium methods of measuring isotherm shapes, batch equilibration and column equilibration. In batch equilibration a known weight of stationary phase is added to a solution of known sample concentration and the mixture is stirred until equilibrium is reached. The final concentration of the sample solution is measured and the amount adsorbed can be calculated by the difference between the initial and final concentrations. The moles adsorbed also can be measured by removing the sample solution, eluting the adsorbed sample with a strong solvent and measuring this quantity. The concentration adsorbed is calculated by dividing the moles adsorbed by the weight of stationary phase.

$$C_s = \frac{\text{moles adsorbed}}{W_s}$$

4.5

The distribution coefficient can be calculated using equation 4.6.

$$K_i = \frac{C_s}{C_m}$$

4.6

The disadvantage to the batch equilibration method is that it is slow and somewhat tedious.

The column equilibration method [4.12] was used for the adsorption isotherm measurement in this thesis. It is based on the same principles as the batch technique but is faster. The procedure was described in Section 2.2.4 but will be briefly reviewed here.

A known weight of stationary phase was packed into a small precolumn. Initially, only mobile phase was pumped through the precolumn. Next, a valve was switched so that a solution of known sample concentration, C_m , was directed onto the

precolumn. The signal that results from this introduction of sample is a breakthrough curve (Figure 4.3).

After equilibrium between the two phases is reached (i.e. the plateau of the breakthrough curve) the total number of moles of sample in the stationary phase (n_t) is measured by eluting the precolumn with a strong solvent onto an analytical HPLC column. Although the analytical column was not really necessary and a detector could be directly connected to the precolumn, the analytical column provided the advantage of separating the sample peak from solvent refractive index peaks and any impurity peaks which may have been present, allowing for more accurate quantification of the sample peak.

The measured quantity n_t includes not only adsorbed sample (n_s) but also that present in the hold-up volume, V_m , of the precolumn. V_m includes the inter- and intraparticle volumes and the connecting tubing, frit and valve volumes as well. Therefore, the moles present in the hold-up volume must be subtracted from the total. The number of moles in V_m is equal to V_m multiplied by the sample solution concentration. The concentration of adsorbed sample can be calculated using equation 4.7.

$$C_s = \frac{n_s}{W_s} = \frac{n_t - C_m V_m}{W_s}$$

4.7

The distribution coefficient corresponding to one point on the isotherm is calculated by dividing C_s by the mobile phase concentration C_m as discussed previously (see equation 4.6). Additional points on the isotherm are obtained by varying the value C_m of the solution pumped through the precolumn.

In the present work the adsorption isotherm of naphthalene in 90% methanol(aq) on PRP-1 was determined by using a 42 mm x 2 mm precolumn packed with the stationary phase. The values of n_t for naphthalene solutions of various concentrations

were measured by determining the area of the eluted peak and comparing it with a calibration curve made from a series of standard solutions. The hold-up volume of the precolumn was measured by determining the number of moles of an unretained compound present in the precolumn system. Once both n_t and V_m were known equation 4.7 was used to calculate C_s . By measuring C_s for a wide range of naphthalene concentrations the adsorption isotherm was obtained.

4.1.3 Relation of Chromatographic Peak Shape and Isotherm Curvature

Several researchers have studied the quantitative relation between isotherm curvature and the corresponding chromatographic peak shape. One goal is to be able to predict the peak shape based on an experimental isotherm. This is important in fields such as affinity chromatography or preparative chromatography, where the quantity of sample used exceeds the linear region of the isotherm. If the peak shape could be predicted, selection of the maximum amount of sample which allows both adequate separation and optimum detectability (or quantity purified) could be determined without experimental trial and error.

One approach used to predict this relation is to set up a mass balance equation [4.13 - 4.16] which relates the flux of sample at any point in a column to processes the sample is undergoing, such as diffusion, sorption-desorption kinetics and the isotherm effects. The inclusion of a non-linear isotherm causes this differential equation to be non-linear and makes solution of the equation quite difficult. Usually the differential equation is solved numerically rather than by trying to obtain an exact analytical solution. While this method can give an exact description of the chromatographic process, the mathematics involved can make it unattractive to use.

Another approach is to simulate the chromatographic separation using models which imitate the physical processes which occur on a column. An imaginary column is

divided into discrete stages or steps and the effects of the physical processes on peak shape at each step are calculated. The final peak shape is the composite of all individual steps.

Eble and co-workers [4.17] used a simulation method based on a Craig distribution model and a Langmuir isotherm (a convex isotherm). They used this method to predict frontal chromatographic elution curves by accounting for non-ideal bandbroadening with the Craig distribution model and isotherm non-linearity with the Langmuir isotherm. However, this simulation took an excessive amount of time which made it inconvenient to use.

Another type of simulation was done by Phillips and co-workers [4.18] to generate chromatographic elution peaks. They used a stochastic model and a Langmuir isotherm to account for non-ideality and non-linearity effects, respectively. This simulation also required a long time to calculate (3 to 6 hours on a Hewlett Packard 2100A minicomputer).

A simulation method was used in this thesis because this approach was simpler mathematically than solving differential equations. Also, the simulation method used invokes a physical picture of the interaction between the non-ideal and non-linear processes. The non-ideal bandbroadening was described by a Gaussian distribution and the shape of the isotherm was described by the Langmuir equation. The Langmuir isotherm equation is given by equation 4.8 [4.19].

$$C_s = \frac{A B C_m}{1 + (B C_m)}$$

4.8

A and B are empirical constants used to fit the equilibrium isotherm data to equation 4.8. They can be easily determined by putting equation 4.8 in the form of an equation for a line.

$$\frac{1}{C_m} = \frac{1}{C_m} + \frac{1}{A}$$

4.9

If $(1/C_m)$ is plotted vs $(1/C_m)$ the slope of this line is equal to $(1/AB)$ and the y-intercept is equal to $(1/A)$.

In the program a "column" was divided into 175 axial positions and sample was initially distributed evenly into the first 3 positions, simulating an injection. A diagram of this is shown in Figure 4.4. The simulation algorithm will be described in a stepwise manner. Details of the program calculations and variables are given in Appendix I.

1. After injection the sample is initially moved down the column to positions 11, 12 and 13. The total concentration of sample at each column position is known and will be referred to as the "sample distribution".
2. The sample distribution is convolved with a Gaussian function, whose variance is related to an assumed plate height which was experimentally measured on a PRP-1 analytical column. This produces a new sample distribution which is broader (it is distributed into a greater number of column positions) and more dilute.
3. Using the total moles of sample present at each position and the adsorption isotherm equation, the equilibrium concentrations in the mobile and stationary phases are calculated. These concentrations are used to calculate the distribution coefficient and the sample velocity, $U(J)$ for sample at each column position via equations 4.6 and 4.10.

$$U(J) = \frac{u_o}{1 + \phi K_i}$$

4.10

4. The sample at each column position is moved down the column a distance X , which is dependent on the individual sample velocities and the time increment, DT , in which sample movement occurs.

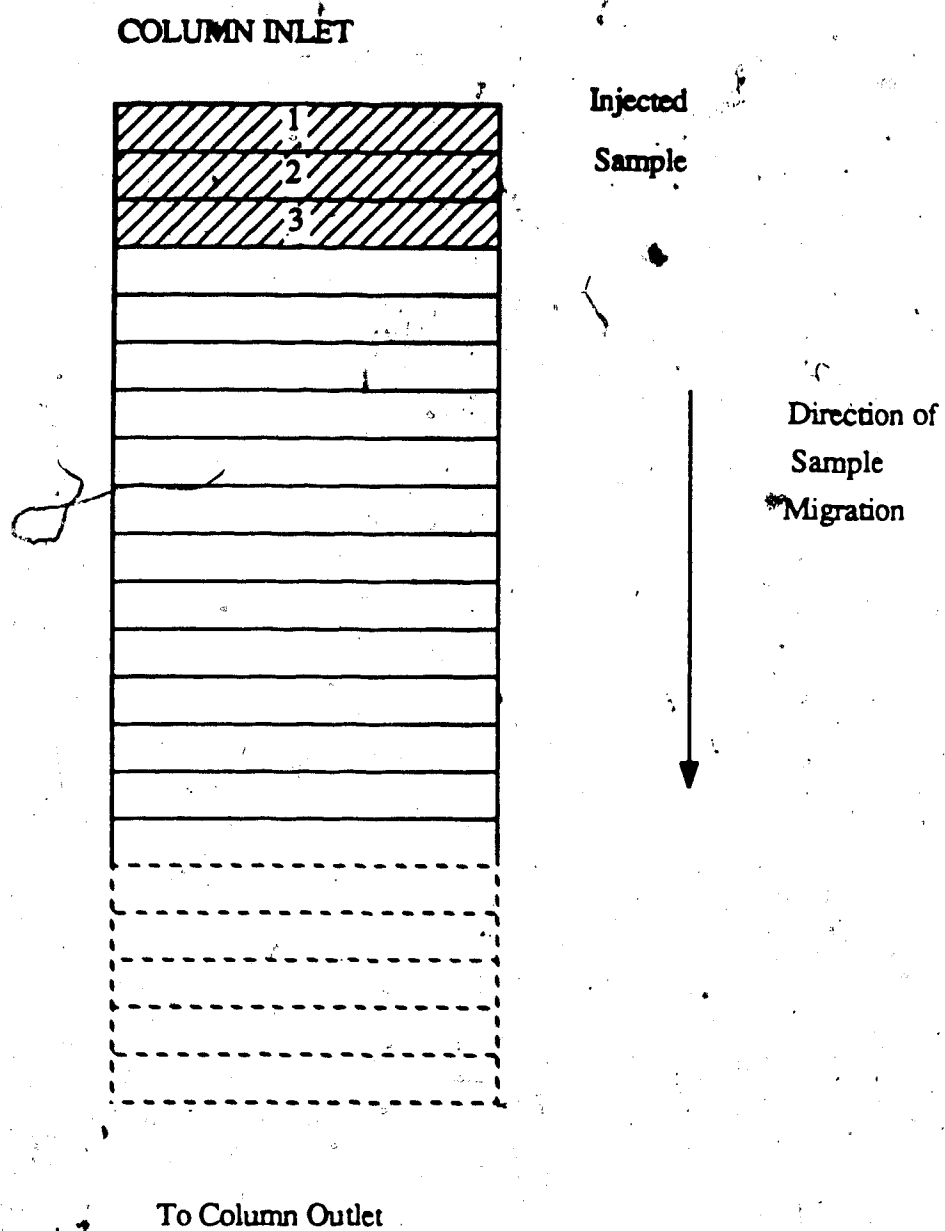


Figure 4.4 Diagram of initial portion of column used in peak simulations.

$$X = U(J) DT$$

4.11

5. Positions past the column outlet (those greater than 175) are checked to see if any sample has eluted. If some has, that amount is stored along with the time of elution.
6. Steps 2 through 5 are repeated until all sample has eluted from the column.

Appendix I gives detailed explanations of each calculation used in the program and justification for the choice of variables.

To test whether the algorithm of this numerical simulation yielded sufficiently accurate results, a simulation was run for a 10^{-4} M naphthalene solution assuming a linear isotherm. The linear isotherm equation was determined by a linear least squares fit through all the experimental naphthalene adsorption isotherm points, ignoring the slight convexity of the data for this test. A simulation was also done for a sample (0.3 M p-toluidine) with a non-linear adsorption isotherm. The data used for the non-linear isotherm was taken from Figure 4b in reference 4.9 and the adsorption isotherm has been replotted in Figure 4.5 of this thesis.

The variables which were entered by the operator to run these simulations are given in Table A2.1 in Appendix II. The plate height which was used to calculate the Gaussian distribution for both simulations was 0.38 mm. This plate height is meant to account for bandbroadening due to "normal" non-ideal processes, such as axial diffusion or some small irregularities in the packing structure. It was not desirable to use the large experimental plate heights measured for naphthalene on PRP-1 since they could be due to an unusual effect, such as slow adsorption-desorption kinetics. The purpose of the peak simulation program was to assume "normal" non-ideality was not the major cause of the naphthalene bandbroadening and to determine whether the isotherm curvature could be responsible for the excessive bandbroadening and peak asymmetry observed for naphthalene. The value of 0.38 mm was chosen because it was the smallest plate height

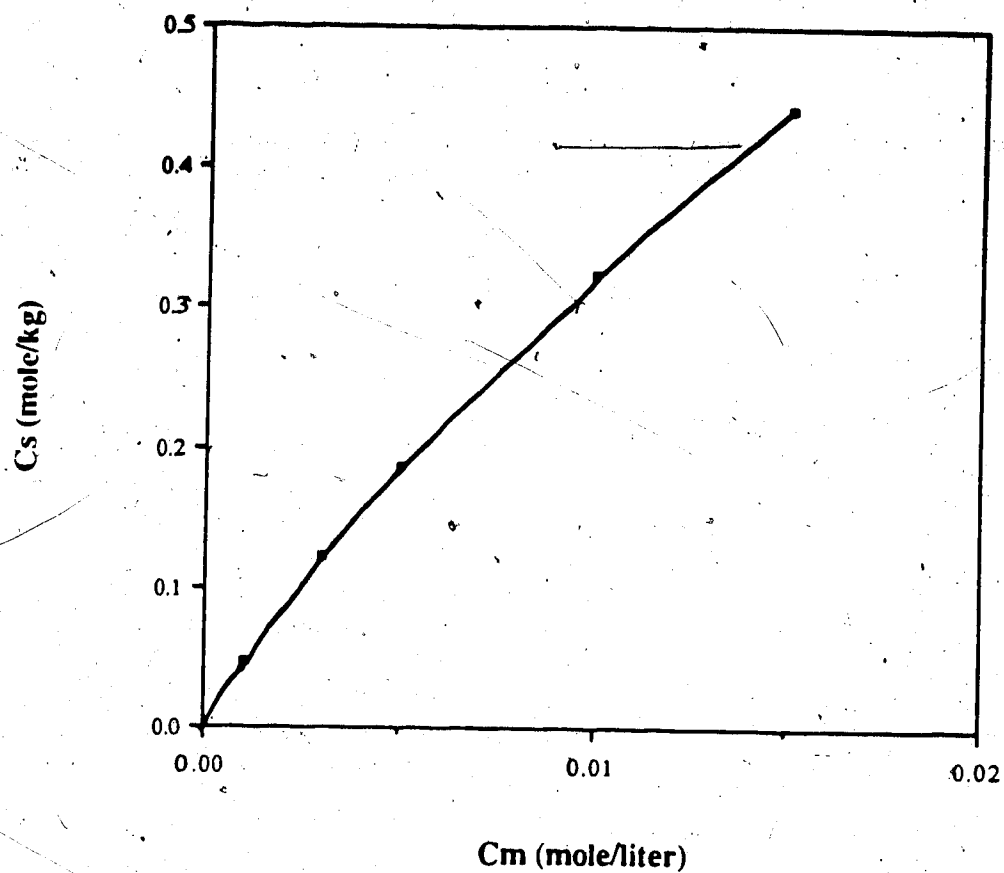


Figure 4.5 Non-linear adsorption isotherm used to calculate the simulated peak shown in Figure 4.6b. The data for the non-linear isotherm was taken from Figure 4b of reference 4.9. The isotherm was fitted by the Langmuir equation and had Langmuir constants of $A = 0.8341$ mole per kg and $B = 59.9226$ liter per mole.

measured for any sample on PRP-1 and hence, was representative of "normal" non-ideal bandbroadening.

The simulated peak shape resulting from the linear isotherm is shown in Figure 4.6a. The dots in 4.6a represent points calculated by the simulation program. The chromatographic parameters measured from the simulated peak and the correct theoretical values are listed in Table 4.1. The theoretical values are calculated from the operator-entered values for plate height, K_i , V_m and W_s . The equations used to calculate the theoretical parameters are given below Table 4.1. It can be seen that the two sets of values agree within twelve percent, suggesting that the simulation algorithm is sufficiently accurate for present purposes. The plate height has increased slightly from 0.38 mm to 0.41 mm because of the discrete method of the simulation, which introduces round-off errors. For example, if sample at a position J is calculated to move a distance equal to 2.5 column positions during one step of the program, it will actually be moved three positions since the movement must occur in integer increments. This is also why the asymmetry factor is 1.1 instead of 1.0 for the simulated peak calculated from the linear isotherm. This error is not very large and could be decreased by increasing the number of column positions in the simulation program. However, this was not done here because it would have substantially increased the computing time.

Figure 4.6b shows the simulation results for the non-linear isotherm. There are no theoretically calculated peak parameters for comparison, as they are not easy to predict by an alternative method. The simulation for the non-linear isotherm case was basically a qualitative test of the algorithm. The simulated peak for the non-linear isotherm is tailed as expected for a convex isotherm and the asymmetry factor for this peak is 1.8. The plate height increases only slightly from the operator-entered value of 0.38 mm to 0.50 mm. The retention volume for this peak is 45.1 mL.

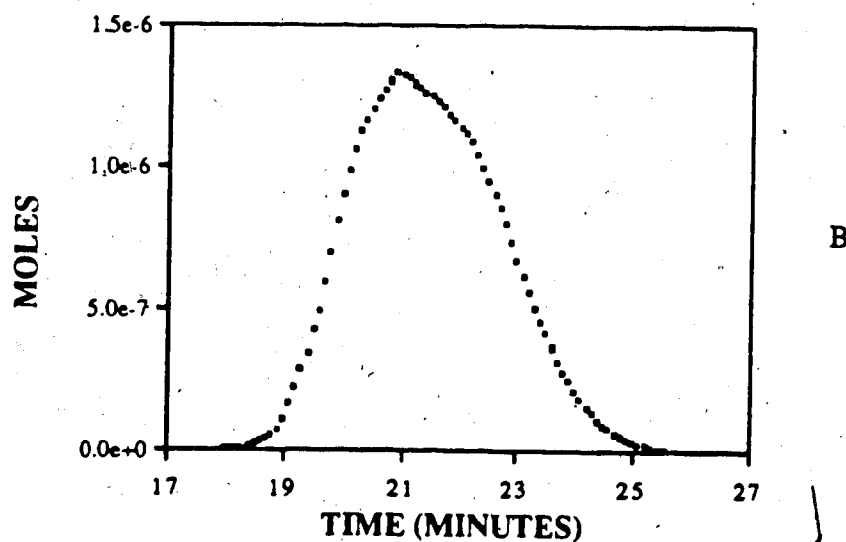
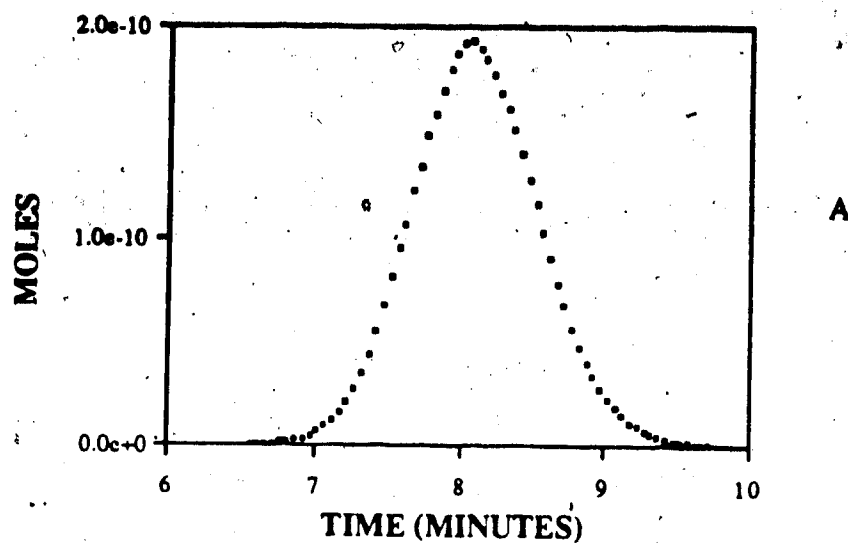


Figure 4.6 Simulated peaks calculated using (A) a linear fit to the (slightly convex) experimental naphthalene data with K_i equal to 16.72 liter per kg and (B) a non-linear Langmuir adsorption isotherm (Langmuir isotherm constants were listed in Figure 4.5). The other parameters used in this calculation are given in Table A2.1 in Appendix II.

Table 4.1 Chromatographic parameters measured for the simulated naphthalene elution peak and theoretical values expected for a linear, non-ideal peak. A linear adsorption isotherm and a plug-shaped injection profile were used. The program variables used to calculate the simulated peak are listed in Table A2.1, Appendix II.

Parameter	Peak		% Difference
	Simulated	Theoretical	
Retention Volume	17.0 mL	15.3 mL	11.1
Capacity Factor	12.1	10.8	12.0
Plate Height	0.42 mm	0.38 mm	10.5
Asymmetry Factor	1.1	1.0	10.0

The theoretical chromatographic parameters were calculated using the following equations :

$$k_i' = K_i \phi$$

$$V_R = k_i' \overline{V_m} + V_m$$

H was measured to be 0.38 mm from an elution chromatogram on PRP-1, K_i was measured to be 16.72 l per kg from the naphthalene adsorption isotherm (assuming a linear least squares fit), and the column $\overline{V_m}$ (1.3×10^{-3} liter) was taken from Table I in reference 4.21.

All computing was done on a Apple Macintosh microcomputer using Microsoft Fortran. Calculations for each simulated chromatogram took between 30 and 45 minutes.

4.2 Results and Discussion

4.2.1 Precolumn Hold-up Volume Determination

The precolumn equilibration method measures the total moles of sample contained within the extracolumn volume as well as adsorbed sample. The quantity of sample which is not adsorbed must be measured and subtracted from the total. The term V_m' will be used to describe the hold-up volume which contains unadsorbed sample. This quantity includes the interparticle and pore volume, the hold-up volume in the frits, inlet and outlet s.s. tubing and the small volume present in the injection valve. An unretained compound, calcium nitrate, was used to measure V_m' .

Before the hold-up volume measurement was done, it was necessary to determine the volume of calcium nitrate solution required to achieve equilibrium between influent calcium nitrate solution and the precolumn. These results are listed in Table 4.2 and it can be seen that 4.7 mL of solution are sufficient for this. V_m' is constant for the three calcium nitrate solution volumes tested, which ranged from 4.7 mL to 23.0 mL. A volume of 15.2 mL was used to be certain.

Two experiments were run to confirm that the nitrate ion of calcium nitrate was truly unretained and could give an accurate value for V_m' . First, the hold-up volume was measured using calcium nitrate solutions of decreasing methanol content. If calcium nitrate was not adsorbed then V_m' should remain constant and not change with % methanol in the mobile phase. The results for this experiment are listed in Table 4.3. It can be seen that V_m' remains constant for the range of methanol content which was studied.

Table 4.2 Volume of calcium nitrate solution pumped through the PRP-1 precolumn vs V_m' . Solution was 4.99×10^{-3} M calcium nitrate.

Volume of calcium nitrate (mL)	Average V_m' (mL)	\pm 95% Confidence Limits
4.7	0.43	0.05
11.6	0.42	0.01
23.0	0.43	0.13

Table 4.3 V_m' vs % methanol. Unretained sample was 4.99×10^{-3} M calcium nitrate dissolved in various methanol - water mixtures. Mobile phases from pump P2 were the same methanol - water solutions that the sample was dissolved in. The stationary phase was PRP-1. The experiments using 90% and 100% methanol(aq) mobile phases were done in duplicate. All others were a single measurement.

% Methanol	Average V_m' (mL)	± 95 % Confidence Limits (mL)	Standard Deviation
100	0.42	0.06	0.0071
90	0.42	0.13	0.014
80	0.40	-----	-----
75	0.42	-----	-----
70	0.40	-----	-----
60	0.41	-----	-----
50	0.40	-----	-----

The value of V_m' was also measured for solutions of increasing calcium nitrate concentration. It has been demonstrated that adsorption of ionic species onto polystyrene-divinylbenzene copolymers is dependent on ionic strength. If calcium nitrate was slightly retained, the retention should increase with increasing ionic strength and increasing concentration of calcium nitrate. These results are given in Table 4.4. The slight decrease in V_m' with increasing calcium nitrate concentration is not statistically significant, as can be seen by noting the 95% confidence limits. This indicates nitrate is unretained under these conditions.

A solution of 2.14×10^{-3} M calcium nitrate in 90% methanol(aq) was chosen to measure V_m' . This concentration gave a suitable absorbance for the final diluted solutions when read on the UV-visible spectrophotometer. The hold-up volume was calculated using Equation 4.12.

$$V_m' = \frac{n_{vm'}}{[Ca(NO_3)_2]_{initial}} \quad 4.12$$

The term $n_{vm'}$ is the number of moles of calcium nitrate in the hold-up volume, as determined in this experiment. The denominator is the concentration of the original calcium nitrate solution (2.14×10^{-3} M) pumped through the precolumn. The value obtained for V_m' was 0.40 ± 0.01 mL (95% confidence limits).

4.2.2 Naphthalene Adsorption Isotherm

Before the adsorption isotherm could be measured, it was necessary to determine the time needed for the naphthalene solutions to reach equilibrium with the PRP-1. A low solution concentration of 4.93×10^{-7} M and a high concentration of 1.02×10^{-3} M were used for this experiment. For both solutions equilibrium times of 6 and 10 minutes

Table 4.4 V_m vs calcium nitrate concentration. Mobile phase was 90% methanol(aq) and stationary phase was PRP-1.

Solution \ Concentration (moles / L)	Average V_m (mL)	\pm 95% Confidence Limits (mL)	Standard Deviation
7.0595×10^{-4}	0.45	0.26	0.028
1.0085×10^{-3}	0.44	0.15	0.017
2.5212×10^{-3}	0.42	0.03	0.0035
5.0425×10^{-3}	0.41	0.01	0.0008
7.0595×10^{-3}	0.42	0.038	0.0042
1.0085×10^{-2}	0.41	0	0

were tested using a flow rate of 1.9 mL per minute. Six minutes was chosen to be the lower value because this was the time it took for the naphthalene peak to elute from the analytical column used in the isotherm experiment. Hence, while one peak was eluting, the next sample could be equilibrating on the precolumn. The peak areas obtained for these equilibration times are given in Table 4.5 where it can be seen that both solutions are at equilibrium within 6 minutes; therefore, this was the time used for the isotherm measurements. Table 4.6 gives the results of the adsorption isotherm for naphthalene on PRP-1 in 90% methanol(aq). The entire concentration range of the isotherm is plotted in Figure 4.7a. There is an additional data point at a C_m of 5.06×10^{-7} M which cannot be seen in Figure 4.7a. The dashed line is the extrapolated isotherm obtained from the points in the linear region at low solution concentrations. The isotherm results for the low solution concentrations are shown in Figure 4.7b. It can be seen from these plots that the isotherm is linear up to a concentration of about 4×10^{-5} M, after which the isotherm deviates perceptibly from linearity. The slope of the 5 data points in the linear region was 18.4 ± 0.6 liters per kg (95% confidence limits).

The linear sample capacity will be defined as the concentration at which K_1 decreases by 10% from its constant value in the linear region. The percent surface coverage of PRP-1 is the fraction of available surface area that is occupied by the naphthalene. The percent coverage at the linear sample capacity can be calculated as follows.

The linear sample capacity of PRP-1 occurred at a mobile phase concentration (C_m) of 9.9×10^{-5} M. The corresponding stationary phase concentration (C_s) is 1.66×10^{-6} moles per gram of PRP-1. Since 0.625 grams of PRP-1 were used, there were 1.02×10^{-6} moles or 6.2×10^{17} molecules of naphthalene. Assuming the area occupied by one naphthalene molecule (8.6×10^{-19} square meters) is twice that of benzene [4.21], this gives 0.53 square meters for the total area of naphthalene. The PRP-1 surface area is the weight of PRP-1 multiplied by the specific surface area (415 square

Table 4.5 Naphthalene peak area vs equilibration time on PRP-1 precolumn. Flow rate = 1.9 mL per minute.

Solution concn (moles / L.)	Equilibration Time (minutes)	Average Peak Area (counts)	± 95% Confidence Limits
4.93×10^{-7}	6	11,059	672
	10	10,770	442
1.02×10^{-3}	6	305,614	1492
	10	307,194	872

Table 4.6 Naphthalene adsorption isotherm results. The parameter n_T is the total number of moles of solute in PRP-1 precolumn before subtraction of moles present in V_m hold-up volume. C_s was calculated using Equation 4.7.

C_m (moles / L)	n_T (moles)	Standard Deviation for n_T	C_s (moles / kg)	Overall Absolute Standard Deviation for C_s
5.06×10^{-7}	9.0×10^{-10}	5.8×10^{-12}	9.7×10^{-6}	8.5×10^{-7}
9.87×10^{-7}	1.7×10^{-9}	4.9×10^{-11}	1.8×10^{-5}	9.2×10^{-7}
2.57×10^{-6}	4.1×10^{-9}	3.3×10^{-11}	5.3×10^{-5}	1.4×10^{-6}
7.90×10^{-6}	1.26×10^{-8}	5.4×10^{-12}	1.5×10^{-4}	3.3×10^{-6}
2.57×10^{-5}	4.0×10^{-8}	3.8×10^{-11}	4.7×10^{-4}	1.0×10^{-5}
9.87×10^{-5}	1.42×10^{-7}	1.7×10^{-10}	1.7×10^{-3}	3.6×10^{-5}

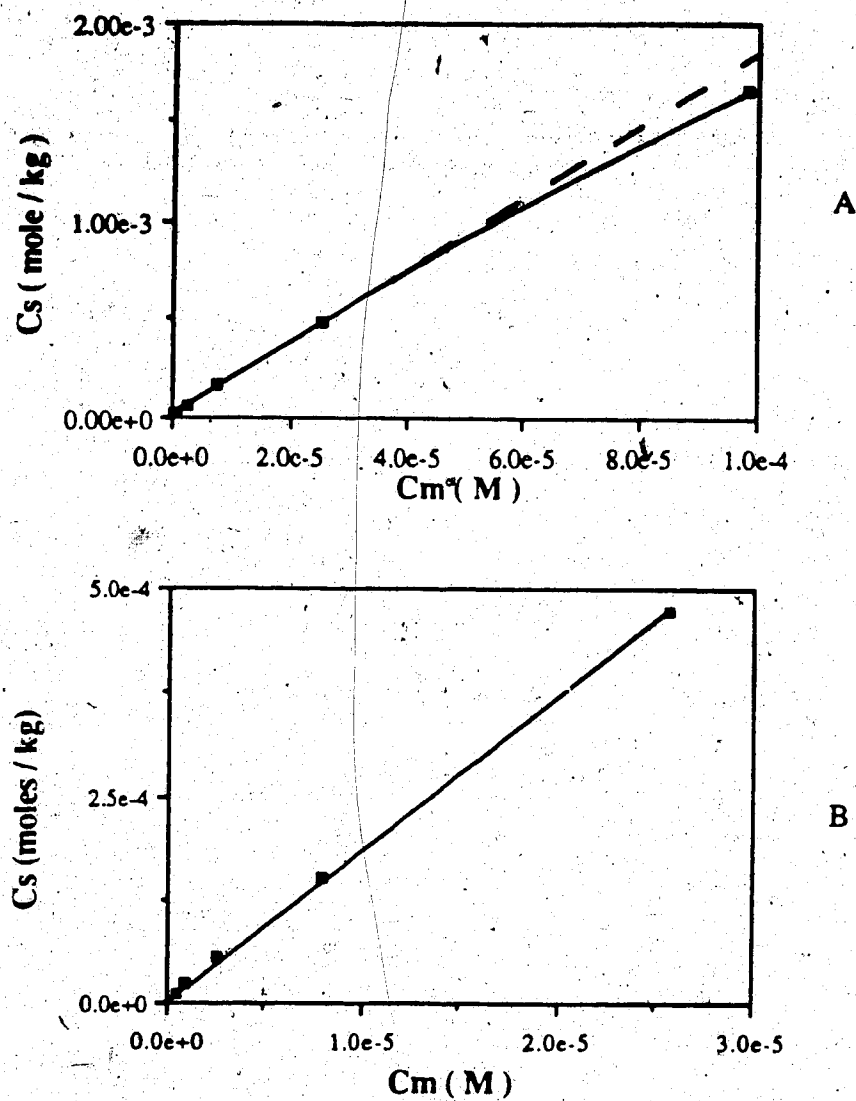


Figure 4.7 (a) Naphthalene - 90% methanol(aq) isotherm on PRP-1. The dashed line indicates the slope of the isotherm extrapolated from the linear region. (b) Lowest solution concentrations which make up the linear isotherm region.

meters per gram) and is equal to 259 square meters. The percent PRP-1 surface coverage at the linear sample capacity can be calculated using equation 4.13 and was found to be 0.2% .

$$\% \text{ coverage} = \frac{\text{total naphthalene surface area}}{\text{PRP-1 surface area}} \times 100 \quad 4.13$$

In order to compare elution peak shape with the isotherm results naphthalene elution chromatograms were run at various concentrations. Also, since the isotherm showed some curvature at higher naphthalene concentrations, peak simulations were done to determine what effect this would have on peak shape. The simulation results are discussed in Section 4.2.4.

4.2.3 Comparison of Results from Elution Chromatograms to Results Predicted from the Adsorption Isotherm

Since the adsorption isotherm was linear up to an equilibrium mobile phase concentration (C_m) of about 4×10^{-5} M, a solution which has equilibrium concentrations lower than this should produce a peak which has no asymmetry or bandbroadening due to isotherm curvature. In order to be able to compare the elution chromatograms with the isotherm results, a relation between the injected solution concentration (C_{inj}) and the equilibrium mobile phase concentration (C_m) was derived. The sample solution is at its highest concentration when it is first injected onto the column because the sample band becomes diluted during migration down the column due to bandbroadening. If the initial solution concentration corresponds to a C_m value in the linear region then the peak shape should not be influenced by non-linearity at any point on the column.

The Langmuir adsorption isotherm equation was rearranged into the form of a second order polynomial which is given in equation 4.14.

$$0 = \left(\frac{B}{V_{m,o}} \right) n_m^2 + \left(1 + \frac{W_{s,o} B A}{V_{m,o}} - \frac{B n_{inj}}{V_{m,o}} \right) n_m - (n_{inj}) \quad 4.14$$

The variables in equation 4.14 are calculated as follows. First, the phase ratio which the injected slug of naphthalene encounters must be determined. Twenty-five microliters of naphthalene were injected onto the PRP-1 column for each elution chromatogram. This volume corresponds to the mobile phase contained in the column positions, as explained in Appendix I. Presumably, this displaced 25 microliters of mobile phase from the bed void volume in the initial portion of the column ($V_{m,o}$). The weight of stationary phase ($W_{s,o}$) that the naphthalene initially encounters can be calculated by knowing what weight of stationary phase corresponds to a void volume of 25 microliters. First, the length of the packed bed of stationary phase which would contain this void volume is calculated.

$$L_o = \frac{V_{m,o}}{0.66 \pi r^2} \quad 4.15$$

The constant, 0.66, is the fraction of the empty column geometric volume which is occupied by interparticle and pore mobile phase and r is the radius of the column. The length is used to calculate the geometric column volume required to contain $V_{m,o}$ and $W_{s,o}$.

$$V_{\text{geometric}} = \pi L_o r^2 \quad 4.16$$

$W_{s,o}$ is calculated by multiplying the geometric volume by the packing density, which is 0.42 grams per cubic centimeter for PRP-1 [4.21].

$$W_{s,o} = \rho_{\text{packing}} V_{\text{geometric}} \quad 4.17$$

The number of moles injected (n_{inj}) is calculated by multiplying the injected naphthalene solution concentration (C_{inj}) by the 25 microliter volume which was injected (V_{inj}).

$$n_{inj} = C_{inj} V_{inj} \quad 4.18$$

The A and B terms in equation 4.14 are the empirical coefficients for the Langmuir isotherm equation. Once all of these values are substituted into equation 4.14, the number of moles present in the mobile phase at equilibrium (n_m) can be calculated using the quadratic formula to solve equation 4.14. The mobile phase equilibrium concentration, C_m , is calculated by dividing n_m by the injected volume of solution.

$$C_m = \frac{n_m}{V_{inj}} \quad 4.19$$

The derivation for equation 4.14 is given in Appendix I, Section A.3.3.

Using this method C_m values for several different C_{inj} values were calculated and are listed in Table 4.7 along with the corresponding C_{inj} values. Since the linear region of the naphthalene adsorption isotherm extends to a C_m of about 4×10^{-5} M, injected solutions with C_{inj} less than approximately 5.2×10^{-4} M would be in the linear region and there should be no peak asymmetry due to isotherm curvature. Above this concentration, some peak asymmetry is expected.

Elution chromatograms were run on four solutions ranging in concentration, C_{inj} , from 5×10^{-5} M to 1×10^{-3} M. Various chromatographic parameters were measured, such as retention volume, plate height and asymmetry factor. All the results shown in

Table 4.7 Naphthalene injected solution concentrations (C_{inj}) and the corresponding mobile phase equilibrium concentration (C_m) at the top of the column.

The C_{inj} and C_m values above the dashed line are in the linear region of the isotherm and the C_{inj} and C_m value below the dashed line is in a curved region of the isotherm.

Shape of Isotherm	C_{inj}	C_m
Linear	5.2×10^{-5}	4.0×10^{-6}
	1.0×10^{-4}	7.9×10^{-6}
	2.0×10^{-4}	1.5×10^{-5}
	3.0×10^{-4}	2.3×10^{-5}
	4.0×10^{-4}	3.1×10^{-5}
	5.2×10^{-4}	4.0×10^{-5}
<hr/>		
Curved	1.3×10^{-3}	1.0×10^{-4}

Figures 4.8 through 4.10 are the average of duplicate chromatograms. The predicted behavior is as follows. In the linear isotherm region the retention volume is expected to remain constant and the asymmetry factor should be equal to 1.0, indicating a perfectly symmetrical peak, neglecting any abnormal non-ideal phenomena which may skew the peak. Once the linear region of the naphthalene isotherm is exceeded, the retention volume should start decreasing and the asymmetry factor should increase as the peaks began to tail, since the adsorption isotherm is slightly convex. The plate height may start to increase slightly, due to the increasing peak asymmetry.

A plot of experimentally observed retention volume vs injected naphthalene concentration, C_{inj} , is given in Figure 4.8. The retention volume for the two lowest solutions is approximately constant and it decreases by 10% for the two high concentration solutions. The slight curvature of the isotherm could be responsible for the decrease in V_r for the highest concentration solution, but the three lower concentration solutions are all in the linear isotherm region and should have a constant V_r . Figure 4.9 gives the experimental asymmetry factor vs concentration. The asymmetry factor increases from 2.6 to greater than 3. Once again, the slight isotherm curvature could be responsible for the peak asymmetry of the highest solution concentration but based on the isotherm results, the three lower concentration solutions should be symmetrical peaks with a constant asymmetry factor of 1.0. Instead, even for the three low concentration solutions which are in the linear part of the isotherm, the asymmetry factor is very large. This peak asymmetry cannot be due to isotherm curvature.

Figure 4.10 shows experimental plate height vs injected naphthalene concentration, C_{inj} . The plate height would be somewhat larger for asymmetric peaks, so some increase in H could be expected for the highest concentration solution. However, the notable point about this figure is that the plate height is very large for all solution concentrations (H is greater than 2 mm). Again, this cannot be the result of isotherm curvature.

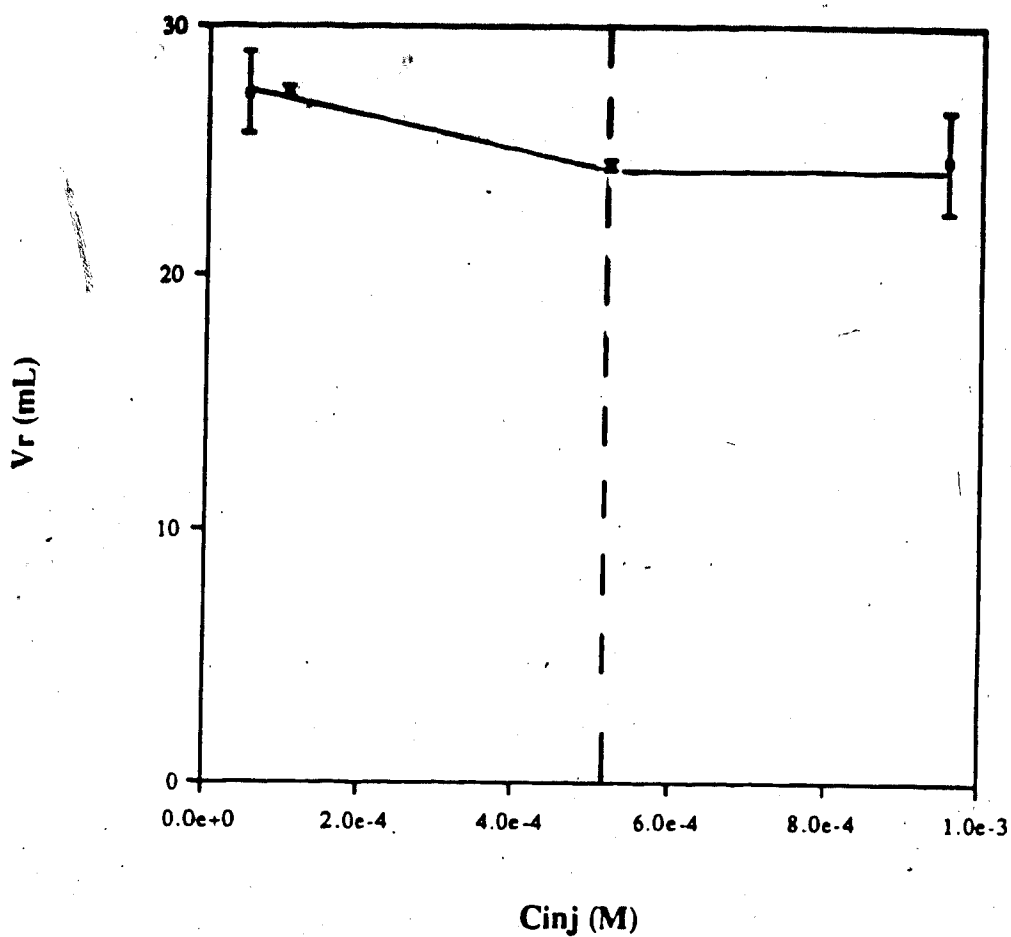


Figure 4.8 Retention volume vs injected naphthalene concentration on PRP-1. The mobile phase was 90% methanol(aq) and the mobile phase linear velocity was 0.35 cm per second. The retention volume was measured using the peak center of gravity. The data points to the left of and on the vertical dashed line are in the linear region of the naphthalene isotherm and the point to the right of the dashed line is in the slightly convex portion of the isotherm.

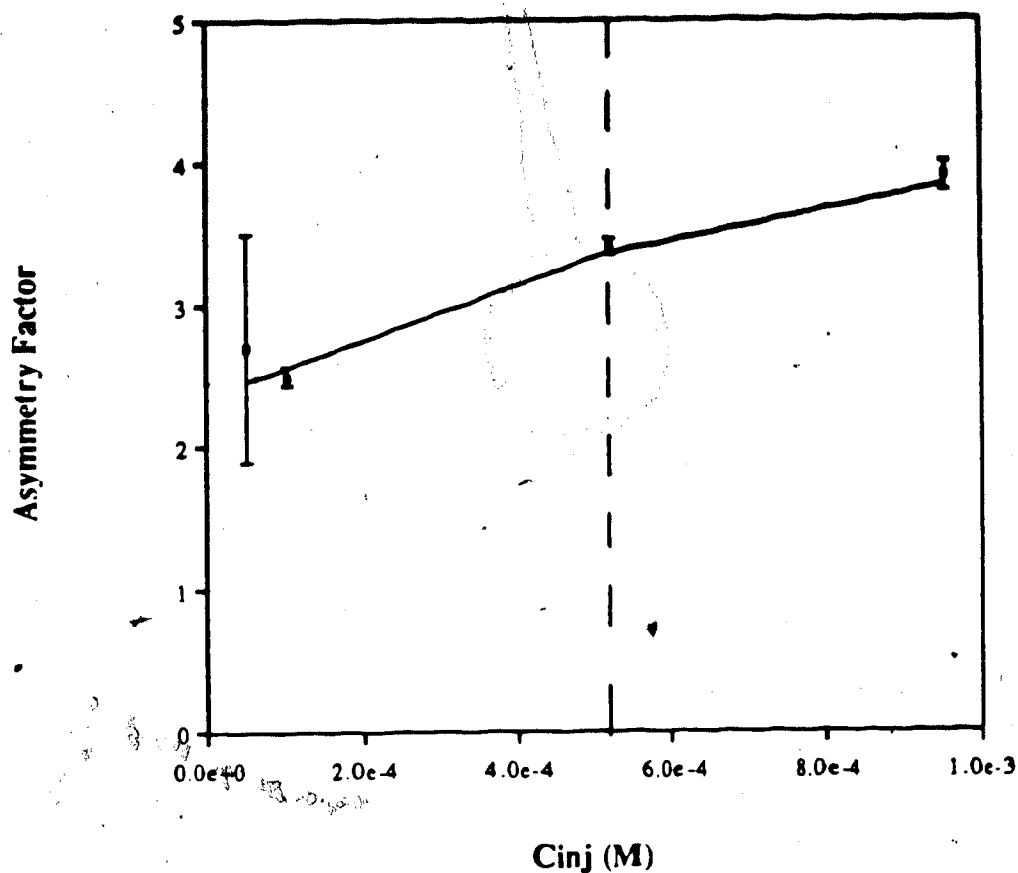


Figure 4.9 Asymmetry factor vs injected naphthalene concentration on PRP-1. The mobile phase used was 90% methanol(aq) and the mobile phase linear velocity was 0.35 cm per second. The data points to the left of and on the vertical dashed line are in the linear region of the naphthalene isotherm and the point to the right of the dashed line is in the slightly convex portion of the isotherm.

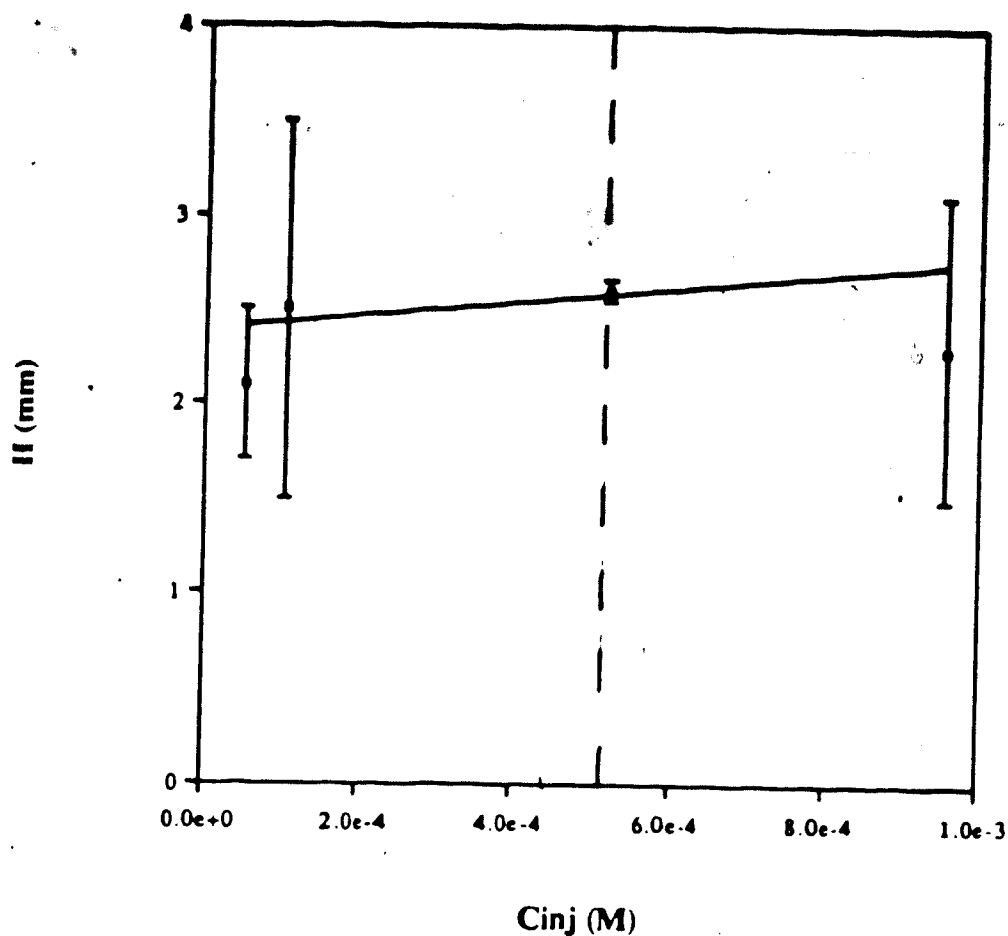


Figure 4.10 Plate height vs injected naphthalene concentration on PRP-1. The mobile phase used was 90% methanol(aq) and the mobile phase linear velocity was 0.35 cm per second. The data points to the left of and on the vertical dashed line are in the linear region of the naphthalene isotherm and the point to the right of the dashed line is in the slightly convex portion of the isotherm.

The conclusion which can be drawn from this experiment is that solutions which are in the linear part of the isotherm show excessive bandbroadening and peak asymmetry. Therefore, these effects are not due to isotherm curvature.

4.2.4 Simulation of Peak Shape Due to Isotherm Curvature

The simulation program described in Section 4.1.3 was used to calculate an elution peak for naphthalene using the experimental adsorption isotherm. The isotherm was fitted the Langmuir isotherm equation. The coefficients for the isotherm equation are listed in Table A2.2 in Appendix II. Other parameters used in the simulation, such as column dimensions and mobile phase linear velocity, are also listed there.

A column plate height of 0.038 cm was used to calculate the Gaussian function for the simulation. The rationale for choosing this value was explained in Section 4.1.3. All other parameters were the same as those used in the experimental elution chromatograms.

The simulated elution peak for a 1.0×10^{-4} M naphthalene solution is shown in Figure 4.11 and the chromatographic parameters measured from this simulated peak are given in Table 4.8. The chromatographic results for a real elution peak resulting from the same injected concentration are also listed in Table 4.8. The retention volume for the simulated peak may differ from the experimental V_R for several reasons. One source of error is that the exact weight of stationary phase was unknown and was estimated using the average packing density of PRP-1. Also, the interparticle and pore void volumes (V_m) were not measured but were taken from reference 4.21. If there was a 10% error in either the packing density or V_m there would be a 10% error in k'_i and V_R . A third source of error is the measurement of retention volume on the experimental elution peaks using moment analysis. Since the elution peaks are asymmetrical, it can be difficult to

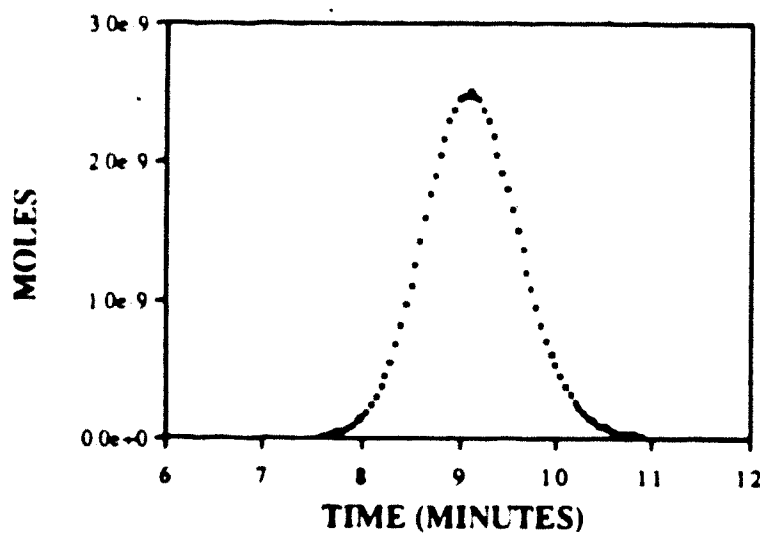
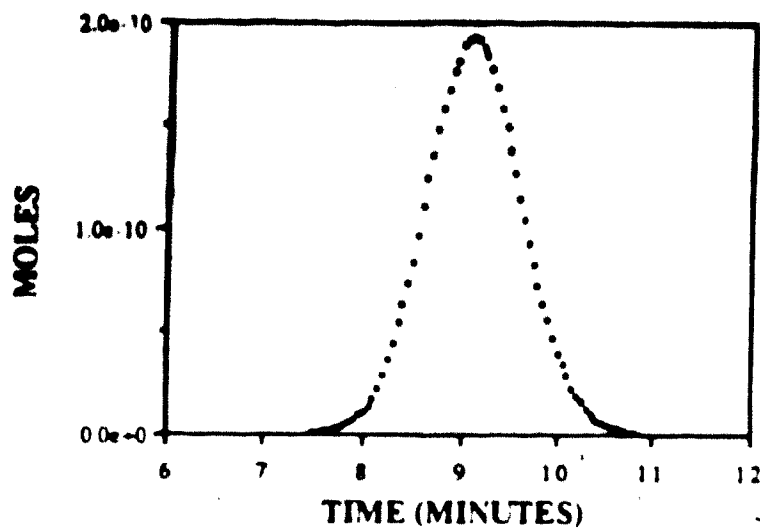


Figure 4.11 Results of the peak simulation program for injected concentrations of (a) 1.0×10^{-4} M naphthalene and (b) 1.3×10^{-3} M naphthalene. The isotherm equation was fitted by the Langmuir equation with isotherm constants of $A = 0.11925$ mole per kg and $B = 159.8$ liter per mole. The other parameters used in the peak simulations are listed in Table A2.2 of Appendix II.

Table 4.8 Comparison of simulated peak results with experimental chromatographic results for two naphthalene solution concentrations. The experimental parameters for the $C_{inj} = 1.3 \times 10^{-3}$ M solution were actually measured on a solution whose $C_{inj} = 9.6 \times 10^{-4}$ M.

Result	C_{inj}	
	1.0×10^{-4} M	1.3×10^{-3} M
V_r (mLs)		
simulated	19.2	19.2
experimental	27.7	24.6
H (mm)		
simulated	0.41	0.42
experimental	2.5	2.3
Asymmetry factor		
simulated	1.1	1.1
experimental	2.7	3.9

decide when the peak has actually ended and this would cause errors in the estimation of V_T and plate height for the experimental elution chromatograms.

However, the most likely explanation for the difference is that abnormal non-ideal processes are not negligible and are contributing significantly to the naphthalene retention volume, plate height and asymmetry factor.

A simulated peak was also calculated for a 1.3×10^{-3} M naphthalene solution and it is shown in Figure 4.11b. This concentration was selected because this value of C_{inj} corresponded to the maximum C_m value measured on the isotherm. At this value of C_m the isotherm deviates from linearity by about ten percent and it was of interest to see what effect this curvature would be predicted to have on peak shape. The chromatographic parameters measured on the simulated peak are listed in Table 4.8. Chromatographic parameters which were measured for an experimental peak of a similar injected concentration (9.6×10^{-4} M) are also listed for a comparison. Once again, the simulated peak is much narrower and symmetric than the experimental elution peak, suggesting non-ideality is responsible for the bandbroadening.

Plate heights were measured on both of the simulated elution chromatograms by moments analysis and found to be about 0.4 mm for both naphthalene concentrations. The asymmetry factors were measured for both simulated peaks and were found to be 1.1. A symmetrical peak would have a value of 1.0. Whether the slight increase in H compared to the input value of 0.38 mm and the slight asymmetry of the peak can be attributed to the slight non-linearity of the isotherm is uncertain since similar "errors" were found in the simulation using a linear isotherm, as a result of the discrete nature of the simulation, as discussed in Section 4.1.3.

The shape of the injected slug of naphthalene solution in these two naphthalene peak simulations was a square wave with the sample evenly distributed into three column positions. This injection shape may not be an accurate model of the real injection profile, which can have an exponential shape, with the highest concentration at the front and the

concentration decreasing toward the back of the profile. An asymmetric injection profile may skew the final elution peak shape, even if the isotherm is linear. To see if there was a significant contribution to elution peak asymmetry from the injection profile, two non-uniform injection shapes were used in the simulation program. The shapes of these injection profiles are shown in Figure 4.12.

The simulated elution peaks in Figure 4.13 were produced using an increasing ramp shaped injection profile, as shown in Figure 4.12b. The lowest concentration was placed in column position 1 in the simulation program and the highest concentration was in column position 3. The concentration in position 1 was 10^{-5} M, position 2 was 2.7×10^{-5} M and position 3 was 10^{-4} M. Simulated elution peak shapes were calculated using both a linear isotherm and the Langmuir isotherm equation. All parameters used in both of these simulations are listed in Table A2.5 in Appendix II. The simulated peaks in Figure 4.14 result from a decreasing ramp injection, Figure 4.12c, which had the concentration in position 1 equal to 10^{-4} M, position 2 was 2.7×10^{-5} M and position 3 was 10^{-5} M.

Table 4.9 gives the retention volume, plate height and asymmetry factor for the simulated peaks which were calculated using the two asymmetric injection profiles, as well as the chromatographic parameters for the simulated peaks which had a uniform, square wave injection profile, as shown in Figure 4.12a. It can be seen that there is little difference between the results, indicating the injection profile has a negligible effect on the naphthalene elution peak shape. The V_r values are different between the simulated peaks for the linear isotherm and the simulated peaks for the Langmuir isotherm because the distribution coefficient for the low C_m solutions of the Langmuir isotherm is larger than the distribution coefficient for the linear isotherm. If these two distribution coefficients were equal, the retention volumes would be equal.

This simulation program could be very useful for predicting elution peak shapes which result from adsorption isotherm curvature. The program is relatively fast and can

Concentration

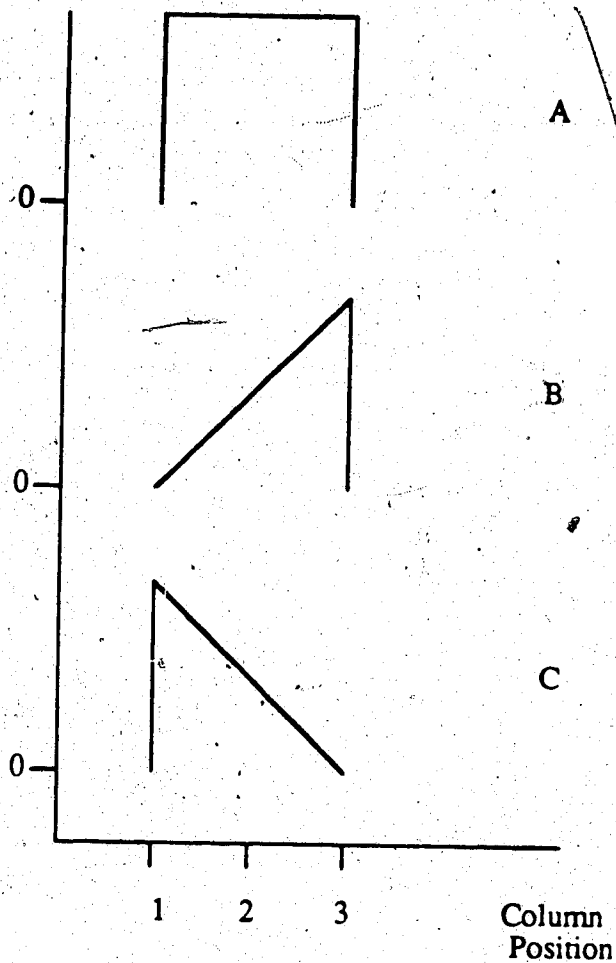


Figure 4.12 Injection profiles used with the peak simulation program. (A) uniform square wave (B) increasing ramp and (C) decreasing ramp.

Table 4.9 Elution peak simulation results for 10^{-4} M naphthalene on PRP-1. The isotherm equation was fit to either a linear equation or the Langmuir equation. The injection profile was either a uniform square wave, an increasing ramp or a decreasing ramp shape (see Figure 4.12 for a diagram of these shapes). Other parameters used in the simulation calculations are listed in Table A2.2 in Appendix II.

Result	Isotherm Equation	
	Linear	Langmuir
Retention Volume (mLs)		
Square wave injection	17.0	19.2
Increasing ramp injection	17.1	19.3
Decreasing ramp injection	17.0	18.8
Plate Height (mm)		
Square wave injection	0.42	0.41
Increasing ramp injection	0.42	0.40
Decreasing ramp injection	0.42	0.40
Asymmetry Factor		
Square wave injection	1.1	1.1
Increasing ramp injection	1.1	1.1
Decreasing ramp injection	1.1	1.1

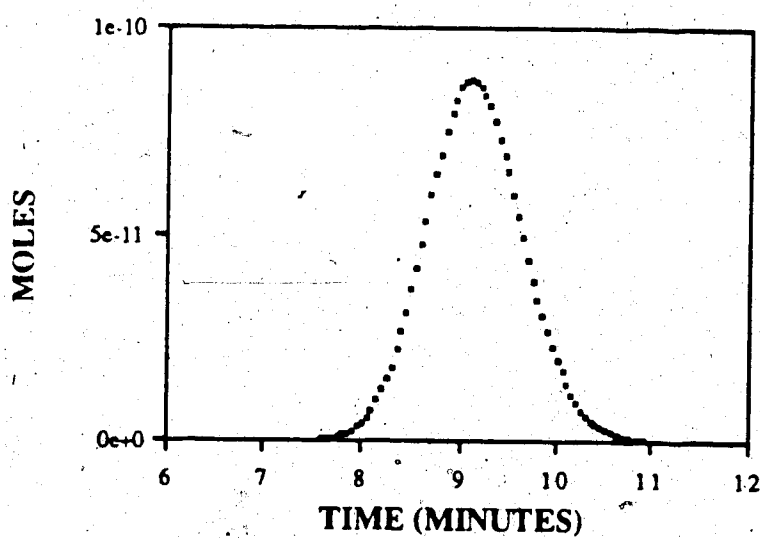
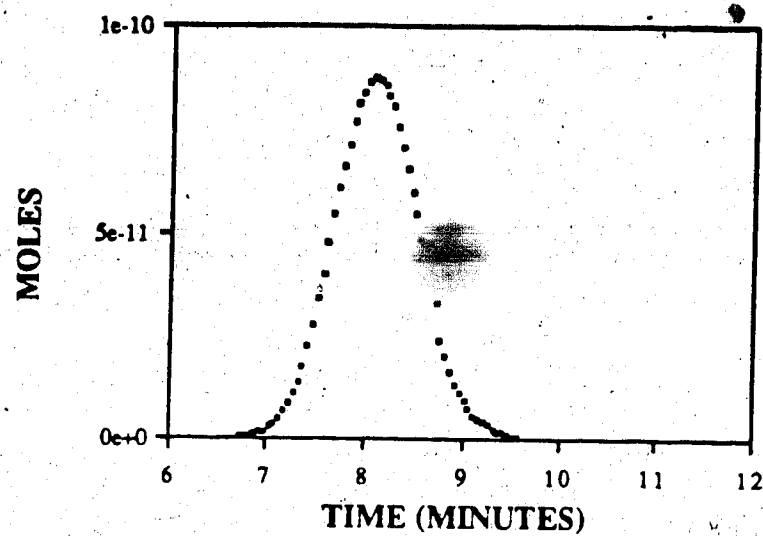


Figure 4.13 Peak simulation results using a (a) linear isotherm equation and (b) Langmuir isotherm equation for naphthalene on PRP-1. An increasing ramp injection profile was used and the injected naphthalene concentration was 1.0×10^{-4} M. Other parameters used in the simulation calculation are listed in Table A2.3 of Appendix II.

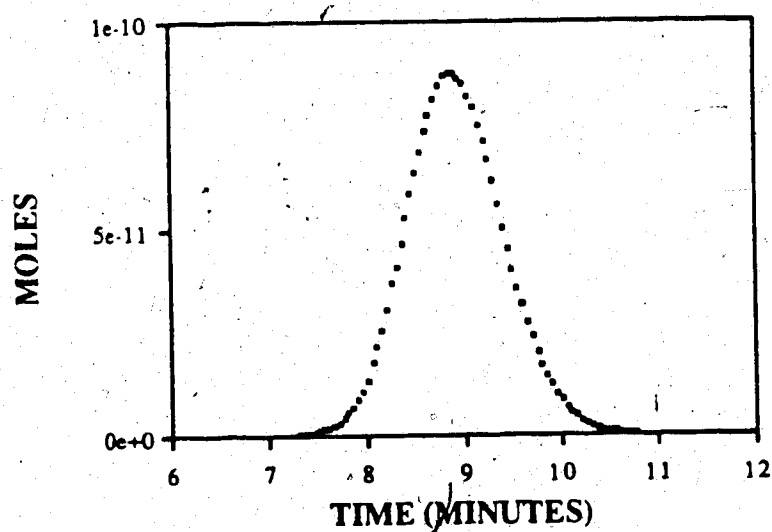
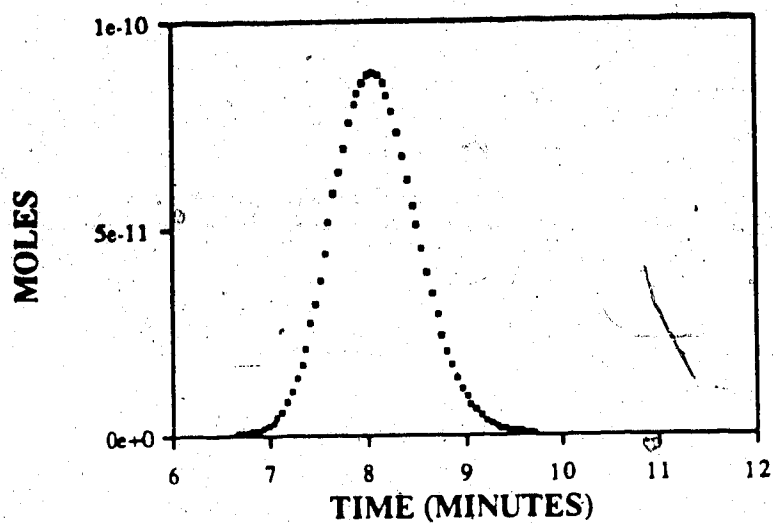


Figure 4.14 Peak simulation results using (a) linear isotherm equation and (b) Langmuir isotherm equation for naphthalene on PRP-1. A decreasing ramp injection profile was used and the injected naphthalene concentration was 1.0×10^{-4} M. Other parameters used in the simulation calculation are listed in Table A2.3 of Appendix II.

be run on small microcomputers. It is based on simple physical concepts of incremental sample movement down a chromatography column with each movement followed by bandbroadening.

When the program was used to predict naphthalene elution peaks from the experimental isotherm data, it was found that no peak asymmetry should occur even for the solution concentrations which fall in the slightly curved portion of the isotherm.

4.3 Conclusions

The purpose of the experiments discussed in this chapter was to determine if a non-linear adsorption isotherm was responsible for the asymmetric elution peak shape observed with PRP-1.

First, the adsorption isotherm of naphthalene in 90% methanol(aq) on PRP-1 was found to deviate only slightly from linearity at the highest solution concentrations used. The distribution coefficient (16.8 liters per kg) for the highest concentration solution was 9% smaller than the distribution coefficient of the linear region (18.4 liters per kg).

Elution chromatograms were run for various naphthalene concentrations in order to compare the chromatographic results with those predicted by the isotherm. It was found the elution peaks were very broad and asymmetrical even in the linear region of the isotherm. This asymmetry could not be caused by isotherm curvature.

A program was developed which simulated elution peaks by calculating the combined effects of adsorption isotherm non-linearity and column non-ideality. The simulation program is based on simple mathematical operations and is relatively fast, compared to other simulation methods.

The simulation program was used to predict elution peaks which corresponded to solution concentrations in the non-linear section of the naphthalene adsorption isotherm.

Even at these concentrations there should be no significant bandbroadening or asymmetry resulting from adsorption isotherm curvature.

CHAPTER 5

Naphthalene Adsorption - Desorption Kinetics on PRP-1

5.1 Theory

5.1.1 Kinetic Processes in Chromatography

The term "adsorption - desorption" kinetics will be defined to include several processes involved in the immobilization and release of a sample molecule by the stationary phase. Basically, there are three steps leading to adsorption onto a porous stationary phase particle and three for desorption [5.1 - 5.5]. Figure 5.1 shows such a particle and each of these steps [5.6].

Initially, the molecule is in the flowing mobile phase between particles. Almost all adsorption occurs on the inner surfaces of the pores because the majority of the total surface area is contained in the pores. The outer surface of the stationary phase particle is surrounded by a film of mobile phase through which the sample must diffuse to get to the pore surface. This step will be referred to as diffusion across the particle outer film. The rate of diffusion across the film is dependent on the film thickness, the diffusion coefficient of the sample in the mobile phase and the sample concentration gradient [5.6,5.7]. The film thickness decreases with decreasing particle diameter at constant u_0 and the total rate of film diffusion increases with decreasing d_p because of both increased surface area and decreased film thickness.

There is also stagnant mobile phase within the pores. The sample must also diffuse through this in a radial direction toward the center of the particle to encounter fresh pore surfaces. The rate of diffusion through this is dependent upon the particle diameter, the effective diffusion coefficient through the pores and the sample concentration gradient [5.7].

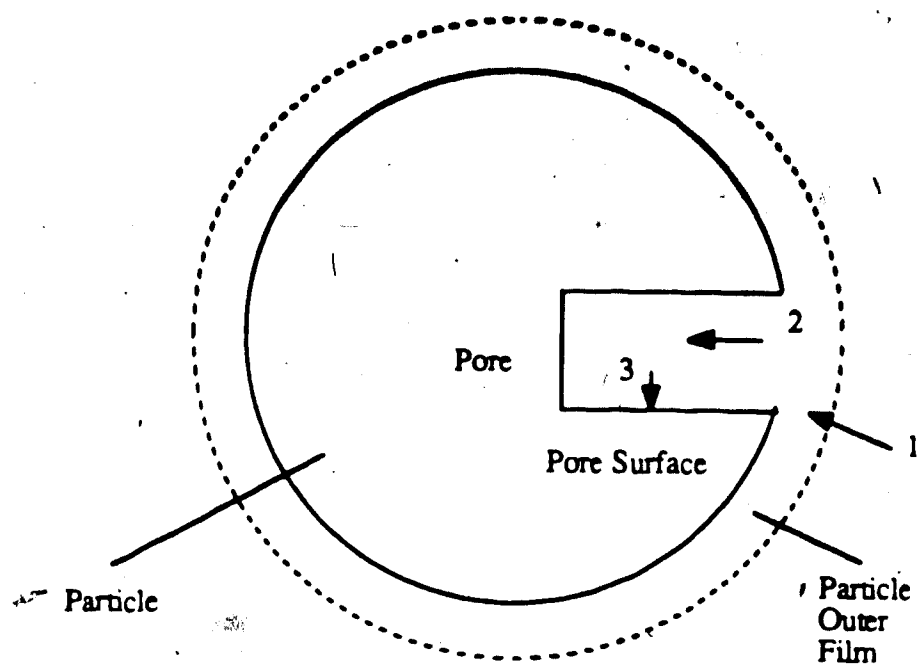


Figure 5.1 Schematic diagram of a spherical stationary phase particle and a pore (pore size is greatly enlarged). Some of the possible steps which can occur in the adsorption-desorption process are shown. (1) Sample diffusion across the film of mobile phase surrounding the outer surface of the particle. (2) Diffusion through the stagnant mobile phase within the pore. (3) Physical adsorption onto the stationary phase surface.

The final step in the adsorption process is adsorption onto the surface of the stationary phase. This step will be referred to as "surface adsorption" (or "surface desorption" in the desorption process) to distinguish it from the overall adsorption process (which includes the diffusion steps). In liquid chromatography, surface adsorption is usually due to Van der Waal forces [5.8], such as dispersion forces or hydrogen bonding, and the rate of surface adsorption is usually quite fast. The rate for a first order surface adsorption step is dependent on the rate constant and the sample concentration in the mobile phase immediately adjacent to the stationary phase. If the surface adsorption reaction can be represented by equation 5.1, then the rate of adsorption is given by equation 5.2.



$$\frac{dC_{i,\text{ads}}}{dt} = k_{\text{ads}} C_{i,\text{soln}} - k_{\text{des}} C_{i,\text{ads}} \quad 5.2$$

The terms $C_{i,\text{soln}}$ and $C_{i,\text{ads}}$ are the sample concentrations in the mobile phase and in the stationary phase. The adsorption and desorption first order rate constants are k_{ads} and k_{des} .

Occasionally, surface adsorption onto the stationary phase surface can involve stronger interactions in which an ionic or covalent bond is formed. This can decrease the rate significantly if a large activation energy is required [5.9]. Additional steps may be involved in adsorption - desorption, such as diffusion into micropores [5.10] or surface diffusion [5.11,5.12], which occurs with some polymer gels.

All three steps occur in the reverse order during the desorption process. If the sample on the stationary phase is desorbing into mobile phase which is free of sample the desorption process is irreversible as shown in equation 5.3.



The rate of this irreversible, first order process is :

$$\frac{dC_{i,ads}}{dt} = -k_{des} C_{i,ads} \quad 5.4$$

For a first order adsorption-desorption process (rate proportional to concentration) the adsorption rate constant is related to the desorption rate constant by a distribution coefficient, K_d , for the process.

$$k_{ads} = K_d k_{des} \quad 5.5$$

The distribution coefficient K_d is unitless and it is related to the distribution coefficient K_i , which was measured in Section 4.2.2, by the density of the PRP-1 matrix, $\rho(\text{PRP-1})$.

$$K_d = \rho(\text{PRP-1}) K_i \quad 5.6$$

The value of $\rho(\text{PRP-1})$ is about 1.07 g per cm^3 [5.13]. The relation between K_i and K_d can be seen by comparing equation 5.7 with equation 5.8. Since K_d is the ratio of the first order rate constants, k_{ads} and k_{des} , K_d must be unitless.

$$K_d = \frac{\left(n_{i,ads} / V_{sp} \right)}{\left(n_{i,soln} / V_m \right)} \quad 5.7$$

Here, $n_{i,ads}$ is the moles of sample i adsorbed on the stationary phase and $n_{i,soln}$ is the moles of i present in the mobile phase. V_{sp} is the volume of the stationary phase solid matrix and V_m is the void volume of the packed bed. V_m is equal to the interparticle volume plus the pore volume. K_i is defined as :

$$K_1 = \frac{(n_{l,ads}/W_s)}{(n_{l,soln}/V_m)}$$

5.8

W_s is the weight of stationary phase. Since K_1 is equal to 18.4 liters per kg, K_d is calculated to be 19.7.

Ideally, all of the steps in the adsorption-desorption process occur fast enough so they do not cause significant bandbroadening. The relation of bandbroadening to slow surface adsorption or slow diffusion through the stagnant mobile phase in the pores was previously discussed in Sections 3.1.4 and 3.1.5. Diffusion through the outer particle film would be described by the k_f' dependent term in the H_m plate height equation which was mentioned in Section 3.1.6. This k_f' dependent term was not discussed in detail because the plate height contribution from this term is usually negligible under normal conditions used in HPLC. Slow kinetic processes lead to non-equilibrium between sample in the mobile and stationary phases and the degree of non-equilibrium increases as the adsorption or desorption rate decreases. The greater the non-equilibrium, the larger the plate height is. Therefore, it is of interest to be able to measure the rates of adsorption and desorption in order to determine the kinetic contribution to H . In the present work, the desorption rate was measured rather than the adsorption rate because experimental conditions could be designed so that the desorption process could be measured under irreversible, first order conditions, which simplified the determination of k_{des} . Also, desorption was a slower process than adsorption for the system being studied, so this minimized the constraints on the operating conditions of the experimental apparatus.

5.1.2 Methods Used to Measure the Rates of Adsorption and Desorption

Both direct and indirect methods have been used for the measurement of adsorption and desorption rates for chromatographic stationary phases [5.14-5.21] Indirect techniques

involve calculation of the rate constants from chromatographic elution peak plate heights and direct methods use non-chromatographic techniques. Indirect methods are more commonly used because of the ease of operation. In order for indirect methods to give accurate values for rate constants, bandbroadening from non-kinetic sources must be negligible or accurately estimated.

Muller and Carr [5.18] used an indirect method to determine the desorption rate constant of carbohydrates in affinity chromatography. The stationary phase in affinity chromatography is an immobilized ligand which retains the sample by a selective interaction. For example, a sample enzyme may be adsorbed by an immobilized substrate. The plate heights in affinity chromatography are often large (1 to 2 mm) and slow desorption from the immobilized ligand is a possible cause. Muller and Carr used equations formulated by Horvath and Lin [5.22] to calculate the desorption rate constant (k_d) from chromatographic plate heights. A value of approximately 0.3 sec^{-1} was obtained for k_d .

In order to determine the slow step in the desorption process they measured the plate heights for both 10 and 50 micrometer particles. Slow diffusion through the stagnant mobile phase or the outer particle surface film is dependent on particle diameter, while slow dissociation from the immobilized ligand is independent of particle size. Their results showed that plate height (H) did increase with increasing particle diameter but not to the extent predicted by Horvath's equations. Based on these results, slow dissociation from the ligand was assumed to be responsible for the slow desorption.

Anderson and Walters [5.19] also used chromatographic plate heights to determine the slow rate step in the same carbohydrate - affinity system used by Muller and Carr. However, they believed Muller and Carr made an incorrect assumption when estimating the plate height contribution from the diffusion processes. Although Anderson and Walters got experimental results similar to those of Muller and Carr, they came to the opposite

conclusion about the slow rate step. They believed that slow diffusion was responsible for the bandbroadening and not dissociation from the ligand.

It is because of these kind of discrepancies that the indirect method for measuring rate constants may not be the best method. In addition, if there are non-kinetic sources of bandbroadening (such as a non-uniform flow profile) and they are incorrectly evaluated, then the rate constant measured by a chromatographic method will be in error.

An example of a rate constant measurement by a direct method is the pressure-jump relaxation kinetics technique used by Marshall and co-workers [5.20]. This was used to obtain the rate of surface adsorption onto a C18 stationary phase. According to their conclusions, the surface adsorption of an ion pair onto the C18 surface was second order and gave a surface adsorption rate constant of 1.4×10^9 liter mole⁻¹ sec⁻¹. As expected they found the surface adsorption a fast process.

A much older study was done by Boyd et al [5.21] to determine the slow kinetic step in ion exchange chromatography. The method they developed will be referred to as the "shallow bed" technique. A very thin layer (approximately three particle diameters thick) of ion exchange resin was placed between two screens in a glass column. The rate of adsorption was determined by passing a solution containing radioactive sample ions through the resin for a predetermined time. A fraction of the sample would adsorb during this time and the amount of adsorbed radioactive sample could be measured. This procedure was repeated for increasing periods of time in order to determine the rate of adsorption. The shallow bed technique was used in a modified form for the work described below.

5.1.3 Shallow Bed Procedure

The shallow bed technique was used in this thesis to measure the rate of desorption of naphthalene from PRP-1. This technique measured a "lumped" rate for desorption,

meaning that this was the overall rate for several steps in the desorption process (both diffusion steps and surface desorption).

The procedure which was described in Section 2.2.4 will be briefly outlined. In the desorption rate experiment a thin layer of PRP-1 was contained within the "s.b.cartridge". Initially, a sample solution consisting of naphthalene dissolved in 90% methanol(aq) flowed through the s.b.cartridge until the PRP-1 was completely equilibrated with the sample, and therefore, a known amount of naphthalene was initially adsorbed on the PRP-1. The bed of stationary phase was then purged with helium to remove excess sample solution. Next, a known volume, V_{inj} , of mobile phase solution was injected and passed through the bed of PRP-1 at a known flow rate, F . The time during which desorption occurred (the contact time, t) was the time during which the mobile phase solution was in contact with the PRP-1 and was calculated using equation 5.9.

$$t = \frac{V_{inj}}{F}$$

5.9

The PRP-1 was purged with helium once again, to remove the majority of the mobile phase present in the void volume. The total moles of sample still adsorbed (n_{ads}) on the column was eluted with a strong solvent and quantified. By repeating this process for various contact times, a plot of n_{ads} vs contact time can be generated. A simulated desorption rate curve is shown in Figure 5.2 to give an impression of the general shape expected for this curve.

The moles remaining adsorbed on the resin were measured rather than the moles desorbed into the mobile phase because there was less error associated with this measurement. This was because the mobile phase exited the s.b.cartridge at a fast flow rate causing some of the solution to splash out of the collection flask at the s.b.cartridge outlet, leading to inaccurate results.

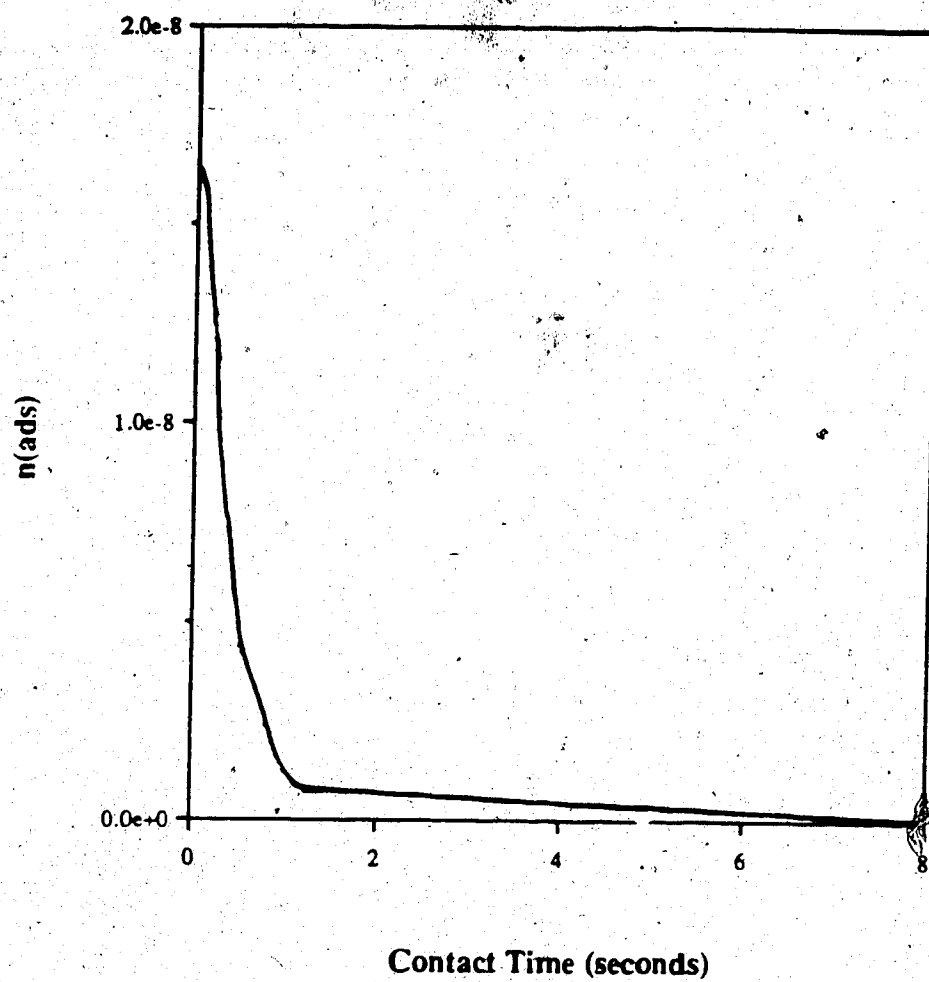


Figure 5.2 Simulated desorption rate curve which would be obtained using the shallow bed technique.

By increasing the sample flow rate and decreasing the length of the adsorbent bed, the measurement of faster desorption rates is possible. Optimizing these two experimental conditions also helps meet another requirement of the shallow bed technique: that the concentration of sample solution in the mobile phase must remain essentially zero as the slug of mobile phase passes through the bed of adsorbent. This is referred to as the "infinite solution volume" or ISV assumption and the error that results from not achieving this condition is discussed in Section 5.3.2. If the ISV assumption is met, the mobile phase solution would encounter every point on the bed at the same time. There would be no sample present in any of the mobile phase and the sample adsorbed on the PRP-1 near the inlet would encounter the same conditions as would sample adsorbed near the outlet. However, if a finite time was required for mobile phase at the inlet to reach the outlet, then sample would have time to desorb into it and the adsorbed sample at the outlet would encounter mobile phase which contained a finite concentration of sample. The concentration gradients between the two phases at the inlet and outlet would be different and so would the rates of desorption. Obviously, the ISV condition is impossible to achieve because sample is desorbing into the mobile phase and, therefore, gives it a non-zero sample concentration. In practice, the ISV condition is met as long as the concentration of sample desorbed into the mobile phase is so low that the observed rate of desorption is equal, within experimental error, to the rate which would be found under truly ISV (i.e. irreversible desorption) conditions. For slower reactions, slower flow rates and longer bed lengths can be tolerated without substantially increasing the error in the measurement.

It is also best to work with a sample concentration in the linear isotherm region because, for a first order desorption reaction, the distribution coefficient is the ratio of the adsorption rate constant to the desorption rate constant (equation 5.10).

$$K_d = \frac{k_{ads}}{k_{des}}$$

If K_d is changing down the length of the bed then the ratio of the two rate constants will also be changing.

A consequence of these requirements of very small sorbent bed and low sample loading is that very small amounts of sample are present on the bed of stationary phase. Detection of these small quantities is difficult. Therefore, the adsorbed sample was eluted by small volumes of strong eluent, in order to facilitate detection.

The experimentally measured desorption rate curve was related to the chromatographic plate height in order to determine if slow kinetic processes were responsible for the excessive bandbroadening observed on PRP-1.

5.2 Results and Discussion

5.2.1 Measurement of Flow Profile

It was necessary for the sample solution to be evenly distributed across the entire PRP-1 bed when it entered the inlet of the s.b. cartridge in order that various portions of the bed will be swept at the same rate.

The s.b. cartridge is shown in Figure 2.4. The bed diameter is 3 mm and the diameter of the outlet and inlet tubing is only 1 mm. This can obviously cause problems as the flow must be spread radially over the larger bed diameter quickly.

The uniformity of the flow profile was determined by injecting 25 μ L of a dye through the PRP-1 s.b. cartridge using the shallow bed apparatus (Figure 2.3). After the injection, the s.b. cartridge was removed from the system and opened. The two frits which held the PRP-1 in place were removed and the bed of PRP-1 was gently extruded. This allowed the dye profile along the outer surfaces of the bed to be examined for uniformity of

dye coloration. After studying the outer surfaces, the bed was sliced open lengthwise and the coloration inside was observed.

This experiment was done first with a 20 micrometer pore diameter inlet frit and a 2 micrometer pore diameter outlet frit. It was thought that perhaps the inlet frit would be sufficient to disperse the flow radially. However, it hardly spread the flow at all, as can be seen by the dye pattern shown in Figure 5.3a. The dye appeared as a small red spot in the center of the PRP-1 bed. Next, the centers of both the inlet and outlet frits (approximately 1 mm in diameter) were pressed partially closed using a hammer and a rod. It was thought that the extra resistance to flow caused by blocking the frit centers would cause the flow stream to move toward the sides. The resulting dye pattern can be seen in Figure 5.3b. Pressing the frit centers had some effect but there was still a large section of the bed which the dye did not encounter. For the next attempt a piece of large mesh screen was placed above the center-pressed frit at the inlet and the experiment was repeated. The dye pattern was slightly better (Figure 5.3c) but still did not completely cover the entire end of the bed. Finally, one more piece of screen was placed at the s.b. cartridge inlet. This resulted in uniform spreading of the dye at the inlet (Figure 5.3d). Slicing open the bed showed that it was uniform throughout the bed. Therefore, this configuration was used for all adsorption and desorption experiments.

5.2.2 Injection Loop Volumes

The volumes of the injection loops had to be measured in order to calculate the contact time using equation 5.9. The procedure used to calibrate the injection loops was described in Section 2.3.6.

The volume of each injection loop (V_{inj}) was calculated by knowing the number of moles collected in the flask and the original solution concentration (equation 5.11).

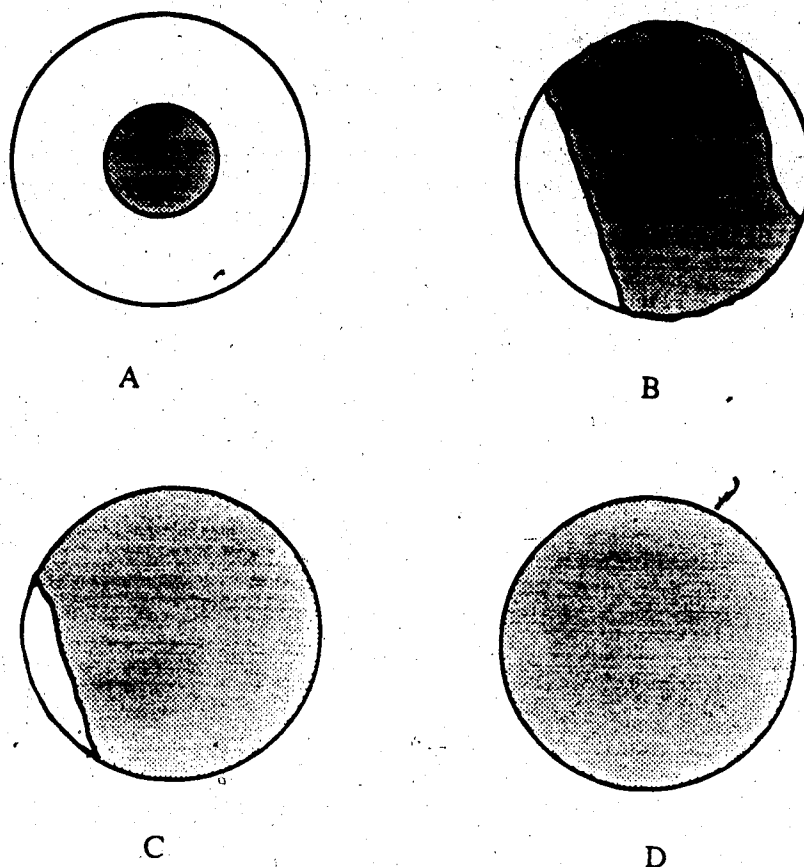


Figure 5.3 Dye patterns observed on the inlet end in the flow profile study. The dye is indicated by the shaded areas. Experimental conditions are: (A) frits only (B) center of frits pressed partially closed (C) 1 piece of large mesh screen at the inlet and center-pressed frits (D) 2 pieces of large mesh screen at the inlet and center-pressed frits. The dye used was 10^{-3}M amaranth and the mobile phase was 90% methanol(aq).

$$V_{inj} = \frac{\text{moles collected in effluent}}{C_{original}}$$

124

The injection loop volumes obtained using both helium and methanol to flush are listed in Table 5.1. The injection volumes obtained using helium were used for the contact times for desorption. These values were chosen because helium was the medium used during the rate experiments. The injection volumes obtained using methanol were consistently larger than those using helium which meant the helium did not flush all the sample from the loop. However, the helium injection volumes were reproducible. The standard deviation of each injection volume was included in the standard deviation of the corresponding contact time for the desorption rate to compensate for this error.

5.2.3 Measurement of Quantity of Naphthalene Adsorbed at Equilibrium

In this experiment the number of moles of naphthalene which were adsorbed on PRP-1 at equilibrium were measured. This was done to test the reliability of the shallow bed apparatus by comparing the value of the equilibrium distribution coefficient obtained with the shallow bed technique to that determined from the adsorption isotherm (Section 4.2.3). The procedure used to measure the moles adsorbed at equilibrium using the shallow bed apparatus is described in Section 2.3.7.

The weight of PRP-1 in the s.b. cartridge was 2.4×10^{-6} kg. The void volume was 0.018 mL with a standard deviation of 0.004 mL. Using equations 4.7 and 4.8, the distribution coefficient was calculated to be 16.1 liters per kg with a standard deviation of 2.4 liters per kg. This result is in agreement with the value obtained in the adsorption isotherm experiment of 16.1 liters per kg. ± 0.4

Table 5.1 Calibration of injection loops. The following solutions were used to calibrate the injection loops : (a) 1.3×10^{-3} M amaranth (b) 0.015 M naphthalene (c) 1.2×10^{-3} M phloroglucinol (d) 1.3×10^{-3} M naphthalene. * indicates the experiment was not done. One standard deviation for V_{inj} is also listed.

Tubing Dimensions		V_{inj} using He (μL)	s.d. for V_{inj} (helium)	V_{inj} using methanol (μL)	s.d. for V_{inj} (methanol)	Sample
Length (cm)	i.d. (cm)					
9	.05	13	2	23.5	0.1	a
22	.05	45	1.32	61	0.4	a
13	.08	91	0.92	111	0.5	a
17	0.1	93	23.2	135	21.9	b
20	0.1	103	11.1	161	3.78	b
26	0.1	176	8.8	222	18.0	b
50	0.1	322	19.8	395	43	b,c
70	0.1	660	40	*	*	d

5.2.4 Hold-up Volume Measurements

The procedure used to measure the desorption hold-up volume is given in Section 2.3.8. The definition of hold-up volume for the desorption experiments will have a different meaning than that for the hold-up volume, V_m' , measured for the adsorption isotherm experiment in Section 4.2.1. In the adsorption isotherm experiment, V_m' was a constant and it was equal to the interparticle volume, pore volume plus extracolumn dead volume. In the desorption rate experiments discussed here the total hold-up volume was also a constant and was defined as the volume of solution contained in the PRP-1 pores, the interparticle spaces, the frits and any other dead spaces in the s.b. cartridge. However, since this experiment has a step where a slug of mobile phase passes through the bed and flushes out most of the hold-up volume, the number of interest is not the total V_m' but the amount of sample left in the V_m' which was not displaced by the slug of mobile phase.

This value is not necessarily constant but could change for different contact times. Failure to compensate for V_m' could give an erroneous value for the desorption rate constant. If the moles in V_m' were not subtracted, there would appear to be a larger number of moles of sample present on the stationary phase for a particular contact time than the "true" value. This would make the desorption rate curve approach a finite value rather than zero at long contact times. As discussed previously in Sections 2.3.5 and 5.1.3, the purpose of the helium purge was to remove solution in V_m' . However, this did not remove all the solution and the solution that remained had to be quantified.

The hold-up volume was calculated using equation 5.12.

$$V_m' = \frac{\text{moles phloroglucinol remaining}}{C_{\text{initial}}} \quad 5.12$$

The numerator is the number of moles of phloroglucinol remaining in the s.b. cartridge after the slug of mobile phase has been injected and passed through the bed. The moles

remaining are eluted with a strong solvent and quantified. C_{initial} is the concentration of the original solution of phloroglucinol which was equilibrated with the PRP-1.

The results for the desorption hold-up volumes are listed in Table 5.2 and plotted vs contact time in Figure 5.4. The smallest contact time (0.085 seconds) had the largest V_m' . For all other contact times measured V_m' was relatively constant and quite small. These results can be explained as follows. The V_m' is determined by measuring the moles present of an unretained compound, phloroglucinol. In the desorption experiment, the s.b. cartridge void volume is initially filled with phloroglucinol and then a slug of mobile phase is injected. The smallest injection volume of mobile phase (which corresponds to a short contact time) is actually smaller than the total V_m' and displaces only part of the phloroglucinol from the hold-up volume. The remaining quantity of phloroglucinol left in the s.b. cartridge is eluted with the strong solvent, methanol, and a relatively large V_m' is measured. As soon as the injection volume of the slug of mobile phase is large enough to displace almost all of the phloroglucinol from the hold-up volume, the amount of phloroglucinol and therefore, the V_m' , drop to low values and remain fairly constant at a small value. These hold-up volumes appear to be slightly dependent on flow rate as well as injection loop volume.

The hold-up volume used for each contact time in calculations of the desorption experiment was read from the plot in Figure 5.4 at the appropriate contact time. The standard deviations for interpolated V_m' values which correspond to contact times of less than 0.2 seconds were taken to be the standard deviation of the nearest experimental point. For all other interpolated V_m' values the standard deviations were calculated using the standard deviations of the slope and intercept of the straight line connecting the points at contact times ≥ 0.2 seconds.

Table 5.2 Hold-up volume results for desorption rate experiment. The sample solutions used were 1.3×10^{-3} M phloroglucinol and 1.8×10^{-3} M phloroglucinol. Both were dissolved in 90% methanol(aq).

V _{inj} (mLs)	Average F (mL / min)	Average t (sec)	Standard Deviation (t)	Average V _m ' (mL)	Standard Deviation (V _m)
0.013	9.2	0.085	0.002	0.0152	0.0005
0.045	13.7	0.198	0.008	1.88×10^{-3}	0.32×10^{-3}
0.091	8.5	0.65	0.009	2.74×10^{-3}	0.82×10^{-3}
0.103	8.4	0.74	0.025	1.41×10^{-3}	0.31×10^{-3}
0.322	6.9	2.79	0.181	2.03×10^{-3}	1.30×10^{-3}
0.66	6.0	6.7	0.45	7.7×10^{-4}	2.0×10^{-4}

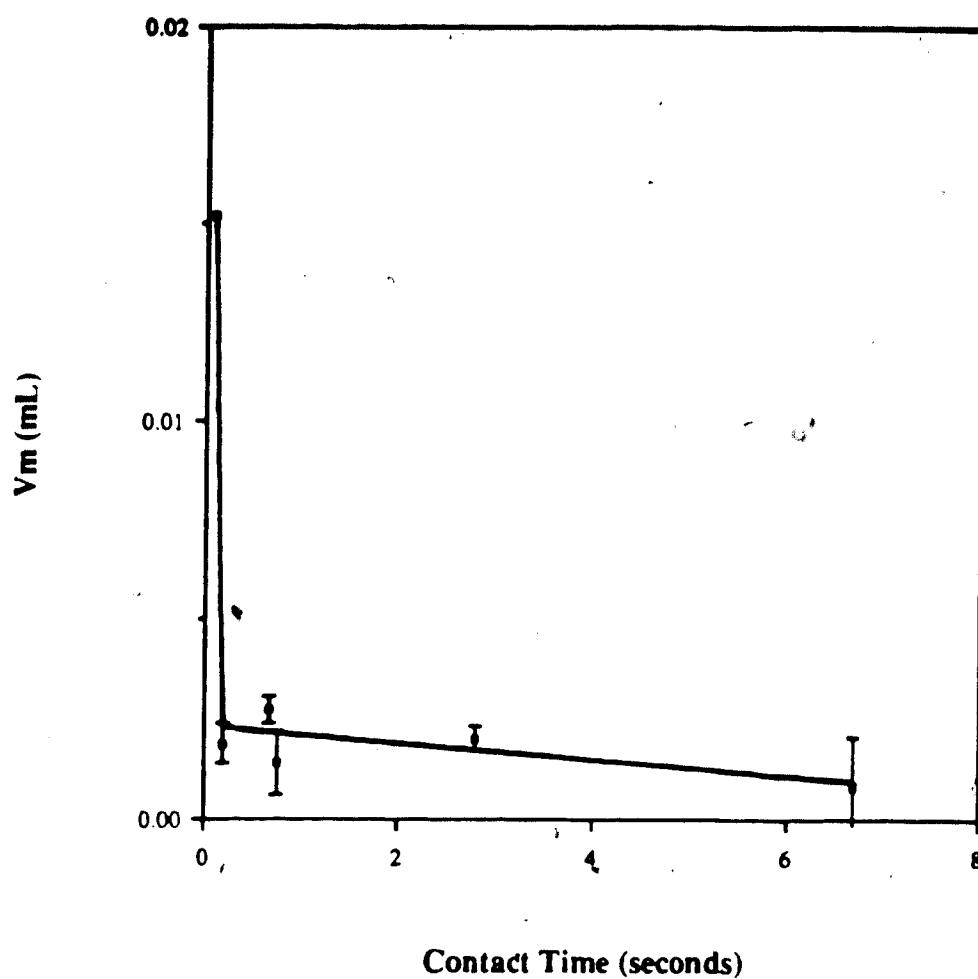


Figure 5.4 V_m results for the desorption rate experiment. The procedure and the experimental conditions are listed in the text. Table 5.2 lists the results and the standard deviations.

5.2.5 Measurement of the Naphthalene Desorption Rate

The results of the desorption rate experiment are listed in Table 5.3 and plotted in Figure 5.5. The absolute overall standard deviation for the contact time included the contributions from flow rate deviations between replicate desorption rate experiments and the standard deviation for the injection loop volume. The overall standard deviation for the moles still adsorbed included deviations between replicate n_{ads} measurements and the standard deviation of V_m .

The rate curve was related to plate height by assuming that either surface adsorption-desorption or diffusion through the stagnant mobile phase in the pores was the slow step in the adsorption-desorption process. These calculations and the results are explained in Section 5.3.

5.2.6 Effect of Fast Flow Rates on Particle Outer Film Diffusion

In chromatography the flow profile between individual stationary phase particles is laminar. Laminar flow is fastest in the center of a channel and slowest at the walls due to the friction caused by the walls. The velocity (u_i) at any radial position (r_i) in a cylindrical channel can be calculated using equation 5.13 [5.23].

$$u_i = 2 u_{ave} \left(1 - \frac{r_i^2}{r^2} \right) \quad 5.13$$

The channel radius is r and the average interparticle mobile phase velocity is u_{ave} . The average interparticle mobile phase velocity does not include the contribution from stagnant mobile phase within the pores and u_{ave} is related to the average mobile phase linear velocity (u_0) by the ratio of the total bed porosity to the interparticle porosity.

Table 5.3 Moles of naphthalene still adsorbed vs contact time for the desorption rate experiment. The sample solution was 5.5×10^{-4} M naphthalene in 90% methanol(aq).

Average t (seconds)	Overall Absolute Standard Deviation (time)	Average n _{ads}	Overall Absolute Standard Deviation (n _{ads})
0	0	1.72×10^{-8}	0.62×10^{-8}
0.072	0.009	1.53×10^{-8}	0.4×10^{-8}
0.183	0.008	1.30×10^{-8}	0.4×10^{-8}
0.32	0.02	7.3×10^{-9}	1.1×10^{-9}
0.48	0.05	4.3×10^{-9}	1.1×10^{-9}
0.81	0.04	2.6×10^{-9}	0.8×10^{-9}
1.45	0.09	9.9×10^{-10}	3.2×10^{-10}
2.25	0.19	8.1×10^{-10}	3.1×10^{-10}
5.9	3.5	1.0×10^{-10}	0.4×10^{-10}

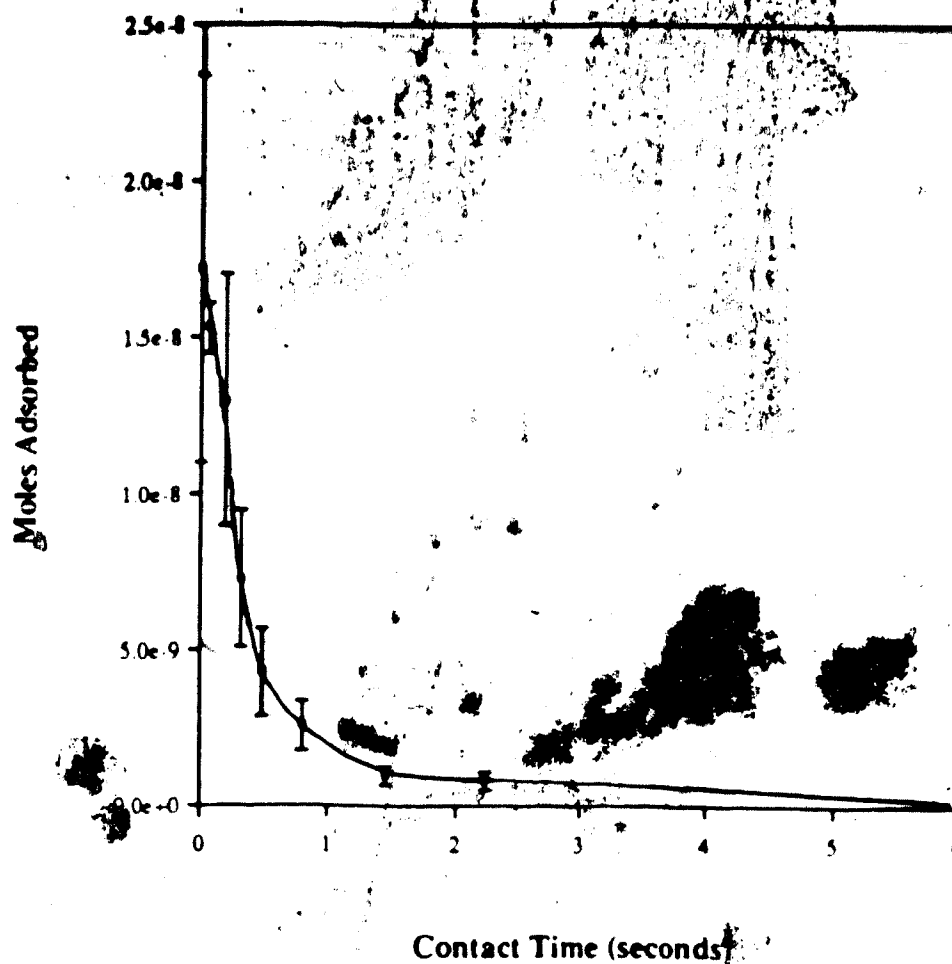


Figure 5.5 Rate of naphthalene desorption from PRP-1 into 90% methanol(aq). The graph depicts moles of naphthalene still adsorbed, n_{ads} , on the PRP-1 vs contact time, t . The squares (\blacksquare) are experimentally measured points shown with error bars representing one standard deviation. A curve is drawn through the data points depicting the shape of the desorption curve.

$$u_{ave} = u_o \frac{\epsilon_t}{\epsilon_{inter}}$$

5.13

Mass transfer through the mobile phase to the outer surface of the particle can be modelled by assuming that a layer of mobile phase exists just outside the particle outer surface which is essentially stagnant (the Nernst film). Diffusion through this film is one of the steps in the adsorption-desorption process which can limit the rate. The thickness of this film is reduced when the mobile phase velocity is increased and it can be estimated using the following empirical equation [5.24].

$$\delta = 0.1 \cdot r \cdot Re^{-0.84}$$

5.14

Here, δ is the film thickness, r is the particle radius and Re is the Reynold's number. Re is defined below in equation 5.18. The time required to diffuse through the film decreases as the thickness decreases. For an adsorption-desorption process whose rate limiting step is film diffusion, the rate of adsorption or desorption is related to the film thickness as shown in equation 5.15.

$$rate = \frac{3 D_m}{2 \cdot \delta \cdot r} \{ C_{i,ads} - C_{i,ads}^* \}$$

5.15

D_m is the solute diffusion coefficient in the mobile phase and the constant $3/2$ is a shape factor used for spherical particles. The term $C_{i,ads}$ is the equilibrium concentration of adsorbed sample in the stationary phase. The two $C_{i,ads}$ terms are calculated by equations 5.16 and 5.17.

$$C_{i,ads} = \frac{n_{ads}}{V_{sp}}$$

5.16

$$C_{i,ads}^* = \frac{n_{ads}^*}{V_{sp}}$$

5.17

Here, n_{ads}^* is the moles adsorbed at equilibrium.

At even higher velocities the flow profile is no longer laminar but turbulent. Velocity and flow direction fluctuate randomly in turbulent flow, rather than being well defined as they are in laminar flow. Turbulence decreases the film thickness. The Reynolds number gives the extent of turbulence and is calculated using equation 5.18 [5.25].

$$Re = \frac{\rho u_{ave} d_p}{\eta}$$

5.18

The density and viscosity of the mobile phase are ρ and η and d_p is the particle diameter.

In a packed bed of particles turbulence begins to develop in some of the larger channels at an Re of 1 and gradually becomes the dominant flow profile as Re increases to 100. At Reynolds numbers less than 1 the flow profile is laminar.

Under typical chromatographic conditions used in this thesis (mobile phase linear velocities of about 0.35 cm per second and a mobile phase consisting of 90% methanol(aq)) the Reynolds number for the PRP-1 column was calculated to be 0.1, indicating the interparticle flow profile was laminar. Using $Re = 0.1$ in equation 5.14, δ is calculated to be about 4×10^{-4} cm. This distance comparable to the average radius of the PRP-1 pores. However, for the shallow bed experiments u_{ave} was about 10x larger, giving a Reynolds number of 1, which means turbulence is starting to develop in some of the larger interparticle channels. The shallow bed experiment would overestimate the desorption rate if slow mass transfer across the interparticle film were the rate limiting step because of the high values of u_{ave} used in the shallow bed experiment. Since the diffusion

distance is about the same for both pore and film diffusion, and pore diffusion was found to be fast, it is likely that film diffusion is equally fast.

5.3 Relation of Desorption Rate Curves to Plate Height

5.3.1 Calculation of the Adsorption-Desorption Plate Height

In order to calculate a plate height from the desorption rate two models were used. The rate limiting step in one model was surface adsorption-desorption and in the other model it was diffusion through the stagnant mobile phase in the pores.

Both models which were used require the assumption that the rate is directly proportional to sample concentration. The results for the desorption rate curve are plotted in Figure 5.6 as $\ln(n_{ads,o}/n_{ads,t})$ vs time. Here, $n_{ads,o}$ is the moles adsorbed on the PRP-1 at time $t = 0$ and $n_{ads,t}$ is the number of moles adsorbed at time t . The value for $n_{ads,o}$ was 1.72×10^{-8} moles. The equation describing the desorption rate process using the shallow bed theory is given in equation 5.3 and the rate of desorption in terms of the adsorbed sample concentration is given by equation 5.4. Integrating equation 5.4 gives equation 5.19

$$\ln \left(\frac{C_{ads,o}}{C_{ads,t}} \right) = k_{des} t$$

5.19

Although equation 5.19 uses adsorbed concentrations rather than moles, the term $\ln(n_{ads,o}/n_{ads,t})$ is equal to $\ln(C_{ads,o}/C_{ads,t})$ because the volumes in the two concentration terms are equal and will cancel out upon division. Therefore, a plot of $\ln(n_{ads,o}/n_{ads,t})$ vs t should be a straight line with a zero y-intercept. The first six data points in Figure 5.6 give a line with a slope of $2.0 \pm 0.6 \text{ sec}^{-1}$. The y-intercept for this plot is 0.13 ± 0.40 . The \pm values are 95% confidence limits.

A second line can be drawn through the last three data points which introduces the possibility of a second slower reaction occurring in parallel with the first faster reaction. However, because of the large standard deviations for each data point, further experiments are necessary to draw conclusions about this. The possibility of a second slower reaction and its effect on plate height is discussed in Appendix III.

If the model used is surface adsorption-desorption the slope of a plot of $\ln(n_{ads,o} / n_{ads,t})$ vs contact time will give the surface desorption rate constant. This value of k_{des} was related to plate height using the surface adsorption-desorption model using equation 5.20 [5.26].

$$H = 2 \frac{k'}{[1 + k']^2} \frac{1}{k_{des}} u_o \quad 5.20$$

Calculated values for the surface adsorption-desorption plate height at various mobile phase linear velocities are listed in Table 5.4. Table 5.4 also compares these plate heights with H measured from elution chromatograms at the same mobile phase linear velocities. The calculated plate heights are 16x to 175x smaller than the elution chromatography values, indicating that surface adsorption-desorption is not responsible for the large plate heights measured on PRP-1.

The second model used assumes that slow mass transfer through the stagnant mobile phase in the pores is the rate limiting step and surface adsorption-desorption is very fast. The rate of mass transfer is assumed to be directly proportional to sample concentration [5.24,5.27]. The rate of transport of sample in the pores is given by equation 5.21 [5.24].

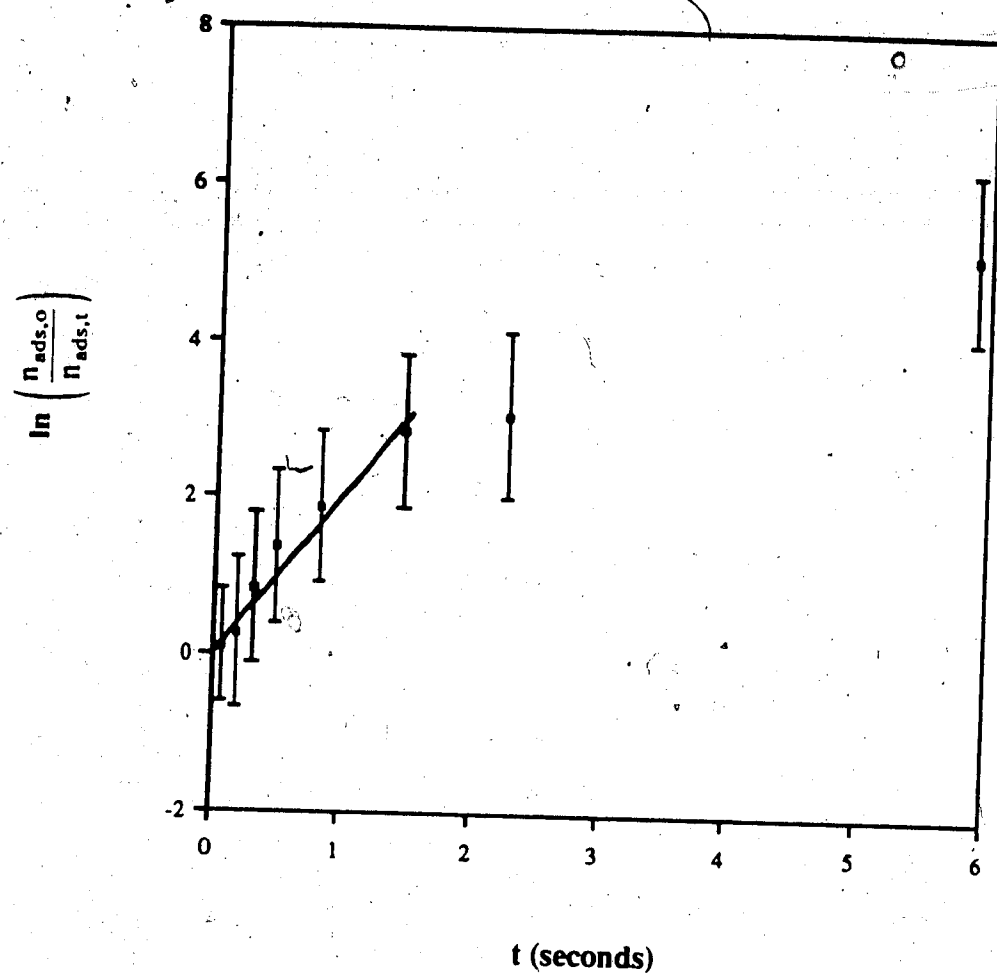


Figure 5.6 First order plot of naphthalene desorption rate data.

$$\frac{dC_{i,ads}}{dt} = - \frac{D_{pore}}{0.07 r^2} C_{i,ads}$$

5.21

D_{pore} is the sample diffusion coefficient within the pores and r is the stationary phase particle radius. Integration of equation 5.21 gives basically the same result as given in equation 5.19 except the slope is equal to $(D_{pore} / 0.07 r^2)$. Once again, moles of adsorbed sample can be used rather than concentrations since the volumes will cancel.

Using 2.0 sec^{-1} for the slope and $5 \times 10^{-4} \text{ cm}$ for the particle radius [5.28], D_{pore} for PRP-1 was calculated to be $3.6 \times 10^{-8} \text{ cm}^2$ per second with a standard deviation of $0.2 \times 10^{-8} \text{ cm}^2$ per second. This value for D_{pore} compares favorably with D_{pore} values measured on two similar polystyrene - divinylbenzene copolymers. D_{pore} was $2.06 \times 10^{-8} \text{ cm}^2$ per second for phenol on XAD-4 [5.29] and $1.2 \times 10^{-8} \text{ cm}^2$ per second for benzaldehyde in water on XAD-1 [5.11]. These workers obtained D_{pore} for the two XAD resins by experimentally measuring the sample breakthrough curve, fitting the data to a theoretical mass balance equation which described diffusion through the stationary phase and solving the mass balance equation for the diffusion coefficient.

The relation between plate height and D_{pore} has been derived by Hawkes [5.30] and is given in equation 5.22. The value of D_{pore} for PRP-1 was substituted into equation 5.22 to calculate plate heights for various mobile phase linear velocities and these results are also shown in Table 5.4.

$$H = \frac{\frac{1}{1+k_i} \left\{ 1 - \left(\frac{\epsilon_{intra}}{\epsilon_t} \right) \left(\frac{1}{1+k_i} \right) \right\} d_p^2 u_o}{30 D_{pore}}$$

5.22

The calculated plate heights for both the surface adsorption-desorption and pore diffusion models are almost the same, which is not surprising since both models assume a first order process is occurring. For both models the plate heights calculated from the

Table 5.4 Plate heights calculated from adsorption-desorption results assuming either surface adsorption-desorption or diffusion in the stagnant mobile phase within the pores is the rate limiting step for various mobile phase linear velocities. The standard deviations for the calculated plate heights are listed as the \pm values. Column 4 of this table lists experimental plate heights obtained from elution chromatograms of 10^{-4} M naphthalene on PRP-1 with a 90% methanol(aq) mobile phase.

u_0 (cm / sec)	Surface Ads.-Des. H (mm)	pore diff. H (mm)	Elution Chrom. H (mm)
0.36	0.18 ± 0.02	0.14 ± 0.016	2.5
0.27	0.14 ± 0.01	0.11 ± 0.012	2.7
0.17	0.087 ± 0.009	0.068 ± 0.008	2.1
0.090	0.046 ± 0.005	0.036 ± 0.004	1.6
0.075	0.038 ± 0.004	0.030 ± 0.003	1.5
9.6×10^{-3}	$4.9 \times 10^{-3} \pm 0.5 \times 10^{-3}$	$3.8 \times 10^{-3} \pm 0.4 \times 10^{-3}$	0.75

results of the adsorption-desorption rate experiments are much smaller than those measured from elution chromatograms. This indicates the kinetics of adsorption-desorption makes only a minor contribution to the bandbroadening.

5.3.2 Infinite Solution Volume Assumption

In Section 5.1.3 it was stated that the shallow bed technique required an unchanging sample concentration in order to measure the desorption rate accurately (the ISV condition). For the desorption experiment this requires that a relatively small amount of sample should be desorbed from the PRP-1 into the mobile phase, so that the concentration of sample in the mobile phase is negligible.

During the desorption experiment a slug of mobile phase solution flows past the adsorbed sample on the bed of PRP-1. If a large amount of sample is desorbed into the slug as the slug first encounters the inlet end of the PRP-1, the PRP-1 which is nearer the outlet will experience a mobile phase solution with a finite concentration of sample instead of being nearly pure mobile phase. Therefore, the desorption rate near the outlet will be slower than the rate at the inlet. This is true because the rates of pore diffusion, film diffusion and surface adsorption-desorption are all dependent on concentration. If the rate is decreasing over the length of the bed, the measured rate value would be an average of all the rates at different points on the bed. The effect that a changing sample concentration in the mobile phase has on the shape of the desorption rate curve is qualitatively shown in Figure 5.7. The measured rate curve is broader than the "true" rate curve as measured under ISV conditions and the measured rate is slower than the "true" rate. This produces an erroneously small value for k_{des} .

In order to estimate the error caused by not meeting the infinite solution volume condition, a stepwise calculation was done using a Microsoft BASIC program written for this purpose. Consider the desorption experiment where the adsorbed moles of sample are

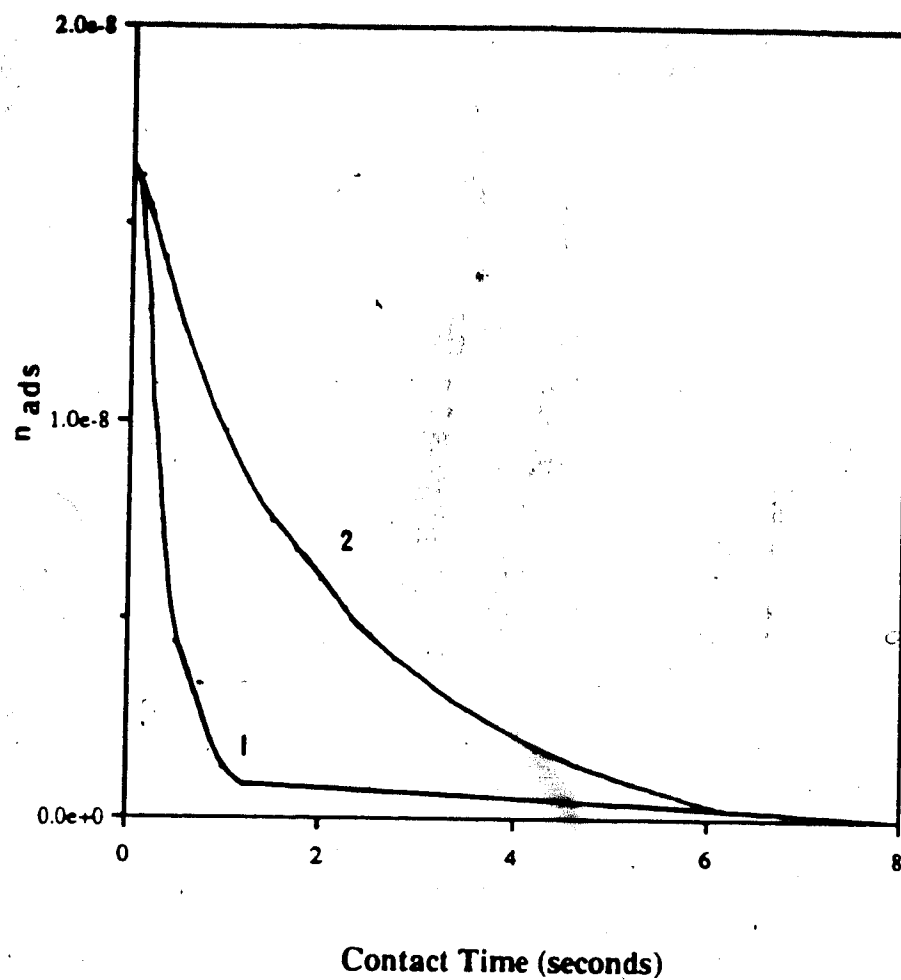


Figure 50 Effect that not meeting the ISV condition or a changing distribution coefficient would have on the desorption rate curve. Curve 1 represents the rate curve for the case where the ISV condition is fulfilled (and a constant K_i). Curve 2 represents the broadened curve resulting from not meeting the ISV condition or from a changing K_i . Both curves are simulated.

desorbing into a slug of mobile phase solution. In the calculation, the bed of stationary phase is divided into segments of equal length and volume as shown in Figure 5.8 and a known amount of sample is initially adsorbed on the PRP-1 stationary phase. A slug of mobile phase solution is injected and flows past the stationary phase and the mobile phase slug is divided into segments of equal volume. The volume of each mobile phase solution segment, V_{soln} , is equal to the bed void volume, V_m , for one stationary phase segment. The number of mobile phase solution segments is equal to the injection volume divided by V_{soln} . The solution segments are moved past the stationary phase segments in a stepwise manner (Figure 5.8b - 5.8c) and as each mobile phase solution segment contacts a stationary phase segment, the number of moles desorbed is calculated. At the end of the program, when all of the solution segments have moved past each stationary phase segment, the total number of moles desorbed is compared with the number of moles which would have been desorbed under ISV conditions. The difference between these two numbers is the error. The basic algorithm for this calculation is listed below.

1. Mobile phase solution segment 1 contacts stationary phase segment 1 as shown in Figure 5.8a. The change in the adsorbed concentration, $\Delta C_{i,\text{ads}}$, on stationary phase segment 1 due to desorption is calculated using the incremental form of equation 5.2.

$$\Delta C_{i,\text{ads}} = \left[(k_{\text{ads}} C_{i,\text{soln}}) - (k_{\text{des}} C_{i,\text{ads}}) \right] * \Delta t \quad 5.23$$

The value used for k_{des} was 2 sec^{-1} as measured by the desorption rate experiment and equation 5.5 is used to calculate a value of 39 sec^{-1} for k_{ads} . For all solution segments, the initial value is zero for $C_{i,\text{soln}}$ at time $t = 0$. For each stationary phase segment the initial value of $C_{i,\text{ads}}$ is known from experimental data. It is determined by first dividing the total number of moles adsorbed on the bed at time $t=0$ (1.72×10^{-8} moles) by the number of stationary phase segments to give the moles adsorbed per segment, $n_{i,\text{ads}}$.

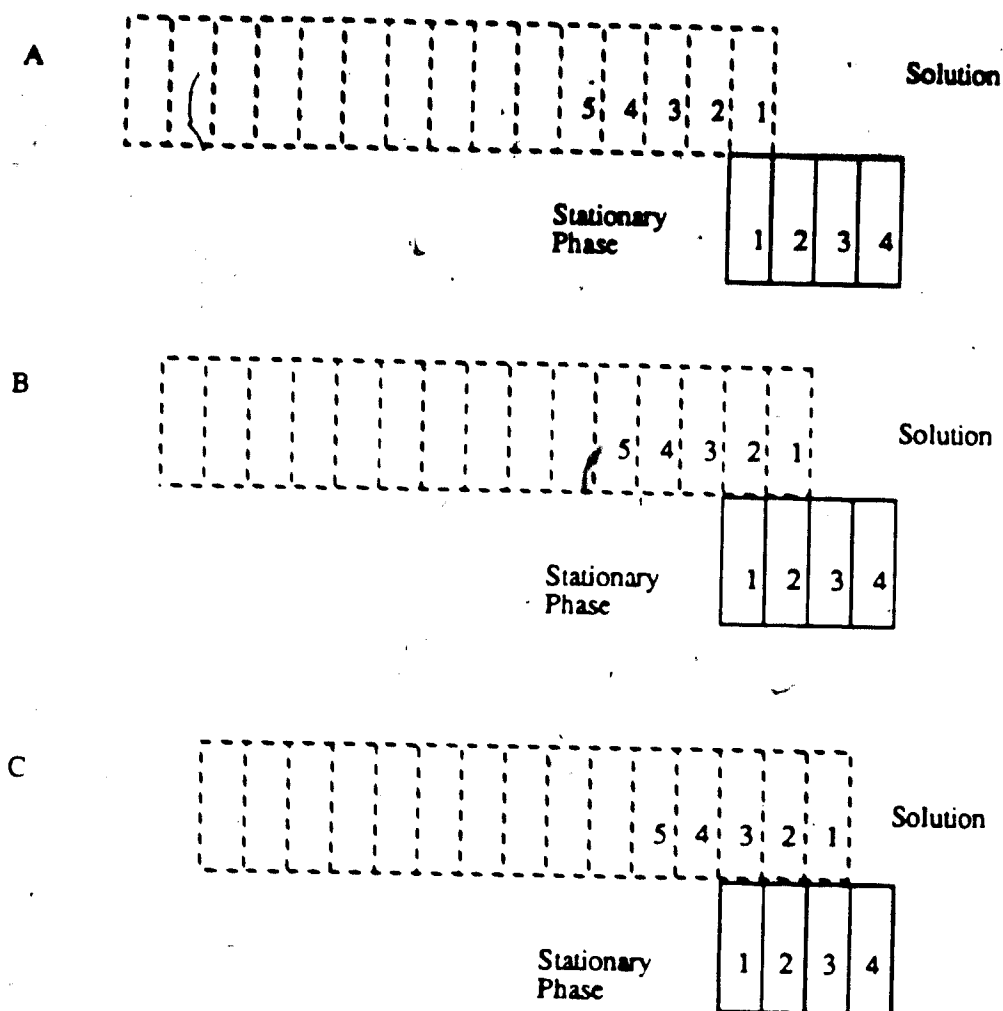


Figure 5.8 Diagram of the steps in the program used to calculate the error caused by not meeting the ISV condition. The stationary phase segments are represented by the solid rectangles and the mobile phase solution segments are the dashed rectangles. The number of solution segments vary with the volume of solution injected. In the calculation for the desorption experiment, mobile phase solution segment 1 is moved past each stationary phase segment one step at a time (5.11a - 5.11c). The number of moles desorbed from each stationary phase segment is calculated at each step. Once solution segment 1 has moved past each stationary phase segment, the process is repeated for the remaining mobile phase solution segments until each solution segment has encountered each stationary phase segment. Although only four stationary phase segments are shown here, ten were used in the calculation.

$$n_{i,ads} = \frac{\text{total moles adsorbed}}{10} = \frac{1.72 \times 10^{-8}}{10} \quad 5.24$$

$C_{i,ads}$ is obtained by dividing $n_{i,ads}$ by the volume of a stationary phase segment, V_{sp} . V_{sp} is calculated by multiplying the weight of stationary phase per segment by the PRP-1 matrix density, $\rho(\text{PRP-1})$. Since the total weight of PRP-1 in the bed was 2.4×10^{-3} g, the weight per segment is one tenth of this. $\Delta C_{i,ads}$ is the decrease in adsorbed concentration due to sample desorption during Δt . Δt is the time period during which the mobile phase solution segment is in contact with the stationary phase segment and it is calculated by dividing the length of the mobile phase solution segment, x , by the velocity of the solution, v .

$$\Delta t = \frac{x}{v} \quad 5.25$$

The solution velocity, v , was calculated by equation 5.26.

$$v = \frac{L F}{60(V_m)} \quad 5.26$$

L is the length in cm of the bed of PRP-1 and F is the mobile phase solution flow rate in mL per minute.

Equation 5.23 is valid to use in place of the derivative form of this equation if Δt is relatively small. Decreasing values of Δt were tried until the final result calculated from this program remained constant. Δt is decreased by increasing the number of stationary phase segments. Ten stationary phase segments were found to be sufficient for the naphthalene desorption process.

Next, the number of moles desorbed from the stationary phase segment into the solution segment is calculated by multiplying $\Delta C_{i,ads}$ by V_{sp} .

$$n_{des} = \Delta C_{i,ads} V_{sp} \quad 5.27$$

The new adsorbed concentration on stationary phase segment 1 is calculated by subtracting moles from the original number of moles adsorbed and then dividing by V_{sp} .

2. The moles of sample desorbed from the first stationary phase segment is added to any moles of sample already present in the solution segment and then this number is divided by V_{soln} to give a new value for $C_{i,soln}$.

3. The solution is moved one step so now solution segment 1 is in contact with stationary phase segment 2 as shown in Figure 5.8b. Steps 1 and 2 are repeated until solution segment 1 has moved past all stationary phase segments. At end of this series of steps, the number of moles in solution segment 1 is the total moles of sample desorbed from the bed of stationary phase into solution segment 1.

4. Steps 1 through 3 are repeated for all the remaining mobile phase solution segments.

5. At the end of the calculation the moles desorbed from all ten stationary phase segments are summed to give the total moles desorbed (n_{total}) from the bed of stationary phase.

6. Only stationary phase segment 1 meets the ISV condition because each segment of mobile phase solution which moved past it had no sample present in it. Therefore, the total number of moles which would be desorbed from the stationary phase bed under ISV conditions (n_{isv}) is equal to the moles desorbed from stationary phase segment 1 multiplied by the total number of stationary phase segments (10).

7. The percent relative error due to not achieving the ISV condition is calculated using equation 5.28. This represents the difference between the number of moles which would have been desorbed under the ISV condition and the number of moles actually desorbed under experimental conditions.

$$\% \text{ error} = 100 \left(\frac{n_{\text{iso}} - n_{\text{total}}}{n_{\text{iso}}} \right)$$

5.28

Table 5.5 lists the error calculated by equation 5.28 as well as the corresponding contact times and injection volumes. The error was determined for the six desorption contact times which were used to calculate k_{des} . The desorption error ranges between 3% and 18%. This means that at a contact time of 0.072 seconds, 18% more moles would have been desorbed than what was experimentally measured, had perfect ISV conditions been achieved. The true value of k_{des} would be about 2.4 sec^{-1} , which is 1.2x larger than the measured value. This error is not very large because the desorption process is essentially irreversible in the shallow bed experiment and the adsorption process has little effect.

The ISV error decreases with increasing contact time. This is because as the contact time increases, the reaction slows down so less sample is desorbed in later solution segments. Therefore, ISV condition is more closely approached in the later solution segments.

5.4 Conclusions

The rate of naphthalene desorption was measured for a PRP-1, 90% methanol(aq) system. Equipment was developed to measure this rate using the "shallow bed" technique. This technique measures an overall desorption rate constant for all steps in the desorption process, both diffusion and surface desorption. The shallow bed apparatus was tested for reliability by comparing equilibrium adsorption results measured with it with the results obtained in Section 4.2.2 in the adsorption isotherm experiment. The results between the two techniques matched well. The shallow bed apparatus could be used to measure many adsorption or desorption processes which have first order rate constants of about 2 to 5

Table 5.5 Error resulting from the departure from infinite solution volume assumption for shallow bed technique in desorption rate experiment for the five data points used to calculate k_{des} . The sample solution was 5.5×10^{-4} M naphthalene in 90% methanol(aq). The \pm values are one standard deviation.

t (seconds)	V _{inj} (ml)	% Error
0.072	0.013	18 ± 4
0.18	0.045	12 ± 3
0.32	0.091	9 ± 2
0.48	0.103	10 ± 2
0.81	0.176	7 ± 0
1.45	0.322	3 ± 1

The % error is calculated by :

$$\% \text{ error} = 100 \left(\frac{n_{isv} - n_{total}}{n_{isv}} \right)$$

n_{isv} is the moles which would be desorbed had the ISV condition been met and n_{total} is the moles actually desorbed.

sec^{-1} or less. This technique also makes it easy to achieve irreversible first order desorption conditions, which simplifies the determination of k_{des} .

Using this equipment, the desorption rate was found to be directly proportional to naphthalene concentration. This rate was related to plate height by assuming either surface adsorption-desorption or diffusion through the stagnant mobile phase within the pores was the rate limiting step.

Both kinetic models gave small calculated plate height values using the experimentally measured desorption rate. Plate heights were calculated for the two models for a range of mobile phase linear velocities and compared to plate heights measured from elution chromatograms. The elution chromatogram plate heights were 16x to 175x larger than those calculated from the desorption result. This means that the adsorption-desorption process makes a negligible contribution to the plate heights measured on PRP-1 and is not responsible for the excessive bandbroadening observed on PRP-1.

CHAPTER 6

Velocity Profile Studies

6.1 Introduction

A heterogeneous packing structure which has regions of different stationary phase density across a column can affect the shape of a sample zone on a chromatographic column in two ways. First, there are areas of differing permeability which causes the mobile phase velocity to vary between the regions of differing packing density. Second, the different regions will have different phase ratios, which causes the sample capacity factor to vary from region to region. Both of these effects were studied in the present work.

6.1.1 Packing Structure Heterogeneity and a Non-uniform Velocity Profile Due to Varying Permeability

As was previously discussed in Section 3.1.6, the packing structure of a chromatographic column affects the dispersion of a sample. In Section 3.2.3 the results were given for an experiment which measured plate height vs mobile phase linear velocity. It was found that although the plate height for naphthalene did decrease with decreasing mobile phase linear velocity, it was still large at very low linear velocities. At a velocity of 9.6×10^{-3} cm per second (flow rate = 0.055 mL per minute) the plate height was 0.7 mm (see Table 3.3). This could be caused by a non-uniform sample velocity profile which is not being relaxed by convective lateral transport (eddy diffusion). The velocity differences are caused by non-uniformities in the packing structure. The permeability and mobile phase linear velocity will be lower in regions with a higher packing density. Also, regions with a higher packing density have a larger W_s , so sample will be retained longer

in these regions. Both of these effects are important and will be discussed in the next two sections. Section 6.1.3 describes a calculation which was used to account for the bandbroadening caused by the combination of the two effects.

Several workers have studied the velocity profiles in preparative and analytical gas chromatographic columns where uneven flow is a problem because of the large radial distances which must be crossed in order to relax the profile. The preparative GC columns used in these experiments were quite large, between 5 and 10 cm in diameter and 100 to 250 cm long. The researchers who measured velocity profiles on these columns monitored sample velocities by inserting detector probes into the column at various positions [6.1]. Another technique used was to coat the stationary phase support with an acid-base indicator prior to coating it with stationary phase. Volatile acidic or basic compounds were added to a carrier gas flowing through the column and the velocity profile could be observed as the vapor encountered the indicator [6.2]. The column walls were made of glass so the color change could be seen. Therefore, these profiles were actually the outer wall profiles and no information was obtained about the velocity at the column center. A dye was used to observe velocity profiles in size exclusion chromatography [6.3] by injecting the dye onto a column and following its migration down the column.

Other studies did yield information about the entire transcolumn velocity profile. One technique was to use an acidic or basic sample [6.4,6.5]. After the sample moved part way down the column, sections of the column were removed, subdivided and titrated. The amount of sample present in each section was proportional to the sample velocity in that section. A second method was used by Littlewood with an analytical GLC column [6.2]. He was able to remove the packing intact by breaking away the glass column because the stationary phase had cemented together during the chromatography process. He then sliced the bed open laterally and measured the velocity distribution. Knox et al [6.5] also studied the entire velocity profile across a 77.5 cm by 11.7 mm i.d HPLC column by placing an

electrochemical detector directly under the outlet frit and monitoring the sample eluted at different radial positions.

In studying the sample velocity profile across an analytical PRP-1 column there were technical difficulties not encountered by earlier researchers. First, because of the high pressures used in HPLC, detector probes could not be easily placed into the column walls and sealed effectively. Secondly, a 4.1 mm i.d. column was used because this was the i.d. of commercial PRP-1 analytical columns used in this thesis. This small diameter made it difficult to measure velocities at different radial positions by any of the techniques described above. Larger diameter columns were not used because it was thought that a larger diameter could change the packing structure significantly and the results would be inapplicable to smaller columns. Also, it was necessary to measure the entire transcolumn velocity distribution, so observing a dye pattern through the glass walls of a column was insufficient. The procedure used involved extruding the bed of stationary phase from short columns after injection of a dye and then slicing the bed along its length to observe the pattern of the colored dye.

Once the sample velocity profile was observed on a PRP-1 HPLC column with standard Swagelok endfittings, the column was modified by using different outlet endfittings which changed the pattern of effluent flow at the outlet end of the column. This was done in order to determine the effect that mobile phase flow configuration at the column outlet end had on the velocity profile and the stationary phase packing structure in the rest of the column. These experiments were repeated for columns packed with C18 stationary phase. Since C18 columns are efficient and give narrow, symmetric peaks, these columns were used as controls to compare with the PRP-1 results.

6.1.2 Packing Structure Heterogeneity and Non-uniform Phase Ratio

In addition to causing an uneven mobile phase velocity profile by creating regions across the packed bed of differing permeability to the flow of mobile phase, a non-uniform packing structure would also cause a non-uniform distribution of stationary phase which would create regions across the bed with differing phase ratios. The capacity factor is dependent on the phase ratio and since the sample velocity (u_i) is inversely proportional to $(1 + k_i')$ this would exacerbate the effect of an uneven mobile phase velocity profile. Regions of the column which have more stationary phase would have lower sample velocities because of both longer retention and decreased permeability.

Giddings [6.6] described the effect of variable phase ratio qualitatively and stated that it would give the same results as a non-uniform velocity profile caused by differences in permeability only. Knox and Saleem [6.7] gave an equation for the plate height, which has a k_i' dependence based on an uneven distribution of stationary phase. They used a random walk model assuming the regions with excess stationary phase caused molecules to be retarded from the main sample band and represented a step backwards, while molecules in the regions with less stationary phase were taking a step forward. Sample dispersion from this source was relaxed by both lateral convection and diffusion which gave a coupled plate height expression. They compared calculated with experimental results for a GLC column. However, the agreement between the results fluctuated from less than 1% to 37%. The agreement was best for samples with k_i' values less than 6 and low carrier gas velocities.

Littlewood [6.2] prepared a GLC column in such a manner as to produce an uneven coating of stationary phase across the bed. He measured the plate height for three compounds with k_i' ranging between 10 to 21 on this column and found that H was 1.3x larger than a control column which had a uniform packing structure and uniform stationary phase distribution. In contrast, a column with regions of differing permeability but a

uniform phase density distribution had a plate height 7x larger than that of the control, indicating a varying k_i' due to an uneven phase density distribution was unimportant compared to permeability differences.

Frisone [6.8] tried to counteract the faster velocity which he found at the wall region of preparative GLC columns by increasing the loading of stationary phase at the wall. He found that this improved peak shape, but he gave no quantitative information.

If we ignore velocity differences due to permeability differences, a qualitative idea of the effect that an uneven radial stationary phase distribution would have on the sample retention time can be obtained as follows: Divide a column into two cylindrical sections of equal volume (the wall section and the center section). Assume the weight of the stationary phase in the wall section is greater than that in the center section. The void volume in the wall section would necessarily be smaller than that in the center region because the packing density (g per cm³) is greater. The capacity factor of a sample is related to the distribution coefficient by the phase ratio.

$$k_i = K_i \frac{W_s}{V_m} \quad 6.1$$

Sample which is in the wall section would have a capacity factor larger than that of sample in the center section because W_s is larger and V_m is smaller in the wall section. The capacity factor is also related to the sample retention time (t_r).

$$t_r = k_i' t_m + t_m \quad 6.2$$

The elution time of an unretained sample is t_m . Since we are ignoring the effects of non-uniform permeability across the column, the mobile phase flow rate is assumed to be constant in both regions. Therefore, it can be seen from equation 6.2 that the retention time of sample in the wall section would be longer than that of sample in the center section.

Since this effect is related to the distribution coefficient, plate height could be related to the distribution coefficient as well.

6.1.3 Calculation of Plate Height Based on Varying Permeability and Non-uniform Phase Ratio Across the Column

For this thesis, a calculation which takes into account both varying permeability and a non-uniform phase ratio distribution was done to predict what effect a changing packing density would have on plate height. A basic program named H(WS) was written to compute this calculation. The program is presented in Appendix IV and the rationale of the program is given below. Basically, the operator enters values for the weight of stationary phase at the wall and center regions of the column and the program calculates the packing density distribution and the regional phase ratios across the column from this information. After the phase ratios are known, the capacity factors and retention times for sample at different points across the column can be calculated as well as the interparticle mobile phase velocities for the different regions across the column. The final results list the moles of sample eluted from different regions across the column, the corresponding retention times and the mobile phase linear velocity for each region. From this information a simulated elution peak can be plotted and a plate height measured from the simulated peak.

1. An imaginary "column" is divided into a number (n) of concentric rings, all of which have the same width. At the center of the column the "ring" is actually a circle numbered $r = 0$ and the ring at the column wall is ring $r = n$. The column dimensions are the same as those used in the velocity profile experiments (5 cm x 4.1 mm i.d.). The area and volume of the rings increase from the column center to wall.
2. A known number of moles of sample (N) is evenly distributed across the column as an infinitely thin slice. The number of moles in each ring, $N(r)$ is proportional to the relative area of the ring, $A(r)$:

$$N(r) = N \frac{A(r)}{A}$$

6.3

Where A is the cross-sectional area of the entire column.

3. The weight of stationary phase in each ring, $WS(r)$, is next specified assuming a linear relation between the packing density and the radial distance from the column center. The volumes, V , of the wall ring and center ring are calculated first.

$$V_{\text{wall}} = V(n) = \pi L R_{r=0,n}^2 - \pi L R_{r=0,n-1}^2$$

6.4

$$V_{\text{center}} = V(0) = \pi L R_{r=0}^2$$

6.5

In these equations, L is the length of the column in cm. $R_{r=0}$ is the radius of the center circle in cm. $R_{r=0,n}$ is the radius of the entire column and $R_{r=0,n-1}$ is the radius up to and including the ring just before the wall ($r = n - 1$). Next, the packing density in the wall ring and the center circle are specified. This is done by specifying the weight $WS(\text{wall})$ and $WS(\text{center})$. From these two values the slope and intercept of the linear equation relating WS with radial position are calculated and the values of WS for all rings can be determined. For the short columns used in the velocity profile experiments, the average packing density was 0.37 grams per cm^3 . The value for $WS(\text{wall})$ is chosen to be slightly larger than the weight corresponding to the average packing density, indicating a more densely packed region and the value for $WS(\text{center})$ is smaller, indicating a more loosely packed region. For a first approximation the packing density of the wall was chosen to be 0.38 and that of the center ring was 0.36.

$$WS_{\text{wall}} = WS(n) = 0.38 V_{\text{wall}}$$

6.6

$$WS_{\text{center}} = WS(0) = 0.36 V_{\text{center}}$$

6.7

4. Using the values of WS at each radial position, the pore (intraparticle) volume can be calculated for each ring using the average pore volume of PRP-1 (0.79 mL per gram) [6.9].

$$V_{\text{pore}}(r) = 0.79 \text{ WS}(r) \quad 6.8$$

5. The interparticle volume, V_{inter} can be calculated for each ring via equation 6.9.

$$V_{\text{inter}}(r) = V(r) - \frac{\text{WS}(r)}{1.07} - V_{\text{pore}}(r) \quad 6.9$$

The term $(\text{WS}(r) / 1.07)$ is the volume of solid stationary phase in the ring. The quantity 1.07 g per cm^3 is the density of the solid styrene-divinylbenzene phase, assuming that Hamilton PRP-1 is like Amberlite XAD-2 in this respect [6.10].

6. The inter- and intraparticle porosities of each ring, ϵ_{inter} and ϵ_{pore} , are calculated by dividing the interparticle and pore volumes by the total geometric volume of each ring, $V(r)$.

$$\epsilon_{\text{inter}}(r) = \frac{V_{\text{inter}}(r)}{V(r)} \quad 6.10$$

$$\epsilon_{\text{pore}}(r) = \frac{V_{\text{pore}}(r)}{V(r)} \quad 6.11$$

7. The total porosity, ϵ_t , for each ring is calculated.

$$\epsilon_t(r) = \frac{V_{\text{inter}}(r) + V_{\text{pore}}(r)}{V(r)} = \epsilon_{\text{inter}}(r) + \epsilon_{\text{pore}}(r) \quad 6.12$$

8. Now, the mobile phase linear velocity, $u_o(r)$, for each ring is calculated by combining the Kozeny-Carmen equation and Darcy's Law (see Section 6.2.1) to give equation 6.13.

$$u_o(r) = X_1 X_2 \epsilon_t(r) \quad 6.13$$

where:

$$X1 = \frac{d_p^2 P}{180 L \eta} \quad 6.14$$

and:

$$X2(r) = \frac{\epsilon_{inter}^3(r)}{[1 - \epsilon_{inter}(r)]^2} \quad 6.15$$

The terms d_p , P and η are the particle diameter, the column pressure and the mobile phase viscosity. All of these are experimentally determined parameters.

The mobile phase linear velocity is the average value of the mobile phase velocity in both the interparticle and pore spaces.

9. The retention time for an unretained sample, t_m is calculated for each ring.

$$t_m(r) = \frac{L}{u_o(r)} \quad 6.16$$

Calculations in steps 8 and 9 determine the velocity difference for an unretained compound due to the changing permeability across the column because of the varying packing density. The second effect that the changing packing density has is the difference in sample retention caused by the changing phase ratios.

10. The sample capacity factor and the sample retention time are calculated for each ring. First, the total void volume in each ring $V_m(r)$ is determined.

$$V_m(r) = V_{inter}(r) + V_{pore}(r) \quad 6.17$$

Then, the capacity factor in each ring is calculated using equation 6.18.

$$k_i(r) = K_i \frac{WS(r)}{V_m(r)} \quad 6.18$$

Finally, the sample retention time for each ring is calculated using equation 6.19.

$$t_r(r) = t_m(r) k_i(r) + t_m(r)$$

6.19

11. Run additional trials by repeating steps 3 through 10 for different values of WS(wall) and WS(center).
12. Compare the calculated mobile phase velocity distribution with the experimental mobile phase velocity distribution after each trial. If they match, then this is the phase density distribution needed to give the experimental velocity profile. A simulated elution peak can be produced by plotting the moles of sample eluted vs retention time and the plate height can be measured from the simulated peak.

Also, the calculated values of the total column void volume and the total weight of stationary phase in the column are listed in the results. These two values can also be compared with experimental values as an additional check on how well the simulated results compare with the experimental. The results obtained using this calculation are presented later in Section 6.2.5.

Rather than using the entire experimental mobile phase velocity distribution, only the fastest and slowest mobile phase linear velocities, $u_{0,max}$ and $u_{0,min}$, were actually used for comparison with the simulated results. The experimental values were measured from the short columns with constricted flow endfittings. The $u_{0,max}$ and $u_{0,min}$ values for only the constricted flow columns were used, since these columns have the same type of endfittings used with commercial PRP-1 columns. The method used to measure these values from a dye profile on an extruded bed is shown in Figure 6.1. The fastest mobile phase linear velocity, $u_{0,max}$, was determined by first measuring the sample linear velocity, $u_{i,max}$, observed on the PRP-1 columns and converting this to $u_{0,max}$. To obtain $u_{i,max}$ the distance (Δd_{front}) from the column inlet to the foremost position of the leading edge of the sample zone was measured. This distance was divided by the time (Δt) in which the sample was on the column to give the sample velocity, $u_{i,max}$.

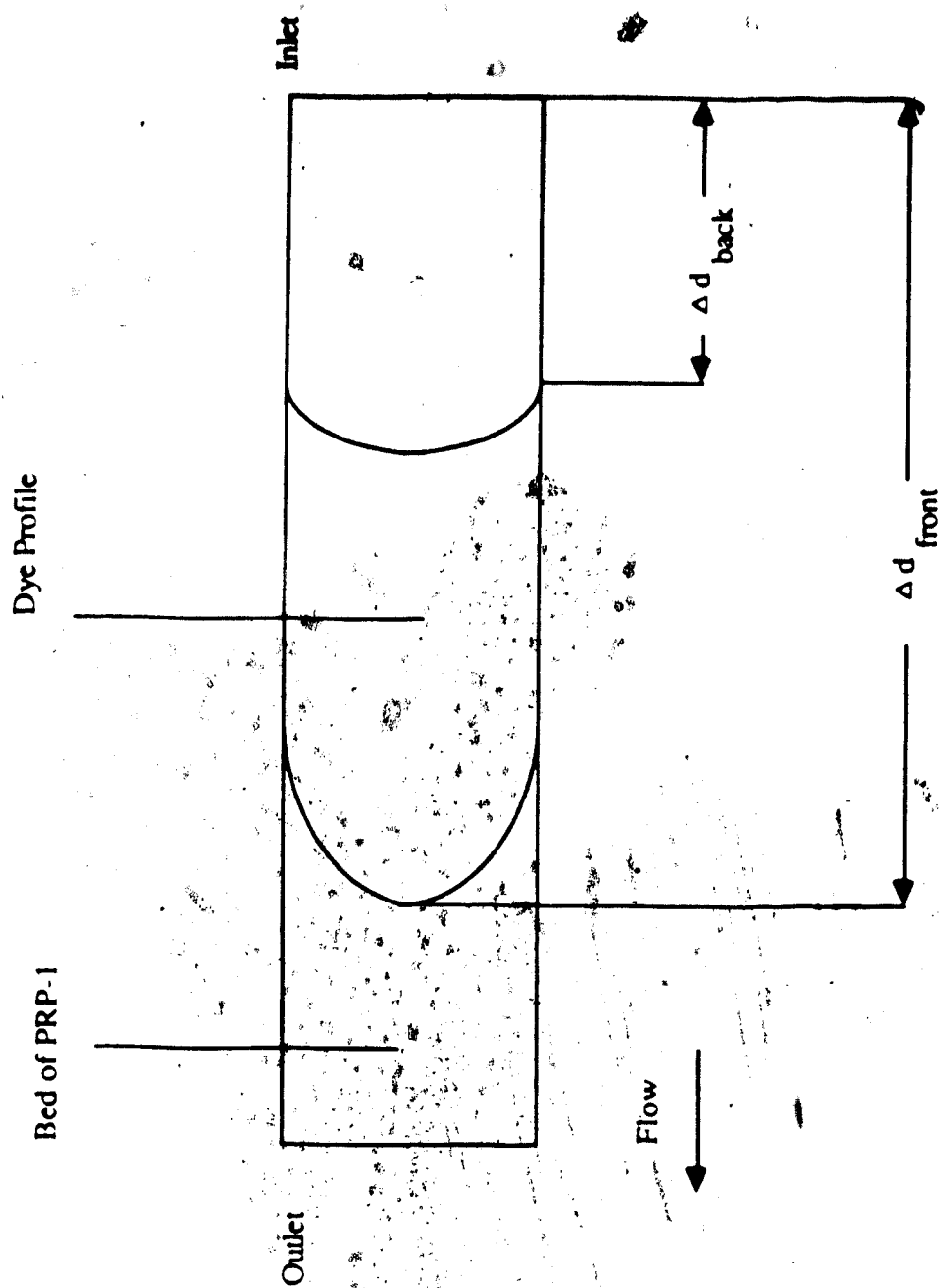


Figure 6.1 Measurement of Δd_{front} and Δd_{back} from a sample profile.

$$u_{i,max} = \frac{\Delta d_{front}}{\Delta t} \quad 6.20$$

The sample linear velocity can be related to the mobile phase linear velocity by using equation 6.21.

$$u_{o,max} = u_{i,max} (1 + k_i) \quad 6.21$$

The slowest mobile phase linear velocity, $u_{o,min}$, was determined by measuring the distance from the column inlet to the hindmost point at the trailing edge of the sample zone (Δd_{back}) as shown in Figure 6.1. This distance was divided by Δt in a manner analogous to that in equation 6.20 to obtain the slowest sample linear velocity, $u_{i,min}$. The slowest mobile linear velocity, $u_{o,min}$ was then obtained by multiplication of ($1 + k_i$) in a manner analogous to equation 6.21.

6.2 Results and Discussion

In order to determine if velocity non-uniformities were contributing to the excessive bandbroadening, it was necessary to obtain a qualitative picture of the sample velocity profile across the packed bed of stationary phase. The procedures used for packing, chromatographic characterization and extruding the bed were already described in Section 2.4.5 and will be referred to as the "velocity profile" technique in following sections.

6.2.1 Packing Structure Non-uniformity Caused by Bed Compression or Expansion

A potential cause of non-uniformities in the packing structure is compression of the bed of stationary phase under the high pressures used in HPLC. A commercially packed Hamilton PRP-1 column was checked for compression by measuring the pressure at

various flow rates in calculating the specific permeability, B^0 . The specific permeability is inversely related to the resistance of a packed bed to fluid flow. The flow through a bed can be described by Darcy's law [6.11] which states that the fluid flux is proportional to the pressure drop across the column.

$$u_0 = \frac{B^0}{L \eta \epsilon_t} \Delta P$$

6.22

Here, η is the viscosity of the mobile phase, L is the length of the bed and ϵ_t is the total porosity (previously defined in Section 3.1.5). Darcy's law is analogous to Ohm's law of electricity with the average mobile phase linear velocity (u_0) and the pressure drop, ΔP , being analogous to current and voltage, respectively. The term $(L \eta \epsilon_t / B^0)$ corresponds to the electrical resistance. B^0 should remain constant with increasing linear velocity and the pressure should increase linearly if Darcy's law is valid for the system. If the resistance of the bed is changing due to greater compression at larger u_0 or greater swelling of the particles in different solvents, B^0 will not be constant and a plot of ΔP vs u_0 will be curved.

Figure 6.2 shows a plot of ΔP vs u_0 . The column was a commercial Hamilton PRP-1 column with a bed diameter of 4.1 mm and a length of 150 mm. The mobile phase was 90% methanol(aq). Table 6.1 gives the measured pressure drop for various mobile phase linear velocities along with the corresponding flow rates and the calculated value of B^0 for each u_0 . The pressures listed in Table 6.1 are the average values of the pressure drop across the chromatographic system, of which the column is responsible for most of the resistance. Because the pumps were reciprocating piston pumps the pressure fluctuated during a pump cycle. The range of values usually extended about 5% from the mean values except for the two lowest flow rates where the range was greater. For these two flow rates, the pressure varied by 10% for $F = 0.27$ and 14% for $F = 0.055$. It can be seen in Figure 6.2 that the pressure increases linearly with increasing mobile phase linear

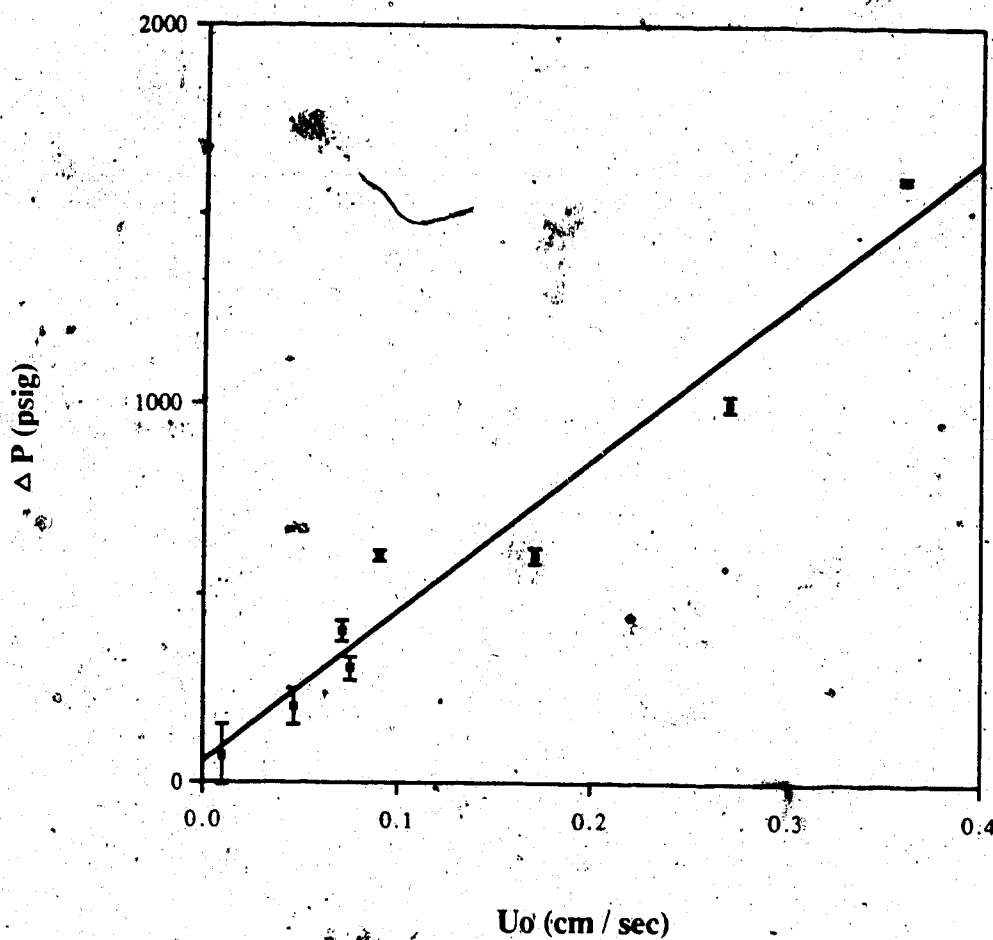


Figure 6.2 Pressure (ΔP) vs average mobile phase linear velocity (u_0) on a PRP-1 column. The column dimensions were 15 cm x 4.1 mm. The mobile phase was 90% methanol(aq).

Table 6.1 Values of the permeability coefficient at various mobile phase linear velocities and column pressure. The mobile phase was 90% methanol and the column was a 15 cm x 4.1 mm i.d. PRP-1 column. The 95% confidence limits for the pressure values are given in the text.

u_0 (cm/sec)	Flow Rate (mL/min)	ΔP (PSIG)	B_0 (cm ²)
0.36	2.1	1600	4.9×10^{-10}
0.27	1.55	1000	5.9×10^{-10}
0.17	1.0	600	6.2×10^{-10}
0.090	0.52	600	3.3×10^{-10}
0.075	0.43	300	5.5×10^{-10}
0.071	0.41	400	3.9×10^{-10}
0.047	0.27	200	5.0×10^{-10}
9.6×10^{-3}	0.055	70	3.0×10^{-10}

velocity, indicating there is no significant change in-column permeability. This can also be demonstrated by looking at B^0 vs pressure listed in Table 6.1. If the particles were being compressed under higher pressures the diameter of the interparticle channels would decrease causing an increased resistance to flow and decreased permeability. Instead, the values are scattered about an average B^0 of $5 \times 10^{-10} \text{ cm}^2$ with 95% confidence limits of $\pm 1 \times 10^{-10} \text{ cm}^2$.

The specific permeability was also measured for several different mobile phases and these results are given in Table 6.2. They can be compared to results obtained by Lee and Kinsvater [6.9] for permeability of PRP-1 in four different mobile phases. They found the permeability coefficient decreased by about 50% when tetrahydrofuran or acetonitrile was used as compared to water. This suggested that the PRP-1 was swelling slightly in the organic solvents. McGinnis and Verzele [6.12] also found that PRP-1 swelled slightly in tetrahydrofuran as compared to water. Swelling was not observed in this lab for aqueous-methanol mobile phases.

The permeability coefficient can also be calculated using the Kozeny-Carmen equation [6.13] which relates it to particle diameter. For spherical particles the Kozeny-Carmen equation is given in equation 6.23.

$$B^0 = \frac{d_p^2}{180} \frac{\epsilon_{\text{inter}}^3}{(1 - \epsilon_{\text{inter}})^2} \quad 6.23$$

Using the Kozeny-Carmen equation, the predicted value for the permeability coefficient was $4 \times 10^{-10} \text{ square cm}$ (Table 6.2) which compares well with the experimental value, suggesting no compression or swelling is occurring.

Permeability coefficients were also measured for a C8 column and these results are listed in Table 6.2, as well. It can be seen that the permeability of PRP-1 was comparable to that of the C8 column.

Table 6.2 Comparison of permeability coefficients obtained by measurement on various columns and mobile phases with literature values for PRP-1 with the theoretical value calculated using the Kozeny-Carmen equation.

Source of Permeability Coefficient	Stationary Phase	Mobile Phase	B_0 (cm^2)
Experiments in this lab	PRP-1	water	5×10^{-10}
		80% methanol(aq)	3×10^{-10}
		90% methanol(aq)	1×10^{-10}
		90% acetonitrile(aq)	1×10^{-10}
	C8	water	1×10^{-10}
		80% methanol(aq)	6×10^{-10}
		90% methanol(aq)	4×10^{-10}
Reference 6.9	PRP-1	water	2.8×10^{-10}
		1:1 acetonitrile:H ₂ O	1.7×10^{-10}
		acetonitrile	1.6×10^{-10}
		tetrahydrofuran	1.3×10^{-10}
Kozeny-Carmen ($d_p = 0.001 \text{ cm}$)	PRP-1		4×10^{-10}

6.2.2 Short Column Characterizations by Chromatography

Most of the short, home-packed columns used in the velocity profile experiments were characterized by measuring the void volume and plate height. This was done to determine if all columns were of equal efficiency so the sample velocity profiles could be compared between columns. Three types of endfittings were used in the velocity profile experiments and are shown in Figure 2.6. The "perforated plate" and the "washer" endfittings were used to allow the column effluent to exit uniformly from the bed. The commercial Swagelok endfitting, which is normally used in chromatography, causes the effluent from the 4.1 mm diameter bed to be constricted down to 0.25 mm (the i.d. of the stainless steel tubing) immediately downstream of the outlet frit. The only columns which were not characterized prior to exclusion were those which were packed with the "perforated plate" outlet endfitting in place, since this fitting could not be connected to a detector. Void volumes for the PRP-1 columns were measured with $\text{Ca}(\text{NO}_3)_2$ and the average column void volume was 0.43 ± 0.02 mL (95% confidence limits). The small deviation from the mean V_m indicates there were no gross differences in the total void space of the columns caused by gaps or channels.

Plate heights were measured using either methyl paraben ($k'_i = 0.9$) or 4-phenylazo-1-naphthylamine ($k'_i = 30$) and these results are listed in Table 6.3. They were calculated from the second moment of the elution peak using equation 3.9. The plate heights for columns which had the "washer" endfitting are listed separately since H will be larger for these because of the dead space caused by the washer. The plate heights for the organic dye compound were large, partly because the high concentration used (10^{-3} M) was probably in the non-linear region of its adsorption isotherm. This concentration was necessary in order to see the dye on the stationary phase. However, isotherm non-linearity does not necessarily interfere with the results observed for a non-uniform velocity profile caused by a heterogeneous packing structure. The only effect that (convex) isotherm

Table 6.3 Plate heights for 10^{-5} M methyl paraben and 10^{-3} M 4-phenylazo-1-naphthylamine on the PRP-1 columns used in the velocity profile experiments. The mobile phase was 90% methanol(aq) and the flow rate was 2 mL per minute. 95% confidence limits are given with the mean values.

Methyl Paraben Plate Height (cm)	4-phenylazo-1-naphthylamine Plate Height (cm)
Consistent flow (Swagelok endfitting)	
0.20	
0.71	
0.30	3.1
0.64	2.9
0.30	2.2
mean = 0.43 ± 0.28	mean = 2.7 ± 1.2
Uniform Flow (Washer endfitting)	
0.64	3.4
1.07	3.9
0.95	3.9
0.43	2.8
0.57	3.7
0.41	2.9
0.39	2.7
mean = 0.64 ± 0.25	mean = 3.3 ± 0.5

non-linearity should have on the flow profile is to cause the sample band to exhibit axial asymmetry. The highest concentration would be at the front edge and would gradually decrease toward the rear (see Figure 6.3a). The concentration distribution would not appear axially symmetrical as it would in a linear, non-ideal case (Figure 6.3b). In contrast, a non-uniform velocity profile would give rise to different positions of advancement at different radial positions across the bed.

Many replicates were done of the PRP-1 extrusions because the dyes were somewhat hard to see against the cream colored, opaque packing material. Also, the PRP-1 beds did not hold together well and often broke into several segments upon extrusion. By repeating the experiment many times, the column extrusion technique could be trusted to give a statistically meaningful picture of the velocity profile. The column extrusion technique was also used with a bonded phase C18 sorbent, Whatman Partisil-10 ODS 3. In contrast to the PRP-1 stationary phase, the C18 bed came out in one piece and was translucent so the outline of the dye could be easily seen. Because of this, the C18 extrusion was done only in duplicate. The average void volume for the C18 columns was 0.48 ± 0.09 mL (95% confidence limits). The plate heights for several samples on C18 were measured by moments analysis on elution chromatograms and are listed in Table 6.4. The plate heights for the two organic dyes are large. This is probably due to both isotherm non-linearity and interactions with residual silanol groups on the C18 silica matrix. Both of these effects would produce axial asymmetry (Figure 6.3a) rather than radial asymmetry and would not interfere with the velocity profile results. Also, the plate heights are larger for the C18 column with the washer at the outlet because of the dead space created by the washer.

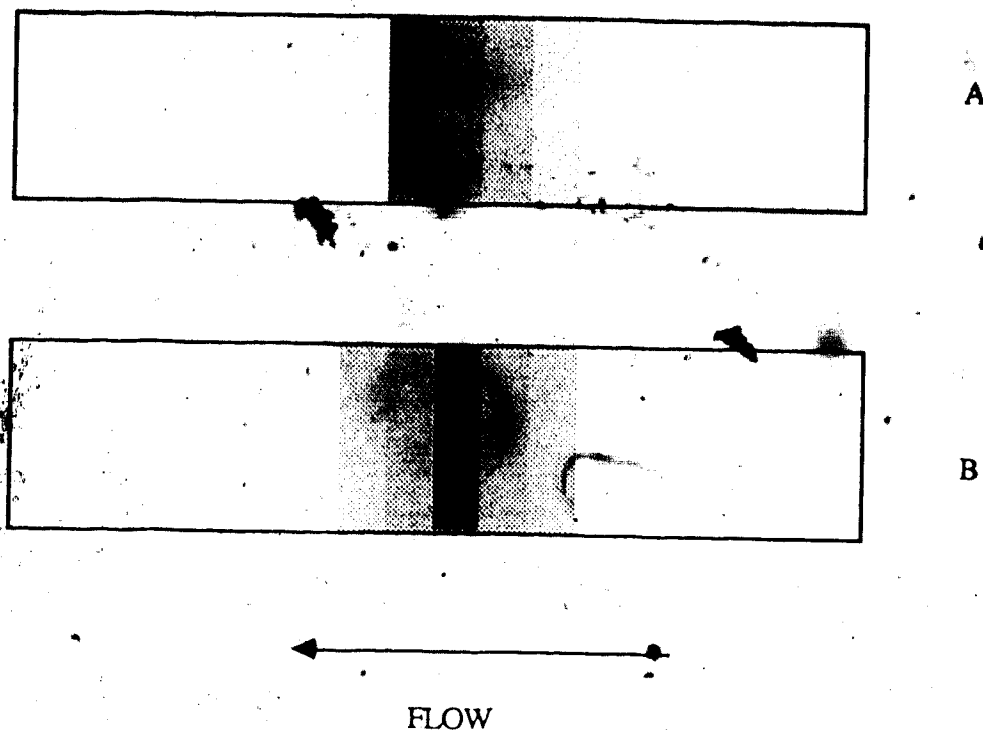


Figure 6.3 Sample profiles on a column with a uniform velocity profile. The sample concentration is in the (A) non-linear isotherm region of a convex isotherm and (B) linear isotherm region. Figure 6.3a also represents a profile for a sample which is adsorbing on residual silanol groups on a bonded phase column.

Table 6.4 Plate heights for C18 columns used in the velocity profile experiments. The mobile phase was 90% methanol(aq) and the flow rate was 2 mL per minute.

Sample	k'_1	H (mm)
Constricted Flow (Swagelok endfitting)		
1.03×10^{-5} M n-butyl paraben	0.2	0.08
1.04×10^{-5} M n-nonyl paraben	0.3	0.11
6.7×10^{-4} M amaranth	1.0	1.9
Uniform Flow (Washer endfitting)		
1.3×10^{-5} M methyl paraben	0.4	1.8
9.9×10^{-5} M 4-phenylazo-1-naphthylamine	0.9	1.8
6.7×10^{-4} M amaranth	1.2	3.8

6.2.3 Velocity Profile Results Using the Constricted Flow Configuration

The velocity profile experiments revealed the sample velocity profile across the bed of stationary phase. The sample velocity profile is not always the same as the mobile phase velocity profile because of diffusive and convective lateral relaxation. For example, if the packing structure was more permeable at the column wall than the column center, the mobile phase velocity would be faster at the wall region. At the same time, if lateral transfer of solute across the column was very fast, the sample zone would appear to be uniform and should not show any significant bandbroadening. This is because sample in the different regions would be exchanged quickly, averaging out the velocity differences. If lateral transfer was slow, sample would stay in the different velocity regions for longer times and would approximate the mobile phase velocity profile more closely.

Therefore, what is of interest in the velocity profile experiments is not only the mobile phase velocity profile but also the rate of solute lateral mass transfer. If a uniform sample profile is observed, the mobile phase velocity profile may be non-uniform but that is inconsequential because the rate of lateral transfer is fast enough to compensate. However, if the sample velocity profile is observed to be non-uniform, then the mobile phase velocity profile is also non-uniform and lateral transfer is too slow to average the velocity differences. Therefore, bandbroadening will occur due to the non-uniform flow profile. According to Giddings [6.14], lateral transfer due to convection (eddy diffusion) should require an axial distance of about 4 cm in order for the sample to move a lateral distance of 0.205 cm (the radius of the PRP-1 columns). In the short 5 cm long columns used in the velocity profile experiments, this means about 1 transcolumn lateral transfer would occur. For the 15 cm long analytical columns about 3 to 4 transcolumn lateral transfers would occur. These numbers are rough estimates but one can see that lateral convection cannot be expected to significantly relax a transcolumn non-uniform velocity profile.

The details of the velocity profile experiment are given in Section 2.4. Basically, there were seven steps in the procedure.

1. Packing of the column.
2. "Pre-chromatographic conditioning" of the column by flowing mobile phase through the column before chromatographic characterization.
3. Characterization of the column using chromatography to measure the void volume and plate height.
4. Post-chromatographic conditioning.
5. Injection of the organic dye and partial elution down the column.
6. Conditioning the bed with 10% glycerin(aq) to enhance particle cohesion prior to extrusion.
7. Extrusion of the packed bed.

For the first set of experiments short, 5 cm long columns were packed with PRP-1 using conventional Swagelok endfittings. The mobile phase flow through this type of fitting will be referred to as "constricted" flow (Figure 2.6). The mobile phase entered the column from a stainless steel tube which had an i.d. of 0.25 mm, passed through a frit (1 mm thick and nominal pore size of 2 micrometers) and then finally entered the bed of stationary phase (diameter of 4.1 mm). The frit should direct some of the mobile phase stream laterally so it would encounter a larger area of stationary phase. The reverse process occurred at the column outlet where mobile phase exited the stationary phase, passed through another frit and finally left through the narrow bore tubing. Table 6.5 gives the volume of eluent passed through the column for each step of the velocity profile experiment run under constricted flow conditions. The sample profiles shown in Figure 6.4 are the shapes obtained under these conditions. Generally, the sample velocity was faster in the center of the column and slower at the walls. Also, there is a difference in the shape of the profiles between the individual columns and between the different samples. The samples were about 1/2 to 3/4 of the way down the column when the flow was stopped and the bed

Table 6.5 Solvent volume passed through the columns during each step in the velocity profile experiment prior to extrusion. Constricted outlet flow conditions were used in each step.

Sample Profile Figure #	EFFLUENT VOLUME PRIOR TO EXTRUSION		
	Packing (mL)	Pre-chromatographic Conditioning (mL)	Chromatographic Characterization (mL)
6.4a	70	30	20
6.4b	70	30	65
6.4c	70	30	20
6.4d	70	40	20
6.4e	70	20	15

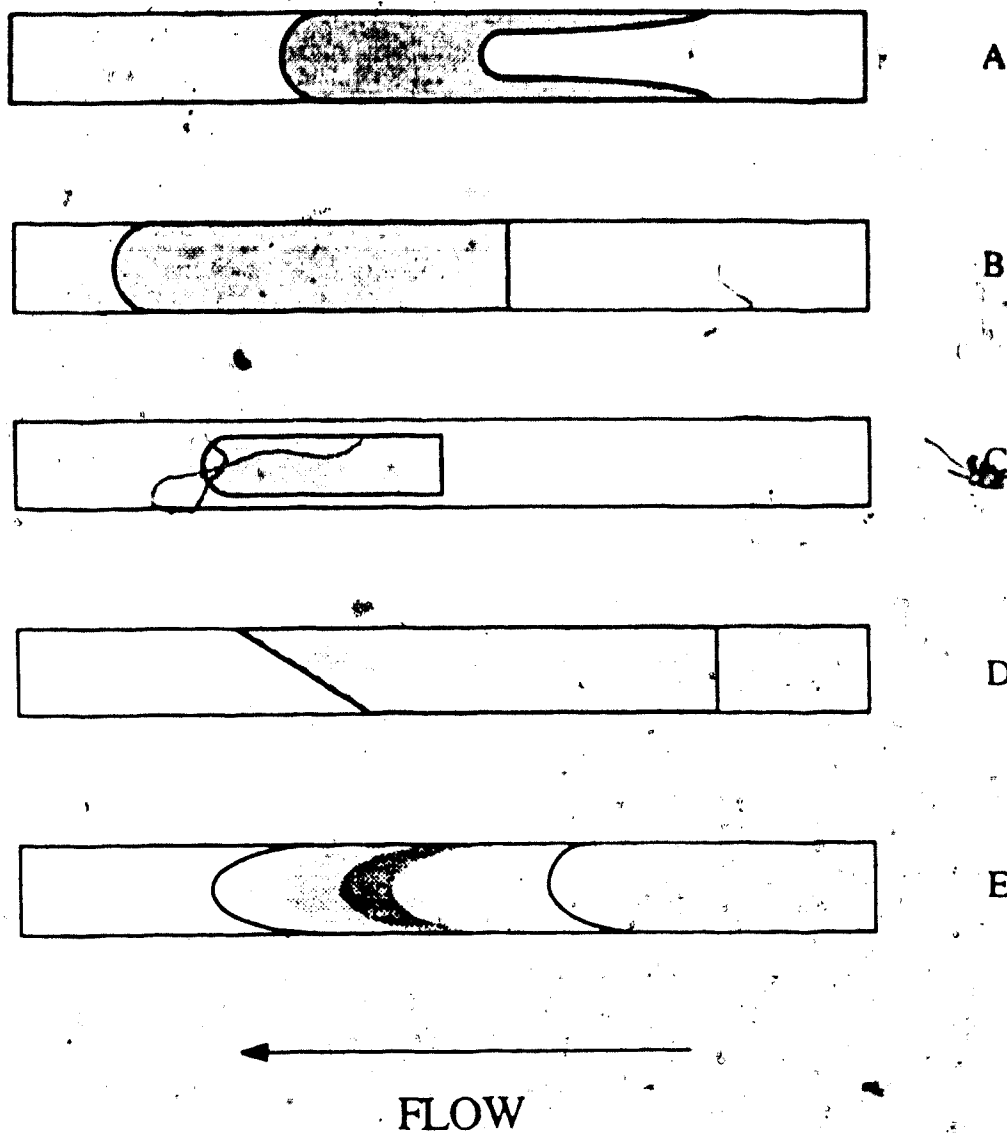


Figure 6.4 Sample profiles obtained on PRP-1 from the velocity profile experiments under constricted flow conditions. The sample compounds are (A) 4-phenylazo-1-naphthylamine $k_i' = 30$ (B) 4-phenylazoaniline $k_i' = 7$ (C) 1-aminoanthraquinone $k_i' = 17$ (D) 4-phenylazo-1-naphthylamine $k_i' = 30$ and (E) amaranth $k_i' = 0.6$. All concentrations were 10^{-3} M.

Table 6.6 Sample velocity at the column wall and center for the front (outlet) and back (inlet) edges of the sample zone. Constricted flow conditions were used in all steps of the velocity profile experiment. The samples used and their corresponding k_i' values are : (6.4a) 4-phenylazo-1-naphthylamine $k_i' = 36$ (6.4b) 4-phenylazoaniline $k_i' = 7$ (6.4c) 1-aminoanthraquinone $k_i' = 17$ (6.4d) 4-phenylazo-1-naphthylamine $k_i' = 36$ (6.4e) amaranth $k_i' = 0.6$. All concentrations were 10^{-3} M.

Sample Profile Figure #	Front Edge of Sample Zone		Back Edge of Sample Zone	
	$u_{i,center}$ (cm / sec)	$u_{i,wall}$ (cm / sec)	$u_{i,center}$ (cm / sec)	$u_{i,wall}$ (cm / sec)
6.4a	0.013	0.012	0.010	4.2×10^{-3}
6.4b	0.080	0.077	0.043	0.043
6.4c	0.025	did not reach wall	0.018	0.018
6.4d	0.012	0.015	4.2×10^{-3}	4.2×10^{-3}
6.4e	0.40	0.38	0.14	0.11

extruded. Table 6.6 lists the wall and center velocities measured for the front and back edges of the sample profile. These results are discussed below and their significance is more apparent when compared to the results from the short columns with uniform flow configurations (Section 6.2.4).

6.2.4 Velocity Profile Results Using the Uniform Flow Configuration

The Swagelok outlet endfitting was replaced by either the perforated plate or washer endfitting, while leaving a conventional Swagelok constricted flow endfitting at the inlet. Now when the stream left the bed, it passed through the frit and then exited more uniformly from the column. In the case of the perforated plate, the effluent flowed through 19 holes (hole diameter = 0.5 mm) which were evenly distributed over the 4.1 mm area. The washer provided a small pool, also of 4.1 mm diameter, in which the mobile phase collected before exiting through the narrow stainless steel tube. The flow through either of these two endfittings will be called "uniform" flow. Table 6.7 lists the volume of eluent passed through the columns in each step using uniform flow conditions. The usefulness of this information is explained later in this Section. Figure 6.5 shows the sample profiles obtained under these conditions and the sample velocities are listed in Table 6.8. These profiles are opposite of those acquired with constricted flow conditions. Now the sample velocity is fastest at the walls and slowest in the center. Under these flow conditions using the washer endfitting the profile was sometimes quite distorted, with tails of sample in the slow central velocity region streaming behind the main portion of the zone. Since the velocity inequalities occur over the entire diameter of the column, this is a transcolumn bandbroadening contribution. Compared to the constricted flow velocity profiles, there is less difference in the sample zone shape between the individual columns with the same type of endfitting. Therefore, the inter-column differences observed for sample zones obtained

Table 6.7 Solvent volume passed through the columns during each step of the velocity profile experiment prior to extrusion. Uniform flow conditions were used in each step and achieved with either a perforated plate (*) or a washer endfitting. The sample was 10^{-3} M 4-phenylazo-1-naphthylamine.

Sample Profile Figure #	EFFLUENT VOLUME PRIOR TO EXTRUSION		
	Packing (mL)	Pre-chromatographic Conditioning (mL)	Chromatographic Characterization (mL)
6.5a *	70	60	n.a.
6.5b *	70	40	n.a.
6.5c	70	20	60
6.5d	70	20	60

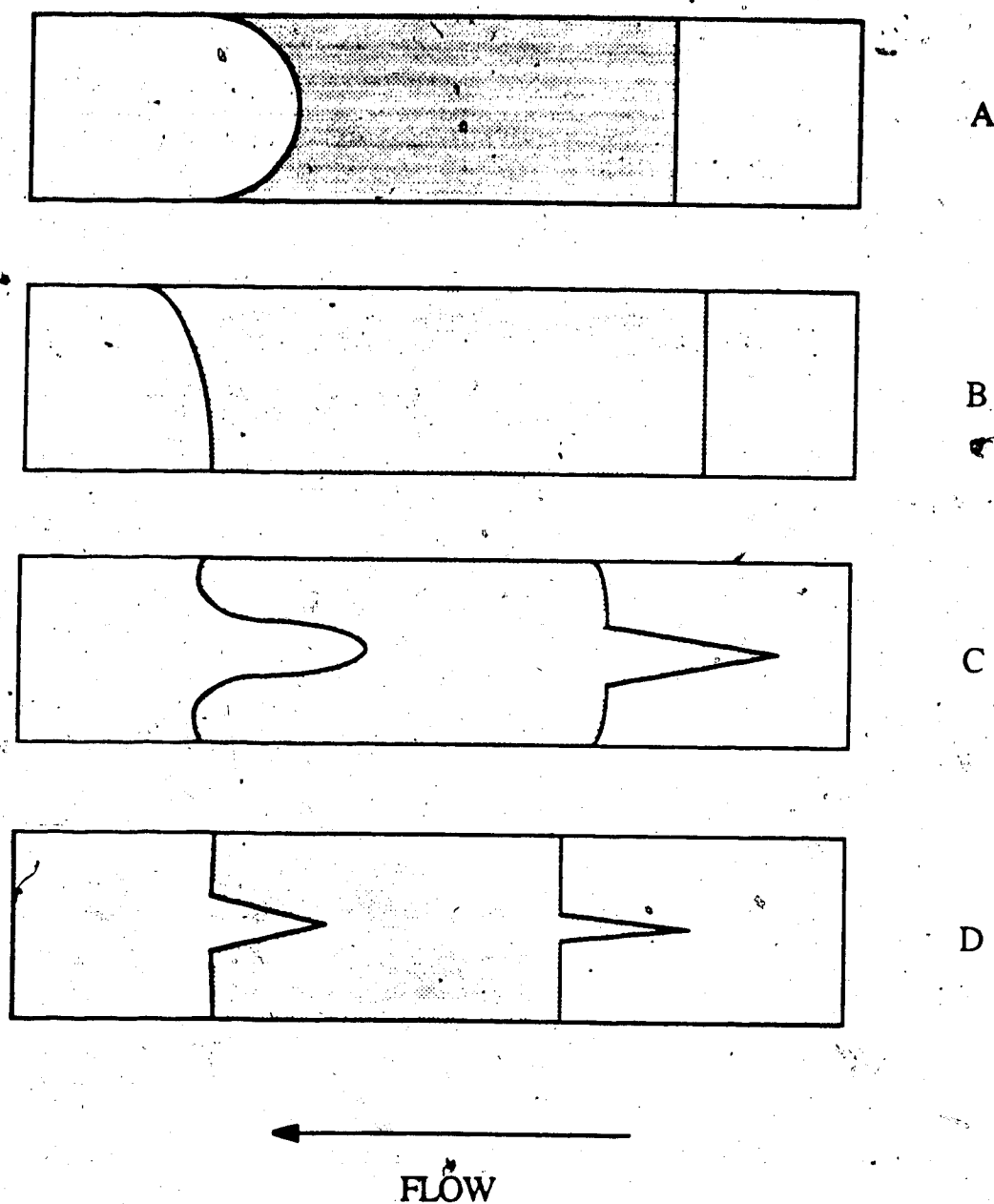


Figure 6.5 Sample profiles obtained on PRP-1 using uniform flow conditions. Uniform flow was achieved using a perforated plate endfitting for (A) and (B) and a washer endfitting for (C) and (D). The sample was 10^{-3} M 4-phenylazo-1-naphthylamine.

Table 6.8 Sample velocity at the column wall and center for the front (outlet) and back (inlet) edges of the sample zone. Uniform flow conditions were used in all steps of the velocity profile experiment. The sample was 10^{-3} M 4-phenylazo-1-naphthylamine and the stationary phase was PRP-1. An asterisk (*) indicates a screen endfitting was used otherwise a washer fitting was used.

Sample Profile Figure #	Front Edge of Sample Zone		Back Edge of Sample Zone	
	$u_{i,center}$ (cm / sec)	$u_{i,wall}$ (cm / sec)	$u_{i,center}$ (cm / sec)	$u_{i,wall}$ (cm / sec)
6.5a *	0.015	0.016	0.0067	0.0067
6.5b *	0.018	0.0018	0.0058	0.0058
6.5c	0.010	0.016	~ 0	0.0071
6.5d	0.011	0.017	0.0042	0.0092

under constricted flow conditions (Figure 6.4) may be due to differences in the types of dye used.

These results demonstrate that there is a non-uniform sample velocity profile caused by a heterogeneous packing structure. The packing structure is different for each of the three endfittings used with the short columns of PRP-1. The fact that the gross shape inverts upon going from constricted flow conditions to uniform flow conditions indicates that the packing structure is dependent on the flow configuration of the mobile phase.

The question arises with reference to both constricted and uniform flow whether the heterogeneous packing structure, which gives rise to the uneven flow pattern, was formed during or after packing. During conditioning and chromatographic characterization, 40 to 100 mL of mobile phase were passed through the column and it was possible that the irregular bed structure developed during these steps rather than during the actual packing. To test this hypothesis, columns were packed under constricted outlet flow conditions and switched to uniform flow (using the washer fitting) for conditioning and chromatographic characterization. The volumes of solvent used in each step of the velocity profile experiment under these conditions are listed in Table 6.9. These volumes have been listed to see if the shape of the sample profile is related to the amount of solvent flowing through the bed under a particular outlet endfitting configuration. Diagrams of the sample profile results are shown in Figure 6.6 and the sample velocities are given in Table 6.10. If a permanent bed structure was formed during packing the flow should be fastest at the center. Instead, the observed profiles are intermediate in shape between those obtained under constricted and uniform flow conditions. In Figures 6.6a and b the linear velocities for half the column are faster than they are in the second half, while in Figures 6.6c and d the flow is slower in the center. Also, the zones depicted in Figures 6.6a and b had only 20 mL of solvent flow through the bed while using the washer endfitting prior to dye injection and bed extrusion while the zones in Figures 6.6c and d had 80 or 110 mL. The sample zone shapes which resulted when the bed had a greater amount of solvent passed

Table 6.9 Solvent volume passed through the columns during each step of the velocity profile experiment prior to extrusion and the corresponding flow conditions for each step. An asterisk (*) indicates uniform flow conditions were used, otherwise constricted flow conditions. The sample was 10^{-3} M 4-phenylazo-1-naphthylamine.

Sample Profile Figure #	Packing (mL)	EFFLUENT VOLUME PRIOR TO EXTRUSION	
		Pre-chromatographic Conditioning (mL)	Chromatographic Characterization (mL)
6.6a	75	30	20 *
6.6b	75	20	20 *
6.6c	70	20 *	60 *
6.6d	70	20 *	90 *

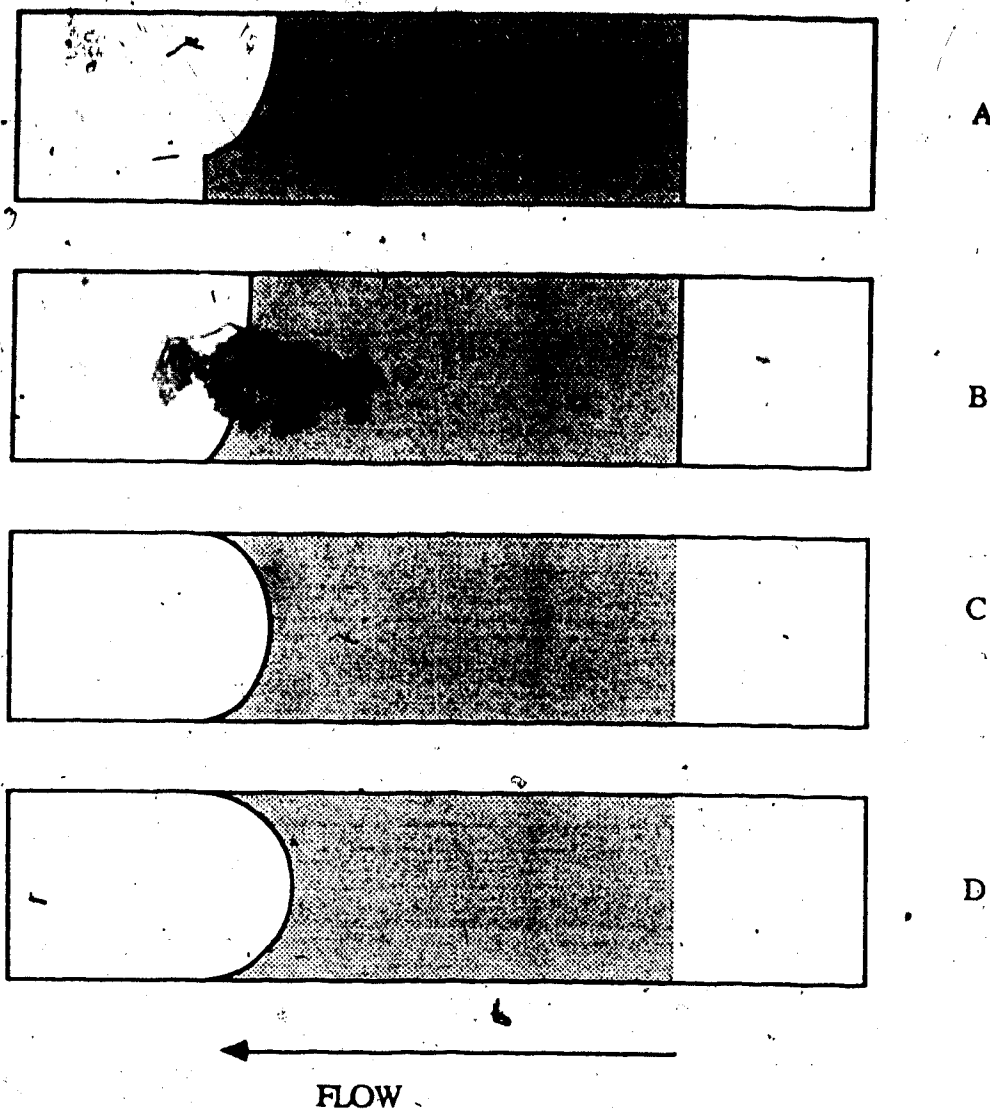


Figure 6.6 Sample profiles obtained on PRP-1 when columns were packed using constricted flow conditions and then switched to uniform flow conditions prior to injection of the dye. See Table 6.9 for the solvent volumes and flow conditions used in each step of the experiments. The sample was 10^{-3} M 4-phenylazo-1-naphthylamine.

Table 6.10 Sample velocity at the column wall and center for the front (outlet) and back (inlet) edges of the sample zones shown in Figure 6.6. The flow conditions for each are given in Table 6.9. The sample was 10^{-3} M 4-phenylazo-1-naphthylamine and the stationary phase was PRP-1. The results for the back edge of samples 6.6c and 6.6d are unknown because this section of the column fell apart before the dye profile could be observed.

Sample Profile Figure #	Front Edge of Sample Zone		Back Edge of Sample Zone	
	$u_{i,center}$ (cm / sec)	$u_{i,wall}$ (cm / sec)	$u_{i,center}$ (cm / sec)	$u_{i,wall}$ (cm / sec)
6.6a	0.018	0.017	0.0046	0.0046
6.6b	0.018	0.017	0.0050	0.0050
6.6c	0.015	0.016	unknown	unknown
6.6d	0.016	0.017	unknown	unknown

through it under uniform flow conditions, had the most exaggerated shapes, suggesting the volume of solvent passed through the bed under a particular outlet endfitting configuration does influence the packing structure. None of these sample zone shapes, which were formed under changing outlet flow configurations, are as exaggerated as those shown in Figures 6.5c and d, where uniform flow conditions were used in all steps. From these results it seems the bed structure is changing after packing in response to the outlet flow configuration. Apparently, the stationary phase does not acquire a stable configuration during packing but shifts, causing large areas of increased permeability and higher velocities.

6.2.5 Velocity Profiles Obtained on C18 Columns

Short columns of C18 were also tested under constricted and uniform flow conditions. In the first extrusion experiment the column was packed, conditioned and characterized using a constricted flow outlet endfitting and in the second experiment a uniform flow washer endfitting was used for all three steps. The solvent volumes used in each step are given in Table 6.11. The sample profiles are shown in Figure 6.7 and the center and wall sample velocities are listed in Table 6.12. The profiles have the same shape under the two sets of flow conditions, with the flow being somewhat faster in the center at the leading edge of the band. The profiles were not nearly as distorted as some of those obtained with PRP-1 and more importantly, they do not change shape with the type of outlet endfitting used. The C18 columns were quite moist (appearing to have the consistency of jelly) and stuck together well. They seemed to be wetted much better by the mobile phase than did PRP-1, which was always crumbly and dry.

Table 6.11 Solvent volume passed through the C18 columns during each step of the velocity profile experiments and the corresponding flow conditions for each step. An asterisk (*) indicates uniform flow conditions (using a washer endfitting)were used, otherwise constricted flow conditions. The sample was 10^{-3} M amaranth for the C18 columns.

Sample Profile Figure #	Packing (mL)	EFFLUENT VOLUME		
		Pre-chrom. Conditioning (mL)	Chromatographic Characterization (mL)	Post-Chrom. Conditioning (mL)
6.7a	70	20	75	0
6.7b	70 *	20 *	150 *	0

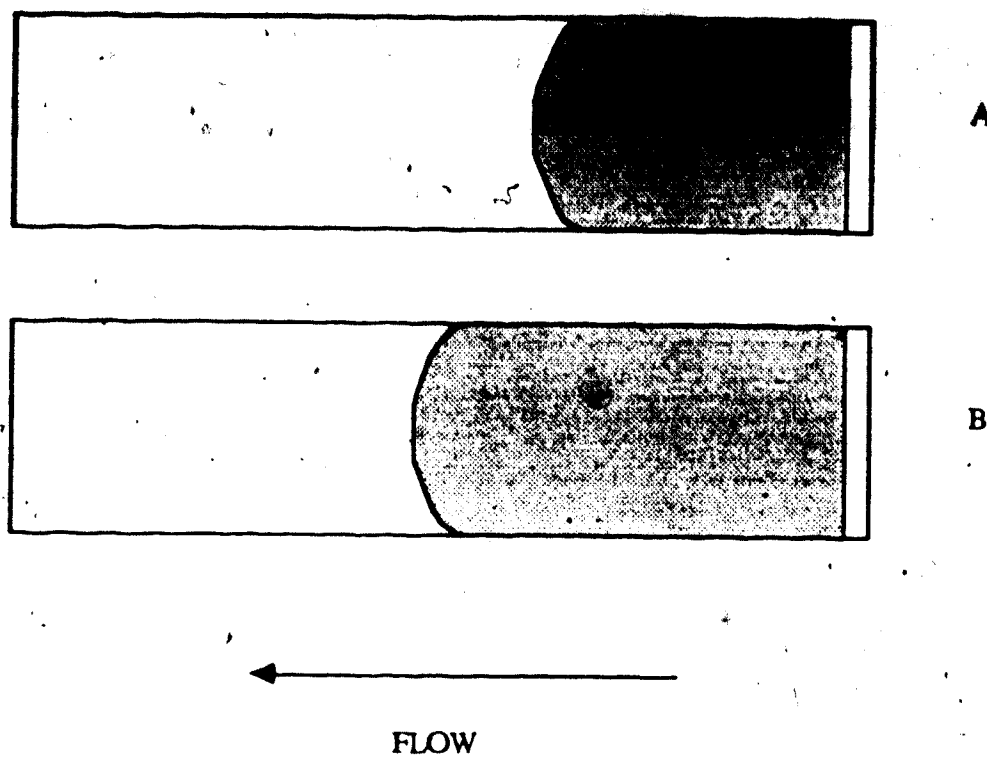


Figure 6.7 Sample profiles obtained using C18 under (A) constricted flow conditions and (B) uniform flow conditions. The sample was 10^{-3} M amaranth.

Table 6.12 Sample velocity at the column wall and center for the front (outlet) and back (inlet) edges of the sample zones shown in Figure 6.7. The flow conditions for each are given in Table 6.11. The sample was 10^{-3} M amaranth for the C18 columns.

Sample Profile Figure #	Front Edge of Sample Zone		Back Edge of Sample Zone	
	$u_{i,center}$ (cm / sec)	$u_{i,wall}$ (cm / sec)	$u_{i,center}$ (cm / sec)	$u_{i,wall}$ (cm / sec)
6.7a	0.24	0.20	-0	-0
6.7b	0.43	0.40	-0	-0

6.2.6 Conclusions from Velocity Profile Experiments

Although under normal conditions a chromatography column is always packed and used with constricted flow endfittings, the results of the present experiment are helpful in explaining the broad sample peaks obtained with PRP-1. The PRP-1 stationary phase does not appear to be wetted sufficiently by the types of solvents commonly used in reverse-phase chromatography and consequently, the particles do not cohere well. Similar problems have been studied in soil science [6.15, 6.16] concerning the cohesiveness of soil. The ability of soil particles to stick together in a stable packing structure depends on two parameters. The first is chemical cohesiveness which results from water wetting the soil particles and pulling them together by capillary action. The second is friction between particles which prevents slippage and collapse of the soil structure. The stabilizing effect of friction is more important for irregular particles and those that are not wetted sufficiently by water. In the case of PRP-1, the spherical particles appear to be dry and not wetted very well by aqueous-methanol mobile phases. Consequently, the particles do not seem to develop a stable packing configuration. They move in response to a stress (the mobile phase flow) which is placed on them by shifting out of the path of the mobile phase stream. In a constricted flow column, normally used in HPLC, this causes the center region to have a higher permeability and a higher velocity than the wall region and this transcolumn velocity inequality cannot be relaxed sufficiently by lateral transfer.

6.2.7 Plate Height Calculation Based on Velocity Profile

If the PRP-1 packing were being pushed toward the walls by the mobile phase stream as suggested above, there would be an increased amount of stationary phase in this region and consequently, a slower mobile phase linear velocity and a larger k_1' for the sample, as discussed in Section 6.1.2 and 6.1.2. The program H(WS), described in

Section 6.1.3, was used to predict plate heights based on both these effects. The parameters used to simulate peaks with this program are listed in Table 6.13.

This calculation was run for samples with K_i equal to 1 liter per kg (methyl paraben) and 45 liter per kg (4-phenylazo-1-naphthylamine) on PRP-1. For both samples, the number of moles eluted from all the rings was plotted vs retention time of solute. These simulated peaks are shown in Figure 6.8. The simulated peaks do not have the same shape as experimental peaks. This program only considers the effect of a non-uniform velocity profile on peak shape and H and it neglects other sources of bandbroadening. Also, in the program it was assumed that no lateral transfer occurred between the velocity regions.

Figure 6.9 shows how the model sample zone shape which was used for the H(WS) program would look during its initial movement down the PRP-1 column. Also, a "real" sample zone with lateral transport is pictured for a comparison. Both the model and the real zones are evenly distributed across the bed cross-section upon injection and this is shown in Figure 6.9a and 6.9d. The model zone actually has an injection shape of zero width (an impulse function) but it is shown having a finite width in Figure 6.9 for diagrammatical purposes. The column has a less densely packed center region and a more densely packed wall region, which causes a faster mobile phase linear velocity in the column center than at the walls. Therefore, after the model sample zone has moved a short distance down the column, it looks like something like a triangle with a uniform width (Figure 6.9b). The plate height would be related to the distance between the foremost point of the zone at the center and the hindmost points at the walls. The plate height would increase as this distance increased. The real sample zone is arc-shaped and because some lateral transport has occurred, the width of the zone is not uniform but resembles the shape drawn in Figure 6.9e.

As the model sample zone elutes farther down the column it becomes an increasingly elongated "triangle" but always retains a uniform width (Figure 6.9c). It is

Table 6.13 Variables used for the program H(Ws) to predict the effect of an uneven packing density on plate height.

Variable	Value
Column Length (L) *	5 cm
Column Radius (R) *	0.205 cm
Number of Rings	30
Moles Injected *	1×10^{-8}
Particle Diameter (DP) *	0.001 cm
Column Pressure Drop (P) *	915 psig
Viscosity (VISC) *	0.014 poise
Distribution Coefficient *	45 and 1 liter / kg
Weight of Packing at Wall	0.0171 g
Weight of Packing at Center	0.000262 g
Average Packing Density *	0.37 g / cm ³

An asterisk (*) indicates an experimentally measured value.

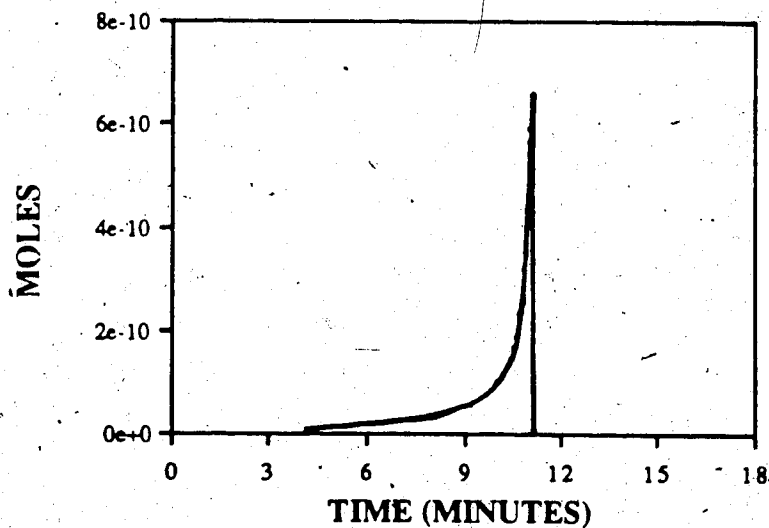
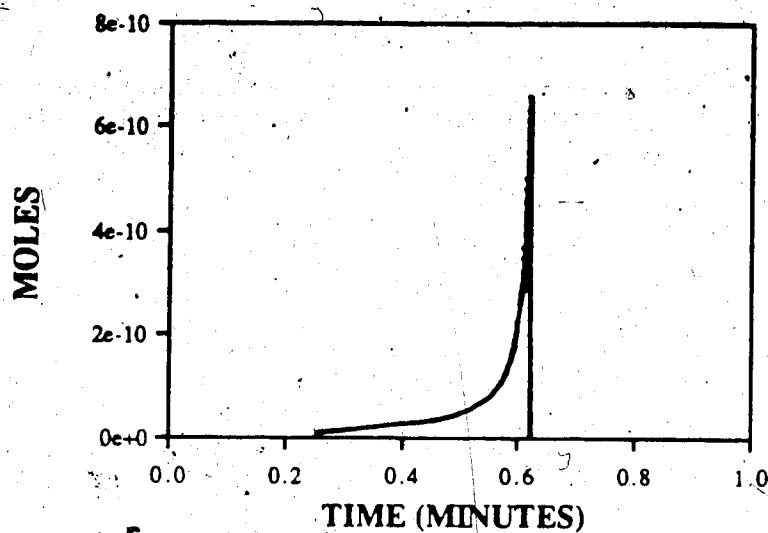


Figure 6.8 Simulated elution peaks for (A) 5×10^{-4} M methyl paraben $K_i = 1$ l/kg and (B) 10^{-3} M 4-phenylazo-1-naphthylamine $K_i = 45$ l/kg. The peaks were calculated using the program H(WS). The "column" used in the simulation was a 5 cm long PRP-1 column. The column i.d. was 4.1 mm.

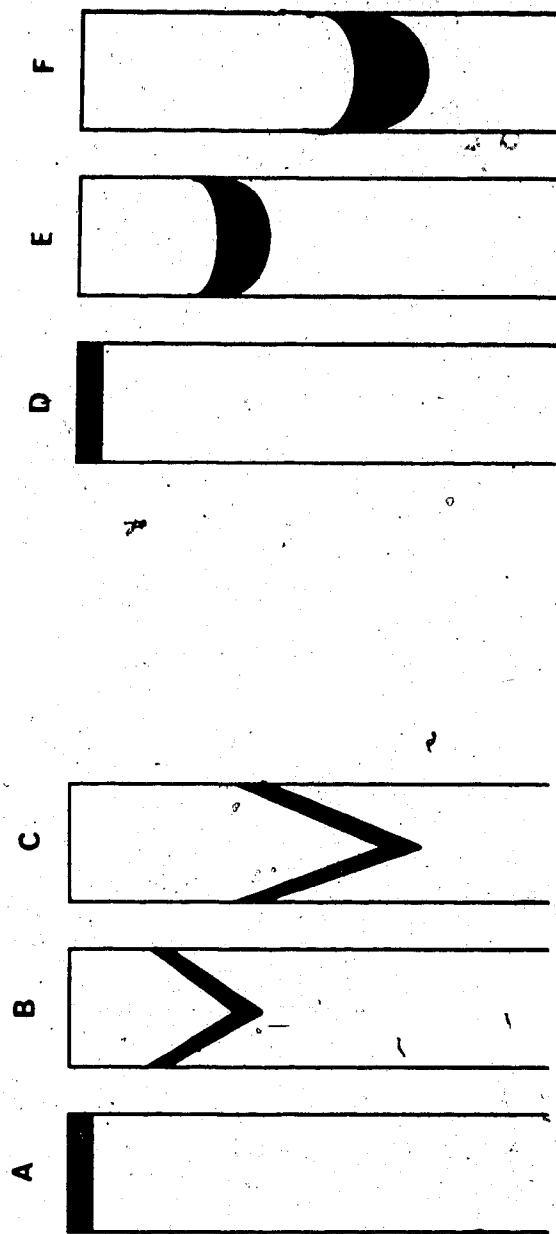


Figure 6.9 Diagram of the model sample zone used in the H(WS) program and a real sample zone at various stages of migration on a column. The model zone has no lateral transport while the real sample zone does have lateral transport. (A) and (C) are the model zone and real zone upon injection. The model zone was assumed to have an infinitely thin width in the simulation but it is shown here with a finite width for diagrammatical purposes. (B) and (D) model and real zone after migrating a short distance down the column. (E) and (F) model and real zone at a later stage of migration.

obvious that the peak shape which will result from this zone will always be fronting, since the faster moving center region has the smallest volume and the least sample. In contrast, the real sample zone becomes broader (Figure 6.9f) as lateral transport moves the sample to different adjacent radial positions, producing a more symmetrical elution peak. The width of the real zone is still quite wide, due to the transcolumn non-uniform velocity profile but the real zone will be narrower than the model zone. If lateral transport is slow, the real zone will more closely resemble the model zone.

Since lateral transport relaxes the effects of a non-uniform velocity profile, the program H(WS) will overestimate the bandbroadening due to a non-uniform velocity profile and the plate height calculated from the simulated peak will be too large. However, since a transcolumn non-uniform velocity profile is not expected to be relaxed much by lateral transport because of the large radial distance to be crossed, this error is not expected to be very large. The plate height obtained from this program will be useful as an upper limit to the bandbroadening caused by the transcolumn non-uniform velocity profile measured on PRP-1.

Table 6.14 lists calculated and experimental values for W_s , V_m , $u_{0,max}$ and $u_{0,min}$. Since these values calculated from H(WS) match the experimental values quite well, it can be assumed the program is reasonably accurate.

The retention volumes, V_r , and plate heights, H , measured for the simulated peaks and for corresponding experimental peaks are also listed in Table 6.14. These values were obtained by determining the center of gravity and variance using moment analysis for the simulated peaks shown in Figure 6.8 and for the experimental peaks. It can be seen the plate heights of the simulated peaks increase very slightly with increasing K_i by comparing the average values of H for $K_i = 1$ and 45 liter per kg. The plate height, H , is 1.25x larger for a sample with a distribution coefficient which is 45x larger. This indicates that the k_i effect on plate height for a column with a non-uniform phase ratio distribution is minor, in agreement with what was found by others [6.2]. Although the range of H , listed in Table

Table 6.14 Comparison of simulated values from the program H(Ws) and experimental values measured from elution chromatograms on PRP-1 columns (5 cm x 4.1 mm i.d.). The error for the experimental values is given as one standard deviation. The experimental values of H and V_r were measured for (a) methyl paraben and (b) 4-phenylazo-1-naphthylamine.

Parameter	Values from Simulation	Experimental Value	
W_s (grams)	0.27	0.26 *	
V_m (mLs)	0.42	0.43 ± 0.02	
$u_{0,max}$ (cm / sec)	0.50	0.51 ± 0.11	
$u_{0,min}$ (cm / sec)	0.22	0.22 ± 0.10	
V_r (mL)			
$K_i = 1$ l/kg	1.1	1.0 ± 0.1	a
$K_i = 45$ l/kg	19.3	12.9 ± 1.2	b
H (mm)			
$K_i = 1$ l/kg	1.2	0.43 ± 0.28	a
$K_i = 45$ l/kg	1.5	2.7 ± 1.2	b
Range of Simulated H (mm)			
$K_i = 1$ l/kg	0.2 - 2.6		
$K_i = 45$ l/kg	0.2 - 3.0		

* This value was obtained by weighing the stationary phase in one column.

6.14, seems to indicate that these values are the same within experimental error, this is not true. The range of H for both samples was calculated as follows. To calculate the lower end of the range, the lowest H was determined by using the smallest difference between $u_{o,min}$ and $u_{o,max}$ to select the correct WS values for the $H(WS)$ program. This is done by calculating the fastest $u_{o,min}$ and the slowest $u_{o,max}$.

$$\text{Fastest } u_{o,min} = \text{Average } u_{o,min} + \sigma = 0.22 + 0.10 \quad 6.24$$

$$\text{Slowest } u_{o,max} = \text{Average } u_{o,max} - \sigma = 0.51 - 0.11 \quad 6.25$$

σ is the standard deviation and is listed in Table 6.14. The upper end of the range (the largest H) was calculated in an analogous manner using the greatest difference between $u_{o,min}$ and $u_{o,max}$. For the largest value of H , the slowest $u_{o,min}$ and the fastest $u_{o,max}$ are the desired numbers. Since the range of H shows the error due to differences in the experimental values of $u_{o,min}$ and $u_{o,max}$, the range should only be used for comparison between the simulated and experimental results. It should not be used for comparison between simulated values of H for samples with different K_i since the range for both samples was calculated using the same differences between $u_{o,min}$ and $u_{o,max}$. The trend of a slightly increasing H as K_i increases is real but the exact value of H for each sample, based on the non-uniform packing density distribution, is somewhere between 0.2 mm and 3.0 mm.

6.3 Conclusions

From the permeability measurements on PRP-1 it appears that the bed is not being compressed as the column pressure increases, therefore, bed compression is not responsible for a non-uniform packing structure and non-uniform velocity profile. There seemed to be no systematic difference in the permeability using different methanol-water

mobile phases, indicating the bed of PRP-1 was not expanding due to particle swelling in these solvents. These results differ from those found for acetonitrile and tetrahydrofuran mobile phases.

Sample velocity profiles were observed directly using the velocity profile technique based on injecting dyes. The profiles were found to change depending upon how the mobile phase exited the column. When the mobile phase outlet flow left in a constricted manner, the sample velocity profile was fastest in the center and slowest at the walls. When the outlet flow uniformly left the column, the sample velocity was now slowest in the center and fastest at the column walls. This phenomenon of a changing velocity profile shape with changing outlet endfitting configuration, was not observed with a C18 packing. Regardless of the mobile phase outlet configuration, the sample velocity on C18 was always fastest in the center and slowest at the walls. Also, the sample velocity profiles on C18 were more uniform and not as exaggerated as those viewed on PRP-1.

Based on these results, it was concluded that the PRP-1 columns had unstable packing structures which shifted in response to the outlet endfitting configuration. An unstable packing structure could be partially responsible for the large plate heights obtained on PRP-1 by causing a uneven transcolumn velocity distribution. Although this could explain the generally low efficiency of PRP-1 relative to the bonded-phase columns, it would not explain the sample-specific bandbroadening observed for some non-polar, highly conjugated compounds.

One possible solution to the problem of the unstable packing structure would be the use of mobile phase solvents which would better wet the PRP-1 stationary phase. Work in this area has been done by Bowers and Pedigo [6.17]. He found that peak shape improved and plate height decreased when methanol-water mobile phases containing 5% to 10% tetrahydrofuran were used. Another possible solution would be to bond a small quantity of polar substituent groups onto the PRP-1 surface. This could improve the wettability of the PRP-1 by typical reversed-phase mobile phases and increase particle coherence. If only a

small percent of the surface were modified, the adsorption properties of the PRP-1 would probably not change substantially. This has been attempted by Yang and Verzele [6.18] for another polystyrene-divinylbenzene copolymer. They used 7 μm diameter particles which had an average pore diameter of either 3 nm or 17 nm (PRP-1 has an average pore diameter of 7.5 nm) and the mobile phases used by Yang and Verzele were acetone-water mixtures, rather than methanol-water as used in this thesis. Because of these differences, a direct comparison between the copolymers used by Yang and Verzele and PRP-1 is not possible. However, their modified polymers did produce lower plate heights than PRP-1. Yang and Verzele measured H values of approximately 0.2 mm for a series of small, polar samples. It is not known what effect this modified polymer would have on non-polar, highly conjugated aromatic samples.

The $H(\text{WS})$ calculation showed that plate height should increase only slightly as the distribution coefficient increases, indicating that bandbroadening due to a non-uniform phase ratio is minor. This agrees with what was found using elution chromatography as discussed in Section 3.2.2, where H was found to be independent of k'_i .

CHAPTER 7

Conclusions and Future Work

The work presented in this thesis was undertaken in order to determine the origin of anomalous bandbroadening observed on polystyrene-divinylbenzene adsorbents used in reversed-phase liquid chromatography. The adsorbent chosen for this study was Hamilton PRP-1. There appears to be two sources of bandbroadening on these stationary phases. A generally low column efficiency is observed for all samples, as compared to silica-based bonded phase columns, and a sample dependent bandbroadening is observed for non-polar, highly conjugated aromatic compounds. The general bandbroadening appears to be responsible for plate heights on PRP-1 which are about 5x larger than plate heights obtained on bonded phase columns. The sample dependent bandbroadening is responsible for plate heights which are about 25x larger than those obtained on bonded phase columns.

The source of the general bandbroadening appears to be a transcolumn non-uniform velocity profile caused by a non-uniform packing density distribution across the column. This varying packing density occurs because the PRP-1 particles are not wetted well by the aqueous-methanol mobile phases commonly used in reversed-phase liquid chromatography and therefore, they do not cohere well. One possible solution to this poor cohesiveness is addition to the mobile phase of organic solvents which wet the PRP-1 more efficiently. It would be of great interest to repeat the velocity profile studies on PRP-1 using such a mobile phase to see the effect on the sample zone profile. Another possible solution is modifying a small percent of the PRP-1 surface by bonding hydrophilic substituents which might improve the wetting characteristics of PRP-1 in the aqueous-methanol mobile phases.

The origin of the sample-specific bandbroadening was not found. Measurement of an adsorption isotherm for a sample (naphthalene) which exhibited this excessive bandbroadening showed the isotherm to be linear in the sample concentration region of

interest. Therefore, isotherm non-linearity was not the cause of the sample dependent bandbroadening.

The desorption rate of naphthalene was also measured and found to be too fast to be responsible for the excessive bandbroadening. It would be interesting to repeat the desorption rate experiment for another sample which does not produce peaks on PRP-1 with excessively large plate heights (such as a paraben compound) and compare these results with the naphthalene results. This could provide some clues to the source of the sample dependent bandbroadening. Also, repeating the desorption rate experiment on C18 with a highly conjugated aromatic could be useful for future direction in discovering the source of this bandbroadening.

The shallow bed technique was modified for measurement of the naphthalene desorption rate. The general technique works well by allowing measurement of first order desorption rate constants of about 5 sec^{-1} or less, under irreversible conditions. Some refinements could be made to the apparatus to improve the accuracy of the measurement and ease of operation. These include decreasing the hold-up volume, V_m' , so that it is approximately equal to the bed void volume, V_m . This would reduce the amount of sample present in V_m' . Alternatively, if the mobile phase could enter and exit the bed in a stream which has the same diameter as the bed, the hold-up volume in the frits and other dead pockets would be swept more efficiently by the mobile phase. This would also decrease the amount of sample present in the hold-up volume.

Also, use of a gas to propel the mobile phase is not ideal because it causes some drying of the stationary phase and even evaporation of the sample under some conditions. A better method would be to use a syringe pump which could operate at pressures of at least 500 psig.

The peak simulation program discussed in Chapter 4 and Appendix I is useful for predicting peak shape from isotherm curvature. Future work suggested in this area

includes running simulations for samples which produce asymmetrical elution peaks caused solely by isotherm non-linearity, in order to further evaluate the accuracy of this simulation.



- 1.18. J.R. Benson and D.J. Woo, *J. Chromatogr. Sci.*, **22**, 386 (1984).
- 1.19. K.A. Kun and R. Kunin, *J. Polym. Sci., A-1*, **6**, 2689 (1968).
- 1.20. J.R. Millar, *J. Polym. Sci.: Polym. Symp.*, **68**, 167 (1980).
- 1.21. R.L. Gustafson, R.L. Albright, J. Heisler, J.A. Lirio and O.T. Reid, Jr., *Ind. Eng. Chem., Prod. Res. Dev.*, **7**, 107 (1968).
- 1.22. F.F. Cantwell, *Anal. Chem.*, **48**, 1854 (1976).
- 1.23. H.Y. Mohammed and F.F. Cantwell, *Anal. Chem.*, **50**, 491 (1978).
- 1.24. R.G. Baum, R. Saetre and F.F. Cantwell, *Anal. Chem.*, **52**, 15 (1979).
- 1.25. I.O. Kibwage, E. Roets, J. Hoogmartens and H. Vanderhaeghe, *J. Chromatogr.*, **423**, 189 (1987).
- 1.26. L.-G. Nilsson, B. Walldorf and O. Paulsen, *J. Chromatogr.*, **423**, 189 (1987).
- 1.27. J.M. Joseph in *Chromatography and Separation Chemistry, Advances and Developments*, Vol. 297, S. Ahuja, ed., American Chemical Society, Washington, D.C., 1987, Chapter 5.
- 1.28. J. Bontemps, L. Bettendorff, J. Lombet, C. Grandfils, G. Dandrifosse, E. Schoffeniels, F. Nevejans, and J. Crommen, *J. Chromatogr.*, **295**, 486 (1982).
- 1.29. D.P. Lee, *J. Chromatogr. Sci.*, **20**, 203 (1982).
- 1.30. D.P. Lee and J.H. Kindsvater, *Anal. Chem.*, **52**, 2425 (1980).
- 1.31. R.I. Greyson and A.M. Parch, *J. Chromatogr.*, **242**, 349 (1982).
- 1.32. J.G. Buta, *J. Chromatogr.*, **295**, 506 (1984).
- 1.33. K.B. Alton, F. Leitz, S. Bariletto, L. Jaworsky, D. Desrivieres, and J. Patrick, *J. Chromatogr.*, **311**, 319 (1984).
- 1.34. S. Bitteur and R. Rosset, *J. Chromatogr.*, **394**, 279 (1987).
- 1.35. W. Dieterle, J.W. Faigle and H. Mory, *J. Chromatogr.*, **168**, 27 (1979).
- 1.36. L.M. Jahangir and O. Samuelson, *J. Chromatogr.*, **193**, 197 (1980).
- 1.37. J. Paleos, *J. Coll. Inter. Sci.*, **31**, 7 (1969).
- 1.38. F.F. Cantwell and S. Puon, *Anal. Chem.*, **51**, 623 (1979).

- 1.39. S. Afrashtehfar and F.F. Cantwell, Anal. Chem., 54, 2422 (1982).
- 1.40. S. May, R.A. Hux and F.F. Cantwell, Anal. Chem., 54, 1279 (1982).
- 1.41. H.J. Liu, Ph.D. thesis, University of Alberta, 1988.
- 1.42. M.D. Grieser and D.J. Pietrzyk, Anal. Chem., 45, 1348 (1973).
- 1.43. D.J. Pietrzyk, E.P. Kroeff and T.D. Rotsch, Anal. Chem., 50, 497 (1978).
- 1.44. D.J. Pietrzyk and C.H. Chu, Anal. Chem., 49, 757 (1977).
- 1.45. D.J. Pietrzyk and C.H. Chu, Anal. Chem., 49, 860 (1977).
- 1.46. T.D. Rotsch, W.R. Cahill, Jr., D.J. Pietrzyk and F.F. Cantwell, J. Canad. Chem., 59, 2179 (1981).
- 1.47. A.M. Tivert and S. Johansson, "Reversed Phase Liquid Chromatography of Omeprazole and Related Compounds on Stationary Phases of Polystyrene-Divinylbenzene and Alkyl-Modified Silica", poster session at 10th International Symposium on Column Liquid Chromatography 1986.
- 1.48. W. Barber and P.W. Carr, personal communication.
- 1.49. D. MacBlane, N. Kitagawa, J.R. Benson, Amer. Lab., p. 134, February 1987.
- 2.1. S. May, R.A. Hux and F.F. Cantwell, Anal. Chem., 54, 1279 (1982).
- 2.2. D.P. Lee and J.H. Kindsvater, Anal. Chem., 52, 2425 (1980).
- 2.3. H.R. Linder, H.P. Keller and R.W. Frei, J. Chromatogr. Sci., 14, 234 (1976).
- 2.4. H.P. Keller, F. Erni, H.R. Linder and R.W. Frei, Anal. Chem., 49, 1958 (1977).
- 2.5. Care and Use of Partisil Columns for HPLC, Technical Bulletin, Whatman Chemical Separation Div., Clifton, NJ.
- 3.1. B.L. Karger, L.R. Snyder and C. Horvath, An Introduction to Separation Science Wiley, Toronto, Chapter 2 1973.

- 3.2. J.A. Jonsson, "Common Concepts of Chromatography", in Chromatography Theory and Basic Principles, ed. J.A. Jonsson, Dekker, New York, Chapter 1 1987.
- 3.3. L.R. Snyder and J.J. Kirkland, Introduction to Modern Liquid Chromatography, 2nd ed., Wiley, Toronto, Chapter 2 1979.
- 3.4. A.B. Littlewood, Gas Chromatography : Principles, Techniques and Applications, Academic Press, Chapter 2 1970.
- 3.5. J.C. Giddings, Dynamics of Chromatography, Dekker, New York, 1965.
- 3.6. J.A. Jonsson, "Dispersion and Peak Shapes in Chromatography", in Chromatographic Theory and Basic Principles, Dekker, New York, Chapter 2 1987.
- 3.7. F.F. Cantwell, class notes.
- 3.8. A.B. Littlewood, Gas Chromatography : Principles, Techniques and Applications, Academic Press, Chapter 6 1970.
- 3.9. C. Horvath and H.-J. Lin, J. Chromatogr., 126, 401 (1976).
- 3.10. C. Horvath and H.-J. Lin, J. Chromatogr., 149, 43 (1978).
- 3.11. E. Grushka, L.R. Snyder and J.H. Knox, J. Chromatogr. Sci., 13, 25 (1975).
- 3.12. E. Grushka, J. Phys. Chem., 76, 2586 (1972).
- 3.13. F.H. Arnold, H.W. Blanch and C.R. Wilke, J. Chromatogr., 330, 159 (1985).
- 3.14. J.C. Giddings, Dynamics of Chromatography, Dekker, New York, p.35 1965.
- 3.15. J.H. Knox and L. McLaren, Anal. Chem., 36, 1477 (1964).
- 3.16. E.R. Bennett and W.E. Bloch, Anal. Chem., 43, 55 (1971).
- 3.17. J.C. Giddings, Dynamics of Chromatography, Dekker, New York, pps.35, 36 1965.
- 3.18. Ibid, p.38.
- 3.19. S.J. Hawkes, J. Chromatogr., 68, 1 (1972).

- 3.20. V.C. Giddings, Dynamics of Chromatography, Dekker, New York, pps. 40-47 1965.
- 3.21. Ibid, p.49.
- 3.22. Ibid, pps. 52 - 61.
- 3.23. J.C. Sternberg, "Extracolumn Contributions to Chromatographic Bandbroadening" in Advances in Chromatography, eds. J.C Giddings and R.A. Keller, Vol. 2, Dekker, New York, Chapter 6 1966.
- 3.24. E. Grushka, Anal. Chem., 41, 889 (1969).
- 3.25. K. DeClerk and T.S. Buys, J. Chromatogr., 63, 193 (1971).
- 3.26. B.A. Bidlingmeyer and F.V. Warren, Jr., Anal. Chem., 56, 1583A (1984).
- 3.27. B.L. Karger, L.R. Snyder and C. Horvath, An Introduction to Separation Science Wiley, Toronto, pps. 72 - 73 1973.
- 3.28. L.R. Snyder and J.J. Kirkland, Introduction to Modern Liquid Chromatography, 2nd ed., Wiley, Toronto, p. 222 1979.
- 3.29. J.R. Conder, J. High Res. Chromatogr., 5, 341 (1982).
- 3.30. J.R. Conder, J. High Res. Chromatogr., 5, 397 (1982).
- 3.31. P.W. Carr and W. Barber, private communication.
- 3.32. A.M. Tivert and S. Johansson, "Reversed Phase Liquid Chromatography of Omeprazole and Related Compounds on Stationary Phases of Polystyrene-Divinylbenzene and Alkyl-Modified Silica", poster session at the 10th International Symposium on Column Liquid Chromatography 1986.
- 3.33. K.Karch, I. Sebestian and I. Halasz, J. Chromatogr., 122, 3 (1976).
- 3.34. International Critical Tables, Vol. 5, McGraw-Hill Book Co., Inc., New York, 1929, p. 73.
- 4.1. L.R. Snyder, Principles of Adsorption Chromatography, Dekker, 1968, Chapter 3.
- 4.2. J.R. Conder and C.L. Young, Physicochemical Measurements by Gas Chromatography, Wiley, Toronto, 1979, Chapters 2, 9.

- 4.3. J.A.Jonsson in Chromatographic Theory and Basic Principles, J.A.Jonsson, ed., Dekker, New York, 1987, Chapter 2.
- 4.4. B.L.Karger, L.R.Snyder and C.Horvath, An Introduction to Separation Science, Wiley, Toronto, 1973, p.134.
- 4.5. J.F.K.Huber and R.G.Gerritse, J.Chromatogr., 58, 137 (1971).
- 4.6. J.R.Conder and C.L.Young, Physicochemical Measurements by Gas Chromatography, Wiley, Toronto, 1979, Chapter 9.
- 4.7. F.Dondi, A.Betti, G.Blo and C.Bighi, Ann. Chim. (Rome), 68, 293 (1978).
- 4.8. A.W.J.DeJong, J.C.Kraak, H.Poppe and F.Neeringedacht, J.Chromatogr., 193, 181 (1980).
- 4.9. J.Jacobson, J.Frenz and C.Horvath, J.Chromatogr., 316, 53 (1984).
- 4.10. J.A.Jonsson and P.Lovkvist, J.Chromatogr., 408, 1 (1987).
- 4.11. J.R.Conder and C.L.Young, Physicochemical Measurements by Gas Chromatography, Wiley, Toronto, 1979, p.354.
- 4.12. S.May, R.A.Hux and F.F.Cantwell, Anal. Chem., 54, 1279 (1982).
- 4.13. J.Funk and G.Houghton, J.Chromatogr., 6, 193 (1961).
- 4.14. H.A.Chase, J.Chromatogr., 297, 179 (1984).
- 4.15. J.L.Wade, A.F.Bergold and P.W.Carr, Anal. Chem., 59, 1286 (1987).
- 4.16. M.J.Gonzalez, A.Jaulmes, P.Valentin and C.Vidal-Madjar, J.Chromatogr., 386, 333 (1987).
- 4.17. J.E.Eble, R.L.Grob, P.E.Antle and L.R.Snyder, J.Chromatogr., 384, 25 (1987).
- 4.18. J.B. Phillips, N.A. Wright and M.F. Burke, Sep.Sci., 16, 861 (1981).
- 4.19. L.R.Snyder, Principles of Adsorption Chromatography, Dekker, 1968, p.58.
- 4.20. A.L. McClellan and H.F. Harnsberger, J.Coll.Inter.Sci., 23, 577 (1967).
- 4.21. D.P. Lee and J.H. Kindsvater, Anal. Chem., 52, 2425 (1980).
- 5.1. C. Horvath and H.-J. Lin, J. Chromatogr., 149, 43 (1978).

- 5.2. O. Grubner in Advances in Chromatography, vol.6, J.C. Giddings and R.A. Keller, eds., Dekker, New York, 1968, Chapter 4.
- 5.3. G.E. Boyd, A.W. Adamson and L.S. Meyers, Jr., J. Amer. Chem. Soc., 69, 2836 (1947).
- 5.4. S.D. Faust and O.M. Aly, Adsorption Processes for Water Treatment, Butterworths, Toronto, 1987, Chapter 3.
- 5.5. F.G. Helfferich in Mass Transfer and Ion Exchange, L. Liberti and F.G. Helfferich, eds., Martinus Nijhoff Publishers, Boston, 1983, Chapter 5.
- 5.6. O. Grubner in Advances in Chromatography, vol.6, J.C. Giddings and R.A. Keller, eds., Dekker, New York, 1968, Chapter 4.
- 5.7. F.G. Helfferich in Mass Transfer and Ion Exchange, L. Liberti and F.G. Helfferich, eds., Martinus Nijhoff Publishers, Boston, 1983, p. 161.
- 5.8. L.R. Snyder, Principles of Adsorption Chromatography, Dekker, New York, 1968, p.40.
- 5.9. L.R. Snyder, Principles of Adsorption Chromatography, Dekker, New York, 1968, pps.40, 92.
- 5.10. R.F. Hirsch and C.S.G. Phillips, Anal. Chem., 49, 1549 (1977).
- 5.11. H. Kuniyama and J.M. Smith, A.I.Ch.E.J., 20, 1110 (1974).
- 5.12. I. Neretnieks, Chem. Eng. Sci., 31, 1029 (1976).
- 5.13. Amberlite XAD-2 Bulletin, Technical Bulletin, Rohm and Haas Co., Philadelphia, PA.
- 5.14. J.R. Sportsman, J.D. Liddl and G.S. Wilson, Anal. Chem., 55, 771 (1983).
- 5.15. M.T.W. Hearn and B. Gregor, J. Chromatogr., 296, 61 (1984).
- 5.16. A.J. Muller and P.W. Carr, J. Chromatogr., 294, 235 (1984).
- 5.17. R.M. Moore and R.R. Walters, J. Chromatogr., 384, 91 (1987).
- 5.18. A J. Muller and P.W. Carr, J. Chromatogr., 284, 33 (1984).

- 5.19. D.J. Anderson and R.R. Walters, *J. Chromatogr. Biomed. Appl.*, **376**, 69 (1986).
- 5.20. D.B. Marshall, J.W. Burns and D.E. Connolly, *J. Chromatogr.*, **360**, 13 (1986).
- 5.21. G.E. Boyd, A.W. Adamson and L.S. Meyers, Jr., *J. Amer. Chem. Soc.*, **69**, 2836 (1947).
- 5.22. C. Horvath and H.-J. Lin, *J. Chromatogr.*, **126**, 401 (1976).
- 5.23. G. Horvai and E. Pungor in Critical Reviews in Analytical Chemistry, vol. 17, W.L. Zulinski, Jr., ed., CRC Press, Inc., Boca Raton, FL, 1986, p. 234.
- 5.24. F.G. Helfferich, Ion Exchange, McGraw-Hill Book Co., Toronto, 1962, pps.253, 454.
- 5.25. J.C. Giddings, Dynamics of Chromatography, Dekker, New York, 1965, p. 218.
- 5.26. J.C. Giddings, Dynamics of Chromatography, Dekker, New York, 1965, p. 38.
- 5.27. W. Rieman, III and H.F. Walton, Ion Exchange in Analytical Chemistry, Pergamon Press, Toronto, 1970, pp. 122 - 126.
- 5.28. D.P. Lee and J.H. Kindsvater, *Anal. Chem.*, **52**, 2425 (1980).
- 5.29. S.D. Faust and O.M. Aly, Adsorption Processes for Water Treatment, Butterworths, Toronto, 1987, p. 111.
- 5.30. S.J. Hawkes, *J. Chromatogr.*, **68**, 1 (1972).
- 6.1. K.P. Hupe, U. Busch and K. Winde, *J. Chromatogr. Sci.*, **7**, 1 (1973).
- 6.2. A.B. Littlewood, Gas Chromatography 1964, ed. A. Goldup, Richard Clay, Ltd. (the Chaucer Press), Suffolk, 1965, p.77.
- 6.3. S.T. Sie and G.W.A. Rijinders, *Anal. Chim. Acta*, **38**, 3 (1967).
- 6.4. F.H. Huyten, Gas Chromatography 1960, ed. R.P.W. Scott, Butterworths, London, 1960, p.224.
- 6.5. J.H. Knox, G.R. Laird and P.A. Raven, *J. Chromatogr.*, **122**, 129 (1976).
- 6.6. J.C. Giddings, *J. Gas Chromatogr.*, **1**, 12 (1963).

- 6.7. J.H. Knox and M. Saleem, *J. Chromatogr. Sci.*, **10**, 80 (1972).
- 6.8. G.J. Frisone, *J. Chromatogr.*, **6**, 97 (1961).
- 6.9. D.P. Lee and J.H. Kindsvater, *Anal. Chem.*, **52**, 2425 (1980).
- 6.10. Amberlite XAD-2, Technical Bulletin, Rohm and Haas Co., Philadelphia, PA.
- 6.11. L.R. Snyder and J.J. Kirkland, Introduction to Modern Liquid Chromatography, 2nd ed., Wiley, New York, 1979, p.36.
- 6.12. F. Nevejans and M. Verzele, *J. Chromatogr.*, **350**, 145 (1985).
- 6.13. J.C. Giddings, Dynamics of Chromatography, Dekker, New York, 1965, p.208.
- 6.14. Ibid, p.52
- 6.15. D.F. McCarthy, Essentials of Soil Mechanics and Foundations, 2nd ed., Reston Publishing Co., Inc., Reston, VA (1982) Chapter 3.
- 6.16. C. Li and J.B. Evett, Soils and Foundations, 2nd ed., Prentice-Hall Inc., Englewoods, NJ (1987) Chapters 2 and 6.
- 6.17. L.D. Bowers and S. Pedigo, *J. Chromatogr.*, **371**, 243 (1986).
- 6.18. Y.-B. Yang and M. Verzele, *J. Chromatogr.*, **387**, 197 (1987).
- A1.1. A.B. Littlewood, Gas Chromatography, Academic Press, New York, 1970, p.151.
- A1.2. M.W. Dubetz, personal communication.
- A3.1. H.A. Mottola, Kinetic Aspects of Analytical Chemistry, Wiley, Toronto, 1988, Chapter 7.
- A3.2. J.C. Giddings, *Anal. Chem.*, **35**, 1999 (1963).

APPENDIX I

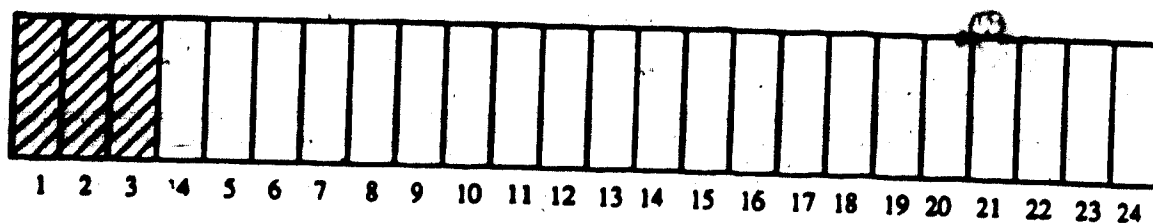
APPENDIX I

Peak Simulation Program

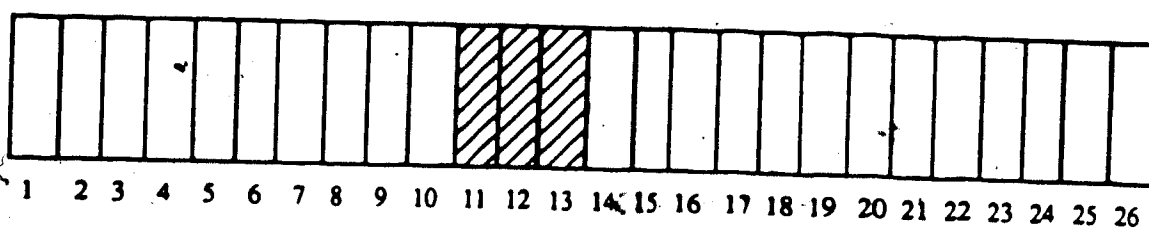
A.1 Basic Algorithm

The algorithm used in this program will be described in a stepwise manner. The basic principle in the calculation is the discreet, stepwise movement of a sample band down a "column". The column is divided axially into increments and the sample zone occupies a certain number of these increments depending upon how much the zone has been broadened by non-ideal chromatographic effects.

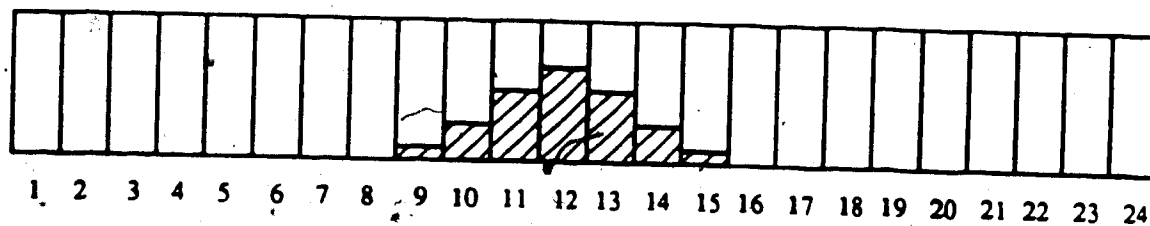
1. Initially the sample is injected into the first few column positions as shown in step 1 of Figure A1.1.
2. The band is moved down ten positions (Step 2 of Figure A1.1).
3. The sample band profile is convolved with a Gaussian distribution to simulate bandbroadening (Step 3 of Figure A1.1).
4. The equilibrium mobile phase concentration is calculated for each column position using the quadratic formula to solve equation A.52. From this concentration, the distribution coefficient and the velocity of sample in each position can be calculated from equations A.54 -A.56. Next, the distance that sample in each position will move (X_j) during a specified time period, DT is determined using equation A.57.
5. The sample at each column position is moved the distance X_j to its new column position farther down the column (Step 4 of Figure A1.1). If the isotherm is non-linear then the distance, X_j , moved by the solute at its various positions will not all be the same and the sample distribution will assume an asymmetric shape as seen in step 4 of Figure A1.1.
6. All positions past the column outlet are checked for sample. If sample is present in these positions, it has eluted and the amount plus the time of elution is stored.



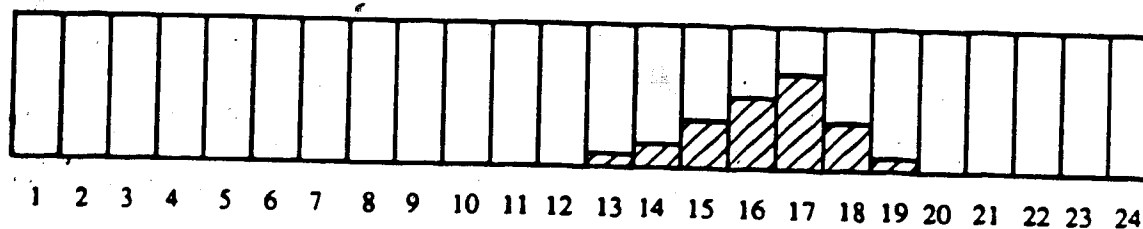
1. Initially, the sample is injected into the first three positions.



2. It is moved down the column 10 positions.



3. The sample distribution is convolved with a Gaussian plate height function.



4. The new sample distribution is moved another step down the column.

Figure A1.1 Diagram of the steps which occur in the peak simulation program.

7. Steps 3 through 6 are repeated until all sample has eluted from the column.

This program was optimized to calculate results for the elution of naphthalene in 90% methanol(aq) on PRP-1. The algorithm calculates the effect on peak shape produced by either a linear isotherm or one that can be described by the Langmuir isotherm equation, although it could be used with any shape isotherm by slightly altering the current program.

One dimensional arrays which contain 256 points are used to monitor the sample as it migrates down the column. Most of these points represent positions on the column and the number of on-column positions is selected by the operator. The remaining points represent positions past the column outlet and are used to monitor eluted sample.

Most numbers must be entered in exponential form.

(ex) 1.0e-3 1.5e1

The few variables which are entered in integer form are the number of steps (STEP), the number of column positions (NPOS), the number of injection positions (INJPOS) and the minimum number of positions to be moved in each step (MINPOS).

There is a glossary of terms used in the program at the end of this appendix.

A.2 Selection of Operator-Entered Values

Several of the parameters which are entered by the operator at the start of the program have obvious meanings and their values are easily chosen. The initial sample concentration, CINJ, is the concentration of sample solution which is injected. The plate height, PLTHT, is an experimental plate height measured from an elution chromatogram run on the real column which is being modelled in the simulation program. The column length (LENGTH), void volume (VM) and weight of stationary phase (WS) are also measured values from the real column. The void volume should be only the inter- and intraparticle volumes and should not include extracolumn void volume. The weight of

stationary phase can be estimated by multiplying the packing density by the empty column geometric volume.

The two isotherm coefficients, A and B, are calculated from the experimental adsorption isotherm of the sample whose elution is being simulated. The average mobile phase linear velocity, UAVE, is also measured during an experimental elution chromatogram of the sample.

Three parameters which are not self-evident are the number of column positions (NPOS), the number of injection positions (INJPOS) and the minimum number of positions to be moved per step (MINPOS). In this program the total number of both column and post-column positions is 256. The total number of positions must be a power of 2 for the FFT and convolution subroutines. The greater the number of positions, the more accurate the peak simulation results will be but the time required for calculations increases in a non-linear manner with an increasing number of positions. The value of 256 was chosen as a compromise since fairly good accuracy was achieved with the simulations taking a reasonable time (30 to 45 minutes).

The number of column positions must be less than 256 but should be as large as possible. The number of post-column positions is the remainder and is calculated using equation A.1.

$$\text{Post-column positions} = 256 - \text{Column positions}$$

A.1

There must be a sufficient number of post-column positions to store all of the eluted sample. If not, both the convolution operation and the number of moles eluted will be incorrect. The number of post-column positions needed is dependent on the plate height. As the plate height increases, the simulated sample zone will become wider and more post-column positions will be necessary. The number of post-column positions necessary

can be roughly calculated by assuming a Gaussian shape for the sample peak and solving for the baseline width.

$$\text{Baseline width} = 6 \sigma_x \quad \text{A.2}$$

The σ_x is related to plate height (PLTHT) and the column length (LENGTH) by equation A.3.

$$\sigma_x = \sqrt{\text{PLTHT LENGTH}} \quad \text{A.3}$$

Substituting gives equation A.4

$$\text{Baseline width} = 6 \sqrt{\text{PLTHT LENGTH}} \quad \text{A.4}$$

To change this to positions it is divided by the number of centimeters per position (DX) using equation A.5.

$$\text{Postcolumn positions} = 256 - \text{NPOS} = \frac{6 \sqrt{\text{PLTHT LENGTH}}}{\text{DX}} \quad \text{A.5}$$

Since DX is dependent on NPOS, this is an iterative calculation which is repeated until the maximum value for NPOS is found which allows for a sufficient number of post-column positions.

INJPOS is the number of column positions the sample is injected into. It is calculated assuming the sample is injected from an injection loop of known volume. First, the void volume in each position is found using equation A.6.

$$\text{VPOS} = \frac{\text{VM}}{\text{NPOS}} \quad \text{A.6}$$

VM is the inter- and intraparticle void volume in liters. The number of injection positions is calculated using equation A.7. INJPOS must be an integer.

$$\text{INJPOS} = \frac{\text{injection loop volume}}{\text{VPOS}}$$

A.7

The number of steps, STEP, is chosen by trial and error. Initially, a small number is selected for STEP, such as 10 or 20. The program is run and the printout of the results will list the sample concentrations, CM(J), and their respective positions, J, on the column for the last step. From this information the number of steps necessary to completely elute the sample can be estimated.

A.3 Calculations Used in the Main Program

This section is meant to correspond with each section of the program and is listed in the same order that each calculation appears in the program. The variables are defined in the glossary at the end of this appendix.

A.3.1 Calculation of Variables which remain constant throughout the program

Calculation of the phase ratio (PHASE) :

$$\text{PHASE} = \frac{\text{WS}}{\text{VM}}$$

A.8

Calculation of the length of each column position (in cm) :

$$\text{DX} = \frac{\text{LENGTH}}{\text{NPOS}}$$

A.9

Calculation of the void volume of each column position (in liters) :

$$\text{VPOS} = \frac{\text{VM}}{\text{NPOS}}$$

A.10

Calculation of the weight of stationary phase in each column position :

$$WPOS = \frac{WS}{NPOS} \quad A.11$$

Calculation of A2, the coefficient of n_m^2 in the second order polynomial (equation A.52) which is used to determine the number of moles present in the mobile phase, at equilibrium for each column position.

$$A2 = \frac{B}{VPOS} \quad A.12$$

Calculation of the denominator, ROOT3, of the quadratic formula which is used to solve for n_m in equation A.52.

$$ROOT3 = 2 \ A2 \quad A.13$$

A.3.2 Calculate plug injection profile

Column positions $J = 1$ through INJPOS have CM(J) set equal to the injected sample concentration, CINJ, to simulate a uniform square wave injection. CM(J) for the rest of the positions is set equal to zero.

A.3.3 Calculation of TMINIT (the initial DT)

The initial time increment, TMINIT, is the time required to move the injected sample 10 column positions. The initial move of 10 column positions is necessary because the sample band will be convolved with a Gaussian plate height function, H(), and there must be positions on both sides of the sample band center of gravity in order to perform the convolution.

To calculate TMINIT the initial sample velocity, UINIT, for the injected sample solution must be determined. First, the equilibrium sample concentration in the mobile phase is calculated by using the quadratic formula to solve equation A.14.

$$0 = \frac{B}{V_{POS}} n_m^2 + \left[1 + \frac{W_{POS} A B}{V_{POS}} - \frac{B N_{INIT}}{V_{POS}} \right] n_m - N_{INIT} \quad A.14$$

Equation A.14 is a rearrangement of the Langmuir isotherm equation. The term n_m is the number of moles of sample present in the mobile phase at equilibrium. The total moles of sample present in both phases is N_{INIT} .

$$N_{INIT} = n_s + n_m \quad A.15$$

The term n_s in equation A.15 is the number of moles present in the stationary phase at equilibrium. For an isotherm which is described by the Langmuir equation, the relation between the mobile phase equilibrium concentration, $MINIT$, and the total moles present can be derived as follows. The isotherm equation is given in equation A.16.

$$CS_{INIT} = \frac{B A MINIT}{1 + B MINIT} \quad A.16$$

CS_{INIT} is the initial equilibrium concentration in the stationary phase. Rewriting equation A.16 in terms of moles gives:

$$\frac{n_s}{W_{POS}} = \frac{B A \frac{n_m}{V_{POS}}}{1 + B \frac{n_m}{V_{POS}}} \quad A.17$$

Eliminating n_s by substituting equation A.15 into A.17 gives:

$$\frac{N_{INIT} - n_m}{W_{POS}} = \frac{B A \frac{n_m}{V_{POS}}}{1 + B \frac{n_m}{V_{POS}}} \quad A.18$$

Rearranging equation A.18 gives the second order polynomial listed in equation A.14.

The coefficients in the quadratic formula are :

$$A_2 = \frac{B^2}{V_{POS}} \quad A.19$$

$$B_2 = 1 + \frac{W_{POS} B A}{V_{POS}} - \frac{B N_{INIT}}{V_{POS}} \quad A.20$$

$$C_2 = -N_{INIT} \quad A.21$$

Solving the quadratic formula gives the number of moles present in the mobile phase at equilibrium for each injection position. To get the equilibrium mobile phase concentration, MINIT, n_m is divided by the void volume of a column position, VPOS.

The next step is to determine the initial stationary phase equilibrium concentration, CSINIT. This is done using equation A.16. Next, the initial distribution coefficient, DISTO, is found by taking the ratio of CSINIT to MINIT.

$$\text{DISTO} = \frac{\text{CSINIT}}{\text{MINIT}} \quad \text{A.22}$$

The initial sample velocity, UINIT, is obtained using equation A.23 :

$$\text{UINIT} = \frac{\text{UAVE}}{1 + \text{DISTO} \text{ PHASE}} \quad \text{A.23}$$

Finally, the initial time increment is found by dividing the distance moved (10 DX) by the initial sample velocity :

$$\text{DT} = \frac{10 \text{ DX}}{\text{UINIT}} \quad \text{A.24}$$

and this is converted from seconds to minutes to give TMINIT.

$$\text{TMINIT} = \frac{\text{DT}}{60} \quad \text{A.25}$$

A.3.4 Calculate minimum value allowed for CM(J)

CM(J) is equal to the total number of moles in each column position divided by VPOS. It is this quantity which is moved and convolved in the program.

During convolution spurious values are generated due to round-off error. These values are very small numbers and should actually be zeroes. In order to make the printouts of the results shorter and easier to read, these spurious values are set to zero by comparing them with a parameter called CUTOFF. To determine CUTOFF the Gaussian plate height function for the entire length of column is calculated. CUTOFF is equal to the

maximum value of the Gaussian function multiplied by CINJ and a factor which sets the lower concentration limit. Currently this factor is 10^{-6} .

$$\text{CUTOFF} = \left[\sqrt{2\pi} \frac{\sqrt{\text{PLTHT LENGTH}}}{\text{DX}} \right]^2 \text{CINJ } 10^{-6} \quad \text{A.26}$$

Any value of CM(J) which is less than this is set to zero. This value is valid for the plate height used for the naphthalene calculations (about 0.4 mm). If the plate height is larger than this CUTOFF should be decreased by decreasing the factor.

A.3.5 Initialize elution chromatogram arrays

This section sets the values to zero for the three arrays used to store the moles eluted and elution times. The three arrays are NTOTAL(), CHROM() and T().

A.3.6 Move one time increment down the column

This loop simulates sample migration down the column using discrete stepwise increments which occur during a time period, DT. STPNUM is the index variable which indicates what step number the loop is in.

A.3.7 Calculation of Gaussian distribution for plate height function

This section calculates the Gaussian distribution used in the convolution to simulate bandbroadening due to non-ideality. The general equation for a Gaussian curve is given in equation A.27 [A1.1].

$$F(x) = \frac{1}{\sigma_x \sqrt{2\pi}} \exp \left[\frac{-(x - \text{AVE})^2}{2 \sigma_x^2} \right] \quad \text{A.27}$$

The standard deviation of the function is σ_x and it has the same units as x . The term x is the distance from the average value, AVE, of the function. In the program the Gaussian distribution was calculated by first finding the center of gravity, FM of the sample profile, CM(.). The first moment is equal to the average x value, AVE of the Gaussian distribution.

$$\text{AVE} = \text{FM} \quad \text{A.28}$$

The standard deviation, SIGMA was calculated using the plate height and the distance the sample band moved during the step, DLNGTH.

$$\text{SIGMA} = \sqrt{\text{PLTHT DLNGTH}} \quad \text{A.29}$$

The standard deviation in units of cm, SIGMA must be changed to the standard deviation in number of column positions, SIG.

$$\text{SIG} = \frac{\text{SIGMA}}{\text{DX}} \quad \text{A.30}$$

The pre-exponential term and the denominator of the exponent in the Gaussian equation are calculated next.

$$Q1 = \frac{1}{\text{SIG} \sqrt{2 \pi}} \quad \text{A.31}$$

$$Q3 = 2 (\text{SIG})^2 \quad \text{A.32}$$

In order to calculate the numerator of the exponential term, a loop was used. First, the difference between each column position, J and the average sample position, AVE was taken.

$$Q2 = -(J - \text{AVE})^2 \quad \text{A.33}$$

Then, the exponential term was calculated.

$$Q4 = \frac{Q2}{Q3} \quad \text{A.34}$$

Finally, the value for the Gaussian distribution, $H(J)$, could be calculated for each column position.

$$H(J) = Q1 \exp(Q4)$$

A.35

If $Q4$ was less than -10, $H(J)$ was set to zero to prevent exponent underflow from occurring. This function, $H(J)$ represents the bandbroadening due to non-ideal phenomena such as diffusion.

A.3.8 Convolve non-linear and non-ideal peak shapes

The sample distribution, $CM()$, and the Gaussian distribution, $H()$, are convolved to produce a new sample distribution which has lower concentrations at each column position and a broader shape. The convolution subroutine, **CONVL**, is called by the following command.

CALL CONVL(RE1,IM1,RE2,IM2,RES,POWER,INVERS)

RE1 and **RE2** are the distributions $CM()$ and $H()$ expanded from their original 256 points to 512. This is necessary because the convolution process will generate $2n - 1$ points for functions of n points and **RE1** is used to store the results of the convolution. The additional 256 data points in the arrays are filled with zeroes prior to the convolution.

RES is the number of points in **RE1** and **RE2** (512). Both **RE1** and **RE2** must have the same number of data points. **POWER** is calculated using equation A.36.

$$POWER = \text{antilog} \left(\frac{\log RES}{2} \right)$$

A.36

INVERS equals 0 for a convolution and 1 for a deconvolution.

The Fourier transforms of $CM()$ and $H()$ are substituted into **RE1**, **IM1** and **RE2**, **IM2**. The convolution is done by solving the following equations for each data point. First, the real part of the convolved function is solved :

$$\text{TEMPR} = \frac{[\text{RE1(J)} \text{ RE2(J)}] + [\text{IM1(J)} \text{ IM2(J)}]}{[\text{RE2(J)} \text{ RE2(J)}] + [\text{IM2(J)} \text{ IM2(J)}]}$$

A.37

Next, the imaginary part of the convolved function is solved using equation A.38:

$$\text{IM1(J)} = \frac{[\text{RE2(J)} \text{ IM1(J)}] - [\text{RE1(J)} \text{ IM2(J)}]}{[\text{RE2(J)} \text{ RE2(J)}] + [\text{IM2(J)} \text{ IM2(J)}]}$$

A.38

Once the imaginary part is calculated the real value in the temporary file TEMPR can be substituted into RE1().

$$\text{RE1()} = \text{TEMPR}$$

A.39

By substituting the convolved values back into RE1 and IM1, computer memory space is saved by eliminating the need for two more arrays to hold the convolved values.

This process is repeated for each of the 512 data points. A reverse Fourier transform is then performed on RE1() and IM1() to obtain the new sample distribution, TEMPCM().

The fast Fourier transform (FFT) algorithm requires the number of data points in each function be a power of 2.

$$\text{Number of positions (\# of J)} = 2 \times$$

A.40

For this program 256 points were used (175 column positions and 81 positions past the column outlet). As mentioned earlier, a greater number of positions would improve the accuracy of the peak shape but would increase the time of the calculation.

The FFT subroutine, FOURI [A1.2] is called within the convolution subroutine by the following command.

CALL FOURI(RE1,IM1,RES,POWER,DX,INVERS)

RE1 is either the sample array, CM() or the plate height function, H(). IM1 is the imaginary part of either of these functions and is an array filled with zeroes. RES is the number of data points (512) and POWER is calculated as shown in equation A.36. DX has a different meaning in the convolution and fast Fourier transform subroutines than it does in the main body of the program and it is calculated by using equation A.41.

$$DX = \frac{1}{RES}$$

224

A.41

Again, a value of zero for INVERS indicates a forward Fourier transform and a value of one indicates a reverse Fourier transform.

A.3.9 Calculate zeroeth and first statistical moments for move back

The convolution process moves the center of gravity of the sample distribution to a new position farther down the column. However, in this simulation, this is undesirable. Any movement down the column is to be due only to the sample migration velocity, $U(J)$, and is related to the distribution coefficient. The results of the convolution should show broadening of the sample zone without movement. Therefore, after the convolution, the center of gravity of the new sample distribution must be moved back to the column position that it occupied before the convolution.

The first moment, AVE, of the pre-convolution sample distribution is already known. In this section the first moment, FM, of the post-convolution sample distribution is calculated and the difference between the two is taken.

$$MOVE = FM - AVE$$

A.42

Each point in the convolved distribution is moved back by the value MOVE. First, the convolved values, TEMPCM(), are put into a temporary file, TEMPH().

$$TEMPH(J) = TEMPCM(J)$$

A.43

The values in TEMPH() are moved back to their correct positions.

$$TEMPPCM(J - MOVE) = TEMPH(J)$$

A.44

The values in TEMPCM() are then substituted into CM(). The area of the convolved function and the number of moles present in the convolved function, CONMOL are calculated for use in the next step in the simulation.

A.3.10 Calculate correct concentrations of convolved function

The convolution process gives results which are lower than the true value. Therefore, the convolved concentrations, CM(J), must be multiplied by a scale factor, RATIO, to correct them. RATIO is equal to the total moles injected, NINJ, divided by the moles present in the convolved function, CONMOL.

$$\text{RATIO} = \frac{\text{NINJ}}{\text{CONMOL}} \quad \text{A.45}$$

Each value in the array CM(J) is multiplied by RATIO (equation A.46).

$$\text{CM(J)} = \text{CM(J)} \cdot \text{RATIO} \quad \text{A.46}$$

A.3.11 Calculate equilibrium concentration in the mobile phase

The value CM(J) is the total moles in both phases at position J divided by VPOS. Therefore, the total moles at position J, N(J), is given by :

$$\text{N(J)} = \text{CM(J)} \cdot \text{VPOS} \quad \text{A.47}$$

In order to calculate the distribution coefficient, the moles present in each phase must be calculated.

If the isotherm is linear the distribution coefficient is equal to the stationary phase concentration divided by the mobile phase concentration. In this program, for a linear isotherm, the distribution coefficient is equal to the parameter B and M(J) is the mobile phase equilibrium concentration. The equilibrium mobile phase concentration can be found using equation A.48.

$$B = \frac{\left(\frac{\text{ns}}{\text{ws}} \right)}{\text{M(J)}} \quad \text{A.48}$$

The moles of sample in the stationary phase, ns, can be related to the total moles in position J, N(J).

$$n_s = N(J) - (M(J) \text{ VPOS})$$

A.49

Substituting this into equation A.49 into A.48 gives :

$$B = N(J) - \frac{[M(J) \text{ VPOS}]}{N(J)} \frac{1}{M(J)}$$

A.50

Solving for M(J) gives equation A.51.

$$M(J) = \frac{N(J)}{\text{VPOS} B + \text{VPOS}}$$

A.51

For an isotherm described by the Langmuir equation, M(J) is found by using the quadratic formula to solve equation A.52 for n_m and then dividing n_m by VPOS.

$$0 = \frac{B}{\text{VPOS}} n_m^2 + \left[1 + \frac{\text{VPOS} A B}{\text{VPOS}} - \frac{B N(J)}{\text{VPOS}} \right] n_m - N(J)$$

A.52

The derivation of equation A.52 was given in Section A.6.3, except NINIT is replaced by N(J).

A.3.12 Find the Lowest M(J) Value to Calculate the Next DT

DT is the time increment necessary to move the slowest moving CM(J) the minimum number of column positions, MINPOS. Therefore, in order to calculate DT for any step, the slowest moving CM(J) had to first be found. This is the CM(J) with the lowest equilibrium sample concentration in the mobile phase, LOWM. To find LOWM it is easiest to find the highest (HIM) mobile phase sample concentration first. This is done by setting HIM equal to M(1) and then comparing each subsequent M(J) value with HIM. If M(J) is greater than HIM, then HIM is set equal to M(J).

Once HIM is found, LOWM is set equal to HIM and each value of M(J) is compared with LOWM. If LOWM is greater than M(J), then LOWM is set equal to M(J). M(J) values which are zero are not included in this comparison. LOWM is then used to calculate

the corresponding CS and DISTCO values. The lowest sample velocity, LOWU, is found in the same manner as UNIT (equation A.23) and the time increment, DT, is obtained using equation A.53.

$$DT = \frac{MINPOS \quad DX}{LOWU} \quad A.53$$

A.3.13 Calculate the sample velocity and distance moved by each CM(J) based on the distribution coefficient for M(J)

For each column position, J, the stationary phase concentration, CS, and the distribution coefficient, DISTCO, are calculated using M(J) and the isotherm equation.

$$CS = \frac{B \quad A \quad M(J)}{1 + B \quad M(J)} \quad A.54$$

$$DISTCO = \frac{CS}{M(J)} \quad A.55$$

Using the distribution coefficient and the average mobile phase linear velocity, UAVE, the sample linear velocity, U(J), can be calculated.

$$U(J) = \frac{UAVE}{1 + DISTCO \quad PHASE} \quad A.56$$

PHASE is the phase ratio. Once the sample velocity is known the distance, X, through which the sample moves during time DT is calculated.

$$X = U(J) \quad DT \quad A.57$$

This distance is in centimeters and must be converted to number of column positions, DPOS.

$$DPOS = \frac{X}{DX} \quad A.58$$

The total sample present at each position, $CM(J)$, is moved by the appropriate value of $DPOS$ to its new position.

$$TEMPCM(J + DPOS) = CM(J) + TEMPCHM(J + DPOS) \quad A.59$$

This process is done for each position. After moving all points, the values in the temporary file, $TEMPCHM(J)$ are substituted into $CM(J)$.

$$CM(J) = TEMPCHM(J) \quad A.60$$

A.3.14 Check for elution

Each time the sample band moves a step down the column, there is a possibility that some sample will have eluted past the column outlet (position $J = 175$). Therefore, the moles of sample which are past the outlet position are monitored and quantified.

First, the moles of sample in every post column position (J is greater than 175) are added together to give the total moles eluted, $NTOTAL(STPNUM)$. This number includes moles eluted in previous steps as well as the present step. Therefore, the moles previously eluted must be subtracted. The moles which elute in a single step are stored in an array called $CHROM()$.

$$CHROM(STPNUM) = NTOTAL(STPNUM) - NTOTAL(STPNUM-1) \quad A.61$$

A.3.15 Calculate zeroeth and first moment for next AVE

Since the sample band, $CM()$, has moved farther down the column, it has a new center of gravity which must be calculated for use in the plate height function for the next step. The distance moved by the center of gravity, $DLNGTH$, is also calculated for the plate height function.

229

A.3.16 Calculate elution time

The elution time corresponding to each step is calculated and stored in a file, T(STPNUM).

$$T(STPNUM) = \left(\frac{DT}{60} \right) + T(STPNUM - 1)$$

A.62

DT is divided by 60 to convert the units to minutes from seconds and then it is added to the time of the previous step. For the first step T(1) is calculated using equation A63.

$$T(STPNUM) = \left(\frac{DT}{60} \right) + TMINIT$$

A.63

The calculations in Sections A.6.6 through A.6.16 are repeated until all sample has eluted from the column. This program prints a list of masses eluted vs elution time as its output.

The program is called PKLANG and is listed on the next seven pages.

```

C
C PKLANG
C PROGRAM TO CALCULATE CHROMATOGRAPHIC PEAKSHAPE
C
  REAL CINJ,PLTHT,LENGTH,CM,TEMPCM,IMAGCM,H,IMAGH,TEMPH
  REAL AVE,SIGMA,SIG,DX,Q1,Q2,Q3,Q4,DT,CSINT,DISTO
  REAL AREA,SUM,FM,CMX,CS,DISTCO,PHASE,UNIT
  REAL U,UAVE,DLNGTH,CHROM,VM,WS,MOVE,RATIO,CHROM,T
  REAL PLTPOS,TMINIT,DL,X
  REAL VPOS,NINIT,N,NELUTE,NTOTAL
  REAL SIGOFF,QOFF,CUTOFF,MOLES
  REAL NINJ,CONMOL,WPOS,LOWM,HIM,LOWU
  DOUBLE PRECISION ROOT4A,ROOT4B,ROOT5,MINT,M
  DOUBLE PRECISION ROOT1,ROOT2,ROOT3,A,B,A2,B2,C2
  INTEGER STPNUM,J,K,STEP,NPOS,INJPOS,MINPOS
  DIMENSION CM(256),IMAGCM(512),TEMPCM(512)
  DIMENSION H(256),IMAGH(512),TEMPH(512)
  DIMENSION U(256),CHROM(200),T(200),NTOTAL(200)
  DIMENSION M(256),N(256)
3  FORMAT(15,3X,E15.7)
5  FORMAT(15.7,3X,E15.7,3X,E15.7,3X,E15.7)
6  FORMAT(I4)
7  FORMAT(E15.7)
  WRITE(9,10)
10  FORMAT('ENTER INITIAL CONCENTRATION')
  READ(9,7)CINJ
  WRITE(9,15)
15  FORMAT('ENTER NUMBER OF COLUMN POSITIONS AS A INTEGER')
  READ(9,6)NPOS
  WRITE(9,20)
20  FORMAT('ENTER NUMBER OF INJECTION POSITIONS AS A INTEGER')
  READ(9,6)INJPOS
  WRITE(9,25)
25  FORMAT('ENTER MINIMUM POSITIONS MOVED PER STEP AS A
  INTEGER')
  READ(9,6)MINPOS
  WRITE(6,27)NPOS,INJPOS,MINPOS
27  FORMAT(3X,NPOS,INJPOS,MINPOS =',I4,3X,I4,3X,I4)
  WRITE(9,30)
30  FORMAT('ENTER PLATE HEIGHT IN CM')
  READ(9,7)PLTHT
  WRITE(9,40)
40  FORMAT('ENTER COLUMN LENGTH IN CM')
  READ(9,7)LENGTH
  WRITE(6,41)CINJ,PLTHT,LENGTH
41  FORMAT(3X'CINJ,PLTHT,LENGTH =',E15.7,3X,E15.7,3X,E15.7)
  WRITE(9,42)
42  FORMAT('ENTER ISOTHERM MONOLAYER VALUE A')
  READ(9,7)A
  WRITE(9,44)
44  FORMAT('ENTER ISOTHERM LINEAR DISTRIBUTION COEF. B')
  READ(9,7)B
  WRITE(9,48)

```

```

48  FORMAT('ENTER VOID VOL. IN LITERS')
    READ(9,7)VM
    WRITE(9,50)
50  FORMAT('ENTER STAT. PHASE WT. IN KG')
    READ(9,7)WS
    WRITE(9,52)
52  FORMAT('ENTER AVE. MOBILE PHASE VELOCITY IN CM/S')
    READ(9,7)UAVE
    PHASE=WS/VM
    WRITE(6,54)A,B
54  FORMAT(3X,'ISOTHERM COEF. ',E17.9,5X,E17.9)
    WRITE(6,56)VM,WS,UAVE
56  FORMAT(3X,'VM,WS,UAVE = ',E15.7,5X,E15.7,5X,E15.7)
    WRITE(9,57)
57  FORMAT('ENTER NUMBER OF STEPS')
    READ(9,6)STEP
    DX = LENGTH/NPOS
    VPOS = VM/NPOS
    WPOS = WS/NPOS
    WRITE(6,59)DX,PHASE
59  FORMAT(3X,'DX,PHASE = ',E15.7,1X,E15.7)
    A2 = B/VPOS
    ROOT3 = 2*A2
    WRITE(6,60)VPOS,WPOS
60  FORMAT(3X,'VPOS,WPOS = ',E15.7,3X,E15.7)

```

```

C
C CALCULATE PLUG INJECTION PROFILE
C

```

```

    NINIT = VPOS*CINJ
    NINJ = INJPOS*NINIT
    DO 61 J=1,256
        CM(J)=0
61  CONTINUE
    DO 62 J=11,10+INJPOS
        CM(J) = CINJ
62  CONTINUE

```

```

C
C CALCULATE INITIAL DT (TMINIT)
C

```

```

    IF(A.EQ.0)THEN
        DISTO = B
    ELSE
        C2 = - NINIT
        B2 = (1 + (WPOS*B*A/VPOS) - (B*NINIT/VPOS))
        ROOT1 = 4*A2*C2
        ROOT2 = SQRT((B2**2) - ROOT1)
        ROOT4A = (-B2 + ROOT2)/ROOT3
        ROOT5 = -B2 - ROOT2
        ROOT4B = ROOT5/ROOT3
        IF(ROOT4A.LT.0)THEN
            MINIT = ROOT4B/VPOS
        ELSE
            IF(ROOT4A.GT.NINIT)THEN

```

```

    MINIT = ROOT4B/VPOS
  ELSE
    MINIT = ROOT4A/VPOS
  ENDIF
ENDIF
CSINIT = (B*A*MINIT)/(1 + (B*MINIT))
DISTO = CSINIT/MINIT
ENDIF
UNIT = UAVE/(1 + (DISTO*PHASE))
DT = (10*DX)/UNIT
TMINIT = DT/60
FM = 12.0
DLNGTH = 10*DX
PLTPOS = PLTHT/DX
WRITE(6,67)CSINIT,DISTO,UNIT
67  FORMAT(3X,'CSINIT,DISTO,UNIT =',E15.7,3X,E15.7,3X,E15.7)
WRITE(6,68)DT,DLNGTH,STEP
68  FORMAT(3X,'INITIAL DT,DLNGTH,STEP =',E15.7,3X,E15.7,3X,I3)
WRITE(6,70)NINJ,NINIT,MINIT
70  FORMAT(3X,'NINJ,NINIT,MINIT = ',E15.7,3X,E15.7,2X,E17.9)
WRITE(6,80)TMINIT
80  FORMAT(3X,'TMINIT =',E15.7)
C
C CALCULATE MINIMUM VALUE ALLOWED FOR CM. CM < CUTOFF IS SET TO
ZERO.
C
SIGOFF = (SQRT(PLTHT*LENGTH))/DX
QOFF = 1/(SIGOFF*(SQRT(2*3.141593)))
CUTOFF = QOFF*CINJ*1.0E-6
C
C INITIALIZE ELUTION CHROMATOGRAM ARRAY
C
DO 100 J=1,200
  NTOTAL(J)=0
  CHROM(J)=0
  T(J)=0
100 CONTINUE
C
C MOVE 1 TIME INCREMENT DOWN THE COLUMN (DT)
C
DO 1000 STPNUM=1,STEP
C
C CALCULATION OF GAUSSIAN DISTRIBUTION FOR PLATE HEIGHT
FUNCTION
C
AVE=FM
SIGMA = SQRT(PLTHT*DLNGTH)
C
C CONVERT SIGMA IN CM TO SIGMA IN #POSITIONS
C
SIG = SIGMA/DX
IF(SIG-INT(SIG).GE.0.5)THEN
  SIG = INT(SIG)+ 1.0
ELSE

```



```

      SIG = INT(SIG)
    ENDIF
    Q1 = 1/(SIG*(SQRT(2.0*3.141593)))
    Q3 = 2.0*(SIG*SIG)
    DO 200 J=1,256
      Q2 = -((J-AVE)*(J-AVE))
      Q4 = Q2/Q3
      IF(Q4.LE.-10.0)THEN
        H(J) = 0
      ELSE
        H(J) = Q1*(EXP(Q4))
      ENDIF
200   CONTINUE
C
C CONVOLVE NONLINEAR & NONIDEAL PEAK SHAPE
C
      DO 250 J=1,512
        TEMPCM(J) = 0
        TEMPH(J) = 0
        IMAGCM(J) = 0
        IMAGH(J) = 0
250   CONTINUE
      DO 300 J=1,256
        TEMPCM(J) = CM(J)
        TEMPH(J) = H(J)
300   CONTINUE
      CALL CONVL(TEMPCM,IMAGCM,TEMPH,IMAGH,512,9,0)
C
C CALCULATE ZEROETH AND FIRST STATISTICAL MOMENTS FOR MOVE
BACK
C
      AREA=0
      DO 430 J=1,512
        AREA=AREA+(TEMPCM(J)*DX)
430   CONTINUE
      SUM=0
      DO 440 J=1,512
        SUM=SUM+(J*TEMPCM(J)*DX)
440   CONTINUE
      FM=SUM/AREA
      IF(FM-INT(FM).GE.0.5)THEN
        FM=INT(FM) + 1.0
      ELSE
        FM=INT(FM)
      ENDIF
C
C MOVE CONVOLVED CM(J) BACK TO ORIGINAL POSITION
C
      MOVE = FM - AVE
      DO 500 J=1,512
        TEMPH(J)=0
500   CONTINUE
      DO 510 J=1,512

```

```

    TEMPH(J)=TEMPCM(J)
510  CONTINUE
    DO 520 J=512*MOVE,MOVE+1,-1
        TEMPCM(J-MOVE)=TEMPH(J)
520  CONTINUE
    CONMOL=0
    DO 550 J=1,256
        CM(J)=TEMPCM(J)
        IF(CM(J).LT.CUTOFF)THEN
            CM(J) = 0
        ENDIF
        CONMOL=CONMOL + (CM(J)*VPOS)
550  CONTINUE
C
C CORRECT CONCENTRATION OF CONVOLVED CM(J)
C
    RATIO=NENJ/CONMOL
    DO 559 J=1,256
        CM(J)=CM(J)*RATIO
559  CONTINUE
C
C CALCULATE EQUILIBRIUM CONCIN IN THE MOBILE PHASE
C
    DO 580 J=1,256
        M(J) = 0
580  CONTINUE
    DO 583 J=1,256
        N(J) = CM(J)*VPOS
        IF(A.EQ.0)THEN
            M(J) = N(J)/((B*WPOS) + VPOS)
        ELSE
            C2 = - N(J)
            B2 = (1 + (WPOS*B*A/VPOS) - (B*N(J)/VPOS))
            ROOT1 = 4*A2*C2
            ROOT2 = SQRT((B2**2) - ROOT1)
            ROOT4A = (-B2 + ROOT2)/ROOT3
            ROOT5 = -B2 - ROOT2
            ROOT4B = ROOT5/ROOT3
            IF(ROOT4A.LT.0)THEN
                M(J) = ROOT4B/VPOS
            ELSE
                IF(ROOT4A.GT.CM(J))THEN
                    M(J) = ROOT4B/VPOS
                ELSE
                    M(J) = ROOT4A/VPOS
                ENDIF
            ENDIF
        ENDIF
    ENDIF
583  CONTINUE
C
C FIND LOWEST M(J) TO CALCULATE NEXT DT
C
    HIM = M(1)
    DO 592 J = 2,256

```

```

      IF(M(J).GT.HIM)THEN
        HIM = M(J)
      ENDIF
592  CONTINUE
      LOWM = HIM
      DO 595 J=1,256
        IF(M(J).EQ.0)GOTO 595
        IF(M(J).LT.LOWM)THEN
          LOWM = M(J)
        ENDIF
595  CONTINUE
      IF(A.EQ.0)THEN
        DISTCO = B
      ELSE
        CS = (B*A*LOWM)/(1 + (B*LOWM))
        DISTCO = CS/LOWM
      ENDIF
      LOWU = UAVE/(1 + (DISTCO*PHASE))
      DT = (MINPOS*DX)/LOWU
C
C CALCULATE U(I) AND DISTANCE MOVED BY CM AT EACH J BASED ON
DIST.COEF. FOR M(J)
C
      DO 600 J=1,512
        TEMPCM(J)=0
600  CONTINUE
      DO 640 J=1,256
        IF(A.EQ.0)THEN
          DISTCO = B
        ELSE
          CMX = M(J)
          CS = (B*A*CMX)/(1 + (B*CMX))
          DISTCO = CS/CMX
        ENDIF
        U(J) = UAVE/(1 + (DISTCO*PHASE))
        X = DT*U(J)
        DPOS = X/DX
        IF(DPOS-INT(DPOS).GE.0.5)THEN
          DPOS = INT(DPOS) + 1.0
        ELSE
          DPOS = INT(DPOS)
        ENDIF
635  TEMPCM(J + DPOS) = TEMPCM(J + DPOS) + CM(J)
C
C CHECK FOR ELUTION
C
      IF((J+DPOS).GT.NPOS)THEN
        NELUTE = TEMPCM(J + DPOS)*VPOS
        NTOTAL(STPNUM) = NTOTAL(STPNUM) + NELUTE
      ENDIF
640  CONTINUE
      IF(STPNUM.GT.1)THEN
        CHROM(STPNUM) = NTOTAL(STPNUM) - NTOTAL(STPNUM - 1)
      ELSE

```

```

    CHROM(1) = NTOTAL(1)
  ENDIF
  IF(STPNUM.EQ.1) THEN
    T(1) = TMINIT + (DT/60)
  ELSE
    T(STPNUM) = T(STPNUM-1) + (DT/60)
  ENDIF
  DO 660 J=1,256
    CM(J)=TEMPCM(J)
660  CONTINUE
    IF(STPNUM.EQ.STEP) THEN
      DO 670 J=1,256
        IF(CM(J).EQ.0) GOTO 670
        WRITE(6,665) J, CM(J)
665  FORMAT(3X, 'J, CM(J) AFTER UI =', I3, 3X, E15.7)
670  CONTINUE
      ENDIF
    C
    C CALCULATE ZEROETH AND FIRST STATISTICAL MOMENTS FOR NEXT AVE
    C
    AREA=0
    DO 700 J=1,256
      AREA=AREA+(CM(J)*DX)
700  CONTINUE
    SUM=0
    DO 710 J=1,256
      SUM=SUM+(J*CM(J)*DX)
710  CONTINUE
    FM=SUM/AREA
    IF(FM-INT(FM).GE.0.5) THEN
      FM=INT(FM) + 1.0
    ELSE
      FM=INT(FM)
    ENDIF
    DLNGTH=(FM-AVE)*DX
1000 CONTINUE
    C
    C WRITE DISTRIBUTION VALUES AFTER FINAL STEP
    C
    WRITE(6,1100)
1100  FORMAT(3X, 'TIME', 3X, 'MOLES')
    DO 1200 J=1, STEP
      IF(CHROM(J).EQ.0) GOTO 1200
      WRITE(6,5) T(J), CHROM(J)
1200  CONTINUE
    WRITE(6,1300) NTOTAL(STEP)
1300  FORMAT(3X, 'TOTAL MOLES ELUTED =', E15.7)
    WRITE(9,1550)
1550  FORMAT('CALCULATIONS FINISHED')
    STOP
    END
  C
  C CONVOLUTION BEGINS
  C

```

```
SUBROUTINE CONVL(RE1,IM1,RE2,IM2,RES,POWER,INVERS)
```

```
REAL RE1,RE2,IM1,IM2,DENOM,DX
```

```
INTEGER RES,POWER,INVERS
```

```
DIMENSION RE1(RES),RE2(RES),IM1(RES),IM2(RES)
```

```
DX = 1.0/RES
```

```
CALL FOURI(RE1,IM1,RES,POWER,DX,0)
```

```
CALL FOURI(RE2,IM2,RES,POWER,DX,0)
```

```
DO 100 J=1,RES
```

```
IF(INVERS.EQ.0)THEN
```

```
  TEMPR = (RE1(J)*RE2(J)) - (IM2(J)*IM1(J))
```

```
  IM1(J) = (RE1(J)*IM2(J)) + (RE2(J)*IM1(J))
```

```
  RE1(J) = TEMPR
```

```
ELSE
```

```
  DENOM = (RE2(J)*RE2(J)) + (IM2(J)*IM2(J))
```

```
  TEMPR = (RE1(J)*RE2(J)) + (IM1(J)*IM2(J))
```

```
  TEMPR = TEMPR/DENOM
```

```
  IM1(J) = (RE2(J)*IM1(J)) - (RE1(J)*IM2(J))
```

```
  IM1(J) = IM1(J)/DENOM
```

```
  RE1(J) = TEMPR
```

```
ENDIF
```

```
100 CONTINUE
```

```
CALL FOURI(RE1,IM1,RES,POWER,DX,1)
```

```
RETURN
```

```
END
```

```
C
```

```
C FFT1 - 1 DIMENSIONAL FAST FOURIER TRANSFORM
```

```
C
```

```
C FOURI(A,B,RES,POWER,DX,INVERS)
```

```
C
```

```
C A = ARRAY OF REAL DATA (LENGTH IS RES)
```

```
C B = ARRAY OF IMAGINARY VALUES (SET TO ZERO IF ALL REAL DATA)
```

```
C RES = NUMBER OF DATA POINTS
```

```
C POWER = IS DEFINED BY RES=2**POWER (RADIX 2 FFT)
```

```
C DX = TIME BETWEEN SAMPLES (OR 1/RES)
```

```
C INVERS = FLAG, FORWARD FFT=0, REVERSE FFT=1
```

```
C
```

```
  SUBROUTINE FOURI(A,B,RES,POWER,DX,INVERS)
```

```
  REAL A,B,DX,TEMP
```

```
  INTEGER RES,INVERS,I,J,SPAN,POWER,REVBIN
```

```
  DIMENSION A(RES),B(RES)
```

```
C
```

```
C REORDER DATA
```

```
C
```

```
  DO 100 I=1,RES
```

```
    J = REVBIN(I,POWER)
```

```
    IF(J.LE.I) GO TO 100
```

```
    TEMP=A(I)
```

```
    A(I)=A(J)
```

```
    A(J)=TEMP
```

```
    TEMP=B(I)
```

```
    B(I)=B(J)
```

```
    B(J)=TEMP
```

```
100 CONTINUE
```

```
C
```

C DO FFT

C

SPAN=1

DO 110 I=1,POWER

CALL STPFFT(A,B,RES,SPAN,INVERS)

SPAN=SPAN*2

110 CONTINUE

C

C SCALE AS REQUIRED

C

IF(INVERS.EQ.1)THEN

TEMP=1.0/(RES*DX)

ELSE

TEMP=DX

END IF

DO 150 I=1,RES

A(I) = A(I) * TEMP

B(I) = B(I) * TEMP

150 CONTINUE

RETURN

END

C

C REVBIN = DETERMINES REVERSE BINARY NUMBER

C

INTEGER FUNCTION REVBIN(VALUE,LENGTH)

INTEGER I,COUNT,LENGTH,RESULT,VALUE

REAL F

C

RESULT = 0

F = VALUE - 1

DO 170 COUNT = 1,LENGTH

F = F/2.

I = INT(F)

RESULT = 2 * RESULT

IF(I.NE.F)THEN

RESULT = RESULT + 1

F = I

ENDIF

170 CONTINUE

REVBIN = RESULT + 1

END

C

C STPFFT = PERFORM ONE STEP OF A FFT

C

SUBROUTINE STPFFT(A,B,RES,SPAN,INVERS)

REAL A,B

INTEGER RES,SPAN,INVERS,I,J

DIMENSION A(RES),B(RES)

REAL TEMPI, TEMPR, TERMI, TERMR

REAL ANGLE,COSINE,DCOSSN,INCCOS,INCSIN,SINE

INTEGER TOSPAN

C

ANGLE = 3.141593/SPAN

INCSIN = SIN(ANGLE)

```
INCCOS = 2. * SIN(0.5*ANGLE) * SIN(0.5 * ANGLE)
DCOSSN = -2. * INCCOS
COSINE = 1.
SINE = 0.
TOSPAN = SPAN * 2
DO 220 I=1,SPAN
  DO 200 J=I,RES,TOSPAN
    IF(INVERS.EQ.1)THEN
      TERMR=COSSINE* A(J+SPAN) + SINE * B(J+SPAN)
      TERMI=-SINE * A(J+SPAN) + COSSINE * B(J+SPAN)
    ELSE
      TERMR=COSSINE * A(J+SPAN) - SINE * B(J+SPAN)
      TERMI=SINE * A(J+SPAN) + COSSINE * B(J+SPAN)
    END IF
    TEMPR = A(J) - TERMR
    TEMPI = B(J) - TERMI
    A(J) = A(J) + TERMR
    B(J) = B(J) + TERMI
    A(J+SPAN) = TEMPR
    B(J+SPAN) = TEMPI
200  CONTINUE
    INCCOS = INCCOS + (DCOSSN * COSINE)
    COSINE = COSINE + INCCOS
    INCSIN = INCSIN +(DCOSSN * SINE)
    SINE = SINE + INCSIN
220  CONTINUE
  RETURN
END
```

Glossary of Terms Used in the Main Program

- A** One of the empirical constants used in the Langmuir equation, sometimes referred to as the monolayer coverage. The units are moles per kg and it is entered by the operator as an exponent. If the adsorption isotherm is linear, A is equal to zero.
- A2** The coefficient for the n_m^2 term in the second order polynomial (equation A.52). This equation is a rearrangement of the Langmuir isotherm equation.
- AREA** The area or zeroth moment of the sample distribution, $CM(J)$.
- AVE** The average value or mean of the Gaussian plate height function, $H(J)$. AVE is equal to the first moment of the sample distribution, $CM(J)$.
- B** An empirical constant used in the Langmuir isotherm equation, sometimes referred to as the distribution coefficient at low concentrations. The units are liters per mole. If the isotherm is linear, B is the distribution coefficient and has units of liters per kg. B is entered by the operator as an exponent.
- B2** The coefficient in the second order polynomial (equation A.52) which precedes the n_m term.
- C2** The constant in the second order polynomial (equation A.52). It is equal to $-N(J)$.
- CHROM()** The number of moles which have eluted from the column in one step.
- CINJ** The molar concentration of the solution which is injected onto the column. This parameter is entered by the operator as an exponent.
- CM()** This array is the sample distribution. For each column position J, the total concentration present at that position is given by $CM(J)$. It is equal

- to the total number of moles in both phases at position J divided by the volume of a column position, VPOS. CM(J) has units of moles per liter.
- CMX The equilibrium concentration of sample in the mobile phase at each column position.
- CONMOL The total number of moles present in the convolved distribution. It is different than NINJ and is related to NINJ by the term RATIO.
- CS The equilibrium concentration of sample in the stationary phase at each column position. The units are moles per kg.
- CSINIT The initial sample equilibrium concentration in the stationary phase for each injection position. The units are moles per kg.
- CUTOFF The minimum sample concentration allowed to be in exponential notation for CM(J). Values less than CUTOFF are set to zero to avoid exponential underflow calculations in the program.
- DISTCO The sample distribution coefficient at each column position. It has units of liters per kg.
- DISTO The initial sample distribution coefficient for each injection position. It has units of liters per kg.
- DLNGTH The distance in cm which the center of gravity of the peak (the first moment of the sample distribution) moves in any step.
- DPOS The number of column positions moved by CM(J) during each step. This value can be different for different CM(J) depending on the isotherm shape and the sample concentration.
- DT The time in seconds required to move the entire sample distribution, CM(), one step down the column. DT can change for each step.
- DX The length of each column position in cm.
- FM The first statistical moment (or center of gravity) of the sample distribution, CM().

- HIM** The equilibrium concentration of sample in the mobile phase with the highest value. It decreases as the sample distribution moves down the column.
- H()** The Gaussian plate height function which is convolved with the sample distribution, $CM()$, to simulate bandbroadening due to non-ideal processes. $H(J)$ represents the value of the Gaussian plate height function at each column position J .
- IMAGCM()** The file which stores the imaginary part of the sample distribution, $CM()$. These values are necessary for the convolution operation. Each value in $IMAGCM()$ is zero prior to convolution.
- IMAGH()** The file which stores the imaginary part of the Gaussian plate height function, $H()$. These values are necessary for the convolution operation. Each value in $IMAGCM()$ is zero prior to convolution.
- INJPOS** The number of column positions into which the sample is injected. This parameter is entered by the operator as an integer.
- LOWM** The equilibrium sample concentration in the mobile phase with the lowest value above the CUTOFF value. It changes as the sample distribution moves down the column.
- LOWU** The linear velocity of the slowest moving $CM(J)$ during a particular step of the sample distribution. For a linear isotherm all $CM(J)$ will have the same linear velocity.
- LENGTH** The column length in cm. This parameter is entered by the operator as an exponent.
- INIT** The initial sample equilibrium concentration in the mobile phase. Units are moles per liter.

- MINPOS** The minimum number of column positions which will be moved per step by the slowest moving $CM(J)$. This variable is entered by the operator as an integer.
- M(J)** The equilibrium concentration of sample in the mobile phase at each column position J . The units are moles per liter.
- MOVE** When the sample distribution, $CM()$, is convolved with the Gaussian plate height function, $H()$, the resulting distribution has a center of gravity which is displaced from the center of gravity of the original $CM()$ by many column positions. **MOVE** is the difference, in column positions, between the two centers of gravity.
- NELUTE** The number of moles of sample eluted into a postcolumn position beyond the end of the column during one step.
- NINIT** The number of moles injected into each injection position.
- NINJ** The total number of moles injected onto the column.
- N(J)** The total number of moles of sample present at each column position J .
- NPOS** The number of on-column positions. This variable is entered by the operator as an integer.
- NTOTAL()** The total number of moles which have eluted in a step and in all the previous steps. It is calculated by keeping a running sum of all moles of sample which have moved past the last column position.
- PHASE** The phase ratio in units of kg per liter.
- PLTHT** The column plate height in cm. This parameter is entered by the operator in exponential form.
- PLTPOS** The plate height which corresponds to the distance ($DLNGTH$) moved by the center of gravity of the sample distribution, $CM()$, moved in one step. It is the fraction of the total column plate height ($PLTHT$), which results from moving the distance, $DLNGTH$.

- Q1-Q4 The Gaussian plate height function, $H()$, is broken down into several terms to make the program easier to follow. Q1 through Q4 are these terms.
- QOFF This is a parameter used to calculate the minimum concentration value, CUTOFF, which is allowed for $CM()$. It is used in the calculation of the Gaussian plate height function, $H()$, which represents the bandbroadening which occurs in one step.
- RATIO When the sample distribution, $CM()$, is convolved with the Gaussian plate height function, $H()$, the resulting distribution has values which are too small. This occurs because the values in $CM()$ and $H()$ are less than one. The convolution operation has a step in which the numbers from both functions are multiplied together, resulting in a smaller number. These convolved values do not represent the true concentrations at each column position J because the total moles of the convolved distribution is less than the moles injected, which is physically impossible. Therefore, the convolved values of $CM()$ must be multiplied by a correction factor, so the total moles in the convolved distribution is equal to the total moles injected. The correction factor, $RATIO$, is equal to $NINJ / CONMOL$.
- ROOT1 to ROOT5 The quadratic formula is used to solve equation A.52 for n_m . It is broken down into a series of terms in order to make the program easier to follow. ROOT1 through ROOT5 are these terms.
- SIG The unitless standard deviation of the Gaussian plate height function, $H()$. SIG is the number of column positions in one standard deviation. Its value depends on the distance moved by the center of gravity of the sample distribution.

SIGMA	The standard deviation of the Gaussian plate height function, $H()$, in units of cm. Its value depends on the distance moved by the center of gravity of the sample distribution.
SIGOFF	This is a parameter to calculate the minimum concentration value, CUTOFF, allowed for $CM()$. It is the standard deviation of the Gaussian plate height function, $H()$, which is calculated for the bandbroadening which occurs in one step. SIGOFF is unitless - it is the minimum number of column positions allowed in one standard deviation.
STEP	The number of steps that the sample distribution will move down the column. This parameter is operator entered as an integer.
SUM	A value used in the calculation of the first moment (or center of gravity) of the sample distribution, $CM()$.
STPNUM	The index parameter which indicates the step number.
TEMPCM()	A file which is used to store values of the sample distribution, $CM()$, temporarily after a calculation.
TEMPH()	A file which is used to store values of the Gaussian plate height function, $H()$, temporarily after a calculation.
TMINIT	The time required to move the sample distribution, $CM()$, the first ten positions down the column. The units are minutes.
UAVE	The average mobile phase linear velocity in cm per second. UAVE is the average of both the inter- and intraparticle velocities. It is calculated by measuring the elution time of an unretained sample from an elution chromatogram and dividing this by the length of the column. This parameter is entered by the operator in exponential form.
UNIT	The initial sample velocity in cm per second.
U(J)	The sample velocity corresponding to the sample concentration, $CM()$, at each column position J. The units are cm per second.

- VM** The column void volume in liters. This is the inter- and intraparticle volume only, not extracolumn void volume. This parameter is entered by the operator in exponential form.
- VPOS** The void volume of each column position in liters.
- WPOS** The weight of stationary phase present in each column position in kg.
- WS** The weight of stationary phase in the entire column. The units are kg and this parameter is entered by the operator as an exponent.
- X** The distance in cm moved by the sample, $CM(J)$, present at each column position J during a step.

Glossary of Terms Used in the Convolution Subroutine

DENOM	An intermediate result in the convolution operation
DX	This parameter DX has a different meaning in the convolution subroutine than it has in the main program but it has the same meaning as DX in the fast Fourier transform subroutine. In the convolution subroutine it is the sampling frequency and is equal to $1/RES$.
IM1,IM2	The imaginary parts of the two arrays which are to be convolved.
INVERS	A flag variable which is used to indicate whether the operation is convolution ($INVERS = 0$) or deconvolution ($INVERS = 1$).
POWER	The power of 2 which gives the number of data points (RES).
RE1,RE2	The real parts of the two arrays which are to be convolved.
RES	The number of data points in RE1 and RE2. There must be the same number of data points in both arrays and it must be a power of 2.
TEMPR	An intermediate result in the convolution operation.

Glossary of Variables Used in the Fast Fourier Transform Subroutine

A	The real part of the array which is going to be transformed. This term has a different meaning in the fast Fourier transform subroutine than it does in the main program.
B	The imaginary part of the array which is going to be transformed. This term has a different meaning in the fast Fourier transform subroutine than it does in the main program.

- DX** The sampling frequency. It is equal to $1/\text{RES}$. This parameter DX has a different meaning in the fast Fourier transform subroutine than it has in the main program but it has the same meaning as DX in the convolution subroutine.
- IM1** This is the same as B.
- INVERS** This is a flag variable which indicates whether the operation is a forward FFT ($\text{INVERS} = 0$) or a reverse FFT ($\text{INVERS} = 1$).
- POWER** The power of 2 which gives the number of data points (RES).
- RE1** This is the same as A.
- RES** The number of data points in RE1. This must be a power of 2.

APPENDIX II

Table A2.1 This table lists the parameters used in the validation of the peak simulation program. The two test samples used were naphthalene, assuming a linear fit through the isotherm data and p-toluidine, which had a non-linear isotherm. The simulated elution peaks are shown in Figure 4.6 in Section 4.1.3.

Parameter		Naphthalene Value	p-Toluidine Value
Concentration injected (M)	*	1.0×10^{-4}	0.3
Plate height (cm)	*	0.038	0.038
Column length (cm)	*	15	15
Void volume (L)	*	1.3×10^{-3}	1.3×10^{-3}
Stationary phase weight (kg)	*	8.4×10^{-4}	8.4×10^{-4}
Mobile phase velocity (cm/sec)	*	0.365	0.365
Number of steps		100	38
Isotherm coefficients		linear isotherm	non-linear
A	*	0	0.83409
B	*	16.72	59.9226
NPOS		175	175
INJPOS		3	3
MINPOS		2	5
Injection Profile		Uniform Square Wave	Uniform Square Wave

An asterisk (*) indicates the parameter was obtained experimentally.

Table A2.2 These are the parameters used in peak simulation program for calculating naphthalene elution peaks based on the experimental adsorption isotherm results presented in Section 4.2.2. The adsorption isotherm results were fit to the Langmuir equation. These parameters were used for the simulated peaks shown in Figure 4.11.

Parameter		1.0 x 10 ⁻⁴ M Naphthalene	1.3 x 10 ⁻³ M Naphthalene
Plate height (cm)	*	0.038	0.038
Column length (cm)	*	15	15
Void volume (L)	*	1.3 x 10 ⁻³	1.3 x 10 ⁻³
Stationary phase weight (kg)	*	8.4 x 10 ⁻⁴	8.4 x 10 ⁻⁴
Mobile phase velocity (cm / sec)	*	0.365	0.365
Number of steps		100	100
Isotherm coefficients			
A		0.11925	0.11925
B		159.8	159.8
NPOS		175	175
INJPOS		3	3
MINPOS		2	2
Injection Profile		Uniform Square Wave	Uniform Square Wave

An * indicates the parameter was obtained experimentally.

Table A2.3 The are the parameters used in peak simulation program for calculating naphthalene elution peaks using uniform and non-uniform injection profiles. The shapes of the injection profiles are shown in Figure 4.12. The same parameters were used in the simulations for all three injection profiles. Two types of adsorption isotherms were used - a linear fit to the slightly curved experimental isotherm data and a Langmuir isotherm fit to the same data.

Parameter		Linear Isotherm	Langmuir Isotherm
Concentration injected	*	1.0×10^{-4}	1.0×10^{-4}
Plate height (cm)	*	0.038	0.038
Column length (cm)	*	15	15
Void volume (L)	*	1.3×10^{-3}	1.3×10^{-3}
Stationary phase weight (kg)	*	8.4×10^{-4}	8.4×10^{-4}
Mobile phase velocity (cm / sec)	*	0.365	0.365
Number of steps		100	100
Isotherm coefficients			
A		0	0.11925
B		16.72	159.8
NPOS		175	175
INJPOS		3	3
MINPOS		2	2
Injection Profiles		Uniform Square Wave, Increasing Ramp and Decreasing Ramp	

An * indicates the parameter was obtained experimentally.

APPENDIX III

APPENDIX III

The Possibility of a Second Slower Reaction

The possibility of a second slower reaction was mentioned in Section 5.3.1. This was based on the observation that a line could be drawn through the last three data points in Figure 5.6 which had a smaller slope than the line extending from $t=0$ to $t=1.45$ seconds. Although the standard deviations of the data points in Figure 5.6 are too large to conclude a second reaction is definitely occurring, the desorption rate constant for such a reaction will be calculated to determine the plate height which would result from it.

Consider the possibility of two irreversible desorption reactions occurring in parallel - reaction 1, where desorption occurs quickly and reaction 2, where desorption is slow. The two desorption reactions are described by equations A3.1 and A3.2.

$$i'_{ads} = i_{soln} \quad A3.1$$

$$i''_{ads} = i_{soln} \quad A3.2$$

The prime (') is used for reaction 1 (fast desorption from adsorption sites) and the double prime (") is used for reaction 2 (slow desorption from adsorption sites). The rate of each reaction is:

$$\frac{d C'_{ads}}{dt} = -k'_{des} C'_{ads} \quad A3.3$$

$$\frac{d C''_{ads}}{dt} = -k''_{des} C''_{ads} \quad A3.4$$

The C_{ads} terms refer to the adsorbed concentration for each reaction and k_{des} is the desorption rate constant for each. The shallow bed experiment described in Chapter 5 measured the total adsorbed concentration, which was the naphthalene adsorbed due to both reactions. The quantity of naphthalene adsorbed due to each reaction must be known in order to calculate accurate values for k'_{des} and k''_{des} .

If reaction 1 (the fast reaction) is assumed to be much faster than reaction 2, then at long contact times reaction 1 is essentially complete and only reaction 2 is occurring. Therefore, for long contact times, a plot of $\ln n''_{ads,t}$ vs t will give k''_{des} [A3.1]. This relation is obtained by integrating equation A3.4 which gives A3.5.

$$\ln C''_{ads,t} = -k''_{des} t + \ln C''_{ads,o} \quad A3.5$$

As previously discussed in Chapter 5, moles can be used rather than concentrations.

$$\ln n''_{ads,t} = -k''_{des} t + \ln n''_{ads,o} \quad A3.6$$

A plot of $\ln (n''_{ads,t})$ vs t has a slope equal to the apparent first order desorption rate constant, k''_{des} . The moles of sample adsorbed due to reaction 2 at $t=0$ can be calculated by taking the anti- \ln of the y intercept. Equation A3.6 is then used to calculate the amount of sample adsorbed due to reaction 2 for all contact times. These values are subtracted from the total moles adsorbed, as measured by the shallow bed experiment, to give n'_{ads} (moles of sample adsorbed due to reaction 1).

$$n'_{ads,t} = n_{ads,t} - n''_{ads,t} \quad A3.7$$

The apparent first order desorption rate constant for reaction 1, k'_{des} , is the slope of a plot of $\ln (n'_{ads,o} / n'_{ads,t})$ vs t . The y intercept of this graph should equal zero. The initial

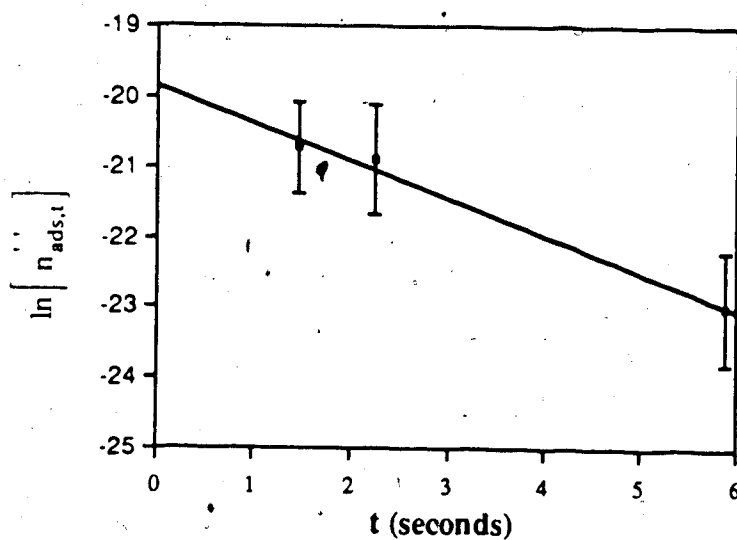
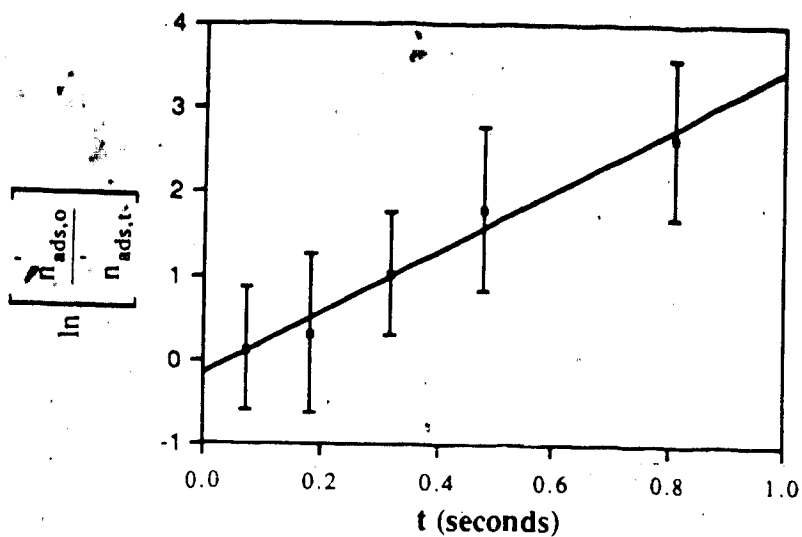
assumption that reaction 1 is much faster than reaction 2 can be tested by calculating the values of $n'_{ads,t}$ for $t=1.45$ through $t=5.9$ seconds. If $n'_{ads,t}$ is negligible compared to $n''_{ads,t}$ then the assumption is valid. This was found to be true for the data obtained from the shallow bed experiment.

The data listed in Table 5.3 was treated in this manner and the two \ln plots are shown in Figure A3.1a and 3.1b. The slope of the plot for reaction 1 (the fast reaction) was $3.6 \pm 0.6 \text{ sec}^{-1}$ and the y intercept was $-0.16 \pm (0.28)$. The \pm values are equal to two standard deviations. The slope of the plot for reaction 2 was $-0.5 \pm 0.1 \text{ sec}^{-1}$ and the y intercept was -19.8 ± 0.4 .

Plate heights were calculated using the pore diffusion model (see Chapter 5), but not the surface adsorption-desorption model. The surface adsorption-desorption model would assume there were two types of adsorption sites on the PRP-1 - a weak site with fast desorption and a strong site with slow desorption [A3.2]. Since only 9% of the total sample undergoes slow desorption, there would be relatively few strong sites as compared to weak sites. The strong sites would preferentially adsorb the sample and the linear capacity of the strong sites would be exceeded before much sample adsorbed onto the weak sites. This would result in non-linearity of the adsorption isotherm. Since the isotherm was linear, it can be assumed that this process is not responsible for the slow desorption and restricted diffusion through some type of narrow, tortuous channel is.

Table A3.1 lists the calculated values of H at various mobile phase linear velocities (u_0) for reactions 1 and 2. These are the plate heights which would be expected if all the sample desorbed solely by reaction 1 or by reaction 2. Therefore, the calculated plate heights for reaction 2 are overestimated since only 9% of the sample desorbs slowly. The actual plate height due to the two parallel desorption reactions would be somewhere in between the H values given for the two reactions.

The plate heights calculated for reaction 1 are just slightly smaller than the plate heights presented in Table 5.4, which were calculated assuming only a single desorption



A3.1 First order plots for (A) reaction 1, fast desorption and (B) reaction 2, slow desorption. Sample was 5×10^{-4} M naphthalene, stationary phase was PRP-1 and mobile phase was 90% methanol(aq).

Table A3.1 Calculated plate heights for reaction 1 (the fast reaction) and reaction 2 (slow reaction) at various mobile phase linear velocities. The \pm values are equal to two standard deviations. Column 4 lists H measured from elution chromatograms using moment analysis.

u_0 (cm/sec)	Reaction 1 H (mm)	Reaction 2 H (mm)	$H_{\text{experiment}}$ (mm)
0.36	0.10 ± 0.02	0.7 ± 0.2	2.5
0.27	0.074 ± 0.013	0.5 ± 0.1	2.7
0.17	0.047 ± 0.008	0.3 ± 0.1	2.1
0.09	0.025 ± 0.004	0.18 ± 0.04	1.6
0.075	0.020 ± 0.004	0.15 ± 0.03	1.5
9.6×10^{-3}	$2.6 \times 10^{-3} \pm 0.5 \times 10^{-3}$	0.019 ± 0.004	0.75

reaction was occurring. This is as expected since 91% of the total sample desorbs via reaction 1 and only 9% by reaction 2. The calculated plate heights for reaction 2 are still about 4x to 40x smaller than experimental plate heights measured from elution chromatograms. However, since it is already known that a non-uniform velocity profile exists which causes some bandbroadening, the combination of a slow desorption process with a non-uniform velocity profile could possibly account for all of the bandbroadening. A slow desorption process could also explain the sample dependent bandbroadening on PRP-1, therefore, the desorption rate experiment should be repeated with emphasis on determining whether a second slower reaction is occurring. A technical difficulty which will have to be overcome is that there is only a very small quantity of sample adsorbed at long contact times making detection and accurate quantification difficult. One possible method which might overcome this problem is the use of a radioactive sample which allows detection at lower concentrations. Fluorescence detection would be another possibility.

APPENDIX IV

```

10 REM PROGRAM H(WS) CALCULATES THE CAPACITY FACTOR AND
12 REM RETENTION TIMES ACROSS A COLUMN WHICH HAS AN UNEVEN
15 REM DISTRIBUTION OF STATIONARY PHASE AND A NONUNIFORM
    VELOCITY PROFILE
19 REM
20 REM DIMENSION AND INITIALIZE ARRAYS
21 REM
30 DIM AREA(50),VOL(50),MOLE(50)
40 DIM WS(50),PD(50)
50 DIM VPORE(50),VINT(50),EINT(50),ET(50)
60 DIM U(50),TM(50),K(50),TR(50),TRMIN(50)
70 FOR I = 1 TO 50
80   AREA(I) = 0
90   VOL(I) = 0
100  MOLE(I) = 0
110  WS(I) = 0
120  PD(I) = 0
130  VPORE(I) = 0
140  VINT(I) = 0
150  EINT(I) = 0
160  ET(I) = 0
170  U(I) = 0
180  TM(I) = 0
190  K(I) = 0
200  TR(I) = 0
210 NEXT I
219 REM
220 REM ENTER VARIABLES
221 REM
260 INPUT "ENTER LENGTH OF COLUMN IN CM ";L
270 INPUT "ENTER COLUMN RADIUS IN CM ";R
280 INPUT "ENTER NUMBER OF SECTIONS COLUMN SHOULD BE DIVIDED
    INTO ";N
290 INPUT "ENTER TOTAL NUMBER OF MOLES INJECTED ";NINJ
300 INPUT "ENTER PARTICLE DIAMETER IN CM ";DP
310 INPUT "ENTER PRESSURE DROP ACROSS COLUMN IN PSI ";P
320 INPUT "ENTER VISCOSITY OF MOBILE PHASE IN POISE ";VISC
330 INPUT "ENTER THE DISTRIBUTION COEFFICIENT IN L/KG ";DIST
339 REM
340 REM CALCULATE CONSTANTS
341 REM
350 R1 = R/N
360 PRESS = P*68947.6
369 REM
370 REM CALCULATE AREAS AND VOLUMES OF SECTIONS AND MOLES
    IN EACH
371 REM
380 AT = 3.14159 * (R ^ 2)
390 AREA(1) = 3.14159 * (R1 ^ 2)
400 A1 = AREA(1)
402 VOL(1) = AREA(1) * L
404 MOLE(1) = (NINJ / AT) * AREA(1)
410 FOR I = 2 TO N
420   A2 = 3.14159 * ((R1 * I) ^ 2)

```

```

430 AREA(I) = A2 - A1
440 VOL(I) = AREA(I) * L
450 MOLE(I) = (NINJ / AT) * AREA(I)
460 A1 = A2
462 NEXT I
464 AVEWW = .37 * VOL(N)
465 MAXWW = 1.07 * VOL(N)
466 AVEWC = .37 * VOL(1)
467 MAXWC = 1.07 * VOL(1)
468 PRINT "AVEWW = "; AVEWW
469 PRINT "MAXWW = "; MAXWW
470 PRINT "AVEWC = "; AVEWC
471 PRINT "MAXWC = "; MAXWC
472 INPUT "ENTER WT. OF STATIONARY PHASE AT WALL "; WW
474 INPUT "ENTER WT. OF STATIONARY PHASE AT CENTER"; WC
479 REM
480 REM CALCULATE WS IN EACH SECTION ASSUMING A LINEAR
    DISTRIBUTION
481 REM
490 M = (WW - WC) / (N - 1)
500 B = WW - (M * N)
510 WS(1) = WC
520 WS(N) = WW
524 WST = WS(1) + WS(N)
530 FOR I = 2 TO N-1
540 WS(I) = (M * I) + B
550 WST = WST + WS(I)
560 NEXT I
569 REM
570 REM CALCULATE PACKING DENSITY IN EACH SECTION
571 REM
580 FOR I = 1 TO N
590 RD(I) = WS(I) / VOL(I)
600 NEXT I
609 REM
610 REM CALCULATE PORE VOLUME IN EACH SECTION
611 REM
615 VMPOR = 0
620 FOR I = 1 TO N
630 VPORE(I) = .79 * WS(I)
635 VMPOR = VMPOR + VPORE(I)
640 NEXT I
649 REM
650 REM CALCULATE INTERPARTICLE VOLUME IN EACH SECTION
651 REM
655 VMINT = 0
660 FOR I = 1 TO N
670 Z = WS(I) / 1.07
680 VINT(I) = VOL(I) - Z - VPORE(I)
685 VMINT = VMINT + VINT(I)
690 NEXT I
695 VMTOT = VMPOR + VMINT
699 REM

```

```

700 REM SOLVE FOR INTERPARTICLE AND TOTAL POROSITIES IN EACH
    SECTION
701 REM
710 FOR I = 1 TO N
720   EINT(I) = VINT(I) / VOL(I)
730   ET(I) = (VINT(I) + VPORE(I)) / VOL(I)
740 NEXT I
749 REM
750 REM CALCULATE LINEAR VELOCITY IN EACH SECTION
751 REM
760 X1 = ((DP ^ 2) * PRESS) / (L * 180 * VISC)
770 FOR I = 1 TO N
780   X2 = (EINT(I) ^ 3) / ((1 - EINT(I)) ^ 2)
790   U(I) = X1 * X2 * ET(I)
800   TM(I) = L / U(I)
810 NEXT I
819 REM
820 REM SOLVE FOR THE CAPACITY FACTOR AND RETENTION TIME IN
    EACH SECTION
821 REM
830 FOR I = 1 TO N
840   VM = VINT(I) + VPORE(I)
850   K(I) = DIST * (WS(I) / VM)
860   TR(I) = (TM(I) * K(I)) + TM(I)
864   TRMIN(I) = TR(I) / 60
870 NEXT I
879 REM
880 REM PRINT RESULTS
881 REM
920 LPRINT "COLUMN LENGTH = "; L
930 LPRINT "COLUMN RADIUS = "; R
940 LPRINT "NUMBER OF SECTIONS = "; N
950 LPRINT "MOLES INJECTED = "; NINJ
960 LPRINT "PARTICLE DIAMETER = "; DP
970 LPRINT "COLUMN PRESSURE DROP = "; P
980 LPRINT "MOBILE PHASE VISCOSITY = "; VISC
990 LPRINT "DISTRIBUTION COEFFICIENT = "; DIST
992 LPRINT "TOTAL VM = "; VMTOT
994 LPRINT "TOTAL WEIGHT OF STATIONARY PHASE = "; WST
996 LPRINT "WS AT COLUMN WALL = "; WW
998 LPRINT "WS AT COLUMN CENTER = "; WC
1000 LPRINT
1010 LPRINT "SECTION"; TAB(15); "PD"; TAB(30); "TR(MIN)"; TAB(50);
    "MOLES"; TAB(70); "M.P. VELOCITY"
1020 LPRINT
1030 FOR I = 1 TO N
1040   LPRINT TAB(5); I; TAB(15); PD(I); TAB(30); TRMIN(I); TAB(50);
    MOLE(I); TAB(70); U(I)
1050 NEXT I
1160 END

```